Elucidating How MLH1 Loss Regulates a Metabolic Phenotype in Endometrial Cancer

Amy Frances Gibson

Submitted in partial fulfilment of the requirements of the Degree of Doctor of Philosophy

April 2023

Centre for Cancer Cell & Molecular Biology

Barts Cancer Institute

Barts and The London School of Medicine and Dentistry

Queen Mary University of London

Charterhouse Square

London

EC1M 6BQ

Statement of Originality

I, Amy Frances Gibson, confirm that the research included within this thesis is my own work or that where it has been carried out in collaboration with or supported by others, this is duly acknowledged below, and my contribution is indicated. Previously published material is also acknowledged below.

I attest that I have exercised reasonable care to ensure that the work is original and does not to the best of my knowledge break any UK law, infringe any third party's copyright or other Intellectual Property Right, or contain any confidential material.

I accept that the College has the right to use plagiarism detection software to check the electronic version of the thesis.

I confirm that this thesis has not been previously submitted for the award of a degree by this or any other university. The copyright of this thesis rests with the author and no quotation from it or information derived from it may be published without the author's prior written consent.

Acknowledgements

Primary Supervisor

Dr Sarah Martin, Reader in Cancer Cell Biology; Director for Graduate Studies for Research; Deputy Centre Lead, Centre for Cancer Cell and Molecular Biology, Barts Cancer Institute.

Secondary Supervisor

Dr Gabriella Ficz, Senior Lecturer; Group Leader, Centre for Haemato-Oncology, Barts Cancer Institute.

Collaborator

Professor Emma Crosbie, Professor of Gynaecological Oncology, Division of Cancer Sciences, The University of Manchester

Funding

This work was supported by Cancer Research UK.

Acknowledgements

First and foremost, I would like to thank CRUK for funding this project. Next, I would like to thank Dr Sarah Martin for welcoming me into her lab. I thank her for all the scientific discussions, advice, and support throughout the last 4 years whilst I juggled pursuing my scientific ambitions alongside my sporting aspirations. Additionally, I'd like to extend gratitude to all my friends and colleagues both from the Martin Lab and Barts Cancer Institute who were a pleasure to work with. From scientific discussions during long tissue-culture days to entertainment whilst waiting for endless westerns to run, you have made my experience all the more enjoyable. Last but not least I would like to thank my wonderful family, particularly my parents, Madeleine and Bob. I thank them for always supporting and believing in me no matter what. I would not be where I am today if it wasn't for them.

Impact of COVID-19

The COVID-19 pandemic disrupted and delayed the completion of this project. During the COVID-19 lockdown (18th March 2020 – 25th June 2020), I had no access to laboratory equipment and therefore could not collect any data. The introduction of laboratory shifts to ensure social distancing when governmental guidelines allowed further limited my time in the lab (26th June 2020 – 29th March 2021). Experiments were performed based on their priority and certain experiments could not be performed due to the time limitation, thus less data was produced.

Abstract

Endometrial cancer is the fourth most common cancer in women and the most common gynaecological malignancy in the developed world. No new systemic treatments for endometrial cancer have been developed in recent years and its incidence is expected to double over the next decade. As such, there is a need to better understand key molecular pathways that are altered in the disease and could be targeted by novel treatments. The DNA MMR pathway is lost in approximately 30% of endometrial cancers. A small proportion of these are caused by germline mutations in one of the four MMR genes, however, the majority result from the epigenetic silencing of MLH1. Recently, our lab has shown that MLH1-deficient cells demonstrate a mitochondrial phenotype characterised by reduced OXPHOS, reduced mtDNA copy number and Complex I inhibition. OXPHOS-deficient cells must adapt their metabolism to compensate for energy defects and the inability to efficiently use the tricarboxylic acid cycle to generate energy. We hypothesise that this altered metabolism is driving tumourigenesis by increasing the tumour cells' metastatic potential. In this PhD we aimed to further investigate the influence MLH1 loss has on cellular metabolism using MLH1 positive and negative paired endometrial cell lines. Ultimately, we aim to understand whether altered metabolism in MLH1-deficient endometrial cancer may be therapeutically targeted.

Abbreviations

1C	One Carbon
2DG	2-deoxyglucose
2HG	2-Hydroxyglutarate
3PG	3-phosphoglycerate
•OH	Hydroxyl Radical
αKG	α-ketoglutarate
AI	Aromatase Inhibitor
ACC	Acetyl-CoA Carboxylase
ACYL	ATP-Citrate Lyase
BCAAs	Branched Chain Amino Acids
BCAT1	Branched-Chain Aminotransferase 1
BER	Base Excision Repair
BSA	Bovine Serum Albumin
CCC	Clear Cell Carcinoma
CN	Copy Number
CRC	Colorectal Cancer
CSS	Cancer-Specific Survival
CTG	Cell Titer-Glo
DDD	DNA Damage Response
DHAP	Dihydroxyacetone Phosphate
DMK	Dimethyl 2-oxoglutarate
DMSO	Dimethyl Sulfoxide
DSB	Double-Strand Break
EBRT	External Beam Radiotherapy
EC	Endometrial Cancer
ECAR	Extracellular Acidification Rate
ECM	Extracellular Matrix
EGFR	Epidermal Growth Factor Receptor
EMT	Epithelial to Mesenchymal Transition
ERK2	Extracellular Signal-Regulated Kinase
ETC	Electron Transport Chain
F2,6BP	Fructose-2,6-Bisphosphate
F6P	Fructose-6-Phosphate
FASN	Fatty Acid Synthetase
FH	Fumarate Hydratase
FCCP	Carbonyl Cyanide-p-Trifluoromethoxy Phenylhydrazone
FFS	Failure-Free Survival
FIGO	International Federation of Gynaecology and Obstetrics
G6P	Glyceraldehyde 3-Phosphate
GAPDH	Glyceraldehyde-3-Phosphate Dehydrogenase
GLDC	Glycine Decarboxylase
GLS	Glutaminase
GLUD	Glutamate Dehydrogenase
GLYCTK	Glycerate Kinase
GOT	Glutamic-Oxaloacetic Transaminase
GPX1	Glutathione Peroxidase 1
H_2O_2	Hydrogen Peroxide
HCC	Hepatocellular Carcinoma Cell
HIF	Hypoxia Inducible Factor

HK	Hexokinase
HR	Homologous Recombination
HNSPCC	Hereditary Non-Polyposis Colorectal Cancer
ICB	Immune Checkpoint Blockade
ICI	Immune Checkpoint Inhibitor
IDH	Isocitrate Dehydrogenase
IDL	Insertion-Deletion Loop
IHC	Immunohistochemistry
InSIGHT	International Society for Gastrointestinal Hereditary Tumours
LC	Liquid Chromatography
LDH	Lactate Dehydrogenase
LDON	6-diazo-5-oxo-L-norleucine
LVSI	Lymphovascular Space Invasion
ME1	Malic Enzyme 1
MDH2	Malate Dehydrogenase 2
MMR	Mismatch Repair
MS	Mass Spectrometry
MSI	Microsatellite Instability
MSS	Microsatellite Stable
mtDNA	Mitochondrial DNA
MTND2	Mitochondrial Encoded Subunit 2
NAC	N-acetyl Cysteine
NEAAs	Non-Essential Amino Acids
NSMP	No Specific Molecular Profile
NER	Nucleotide Excision Repair
NHEJ	Non-Homologous End Joining
NSCLC	Non-Small Cell Lung Cancer
OCR	Oxygen Consumption Rate
OS	Overall Survival
O2•−	Superoxide Anion
OXPHOS	Oxidative Phosphorylation
PBS	Phosphate Buffered Saline
PCNA	Proliferating Cell Nuclear Antigen
PCR	Polymerase Chain Reaction
PCK1	Phosphoenolpyruvate Carboxykinase
PDAC	Pancreatic Ductal Adenocarcinoma
PDC	Pyruvate Dehydrogenase Complex
PDH	Pyruvate Dehydrogenase
PD-1	Programmed Cell Death Protein 1
PD-L1	Programmed Death-Ligand 1
PEP	Phosphoenolpyruvate
PHGDH	Pyruvate Dehydrogenase
PKM1/2	Pyruvate Kinase
PFK	Phosphofructokinase
PFKBP	Phosphofructo-2-Kinase/Fructose-2,6- Bisphosphatases
PFKP	Phosphofructokinase Platelet
PFS	Progression Free Survival
PI3K/Akt/mTOR	Phosphatidylinositol 3 Kinase/Akt/Mammalian Target of Rapamycin
PKM2	Pyruvate Kinase Isozyme 2
PLC	Phospholipase C
POLD	Polymerase δ

POLE	DNA Polymerase Epsilon
PPAR	Peroxisome Proliferator-Activated Receptors
PSAT1	Phosphoserine Aminotransferase
PPP	Pentose Phosphate Pathway
PSPH	Phosphoserine Phosphatase
qPCR	Quantitative PCR
RFC	Replications Factor C
RFS	Recurrence-Free Survival
ROS	Reactive Oxygen Species
RPA	Replication Protein A
SC	Serous Carcinoma
SDH	Succinate Dehydrogenase
SHMT	Serine Hydroxymethyltransferases
siRNA	Small Interfering RNA
SLC2A1	Solute Carrier Family 2 Facilitated Glucose Transporter Member
SoC	Standard of Care
SOD	Superoxide Dismutase
SRC	Spare Respiratory Capacity
SSB	Single-Strand Break
SSP	Serine Synthesis Pathway
TCA	Tricarboxylic Acid Cycle
TIC	Total Ion Count
TMB	Tumor Mutational Burden
TNBC	Triple Negative Breast Cancer
UCS	Uterine Carcinosarcoma
UDP-GlcNAc	Uridine Diphosphate-*N*-Acetylglucosamine
VBT	Vaginal Brachytherapy

List of Figures

List of Tables

Table of Contents

1.0 Introduction

1.1 Endometrial Cancer

Endometrial cancer (EC) initiates in the cells which line the uterus (endometrium) and is the sixth most frequently diagnosed cancer and the fourteenth leading cause of cancer mortality in women, comprising approximately 90% of all uterine cancers [1, 2]. Worldwide, it is the second most common gynaecological malignancy, and the first in developed countries [3]. The primary treatment strategy for patients with early-stage disease is surgery, and these women usually have excellent overall 5-year survival rates of 75-86% [4, 5]. However, there are no evidence-based treatments for women with advanced (stage III/IV) or recurrent disease, and this is reflected in poor survival outcomes. Five-year survival for advanced EC is 20-60% [6], while in those with recurrent disease (10-15%), 5-year survival is 13-65% [7]. A study characterising real-world outcomes of women with advanced EC in the US indicated the median overall survival (OS) for these patients was 49.6 months and was shorter in patients with serous carcinoma (31.3 months) and other ECs (29.4 months) than in patients with endometrioid carcinoma (70.8 months) [8]. Increasing our knowledge of the molecular profile of EC is crucial to identify high-risk groups at an early stage [9], as well as for recurrent or metastatic disease where personalised adjuvant treatment is proving beneficial, such as in breast cancer for instance [10].

1.1.1 Diagnosis and molecular characterisation

In the last three decades, the incidence of EC has increased by approximately 1% per year and is now associated with a higher mortality [9]. Observational analyses have associated age at the time of diagnosis, and the presence of other health conditions such as diabetes or obesity, with increased mortality [11]. Investigations for EC usually follow abnormal uterine bleeding which is the most common symptom. Transvaginal ultrasounds are usually performed in postmenopausal women or those with high-risk factors, and if EC is suspected, a biopsy and histological confirmation are required. EC was historically characterised into two distinct subtypes according to clinical and endocrine features: type I (endometrioid, 80-90% of cases) and type II (non-endometrioid, 10-20% of cases) tumours. Type I ECs were characterized by low-grade, excess oestrogen exposure, positive hormone receptor status, and a generally favourable prognosis, while type II tumours were hormone-independent, and associated with higher mortality and rates of recurrence [8, 12, 13]. Nowadays, EC is classified by the following histologic subtypes: 1) endometrioid carcinoma, 2) serous carcinoma, 3) clear cell carcinoma, 4) uterine carcinosarcoma, 5) other: mucinous, neuroendocrine, undifferentiated, and dedifferentiated carcinomas. Endometrioid adenocarcinomas (EECs) are the most frequently identified subtype accounting for approximately 80% of EC cases and typically have a

favourable prognosis [14]. However, they can be heterogenous, varying from relatively slow growing and non-invasive to very aggressive tumours [9]. Accounting for <10% of ECs, serous carcinomas (SC) are the second most frequent EC. They are typically aggressive and are frequently associated with myometrial involvement and lymphovascular invasion [9]. Clear cell carcinomas (CCC) are a rare subgroup, accounting for <8% ECs and characterized by the clearing of tumour cell cytoplasm. CCC are patients have an increased chance of presenting with a higher FIGO stage than EEC, and thus are associated with a poorer prognosis [15]. Uterine carcinosarcoma (UCS) is a rare (<2% of ECs), aggressive tumour composed of a mix of malignant epithelial and mesenchymal/sarcomatous components [9, 16]. If EEC coexists in the presence of SC and CCC it is classified as a mixed carcinoma [9].

Once diagnosed, ECs are classified by tumour stage (**FIGURE 1.1)** followed by a widely used three-grade system created by FIGO (International Federation of Gynaecology and Obstetrics): low grade (1–2) vs high grade (3) [17]. Significant progress in understanding the molecular mechanisms that drive EC has been made, with a range of alterations identified in tumours important for determining prognosis [8]. In 2013, after analysing exome sequencing data, the Cancer Genome Atlas Research Network identified a molecular classification system for EC based on gene mutation pattern and frequency, copy number variation and microsatellite instability (MSI) status [18]. These molecular subgroups correlate with progression-free survival and include POLE (ultra-mutated) (7%), microsatellite instability (MSI)/hypermutated (28%), copy number low/microsatellite stable (39%), and serous-like/copy number high (26%) [19, 20]. The POLE ultra-mutated is characterised by somatic mutations in the DNA polymerase epsilon (POLE) exonuclease domain [9]. POLE mutations are usually associated with low and high-grade EEC and typically have a good prognosis. The microsatellite instability-high (MSI-h) subtype is characterised by mismatch repair (MMR) deficiency, which results in a hypermutated status [9]. Most MSI-h tumours are EEC [9]. The copy number (CN) low subgroup or microsatellite stable subgroup, accounts for the majority of the low-grade endometrioid tumours [9]. The CN high subgroup commonly harbours TP53 mutations and includes most of the SC and mixed-type carcinomas and carcinosarcomas [9]. This knowledge informed the classification of a less complex system which is widely used in clinical practice: 1) POLE-mutant, 2) microsatellite instable, 3) p53 abnormal, and 4) no specific molecular profile (NSMP) (**TABLE 1.1**) [9].

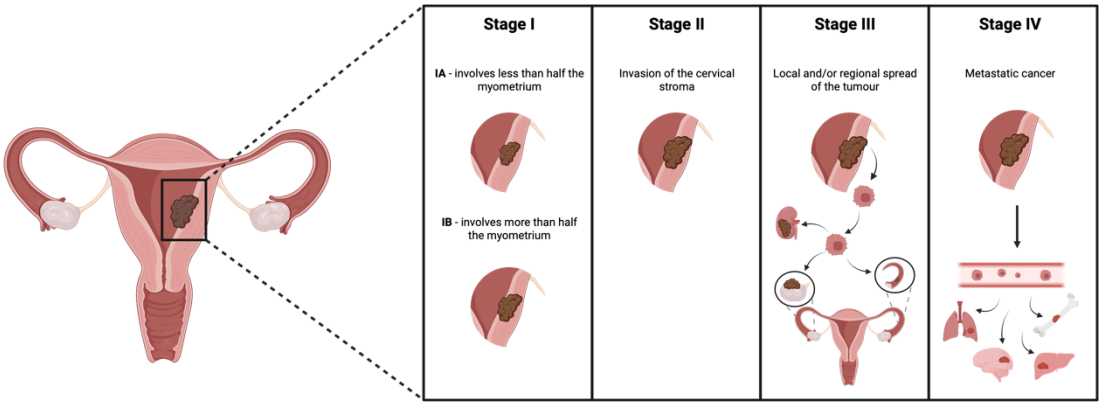

FIGURE 1.1. Federation of Gynaecology and Obstetrics (FIGO) endometrial cancer staging (2009). Stage I – tumour confined to the uterus; Stage II – tumour invades the cervical stroma; Stage III – local or regional spread of the tumour; Stage IV – extension to the bowel, bladder, or distant metastatic sites. *(Created with BioRender*, adapted from [21]).

EC Type	NSMP	MMR-deficient or MSI	POLE-mutated	P53 abnormal
Endometroid carcinoma G1-2	>50%	10-50%	<10%	<10%
Endometroid carcinoma G3	10-50%	10-50%	10-50%	10-50%
Serous carcinoma	<10%	<10%	0%	>50%
Clear cell carcinoma	>50%	<10%	<10%	10-50%
Uterine carcinosarcoma	<10%	10-50%	<10%	>50%

TABLE 1.1. Relationship between EC histotype and molecular classification. (Adapted from [9]).

1.1.2 Endometrial cancer treatment algorithm

Once diagnosed, ECs are surgically staged into risk groups (low to high) that factor in the likely risk of recurrence to identify those that could benefit from adjuvant therapy [9]. These risk groups (**TABLE 1.2**) take into consideration EC clinicopathological features including histological subtype, tumour differentiation grade, FIGO stage, age, depth of myometrial invasion and lymphovascular space invasion (LVSI), and may help to establish a recurrence risk group and to define resulting surgical management [9, 22]. Standard surgery in early-stage EC involves a hysterectomy with bilateral salpingo-oophorectomy without vaginal cuff resection [9]. The aim of the surgery is to remove macroscopic tumour, examine for microscopic metastases and stage the tumour to assess the need for adjuvant therapy. As previously discussed, molecular classification has been proposed to improve the evaluation of recurrence risk (**TABLE 1.2**) and is now incorporated into guidelines to aid decision-making regarding adjuvant treatment (**TABLE 1.3**) [23]. ESMO Clinical Practice Guidelines recommend that all EC pathology samples have histological type, FIGO grade, myometrial invasion and LVSI

(focal/substantial) defined, followed by molecular classification for p53 and MMR proteins (MLH1, PMS2, MSH2, MSH6), in combination with targeted tumour sequencing (POLE hotspot analysis) [9, 23].

Risk Group	NSMP
Low	• Stage I–II POLE-mutated EC, no residual disease • Stage IA MMR-deficient/NSMP endometrioid carcinoma G1-2, with no or focal LVSI
Intermediate	• Stage IB MMR-deficient/NSMP endometrioid carcinoma G1-2, with no or focal LVSI • Stage IA MMR-deficient/NSMP endometrioid carcinoma G3, with no or focal LVSI • Stage IA p53 abnormal without myometrial invasion • Stage IA non-endometrioid (serous, clear cell, undifferentiated carcinoma, carcinosarcoma, mixed) without myometrial invasion
High-intermediate	• Stage IB MMR-deficient/NSMP endometrioid carcinoma with LVSI • Stage IB MMR-deficient/NSMP endometrioid carcinoma G3 • Stage II MMRd/NSMP endometroid carcinoma
High	• Stage III–IVA MMR-deficient/NSMP endometrioid carcinoma with no residual disease • Stage I–IVA p53 abnormal endometrial carcinoma with myometrial invasion, with no residual disease • Stage I–IVA NSMP/MMR-deficient serous, undifferentiated carcinoma, carcinosarcoma, with myometrial invasion, with no residual disease
Advanced Metastatic	• Stage III–IVA with residual disease of any molecular type • Stage IVB regardless molecular type

TABLE 1.2. EC Prognostic risk groups. (Adapted from [9, 24]).

In low-risk EC, there is no indication for adjuvant therapy with several studies demonstrating that adjuvant treatment in low-risk EC does not improve survival chances as the risk of recurrence is low [23, 25-28]. Adjuvant vaginal brachytherapy (VBT) is recommended for all intermediate-risk EC patients except those with stage IA p-53 abnormal tumours without myometrial invasion as these patients were not included in the randomised trials [23] following the PORTEC-1 study which demonstrated that pelvic radiotherapy significantly reduced locoregional recurrence in this group [26]. PORTEC-2 evaluated the efficacy and toxicity of VBT compared with external beam radiotherapy (EBRT) as the majority of recurrences for those cases were in the vaginal vault, and both treatment arms demonstrated exceptional vaginal control rates (>96%), in addition to similar rates of isolated pelvic recurrence, distant metastasis and overall survival (OS) [29, 30]. High-intermediate risk EC is a group with a higher risk of recurrence; hence the potential benefit of chemotherapy has been evaluated in several trials [31, 32]. Pooled analysis of two studies (NSGO-EC-9501/EORTC-55991 and MaNGO ILIADE-III) combining radiation therapy and chemotherapy demonstrated a trend towards

improved overall survival (OS), though not significant (OS 16%), but improved cancer-specific survival (CSS) (CSS 11%) [33]. Another study found minor improvements in 5-year OS in patients with high-risk EC when receiving chemoradiation (OS 81.8%) vs. radiotherapy alone (OS 76.7%). However, more frequent adverse events were identified in patients receiving the combination with 60% experiencing ≥ Grade 3 adverse events, vs. 12% of patients who received radiotherapy alone [34]. More recently, GOG-249 analysed the effect of replacing pelvic RT for VBT on recurrence-free survival (RFS), followed by three cycles of paclitaxel and carboplatin in patients with high-intermediate-risk EC [35]. 5-year RFS and OS showed no differences between both arms, however, acute adverse events of grade ≥2 were found in 94% of patients receiving chemotherapy and VBT vs. 44% of those assigned to radiotherapy, leading to the conclusion that pelvic radiotherapy was the appropriate treatment of high-risk early-stage disease [36]. The PORTEC-3 trial provides further data to define better treatment approaches having assessed the impact of chemotherapy during and after radiotherapy vs. pelvic radiotherapy alone in patients with high-intermediate-risk and high-risk EC [34]. Though the results did not demonstrate a significant improvement in 5-year OS or failure-free survival (FFS), when analysing results by stage, small absolute improvements were observed in patients with stage I-II non-serous cancers receiving combined adjuvant treatment (i.e. 2% in 5-year OS and 4% in FFS) [34]. Consequently, the decision to combine treatment in early-stage EC should weigh the balance between adverse events and outcome benefits and be discussed on a case-by-case basis [23].

Results from PORTEC-3, GOG-249 and GOG-258 have led to a shift in the treatment paradigm for high-risk EC patients. PORTEC-3 demonstrated a 5% OS benefit and a 7% benefit in FFS in the concurrent plus adjuvant chemotherapy group, compared with radiotherapy alone [34]. In the subgroup analysis, women with stage III EC and serous histology obtained the greatest benefit from the combination. In the GOG-258 trial, no differences in RFS and OS were found in patients with stage III-IVA EC who received pelvic radiotherapy with concurrent and adjuvant chemotherapy or chemotherapy alone, however, significantly more vaginal and pelvic recurrences were seen in women treated with chemotherapy alone [37]. While chemoradiotherapy is the recommended regimen for high-risk patients, radiotherapy alone may be recommended in cases of major comorbidities and contraindications to chemotherapy [23]. Moreover, given the strong emerging prognostic value of the EC molecular classification, chemotherapy outcomes for each molecular subgroup were reported in PORTEC-3. This demonstrated that patients with p53-abnormal EC had the poorest prognosis regardless of histology, whereas POLE-mutated was the strongest favourable prognostic factor [34]. Patients with p53-abnormal EC had a highly significant benefit from chemotherapy regardless of the histological subtype and stage, whereas patients with POLE-mutated EC had excellent survival in both

treatment arms [23, 34]. MMR-deficient and NSMP EC patients had an intermediate outcome, however, no benefit was observed between chemoradiotherapy vs. radiotherapy alone in MMR-deficient patients, and a trend toward benefit from chemotherapy was observed in NSMP EC [38].

The treatment of recurrent or metastatic EC requires a multidisciplinary approach, however, 5-year survival outcome rates remain poor. Radiotherapy is the preferred treatment for patients who have not received prior irradiation, and with isolated vaginal or locoregional recurrence, however, the use of primary radiotherapy influences sites of recurrence and survival after relapse, and it has been demonstrated that survival is longer for patients with recurrent disease not previously treated with adjuvant radiotherapy [26, 39]. Complete debulking surgery is the only treatment option associated with an improved OS in women with recurrent disease who have received prior radiotherapy [40]. The role of chemotherapy after surgery is yet to be established, as there are a lack of studies addressing this treatment approach [23]. For relapsed disease not amenable to surgery and or radiotherapy, the standard approach remains chemotherapy or hormonal therapy. GOG-209 demonstrated paclitaxel-carboplatin was not inferior to the cisplatin-doxorubicin-paclitaxel efficacy-wise and was associated with a more favourable toxicity profile [41]. The combination of carboplatin-paclitaxel with the antiangiogenic agent bevacizumab failed to demonstrate a clear benefit in PFS and OS with respect to the standard of care [42]. Hormonal therapy has been accepted as first-line therapy for advanced EC, with progestins used as the standard of care. A recent analysis of progestins used as first-line therapy for metastatic or recurrent EC demonstrated an ORR of 23.3%, a median PFS of 2.9 months and a median OS of 9.2 months [43, 44]. Alternative options include tamoxifen, fulvestrant and aromatase inhibitors (AIs) [23].

Moreover, given approximately 30% of primary ECs are MSI-high or MMR-deficient indicating immune dysregulation, immune checkpoint blockade (ICB) therapy has been explored as a monotherapy and in combination with other anti-cancer agents including chemotherapy, other immunotherapies or targeted agents [45]. EC cells activate PD-1 signalling, which downregulates the immune response following the overexpression of PD-L1 and PD-L2 on the surface of tumour cells [46]. Immunotherapy augments the host immune system to generate an antitumor effect. Immune checkpoints are pathways with inhibitory or stimulatory features that maintain self-tolerance and assist with immune response [47]. Molecules that inhibit these pathways, and instigate the hosts immune system to target tumours, have been developed and have become the primary treatment for several cancers [47]. Immunohistochemical studies have identified PD-1 and PD-L1 expression levels, one of the most well-described checkpoints, (40%-80% in endometrioid, 10%-68% in serous, and 23%-69% in clear cell

subtypes, respectively) in ECs, the highest expression amongst gynaecologic cancers [24, 45]. Several anti-PD-1 and PD-L1 inhibitors have now been approved and show efficacy in MMR-deficient ECs. Pembrolizumab, an antibody targeting PD-1, has shown efficacy in a phase 2 trial including patients with MMR-deficient tumours, with 20% complete responses and 33% partial responses among EC patients [48-50]. Moreover, in a phase 1 trial of dostarlimab, another PD-1 targeting monoclonal antibody, the response rate was 42.3%, 12.7% had a complete response, and 29.6% had a partial response [51]. Other anti-PD-1/PD-L1 agents that have shown encouraging activity in MMR-deficient EC include avelumab and durvalumab [52, 53]. Additionally, immunotherapies are being investigated in combination with other approved anticancer therapies. A phase 3 study investigating pembrolizumab in combination with lenvatinib (a tyrosine kinase inhibitor) vs. standard-of-care therapy following platinum-based therapy in advanced EC (NCT03517449) led to the accelerated approval of this combination in the US, Australia, and Canada. The combination demonstrated statistically significant improvements in OS (18.3 vs. 11.4 months) and PFS (7.2 vs. 3.8 months), however, was associated with considerable toxicity vs. chemotherapy [54]. In addition, this combination is under investigation as first-line therapy vs. carboplatin and paclitaxel chemotherapy in advanced EC (NCT03884101). In the EU this combination is approved in adult patients ineligible for surgery or radiotherapy, with advanced or recurrent EC who have progressed on, or following prior treatment with a platinum-containing therapy in any setting, irrespective of MMR status [23]. More recently, results of the Ph3 KEYNOTE-868 (NCT03914612) study investigating the addition of pembrolizumab to standard chemotherapy resulted in significantly longer PFS than with chemotherapy alone in patients with advanced or recurrent EC. In the 12-month analysis, Kaplan-Meier estimates of PFS in the MMR-deficient cohort were 74% in the pembrolizumab group and 38% in the placebo group [55]. Results from the RUBY (NCT03981796) trial demonstrated that dostarlimab plus carboplatin-paclitaxel significantly increased PFS (36.1% vs. 18.1%) and OS (71.3% vs. 56.0%) among patients with primary advanced or recurrent EC, with a substantial benefit in the MMR-deficient MSI-h population [56]. Furthermore, targeted therapy approaches such as inhibition of cyclin-dependent kinases have demonstrated some success in advanced EC. Interim results of the ENGOT EN3 PALEO trial in previously treated EEC tumours that were ER-positive demonstrated that aromatase inhibitor letrozole in combination with palbociclib significantly improved PFS compared with letrozole plus placebo, median 8.3 vs. 3.0 months, respectively [57]. Moreover, WEE1 inhibitor adavosertib, reported 29.4% ORR and 38.2% clinical benefit in a population of 34 heavily pre-treated serous EC patients and warrants further investigations [58].

Until recently, women with recurrent or metastatic EC had few therapeutic options, however, as our understanding of the disease improves, molecular classifications have started to inform the treatment

algorithm, providing both new directions for clinical studies as well as new prognostic implications [59]. More importantly, the consensus that "one size does not fit all" for women with EC is gaining tract. Beyond molecular classifications, many women have comorbidities such as obesity or diabetes, or specific health needs related to age which can affect the tolerability of treatment [60]. Currently (as of 13/02/2023) there are 573 EC 'interventional' phase 1-3 clinical trials registered on CT.gov, and this number is expected to increase.

Risk Group	Treatment Recommendation
Low	• For patients with stage IA (G1 and G2) with endometrioid (MMR-deficient and NSMP) type and no or focal LVSI, adjuvant treatment is not recommended • For patients with stage IA non-endometrioid type (and/or p53 abnormal), without myometrial invasion and no or focal LVSI, adjuvant treatment is not recommended • For patients with stage I-II POLE-mutated cancers adjuvant treatment is not recommended • For patients with stage III POLE-mutated cancers, treatment within the scope of clinical trials is recommended but note adjuvant treatment is also an option
Intermediate	• For patients with stage IA G3 endometrioid (MMR-deficient and NSMP) type and no or focal LVSI, adjuvant VBT is recommended to decrease vaginal recurrence • For patients with stage IB G1-G2 endometrioid (MMR-deficient and NSMP) type and no or focal LVSI, adjuvant VBT is recommended to decrease vaginal recurrence • For patients with stage II G1 endometrioid cancer (MMR-deficient and NSMP) and no or focal LVSI, adjuvant VBT is recommended to decrease vaginal recurrence • Omission of adjuvant VBT can be considered (especially for patients aged <60 years) for all above stages, after patient counselling and with appropriate follow-up

High-intermediate	• For patients with stage IA and IB with substantial LVSI, stage IB G3, stage II G1 with substantial LVSI and stage II G2-G3 (MMR-deficient and NSMP):
	  ○ Adjuvant EBRT is recommended
	  ○ Adding (concomitant and/or sequential) chemotherapy to EBRT could be considered, especially for G3 and/or substantial LVSI
	  ○ Adjuvant VBT (instead of EBRT) could be recommended to decrease vaginal recurrence, especially for those without substantial LVSI
	  ○ With close follow-up, omission of any adjuvant treatment is an option following shared decision-making with the patient

High	• Adjuvant EBRT with concurrent and adjuvant chemotherapy is recommended • Sequential chemotherapy and radiotherapy can be used

	• Chemotherapy alone is an alternative option

Advanced Metastatic	• Hormonal therapy
	• Chemotherapy
	• MSI-high/ MMR-deficient:
	  ○ Re-challenge with platinum-based therapy
	  ○ Chemotherapy
	  ○ Immune-checkpoint blockade (dostarlimab or pembrolizumab-lenvatinib)
	• MSS/ MMR-proficient
	  ○ Re-challenge with platinum-based therapy
	  ○ Chemotherapy
	  ○ Pembrolizumab-lenvatinib

TABLE 1.3. EC treatment and management algorithms according to risk groups and for advanced/metastatic or recurrent disease. (Table adapted from [23]).

1.1.3 MMR loss in endometrial cancer

With the DNA MMR pathway predominantly functioning to maintain genomic stability during DNA replication, dysfunction leads to MSI which promotes cancer formation. Loss of MMR genes results in an accumulation of DNA replication errors in repetitive sequences (microsatellites) and eventually can be associated with genome-wide instability, predisposition to particular cancers, alongside resistance to many chemotherapeutic agents [61]. Disruption of genes involved in the MMR pathway in EC results in the loss of key MMR proteins, namely MLH1, PMS2, MSH2, or MSH6 [62]. The majority of ECs are sporadic (90%), while up to 5% are inherited cases such as Lynch syndrome [63].

1.1.4 MMR loss in hereditary endometrial cancer

All ECs are molecularly screened to assess for Lynch syndrome, also known as hereditary non-polyposis colorectal cancer (HNPCC). Lynch syndrome is an autosomal dominant familial cancer affecting approximately 1 in 400 people and can be caused by a mutation in any of the genes involved in MMR [64, 65]. Patients with Lynch syndrome are generally heterozygous for a pathogenic MMR gene variant; in order to develop a carcinoma for the respective cell type, a somatic inactivation of the second allele is required [66]. Women with EC are screened accordingly, as those with Lynch syndrome have up to a 60% chance of developing EC, and a 40-50% chance of developing it as the first clinical manifestation of the disease [67]. Given the clinical implication of diagnosing Lynch syndrome for the patient and family members, universal screening of EC for MMR deficiency has become standard-of-care. This testing is conducted in one of two ways: direct assessment for MSI, or indirect assessment reflected in the loss of MMR protein expression. Although these techniques are

sometimes used interchangeably, they are functionally evaluating different factors. MMR protein expression is typically assessed via immunohistochemistry (IHC), as it is sensitive, cheap, and easily accessible. This testing evaluates the loss of expression of any of the four most common mismatch repair proteins: MLH1, MSH2, MSH6, and PMS2 [68]. Loss of expression of any of those proteins on IHC suggests the possibility of a germline mutation in one of the genes associated with Lynch syndrome, though MLH1 loss is also commonly associated with epigenetic modification [69]. For this reason, MLH1 deficiency is usually followed by an assessment of MLH1 promoter methylation prior to germline sequencing. If methylation is not present, the likelihood that MLH1 loss is due to a germline mutation is much higher [70]. Testing MSI involves a polymerase chain reaction (PCR) test which evaluates for insertions and deletions of microsatellite repeats in five to seven DNA regions [71]. MSI testing categorizes tumours as having high microsatellite instability (MSI-high), low microsatellite instability (MSI-low), or being microsatellite stable (MSS) [70, 71]. An alternative approach is to measure MSI by next-generation sequencing, however, this is less widely available, more costly, and less sensitive than immunohistochemistry in the endometrium [67]. Moreover, measuring MSI for the detection of Lynch syndrome in women with EC is not necessarily helpful in the diagnosis as 15-25% of sporadic ECs also result in MSI [65, 72].

Lynch syndrome accounts for approximately 2-5% of all colorectal cancer (CRC) cases, is the most common presentation of hereditary CRC, [73-75]. Significant progress has been made to elucidate molecular pathogenesis, risks, genetic basis, and cancer prevention in Lynch syndrome-related CRC, however, recently, the focus has shifted to Lynch syndrome-related EC as women with Lynch syndrome have a 40-60% chance of presenting with EC as the first clinical manifestation [65, 76]. Among Lynch syndrome-related EC, the mutation rate of MMR genes shows a frequency in the MSH2 gene of 50-66%, in MLH1 of 24-40%, and in MSH6 of 10-13%, respectively [77]. The overall 5-year cumulative survival rate is approximately 88% for patients with Lynch syndrome-associated EC vs. 82% for patients with sporadic EC [68]. Lynch syndrome-associated EC is associated with a trend towards better RFS but a higher risk for second cancers compared with patients with MLH1-methylated EC, as demonstrated by a study by Post *et al*. [78]. In comparison, the OS of patients with Lynch syndrome-related CRC was approximately 90% at 5 years [79].

1.1.5 MMR loss in sporadic endometrial cancer

Sporadic EC can be caused by a somatic mutation in one of the four MMR genes, or by gene promoter methylation. Methylation is the main cause of sporadic tumours with MMR deficiency [66]. 62%-73% of sporadic MMR-deficient ECs arise from somatic hypermethylation of the MLH1 gene promoter region [66]. The relationship between MMR deficiency and outcomes in EC has not been fully

established, and there is no consensus regarding the impact of MMR abnormalities on patient outcomes in EC. In some cases, it has been reported that MMR deficiency in EC is a good prognostic indicator and is associated with increased OS and PFS compared to MMR-proficient patients [80-82]. Shikama *et al.* demonstrated that deficiency in MMR showed trends towards favourable OS compared with MMR-proficient ECs, a trend that was stronger in advanced-stage vs. early-stage disease [83]. Moreover, Mackay *et al.* demonstrated MSI tumours were more common in early-stage EC and these patients were associated with a worse prognosis [84]. Additionally, when evaluating the response rate of first-line chemotherapy in EC patients, Kato *et al.* demonstrated a higher response rate in MMR-deficient cases (67% vs. 44%). Moreover, MMR-deficient cases had significantly better progression-free and OS compared with MMR-proficient cases [85]. Consistent with these findings, Fountzilas *et al*. demonstrated MMR-deficient ECs were more likely to be low-grade (80% MMR-deficient vs. 69% for MMR-proficient) and favourably associated with OS in patients with nonmetastatic EC, but not in patients with nonmetastatic CRC who received adjuvant chemotherapy [86]. Interestingly, outcomes analysed by MMR status demonstrated that MSH2 deficiency was associated with better outcomes, whereas in CRC no association between MMR status and OS was identified [87].

On the contrary, several studies have noted an association between MMR defects and the presence of poor prognostic features in EC including higher tumour grade, presence of deep myometrial invasion, and lymphovascular invasion [88-93]. Some of these have found unfavourable or no differences between prognosis and survival outcomes in MMR-deficient and proficient endometrial tumours, however, not many have comprehensively discriminated between MMR-deficient ECs caused by somatic alterations from germline variations in MLH1, MSH2, MSH6, or PMS2. A study by Nagle *et al.* evaluating MMR status and EC risk demonstrated that among women with MMR-proficient and somatic MMR-deficient ECs, >70% had early-stage grade 1/2 endometrioid tumours, and women with germline MMR-deficient EC were more likely to have high-grade endometrioid or non-endometrioid tumours, and higher stage disease [87]. Moreover, analysis restricted to the endometrioid histologic subtype demonstrated a survival disadvantage for women with somatic MMR-deficient EC vs. MMR-proficient EC [87]. Consistent with these findings Black *et al*. have shown that MSI-high EC tumours were associated with early-stage tumours (92% v 81%) and worse prognosis [81]. Moreover, Garg *et al*. demonstrated MMR-deficient and Lynch syndrome ECs were distinct, with MMR-deficient ECs displaying worse prognostic factors, inferior 5-year survival and, possibly, worse clinical behaviour [88]. Loukovara *et al.* concluded that complete classification into molecular subgroups is required to appreciate the prognostic significance of MMR status in EC [94]. In this study, there was no association between EC-related survival and MMR deficiency when assessed solely by

MMR protein immunohistochemistry, however, when MMR-proficient ECs were defined as those lacking a specific molecular profile, MMR deficiency was associated with poor survival [94]. The current classification system includes copy-number high and POLE ultramutated subgroups (those associated with the respective poorest and best outcomes) in the MMR proficient category, and possibly explains the lack of consistent findings observed to date [94].

It is important to note that due to the respective nature of these studies, they have some limitations. More, current, and larger studies are required to further elucidate the role of MMR in EC and the use of MMR proteins as predictive and prognostic biomarkers in the disease given the mixed findings to date.

1.2 DNA Mismatch Repair Pathway

1.2.1 DNA damage

DNA is constantly challenged by endogenous and exogenous sources which can lead to genomic changes [95]. Endogenous sources of damage include replication stress, telomere shortening, reactive aldehydes, and reactive oxygen species (ROS) produced by cellular metabolism, whilst exogenous sources can consist of UV light, ionising radiation (IR) and various chemical agents such as alkylating agents. DNA damage can also occur due to aberrant DNA processing reactions, including DNA replication, recombination, and repair, which can result in nucleotide substitutions, insertions, deletions and changes in chromosomal copy number and structure [61]. If unrepaired, DNA damage can generate mutations in somatic or germline cells resulting in dysfunction and instigating disease [61]. A complex network of pathways has evolved to protect the integrity of the genome and collectively these are known as the DNA damage response (DDR). These are base excision repair (BER), nucleotide excision repair (NER), MMR, homologous recombination (HR) and non-homologous end joining (NHEJ) (**FIGURE 1.2**) [96]. More than 150 proteins are involved in the DDR and coordinate to stall the cell cycle and enable DNA repair [95]. As such, mutations in genes involved in many of these pathways have been associated with several cancers [97]. Loss of the DDR can result in a higher mutagenesis rate and an increase in genomic instability, which contributes to cancer promotion and progression [98-100]. A significant amount of ongoing research is aiming to understand and develop novel strategies to therapeutically target the DDR for treatment across various cancers.

The MMR pathway plays a key role in maintaining genomic stability, primarily repairing base-base mismatches and insertion/deletion loops (IDLs) which arise during DNA replication, in order to prevent these mutations from becoming permanent in dividing cells [61]. Though nucleotide insertion errors

can occur around 10^5 times during DNA replication [101], repair of these errors improves the overall fidelity of replication by up to a 1000-fold [102].

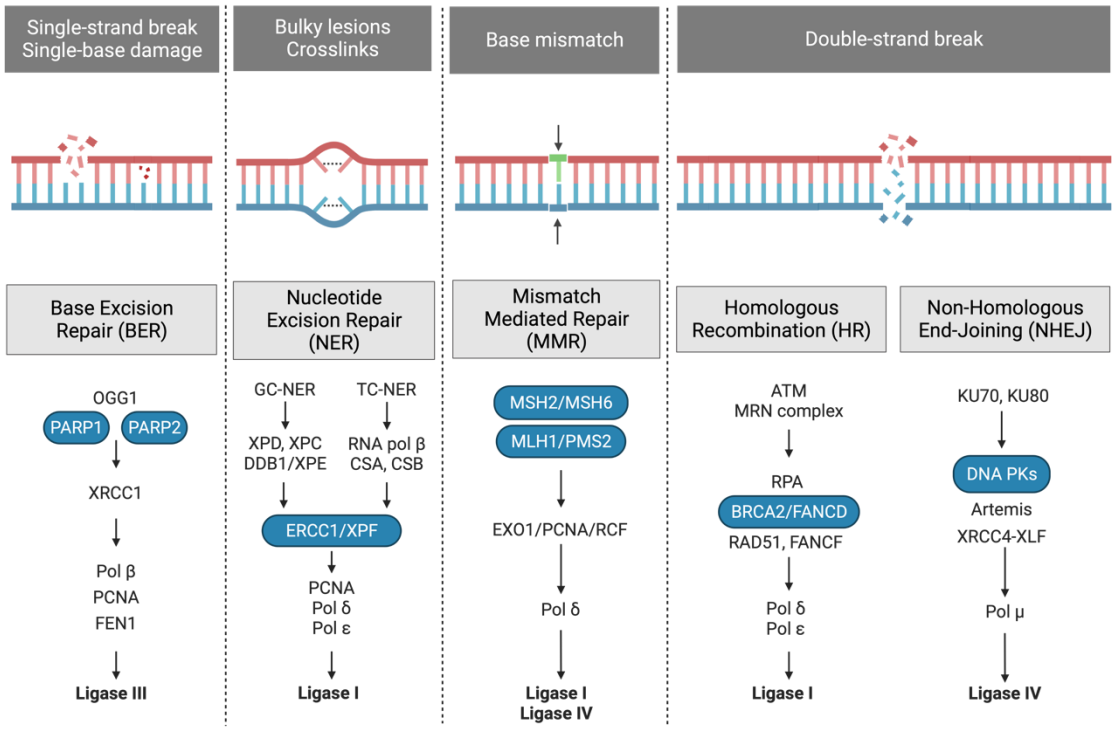

FIGURE 1.2. Different DNA repair pathways respond to different types of damage. At least five major DNA repair pathways: 1) base excision repair (BER), 2) nucleotide excision repair (NER), 3) mismatch repair (MMR), 4) homologous recombination (HR) and 5) non-homologous end joining (NHEJ)—are active throughout different stages of the cell cycle, enabling cells to repair DNA damage caused by varying sources [103]. *(Created with BioRender)*

1.2.2 Canonical MMR pathway in eukaryotes

MMR is highly conserved between eukaryotes and prokaryotes, though some differences have been identified [101]. Both mechanisms have three key steps: 1) recognition, 2) excision and 3) re-synthesis (**FIGURE 1.3**), as well as sharing similarities including substrate specificity, bi-directionality, and nick-directed strand specificity [61]. The human MMR pathway comprises seven genes; MLH1, MSH2, PMS2, MSH6, MSH3, PMS1 and MLH3. Several of these MMR proteins were identified based on their homology to *E. coli* MMR proteins [101]. MMR proteins form heterodimer complexes that interact with each other to coordinate DNA repair. Double helical distortions caused by the DNA mismatch are recognised by the MutS protein complex, which is a heterodimer comprised of MSH2 in combination with MSH6 (MutSα) or MSH3 (MutSβ), both of which are ATPases [61]. These two complexes have distinct roles in the recognition of DNA mismatches. MutSα is involved in recognising single base-base mismatches and small IDLs of 1-2 base pairs, whereas MutSβ recognises longer IDLs of up to 16

nucleotides long [104, 105]. The ratio of MutSα:MutSβ is around 10:1 [106]. The MutS heterodimer binds to DNA, forming a sliding clamp that can translocate along the DNA strand in search of a mismatch [101]. Once located, it undergoes an ATP-dependent conformational change, recruiting MutL. MutL is another heterodimer conserved across species, which is comprised of MLH1 in combination with either PMS2 (MutLα), PMS1 (MutLβ), or MLH3 (MutLγ) [102, 107]. MutLα is the most common and excises the lagging strand from the mismatch due to its endonuclease activity. MutLγ has a role in meiosis though the role of MutLβ remains unkown [61, 107]. MutLα has both ATPase activity and PCNA/replication factor C (RFC)-dependent endonuclease activity which is thought to be critical for 3' nick-directed MMR involving EXO1 [108]. The endonuclease capabilities of MutLα are activated upon interaction with proliferating cell nuclear antigen (PCNA) [101]. PCNA is a ring-shaped homotrimeric sliding clamp that interacting with both MLH1 and MSH2 to coordinate the DNA repair function of MMR [61, 109]. While PCNA is required during 3' nick-directed MMR, 5' nick-directed excision is independent of PCNA [110]. Subsequently, Exonuclease 1 (EXO1) nicks the DNA and excises nucleotides in a 5'-3' direction MMR from the incision site, in the presence of replication protein A (RPA) which stabilises the single-stranded DNA and prevents further degradation of the strand by inhibiting EXO1 [108]. EXO1 can also mediate 3' nick-directed repair, however, it requires the MutLα endonuclease, which is activated by PCNA and RFC [108]. DNA polymerase δ resynthesises the DNA, followed by ligation with DNA ligase I [111].

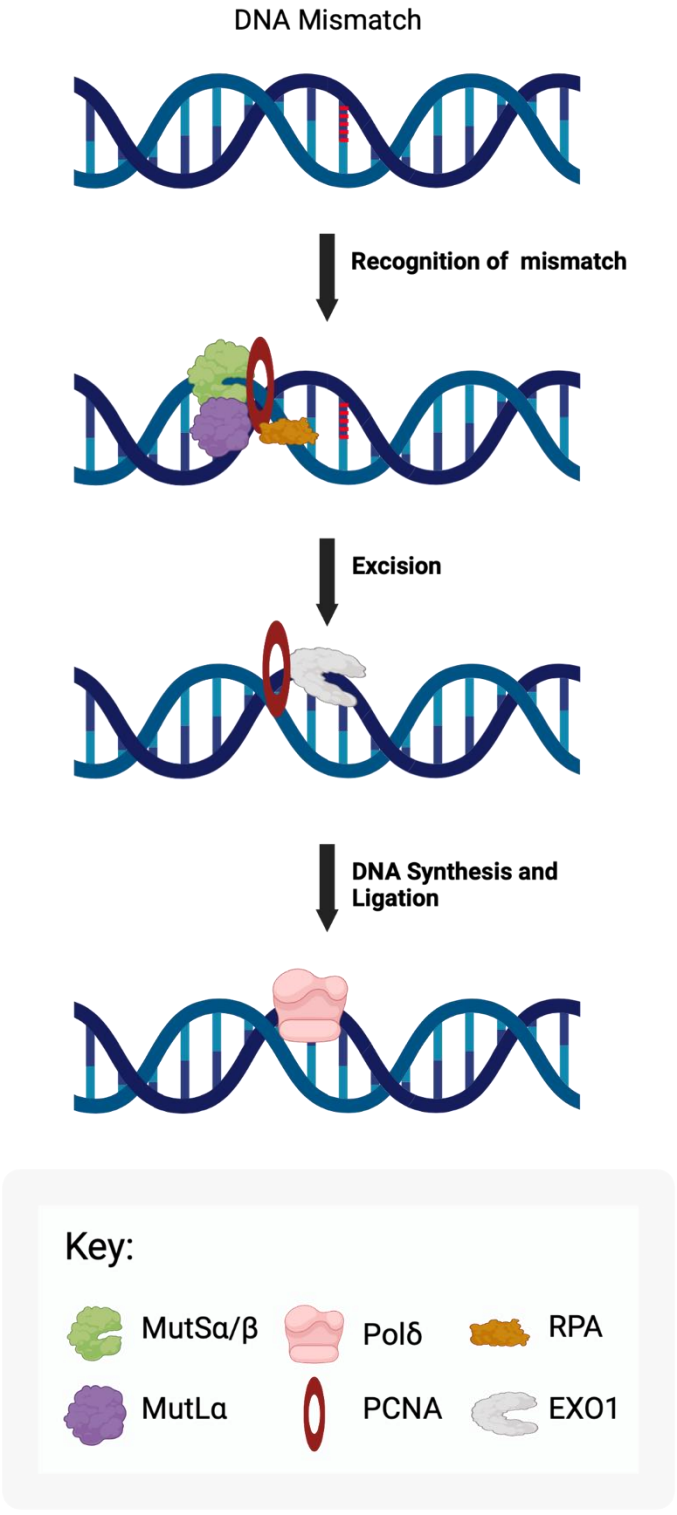

FIGURE 1.3. Schematic diagram of the eukaryotic DNA MMR pathway. MutS recognises base-base mismatches or insertion-deletion loops that arise during DNA replication. MutL interacts with the activated MutS homolog forming a ternary complex. This enables EXO1 and DNA polymerase to excise the mispaired bases and resynthesise DNA, respectively. PCNA interacts with MSH2 and MLH1, playing a role in initiation and DNA resynthesis. *(Created with BioRender)*

1.2.3 The role of MLH1 in the DNA MMR pathway

Several studies in both yeast and mammalian cell lines have described the essential function of MLH1 in the MMR pathway [112, 113]. Since the discovery of major human MMR genes, the clinical significance of mutations in these genes has been extensively studied [64]. According to the database maintained by the International Collaborative Group on Lynch syndrome, and current InSiGHT (International Society for Gastrointestinal Hereditary Tumours), >500 Lynch syndrome-associated MMR gene mutations have been identified, with mutations in MLH1 accounting for approximately 50% of these, mutations in MSH2 approximately 40%, and mutations in MSH6 approximately 10% [64]. Given MLH1 is the most important susceptibility gene in Lynch syndrome, a range of studies aiming to further characterise the structure of MLH1 and determine the functional significance of these mutations are ongoing [114, 115].

One of the most striking features of MLH1 is its ability to interact with a wide variety of proteins including DNA clamp PCNA, EXO1 in addition to various other factors involved in DNA damage response, as previously described [116]. The most important protein interaction in the pathway is the interaction of MutLα with MutSα which is dependent on ATP. MLH1 is predominantly responsible for this interaction due to its ATPase domain [117]. The N-terminal domain of MLH1 contains a GHKL class ATPase domain, while the C-terminus confers dimerization to PMS2, and the metal binding site essential for its endonucleolytic function (**FIGURE 1.4)** [108]. The binding and hydrolysis of ATP induce a conformational change in the MLH1 protein which in turn mediates the downstream events of the MMR pathway by controlling the binding and activation of the downstream repair factors MutS interacts with [118-121]. The resultant ATPase cycle, involving ATP binding, transient N-terminal dimerization, hydrolysis, subsequent separation of the N-termini and release of ADP, is thought to be a switch in the repair process [122]. It has been established that MLH1 mutations can abolish the interaction between MutS and MutL, eliminating MMR activity [121].

Furthermore, MutLα is an endonuclease that is required for MMR [108]. The endonuclease activity of MutLα introduces 5′ and 3′ nicks into the daughter strand of DNA in a manner that depends on MutSα or MutSβ, PCNA, RFC, ATP, a mismatch, and a DNA strand break [61, 108, 121]. Though MutLα is more commonly described in the literature, Kadyrova *et al.* more recently described the unique MutSβ-dependent endonuclease activity of human MutLγ which can initiate triplet repeat DNA expansions by incising loop-containing DNAs in the strand that does not have the loop [123]. After recognizing a small loop, MutSβ either acts alone to activate MutLγ or interacts with loaded PCNA to activate MutLα,. The activated MutLα or MutLγ incises the loop-containing DNA. The incision of the loop-

containing DNA by the activated MutLα endonuclease occurs in the loop-containing or loop-lacking strand. MutLγ only cleaves loop-containing DNA in the loop-lacking strand [121, 123]. Despite playing a minor role in MMR, MutLγ has been known to have an essential function in meiotic recombination [124, 125]. It has been established that MLH1 is required for MLH1 binding to meiotic chromosomes and localizes to meiotic chromosomes from the mid-pachynema stage of prophase I [125].

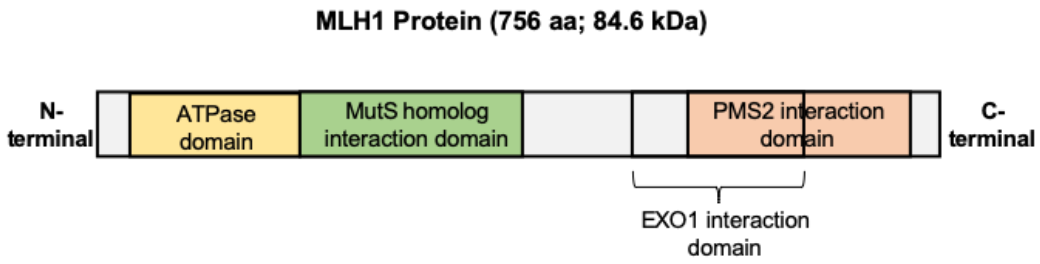

FIGURE 1.4. Schematic of MLH1 protein. MLH1 contains an ATPase domain and two interaction domains, MutS homolog interaction domain and PMS2 interaction domain. MLH1 forms a heterodimer with PMS2 (MutL). This heterodimer subsequently binds to MutS (MSH2-MSH6). The heterodimer formed by MLH1 recruits the proteins required for DNA repair to the site of the error [126].

1.2.4 Non-canonical roles of MMR genes

There is evidence for several non-canonical roles of the MMR pathway, in addition to its main function in the repair of DNA replication errors [107]. MMR plays a role in cell cycle arrest and/or programmed cell death in response to exogenous DNA damage by alkylating agents [127]. Functioning as lesion sensors, MMR proteins activate cell cycle checkpoints and signalling apoptosis by binding to DNA adducts activating a signalling cascade that results in the phosphorylation of p53 and/or p73, the functional homologue of p73 [127, 128].

Studies have also demonstrated that MMR proteins play a role in meiotic and mitotic recombination [129-133]. To carry out its function in meiotic recombination Allers *et al.* demonstrated that MLH1 and MLH3 interact with a MutS homologue, hMSH4/hMSH5, which has no identified role in the conventional MMR pathway, suggesting MMR directs meiotic DNA double-strand break repair towards a crossover pathway [134]. Lipkin *et al.* uncovered a role for MLH3 in mammalian meiosis and demonstrated that MLH3 is required for MLH1 binding to meiotic chromosomes [125]. In mitotic recombination, MMR proteins prevent strand exchange and recombination between divergent sequences though the mechanism is unclear [135]. MMR deficiency has been shown to result in increased recombination between homologous sequences [129-131].

Furthermore, MMR proteins are involved in chromatin assembly. Several studies have demonstrated that nucleosome loading in human cell extracts is delayed in the presence of a mismatch in nicked plasmid heteroduplex DNA and once removed, the single-strand gap is repaired, followed by nucleosome loading [136, 137]. The study also demonstrated that MSH6 interacts with the chromatin assembly factor, CAF-1 [137]. Kadyrova *et al.* demonstrated that MutSα suppresses CAF-I-dependent histone H3-H4 deposition in a mismatch-dependent manner, hypothesizing that there is active between MMR and replication-dependent nucleosome assembly during DNA replication error corrections [136].

While our understanding of the MMR pathway and its function in the repair of replication errors has improved, challenges remain. Improved understanding of the mechanisms of MMR could benefit by developing approaches to study the repair of mismatches that are made by the replication machinery and not induced exogenously. Given several studies have demonstrated loss of MMR functions decreases apoptosis, increases cell survival, and results in resistance to chemotherapy [138-140], understanding the mechanisms by which replication errors are repaired will provide important insights into the non-canonical roles of MMR proteins which are also biologically relevant and important to human health [107].

1.2.5 The role of MMR in the repair of oxidative DNA damage

Evidence has also suggested a role for MMR in the repair of oxidative DNA lesions which may be associated with carcinogenesis caused by an accumulation of oxidative DNA damage in the context of MMR deficiency [141, 142]. Cellular macromolecules are constantly exposed to potentially damaging reactive oxygen species (ROS), including free radicals with unpaired electrons, such as the superoxide anion (O2•−), the hydroxyl radical (•OH), and non-radical hydrogen peroxide (H_2O_2) [143, 144]. ROS can be generated during normal cellular metabolism, or by exogenous agents including UV exposure, ionising radiation, carcinogenic compounds, and redox-cycling drugs (**FIGURE 1.5**). During OXPHOS (described in section 1.3.1) electrons are continuously released in the form of O2•− predominantly from the complexes I and III. The majority of O2•− released by endogenous and exogenous means is converted into H_2O_2 by superoxide dismutases (SOD) and superoxide reductases [144]. H_2O_2 can modify proteins by reacting with thiol groups. In the context of DNA damage, hydroxyl radicals are the more pertinent oxidant species as they can react with both purine and pyrimidine bases and the sugar moiety of the DNA backbone [143]. Hydroxyl radicals form in the presence of copper or iron catalysts from H_2O_2 and O2•− via the Haber-Weiss and Fenton reactions [144]. These are damaging as there are no known enzymes or biological binding partners that can neutralise their activity [144]. Due to

the high electron density of DNA bases, the carbon-carbon double bonds are often sites of 'attack'. Addition reactions occurring at these sites generate radical intermediates of guanine, adenine, thymidine and cytosine which are then subjected to further oxidation and reduction reactions to generate a plethora of DNA lesions [143]. Given the mutagenic nature of oxidatively-induced DNA lesions and the high rate of oxidative DNA damage, approximately 10^5 lesions per cell per day, several DNA repair mechanisms have evolved to remove them [144].

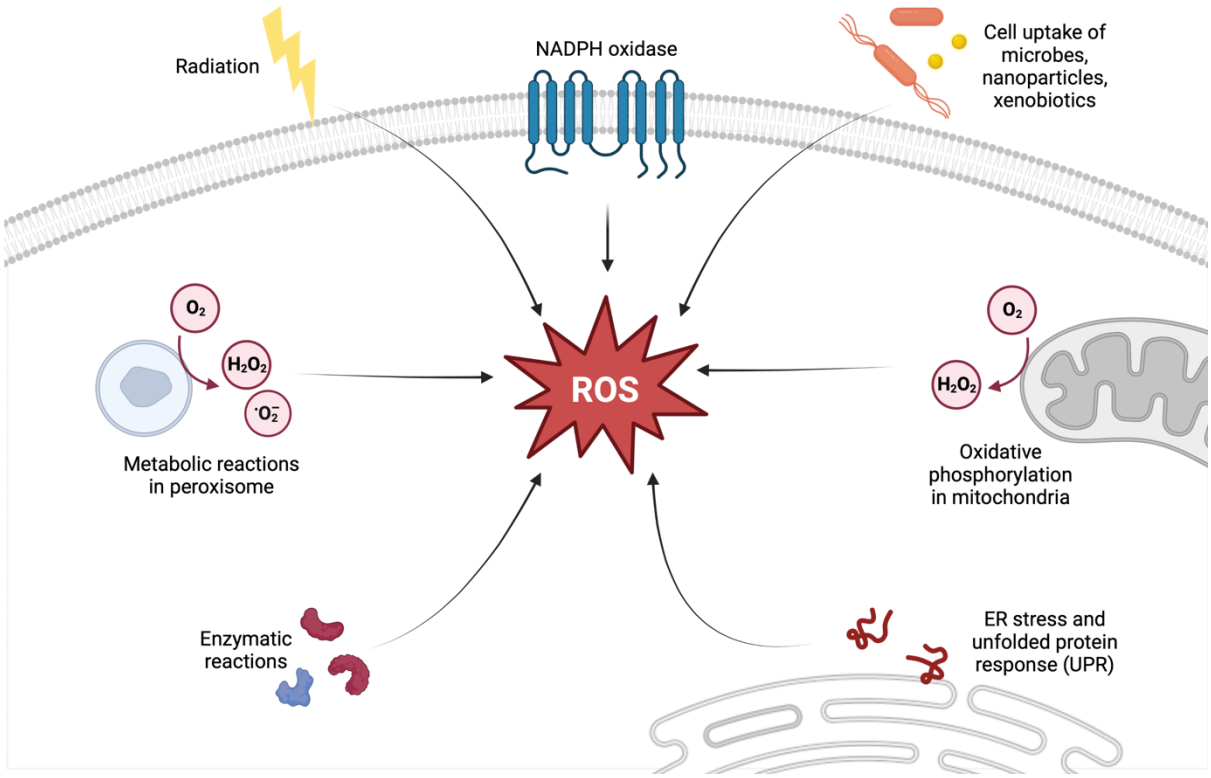

FIGURE 1.5. The main sources of ROS generation in normal and tumour cells. In normal and tumour cells ROS can be generated by many sources including ionizing radiation, oxidizing chemicals and enzymes, immune cells, and mitochondrial respiration. In cells, excessive ROS can result in oxidative stress which can cause harmful effects including DNA damage, lipid peroxidation, protein oxidation, and enzyme degradation. *(Created with BioRender)*

BER and NER are the main pathways that function to repair ROS-induced DNA damage, however, the MMR pathway has also been implicated in the response to oxidative DNA damage, particularly in the repair of 8-oxoG residues [145]. Our lab has demonstrated that inhibition of several mitochondrial genes, including POLG and PINK1, results in an accumulation of oxidative 8-oxoG lesions specifically in mitochondrial DNA (mtDNA) that can induce synthetic lethality in MLH1-deficient cells [146-150]. Additionally, we and others have identified the presence of MLH1, but not MSH2, in the mitochondria [146, 151, 152]. Moreover, several studies report less efficient repair of DNA lesions caused by oxidative damage upon MMR loss [147, 153-156]. DeWeese *et al*. demonstrated embryonic stem cells

and mouse embryo fibroblasts derived from mice deficient in MSH2 have higher levels of both basal and ROS-induced genomic 8-oxoG vs. the control [144, 157]. Furthermore, the role of the MMR's pathway in the repair of oxidative DNA damage is further evidenced by Mishra *et al.* who demonstrated loss of MMR was associated with an accumulation of mismatches in the non-coding D-loop in the mtDNA of retinal endothelial cells, which was associated with decreased respiration and increased apoptosis [151]. The observed phenotype could be rescued by the addition of MLH1, but not MSH2.

MMR proteins have distinct roles in the repair of oxidative DNA damage. Mazurek *et al*. demonstrated that 8-oxoG lesions lead to the activation of MutSα, but not MutSβ, and MutSα could bind different mismatches with differing affinities [145]. Moreover, MMR proteins have been implicated in the repair of clustered DNA lesions, a consequence of DNA damage following exposure to chronic oxidative stress [144]. These lesions can arise on single a single strand or bistrand, which are further classified into double-strand break (DSB) or non-DSB (single-strand breaks (SSBs)). Non-DSB clusters mostly contain oxidized base damage and are also known as bistranded oxidatively induced clustered lesions (OCDLs) and are highly mutagenic and difficult to repair. Several studies have elucidated the importance of MSH2 in the repair of OCDLs by demonstrating that MSH2-deficient cells were less able to facilitate the repair of these lesions [144, 158, 159]. For this pathway, MutSα is crucial for the interaction with the monoubiquitinated form of PCNA to recruit Polŋ and remove OCDLs [159]. Moreover, Barone *et al.* demonstrated MutSα can recognise 2-hydroxyadenine-containing structures supporting the hypothesis that the MMR pathway could play a role in the repair of frameshifts caused by oxidation of adenine within repetitive sequences [160]. *In vivo* studies to understand the relative contribution of MMR and BER to oxidative DNA damage repair and whether the pathways had overlapping roles, identified synergistic accumulation of 8-oxoG in several organs of MSH2 and MutY homolog (MUTYH)-deficient mice [161]. MUTYH is a DNA glycosylase of the BER pathway that removes 8-oxoG, thus the authors concluded that both MSH2 and MUTYH contribute significantly to the repair of oxidative DNA damage, though act independently of each other [144, 161].

1.2.6 MLH1-deficient endometrial cancers

Whilst a small proportion of MMR-deficient ECs are caused by germline mutations in one of the four mismatch repair genes, the majority result from the epigenetic loss of MLH1 [93, 162]. MLH1 plays a key role in the MMR pathway (as outlined in section 1.2.2), heterodimerising with PMS2 and recruiting proteins required for excision and repair synthesis. MLH1 contains an ATPase domain and two interaction domains to enable it to carry out its function (**FIGURE 1.4**). Though MMR proteins have

been extensively studied as predictive and prognostic biomarkers of EC, no consistent association with poor outcomes has been identified. Furthermore, the impact of MLH1 methylation status on prognosis and treatment response is yet to be elucidated. Studies have associated EC with MLH1 hypermethylation with reduced disease-specific survival and poor prognostic indicators, however, we do not know why this is the case and how this may impact treatment approaches and survival outcomes.

Pasanen *et al.* demonstrated reduced disease-specific survival and OS rates in MLH1-methylated MMR-deficient ECs vs. non-methylated MMR-deficient ECs (83.2% and 71.3% vs. 91.7% and 83.3%, respectively) [163]. Similarly, Cosgrove *et al.* reported that epigenetic MMR defects were associated with advanced stage, higher grade, presence of lymphovascular space invasion, and older age [93]. In this study, MMR class was significantly associated with tumour volume. Additionally, EEC cases with epigenetic MMR defects had significantly reduced recurrence-free survival and recurrence was more likely to recur compared to the MMR proficient group (47.7% vs 3.4%) among advanced stage (III/IV), despite receiving similar adjuvant therapy [93]. Shikama *et al*. reported poor overall survival in patients with sporadic EC compared with nonmethylated (presumed LS) MMR-deficient tumours [83]. In line with these studies, McMeekin *et al.* reported epigenetic and probable mutations in MMR were significantly associated with higher grade and more frequent lymphovascular space invasion [93, 164]. Though there were no differences in outcomes, PFS was worse in epigenetic MMR-deficient tumours compared with the MMR-proficient group. Moreover, exploratory analysis of the interaction between MMR status and adjuvant therapy indicated probably MMR-deficient ECs exhibited a trend toward improved PFS [93, 164].

Previously, our lab has highlighted the importance of MLH1 in the MMR pathway by demonstrating that silencing of the mitochondrial DNA polymerase POLG (involved in the repair of 8-oxoG DNA lesions in the mitochondria) is synthetically lethal with MLH1 deficiency due to an increase in oxidative DNA lesions in the mtDNA [146]. Interestingly, MSH2 deficient cells were not sensitive to POLG silencing but showed selectivity with depletion of the nuclear polymerase POLB, which was associated with an increase in nuclear 8-oxoG [165]. This phenotype is possibly explained by the fact that MLH1 is expressed in both the mitochondria and nucleus whereas MSH2 is only expressed in the nucleus [146]. Several other mitochondrial proteins that do not function in DNA repair, have also been found to be synthetically lethal with deficiencies in a range of MMR genes (MLH1, MSH2 and MSH6) as a result of nuclear and mitochondrial oxidative DNA damage [150]. Furthermore, our group demonstrated that MSH2-deficient cell lines *in vitro* and *in vivo* are selectively lethal to treatment with

the oxidative damage-inducing agent, methotrexate, findings that led to further clinical investigations in CRC [147]. It is evident that MMR protein expression and MLH1 methylation profiles define distinctive phenotypes that likely correlate with prognostic factors of EC, however, further research is required to determine the prognostic value of these classes and whether they will inform treatment choices [163]. There is a need to elucidate the mechanism underpinning this more aggressive phenotype in MLH1-deficient ECs, which may offer more targets, lead to more personalised therapies, and ultimately prolong survival.

1.3 The Mitochondria

Mitochondria are ubiquitous organelles found in all nucleated mammalian cells. They play a vital role in bioenergetic and biosynthetic pathways, rapidly adjusting to meet the metabolic requirements of the cell. Mitochondria house the machinery for generating ATP and other metabolites which are important for numerous cellular functions. Additionally, they play a role in iron-sulphur cluster biogenesis, haem production and calcium regulation to name a few (**FIGURE 1.6**) [166].

The mitochondrial genome is maternally inherited and is present in multiple copies within a cell, varying based on the metabolic requirements of the cell and on tissue type [167, 168]. Mitochondria possess their own circular genomic material (mtDNA) which is small and only encodes 37 genes. Most of these genes (13) function to produce components of the OXPHOS pathway. The other proteins required for OXPHOS function come from nuclear-encoded gene products [169]. mtDNA is subject to the same DNA lesions as the nuclear genome, however, does not code for the genes involved in DNA maintenance and repair. Most mitochondrial proteins are in fact nuclear-encoded, thus mito-nuclear cross-talk is important and synthesis must be well coordinated to enable the translocation of these elements to within [170].

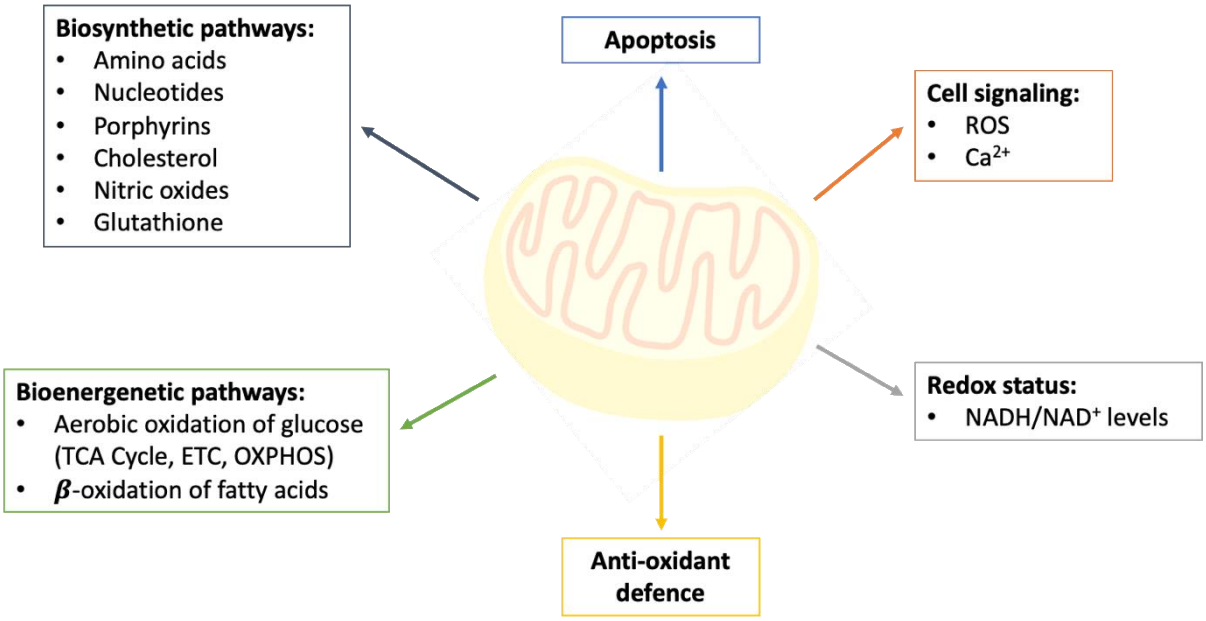

FIGURE 1.6. Mitochondrial involvement in fundamental cellular pathways and processes. Mitochondria play a vital role in bioenergetic and biosynthetic pathways, antioxidant defence, redox sensing, and cell signalling. Figure adapted from [171].

1.3.1 Oxidative phosphorylation

One of the main functions of mitochondria is to produce ATP through OXPHOS (**FIGURE 1.7**). OXPHOS occurs in the inner mitochondrial membrane and requires five membrane-bound enzyme complexes to carry out its function: Complex I (NADH-ubiquinone oxidoreductase, CI), Complex II (succinate-quinone oxidoreductase, CII), Complex III (cytochrome bc1, CIII), Complex IV (cytochrome c oxidase, CIV) and Complex V (F1FO-ATP synthase, CV), as well as two electron mobile carriers coenzyme Q and cytochrome C. The majority of the OXPHOS complex subunits are encoded by nuclear DNA (approximately 70 subunits), with the remainder (only 17) encoded by mtDNA [172]. The system functions to generate ATP using the electrons from $NADH_2$ and $FADH_2$ produced during glycolysis, fatty acid oxidation, and the TCA cycle. Glycolysis and the citric acid cycle generates approximately 4 molecules of ATP, while the OXPHOS system generates the remaining 32–34 ATP molecules (discussed further in section 1.4.1). Initially, electrons from NADH enter CI and are then transferred to CIII via flavin mononucleotide and the electron carrier coenzyme Q [173]. Subsequently, the electrons are transferred from cytochrome b to cytochrome c, within CIII, and finally to CIV. CIV transfers the electrons to O_2 which in turn is reduced to form H_2O. CII accepts electrons from $FADH_2$ as opposed to NADH, and these are also transferred to O_2 via coenzyme Q, CIII and CIV [173]. The series of redox reactions that occur as electrons progress through the chain, lead to the formation of an electrochemical gradient caused by the simultaneous pumping of protons from the mitochondrial matrix. This proton gradient powers the synthesis of ATP via ATP synthase [173]. The transferring of

protons is proposed to occur directly through the protonation and de-protonation of redox intermediates (CIII and CIV) or indirectly through the conformational change of the complexes (CI and CIV). It is estimated that per 1 oxidised NADH molecule, approximately 10 protons are transported from the mitochondrial matrix to the inner membrane space [174].

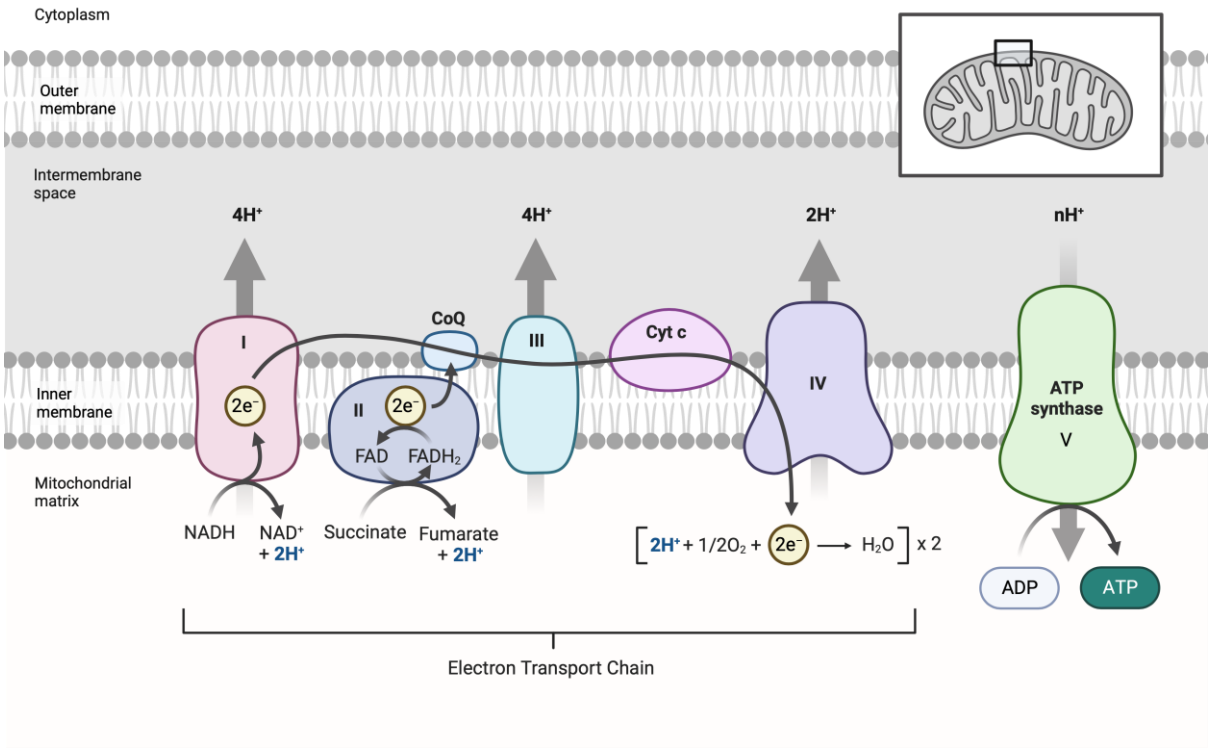

FIGURE 1.7. Oxidative Phosphorylation. This image depicts the process of oxidative phosphorylation (OXPHOS) via the electron transport chain (ETC), which is composed of five membrane-bound complexes: Complex 1 (NADH–ubiquinone oxidoreductase), Complex II (succinate- quinone oxidoreductase), Complex III (cytochrome bc1), Complex IV (cytochrome c oxidase), Complex V (F1FO-ATP synthase) [174]. *(Created with BioRender.com)*

1.3.2 Complex I and antioxidant system

Our lab has previously shown that inhibition of a number of mitochondrial genes, including *POLG* and *PINK1* and induction of oxidative stress can induce synthetic lethality in MLH1-deficient cells [146-150]. More recently, the lab has identified that loss of MLH1 results in a mitochondrial phenotype, characterised by reduced OXPHOS as determined by the basal oxygen consumption rate (OCR), and reduced spare respiratory capacity (**FIGURE 1.8 A-C**; [175]). No significant difference was observed upon MLH1 loss on glycolysis as determined by analysing the extracellular acidification rate (ECAR) of the surrounding media (**FIGURE 1.8 D**). Furthermore, MLH1-deficient HCT116 cells display a significant reduction in the activity of respiratory chain Complex I (**FIGURE 1.9 A&B**) and reduced mtDNA copy number (**FIGURE 1.9 C**). As a functional consequence of this perturbed mitochondrial metabolism,

MLH1-deficient cells have a reduced antioxidant response (**FIGURE 4D**) and show increased induction of ROS (**FIGURE 4E**) [175].

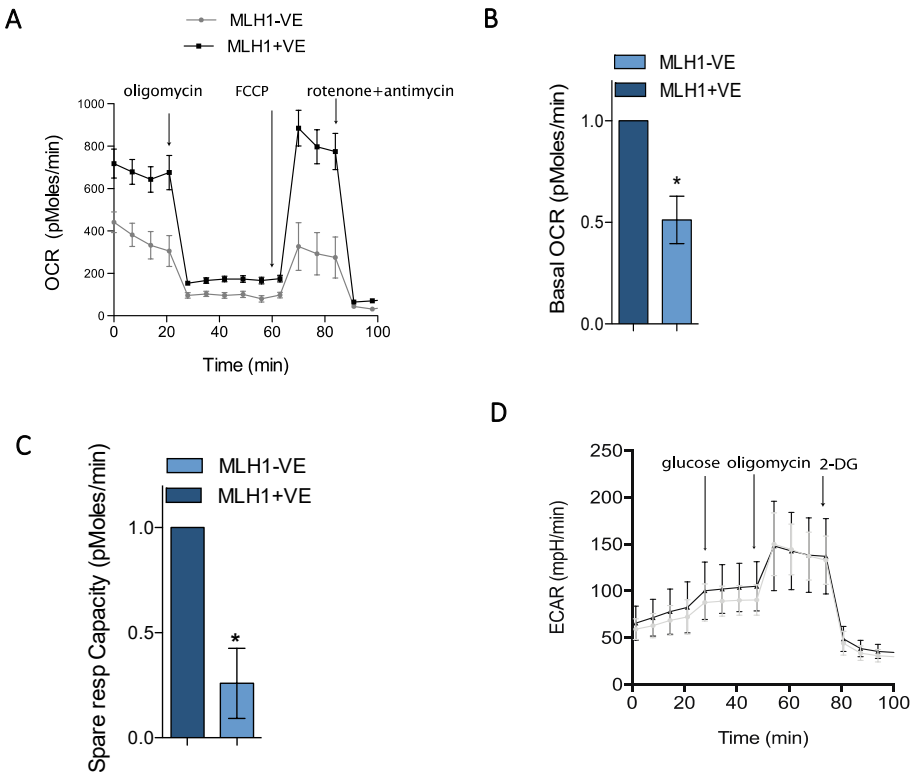

FIGURE 1.8. MLH1 loss leads to deregulated mitochondrial metabolism. The Seahorse Bioscience XF24 extracellular flux analyzer was used to measure OCR (pMoles/min), indicative of oxidative phosphorylation (OXPHOS) in the MLH1-deficient and the MLH1-proficient HCT116 cell lines. (**A**) After establishing a baseline, oligomycin (1 µM), FCCP (0.25 µM), rotenone (1 µM) and antimycin (1 µM) were sequentially added, as indicated by arrows. (**B**) The basal OCR was calculated using the difference between the mean of time points in baseline and in oligomycin treatment (baseline minus oligomycin OCR). (**C**) The spare respiratory capacity was calculated as (OCR following FCCP – baseline OCR). **(D)** EACR, indicative of glycolysis was measured of the surrounding media, by measuring the excretion of lactic acid per unit time after its conversion from pyruvate. All experiments were carried out in triplicate and error bars represent the SEM. *p<0.05. (Rashid *et al.* [175])

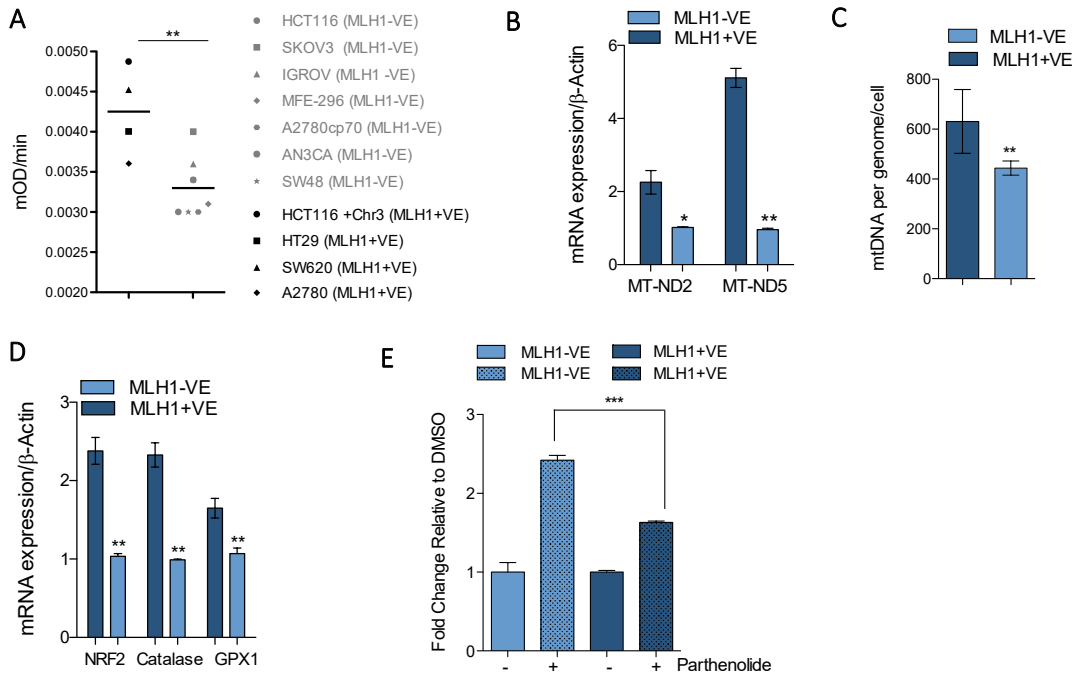

FIGURE 1.9. MLH1 loss leads to decreased Complex I and mtDNA copy number, resulting in a reduced antioxidant response. (**A**) Complex I activity was measured using an ELISA assay. Protein lysates were isolated from a panel of MLH1-ve and MLH1+ve cell lines, as indicated. Equal amounts of protein were incubated to determine the activity of Complex I by measuring the oxidation of NADH to NAD^+ and the simultaneous reduction of a dye leading to increased absorbance at 450 nm, over time. (**B**) Quantitative RT-PCR analysis of RNA extracted from ISHIKAWA EC cells (MLH1-ve) and ISHIKAWA+MLH1 (MLH1+ve) cells. mRNA expression was measured using Taqman probes against the mitochondrial-encoded Complex I subunits MT-ND2 and MT-ND5. β-actin was used as a control. (**C**) Reduced mtDNA copy number in MLH1-deficient cells by determining the ratio of the mitochondrial *tRNA* gene, relative to the nuclear housekeeping gene, *β2M.* Relative mtDNA copy number is expressed as a ratio of total genomic DNA. (**D**) Quantitative RT-PCR analysis of RNA extracted from ISHIKAWA EC cells (MLH1-ve) and ISHIKAWA+MLH1 EC (MLH1+ve) cells. mRNA expression was measured for the antioxidant response genes, NRF2, Catalase and GPX1 using Taqman probes. β-actin was used as a control. (**E**) Increased ROS levels in MLH1-deficient cells upon Parthenolide treatment. The MLH1-deficient ISHIKAWA and the MLH1-proficient ISHIKAWA+MLH1 cell line were treated with either DMSO or Parthenolide (1µM) for 30 min. Cells were washed and treated with 10 µM DHE, and fluorescence was measured on the MitoXpress fluorescent microscope as a measure of ROS production. All experiments were carried out in triplicate and error bars represent the SEM. *p<0.05, **p<0.005, ***p<0.0005. (Rashid *et al.* [175])

Complex I is the first enzyme of the respiratory chain and enables the transfer of 2 electrons from NADH produced by the TCA cycle to ubiquinone, coupling this to the translocation of 4 protons across the inner membrane [176]. With a molecular mass of about 1 MDa, it is the largest and most complicated multi-subunit complex in the respiratory chain. It is formed of 45 subunits, 14 core subunits (**TABLE 1.4**) that are essential to its enzymatic function, and 31 accessory subunits, 25 of which are required for structural assembly and 1 essential for cell viability [177, 178].

The structure of Complex I was solved first using electron microscopy for the *Neurospora crassa* enzyme from a detergent-solubilized preparation on two-dimensional crystals, which uncovered that it has an L-shaped architecture and is located within the mitochondrial inner membrane [179]. The hydrophobic membrane arm contains all the mtDNA-encoded subunits and is embedded in the inner mitochondrial membrane, while the hydrophilic peripheral arm protrudes into the matrix [176]. Complex I can also be divided into three modules based on function: the NADH-oxidising dehydrogenase module (N module) which is connected to the Q module, and finally the proton translocation module (P module). The N nodule accepts electrons and feeds them into a chain of iron-sulphur clusters via its NADH oxidation site with a flavin mononucleotide molecule. In the Q module electrons from the N module are passed to its ubiquinone reduction site. The P module exists in membrane arm which is responsible for the translocation of protons. Electron transfer and proton translocation are spatially separated within Complex I [180, 181].

Module	Subunit Name	Mitochondrial or Nuclear Encoded
N-module	NDUFS1	Nuclear
	NDUV1	Nuclear
	NDUFV2	Nuclear
Q-module	NDUFS2	Nuclear
	NDUFS3	Nuclear
	NDUFS7	Nuclear
	NDUFS8	Nuclear
P-module	ND1	Mitochondrial
	ND2	Mitochondrial
	ND3	Mitochondrial
	ND4	Mitochondrial
	ND4L	Mitochondrial
	ND5	Mitochondrial
	ND6	Mitochondrial

TABLE 1.4. Mitochondrial Complex I core subunits. Adapted from [176].

1.3.3 Complex I dysfunction in cancer

Defects in mtDNA lead to debilitating metabolic disorders, often with no effective treatments. mtDNA mutations have been associated with neuromuscular and neurodegenerative mitochondriopathies, as well as complex diseases such as diabetes, cardiovascular diseases, gastrointestinal disorders, skin disorders, ageing and cancer [171]. mtDNA is one of the most mutated regions of the cancer genome, with somatic mutations present in approximately 50% of all tumours [182]. Cancer cells accumulate defects in the mitochondrial genome, including the small repertoire of protein-coding genes, non-protein-coding tRNAs and rRNAs, and non-coding DNA that are essential for OXPHOS [171]. These can lead to deficient mitochondrial respiration and increased ROS production, which makes mtDNA more vulnerable to oxidative injury and likely accounts for some of the increased mtDNA mutations observed in cancer [176]. Complex I deficiency caused by mutations in genes encoding its subunits and assembly factors has been associated with mitochondrial dysfunction and various human diseases over the last two decades [176].

The most common mtDNA mutations affect the translation of respiratory subunits, resulting in impaired OXPHOS [171]. Out of all respiratory chain defects, complex I deficiency is the most common [181]. Complex I contributes significantly to the formation of mitochondrial ROS; thus, its dysfunction has been linked to several hereditary and degenerative diseases including neurodegenerative diseases, diabetes, and cancer [181]. It has been established that mutations within the core subunits, both mitochondrial and nuclear, can lead to Complex I deficiency alongside a heterogeneous group of clinical manifestations related to defects in energy metabolism [183]. Although the role of the accessory complexes is unclear, mutations in genes such as NDUFB8 [184], NDUFB10 [185], NDUFA2 [186] and NDUFA10 [187] correspond with a decrease in Complex I function have also been identified [176]. The role of Complex I deficiency in cancer has been debated, however. Several studies have suggested that Complex I subunits are tumour suppressors [188-190]. Moreover, several studies have demonstrated Complex I gene mutations are linked to cancer progression in a range of cancers including prostate, thyroid, breast, lung, renal, colorectal, and head and neck tumours [191-200].

Nonetheless, given its pivotal role in OXPHOS and ATP synthesis, it is unsurprising that Complex I supports cancer cell proliferation. More recently, however, evidence suggests that non-energetic roles of mitochondrial respiration, and specifically Complex I activity, support proliferation by providing electron acceptors and regenerating oxidized cofactors [201, 202]. Cellular NAD^+ pool and the NAD^+/NADH ratio are maintained by Complex I activity which is necessary to sustain mitochondrial malate dehydrogenase (MDH2) enzyme activity, and aspartate generation [201, 202]. Numerous

studies have demonstrated that the inhibition of ETC activity using Complex I inhibitors (metformin, rotenone, and piericidin) affects the NAD+/NADH balance, resulting in a decrease in electron acceptors and limiting aspartate synthesis. Aspartate is a precursor of purine and pyrimidine synthesis which is required for the biosynthesis of nucleic acids and macromolecules during cell proliferation [191, 201, 202]. Moreover, maintenance of the NAD^+/NADH ratio by Complex I is important for the induction of adaptive mechanisms to hypoxia and to promote a metabolic remodelling toward aerobic glycolysis [189, 203, 204]. NADH accumulation as a result of Complex I inhibition allosterically inhibits α-ketoglutarate (αKG) dehydrogenase, a member of the TCA cycle. This increases the αKG/succinate ratio, favouring the activity of the prolyl-hydroxylases which control the degradation of HIF1α, and tumour growth arrest [189, 191]. Moreover, mutations in mtDNA-encoded Complex I core subunits that result in OXPHOS defects have pro-tumorigenic effects [191, 205]. For instance, cancer cells with mutations in *ND4* and *ND6* have a mild decrease in OXPHOS function that promotes tumour growth when injected in nude mice [206]. Furthermore, *ND6* mutations which result in deficient Complex I activity and high ROS generation, increase the metastatic potential of cells, a characteristic that is suppressed by ROS scavengers [207]. Moreover, lack of OXPHOS caused by an absence of functional Complex I in osteosarcoma cells induces an imbalance of the αKG/succinate ratio, destabilizing HIF1α and reducing the ability of these cells to grow in an anchorage-independent fashion, consequently forming tumours *in vivo* [188].

Complex I also plays a role in metastasis. Both *in vitro* and *in vivo* studies have demonstrated that the downregulation of certain Complex I subunits, such as NDUFB9 and MTND6, genetically or pharmacologically, increases the migratory and metastatic potential of cancer cells [190, 207, 208]. For instance, the downregulation of NDUFA13 and NDUFS3 subunits in HeLa cells promotes the loss of epithelial morphology and acquisition of mesenchymal properties, a key event for the development of metastasis known as epithelial-mesenchymal transition (EMT) [191, 209, 210]. During EMT, secretion of fibronectin and increased expression of its receptor integrin α5, N-cadherin, and vimentin results in a high cell-matrix adhesion which promotes migration and invasion. These events are accompanied by an increase in ROS generation and can be reversed with the presence of ROS scavenger N-acetyl cysteine (NAC) [191, 210, 211]. Similarly, highly invasive breast cancer cells have been associated with reduced levels of NDUFA13, NDUFS3, and accessory subunit NDUFB9 [211, 212]. Moreover, highly metastatic breast cancer cells have reduced expression of nuclear-encoded NDUFB9 subunit, with knockdown of this subunit generating high levels of mitochondrial ROS and a decrease in NAD^+/NADH ratio [190, 191]. Given mtDNA mutations are an early event during breast tumorigenesis and produce defective OXPHOS with a metabolic shift toward glycolysis, it has been

hypothesised that this could be used as a potential biomarker for early detection and prognosis [213]. Conflicting observations, however, imply Complex I's role in tumourigenesis may be cancer cell-specific and is likely influenced by the level of Complex I inhibition. For instance, lung adenocarcinoma patient data associated an elevated expression of OXPHOS-encoding genes with poor prognosis. This study demonstrated that cisplatin-resistant lung cancer cells exhibited high Complex I activity, elevated mitochondrial transmembrane potential, high ATP content, and increased migration and invasion compared with parental cells [191, 214].

Ultimately, there is still more to be learnt about the tumourigenic role of Complex I subunits. Increasing evidence suggests changes in the expression of, or mutations in nuclear and mitochondrial genes encoding Complex I subunits are pro-tumourigenic [191]. Targeting mitochondrial metabolism is a promising anticancer strategy, however, new molecules need to be discovered.

1.4 Metabolic Rewiring in Cancer

Cancer is widely accepted as a 'metabolic disease', influenced by complex interactions between tumours and their microenvironments. Proliferating cells rewire their metabolism to generate macromolecules such as proteins, lipids, and nucleic acids, which are required for cellular growth and division [215, 216]. An adequate nutrient supply, i.e., carbohydrates, amino acids, and fatty acids, is essential for the execution of metabolic reactions. These nutrients can be supplied by diet and, once resorbed in the gut, are transported in the blood to sites of consumption where they are taken up by the cells through specific transporters [217]. Furthermore, cells rely on sufficient oxygen supply. The vascular system sustains nutrient and oxygen supply under normal conditions; however, tumours can outgrow the vasculature resulting in inefficient nutrient supply and hypoxic areas. The knowledge that healthy cells and cancer cells utilise distinct energy-generating pathways, could serve as a potential therapeutic target [217]. Identifying the unique metabolic dependencies of specific cancer cells may enable the non-invasive recognition of tumours, making it possible to directly target their essential pathways to prevent tumour progression [218].

1.4.1 Glycolysis provides precursors for anabolic processes

In non-cancerous cells with adequate oxygen supply, the tricarboxylic acid (TCA) cycle, associated with OXPHOS via the ETC in the mitochondria, is the main site of ATP generation. In the 1920s Otto Warburg identified that cancer cells exhibited high glucose consumption rates concurrent with high lactate secretion rates, even in the presence of functioning mitochondria, a sign of a high glycolytic flux [217]. A high rate of glycolysis is advantageous for the growth and survival of cancer cells as it generates ATP

at a faster rate than OXPHOS [219] and is a source of intermediates for other biosynthetic pathways. This phenomenon has become known as the Warburg effect.

Glycolysis takes place in the cytoplasm and is the multi-step conversion of glucose to pyruvate in the presence of oxygen (aerobic glycolysis) or lactate in the absence of oxygen (anaerobic glycolysis). During aerobic glycolysis pyruvate derived from glucose will enter the mitochondria to undergo oxidative phosphorylation, whereas in anaerobic conditions pyruvate will be converted to lactate by the enzyme lactate dehydrogenase. Via the mitochondrial TCA cycle and OXPHOS, the conversion of a single glucose molecule to CO_2 yields ~36 ATP molecules (corresponding to 2 ATP, 8 NADH, 2 $FADH_2$), whereas, the net yield from glycolysis for a glucose molecule is only 2 ATP and 2 NADH molecules (**FIGURE 1.10**) [220].

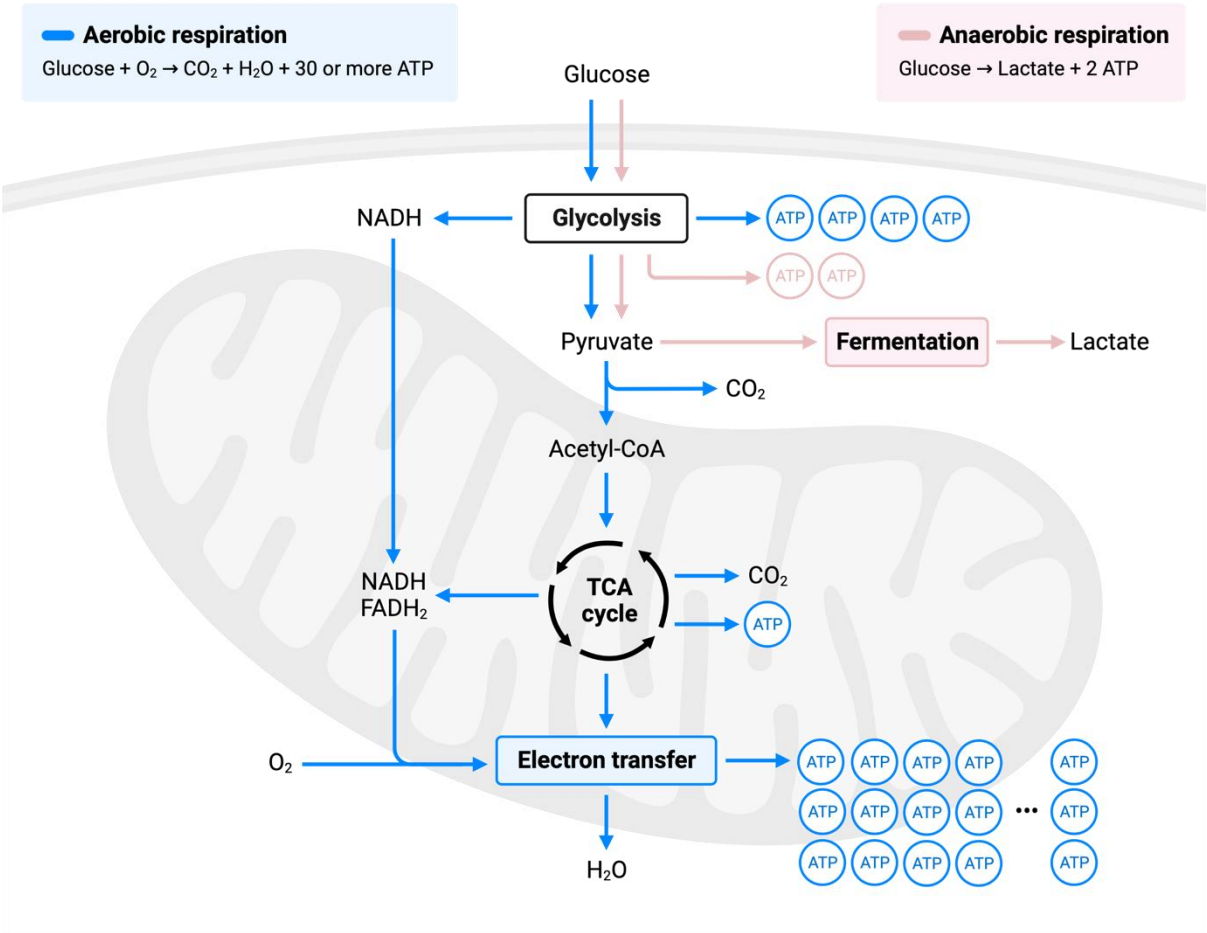

FIGURE 1.10. Anaerobic and Aerobic Glycolysis. Under aerobic conditions, pyruvate enters the TCA cycle and undergoes OXPHOS which produces 32 ATP molecules. Under anaerobic conditions, pyruvate is converted to lactate through anaerobic glycolysis, leading to the production of only 2 ATP molecules. *(Created with BioRender)*

The multistep pathway was elucidated by the 1940s [221]. Glucose is initially converted to glucose-6-phosphate (G6P) by hexokinase or glucokinase. Subsequently, G6P is converted to fructose-6-

phosphate (F6P), an isomer, by phosphoglucose isomerase. Phosphofructokinase catalyses the subsequent reaction to produce fructose-1,6-bisphosphate. Dihydroxyacetone phosphate (DHAP) and glyceraldehyde 3-phosphate (G3P) are then produced from fructose-1,6-bisphosphate catalysed by fructose bisphosphate aldolase. Glyceraldehyde-3-phosphate is oxidized in an exergonic reaction into 1,3-bisphosphoglycerate, reducing an NAD^+ molecule to NADH and H+. 1,3-bisphosphoglycerate is then converted into 3-phosphoglycerate (3-PG) catalysed by phosphoglycerate kinase. 3-phosphoglycerate is then converted into 2-phosphoglycerate catalysed by phosphoglycerate mutase. Enolase subsequently generates phosphoenolpyruvate (PEP) from 2-phosphoglycerate. Pyruvate kinase finally facilitates the production of pyruvate from PEP.

Cancer cells have high glycolytic rates as glycolytic intermediates serve as precursors for the biosynthesis of nucleotides, amino acids, or phospholipids, [222]. For instance, via the oxidative arm of the pentose phosphate pathway (PPP), G6P and F6P serve as precursors for purine and pyrimidine biosynthesis. Additionally, NADPH is generated as a by-product of these reactions, which is an important cofactor for enzyme-mediated redox reactions and is essential for maintaining cellular redox homeostasis. The glycolytic intermediate 3-PG is a precursor of serine, which is a substrate or precursor for purine and pyrimidine, glycine, and cysteine biosynthesis. Moreover, as well serine connects glycolysis with the PPP, amino acid biosynthesis and one-carbon metabolism (**FIGURE 1.10**). G3P, another glycolytic intermediate, is converted to glycerol-3-phosphate and phosphatidic acid to support phospholipid synthesis, while pyruvate can be converted into alanine [223].

Glycolytic genes are ubiquitously overexpressed in over 70% of human cancers [224, 225]. Under hypoxia, cancer cells frequently upregulate the expression of glucose transporters (GLUT1-5), in particular GLUT1 and GLUT3, to enhance glucose uptake and support increased glycolytic flux in many cancer cells [226]. Moreover, Hexokinase 2 (HK2) is also frequently upregulated in different cancer cells [227, 228]. HK2 is one of the four glycolytic enzyme isoforms (HK1-3 and GCK) that designates glucose to the glycolytic pathway through its irreversible conversion to G6P [227, 228]. Bifunctional 6-phosphofructo-2-kinase/fructose-2,6- bisphosphatases (PFKFBs) mediates the reversible conversion of F6P to fructose-2,6-bisphosphate (F2,6BP). The activity of phosphofructokinase 1 (PFK1) is allosterically regulated by F6P, which converts F6P into F1,6BP, enhancing glycolytic flux. PFK2 activity catalyses the ATP-dependent phosphorylation of F6P, whereas FBPase activity catalyses F2,6BP dephosphorylation. Many cancer types show high expression of PFKFB3, one of the four members of the PFKFB family, to sustain a high rate of glycolysis [229].

As mentioned, under aerobic conditions pyruvate is converted into lactate as opposed to entering the TCA cycle in mitochondria, coupled with the oxidation of NADH to NAD^+, in the reaction catalysed by lactate dehydrogenase (LDH). There are two LDH isoforms, LDHA and LDHB, and LDHA has been found upregulated in several tumour types and has been linked to tumour growth, maintenance, and invasion [230-232]. An immunohistochemical study found that LDHA is primarily expressed in cancer cells whereas LDHB is comparably expressed in normal and carcinomatous tissues. Consequently, LDHA can be utilised as a biomarker in several malignancies, including lymphoma, prostate cancer, renal cell carcinoma, and melanoma [230, 233-237]. LDHA expression is impacted by several factors including Myc (c-Myc), HIF-1, pyruvate kinase isozyme M2 (PKM2) and epidermal growth factor receptor (EGFR) expression [237]. c-Myc promotes the expression of critical enzymes involved in aerobic glycolysis, such as HK2 and LDHA. HIF-1 can be activated by the Phosphatidylinositol 3 Kinase/Akt/Mammalian Target of Rapamycin (PI3K/Akt/mTOR) pathway initiating the transcription of genes encoding glycolytic enzymes, including HKM and LDHA [237]. As a consequence, glycolysis and glucose consumption for conversion to lactate is increased, alongside an increase in mitochondrial respiration through the induction of pyruvate dehydrogenase kinase 1 [238]. Moreover, induction of transcriptional coactivator PKM2 by prolyl hydroxylation 3 promotes HIF-1 binding to hypoxia response elements, leading to recruitment of coactivator p300, histone acetylation, and subsequent transactivation of LDHA target genes, thereby promoting the shift from oxidative phosphorylation to glycolysis as summarised by Miao *et al.* [237, 239, 240]. EGFR controls LDHA expression by inducing the Warburg effect via the activation of extracellular signal-regulated kinase (ERK2). ERK2 binds directly to PKM2, resulting in PKM2 phosphorylation and recruitment of isomerase Pin1, which promotes PKM2 translocation into the nucleus; nuclear PKM2 acts as a coactivator of β-catenin to induce c-Myc expression, which in turn transcriptionally induces expression of GLUT1 and LDHA [237, 241].

1.4.2 Glutaminolysis provides precursors for anabolic processes

Glutamine, the most abundant amino acid, serves as another pertinent source of carbon for anabolic processes in cells and in addition provides nitrogen for the synthesis of non-essential amino acids and nucleotides. High glutamine consumption has been identified in many cancer types, including pancreatic, ovarian, and breast cancers [242]. Glutamine flux is mediated by transporters such as SLC1A5 (ASCT2) on the cell membrane [243, 244]. Upon uptake, glutamine is converted to glutamate and ammonia via glutaminase (GLS) in a process called glutaminolysis. While GLS is a key player in glutaminolysis, various enzymes contribute to the diverse metabolic pathways of glutamine within cells. Numerous amidotransferases involved in nucleotide synthesis utilize glutamine as a nitrogen donor during the de novo production of purine and pyrimidine nucleotides, concurrently generating

glutamate as a by-product [245]. Additionally, asparagine synthetase plays a pivotal role in synthesizing asparagine, using glutamine and producing glutamate as a by-product. This becomes particularly crucial in situations of heightened asparagine demand, as observed during rapid cell growth and proliferation [245]. Glutamate subsequently has a choice of metabolic fates and is either converted by glutamate dehydrogenase (GLUD) into αKG to fuel the TCA cycle, or its amino group can be transferred to oxaloacetate, in a reaction catalysed by glutamic-oxaloacetic transaminase (GOT), to form aspartate. The latter biosynthetic pathway fuels the production of non-essential amino acids (NEAAs) via aminotransferases [242].

αKG can serve as an anaplerotic substrate in the TCA cycle, fuelling energy production via TCA cycle metabolism. Alternatively, α-KG can generate precursors for other biosynthetic reactions such as citrate, which connects mitochondrial metabolism to *de novo* lipogenesis via ATP-citrate lyase (ACLY) and fatty acid synthetase (FASN) [242]. Citrate can be generated when glutamine-derived OAA condenses with acetyl-CoA, or when αKG undergoes isocitrate dehydrogenase (IDH)-mediated reductive decarboxylation to directly yield citrate [246, 247]. Hypoxic cancer cells and clear cell renal cell carcinoma cells utilise this reductive glutamine metabolism for lipogenesis [246]. Glutamine-derived carbons from TCA cycle metabolites can also be released into the cytoplasm through mitochondrial shuttles and carriers. These mechanisms facilitate the transfer of TCA cycle intermediates and contribute to the integration of metabolic processes between the mitochondria and the cytoplasm including for instance, when glutamine-derived aspartate is transported to the cytoplasm, it serves as a versatile metabolite. It can contribute to nucleotide biosynthesis for DNA and RNA, participate in the synthesis of other amino acids, play a role in the urea cycle for ammonia detoxification, and engage in transamination reactions to form different amino acids [242]. Consequently, glutamine anaplerosis in the TCA cycle provides critical precursors for NEAAs, nucleotides, and lipids (**FIGURE 1.11**) [242].

Accumulating studies have shown that OXPHOS-deficient cells, caused by mtDNA mutations, undergo a metabolic rewiring to compensate for energy defects and the inability to use the TCA cycle effectively [201, 248]. In the presence of complete OXPHOS impairment, studies indicate that glutamine undergoes a complete reductive flux via the TCA cycle, resulting in aspartate biosynthesis, an essential metabolic role of the ETC which is required to sustain cell proliferation [201, 202]. The metabolic fate of αKG (oxidative vs reductive) depends on the severity of OXPHOS impairment. The oxidative flux of αKG prevails over reductive flux when residual mitochondrial respiration levels exceed 45% of control levels [249]. Moreover, Lombardi *et al.* proposed that changes in intermediary

TCA metabolites (notably αKG) provide a mechanism that links changes in mitochondrial calcium to cell fate and function [250]. This study demonstrated that a decrease in mitochondrial calcium uptake may be important in remodelling metabolism in myofibroblasts in a manner that drives epigenetic changes important in differentiation [250].

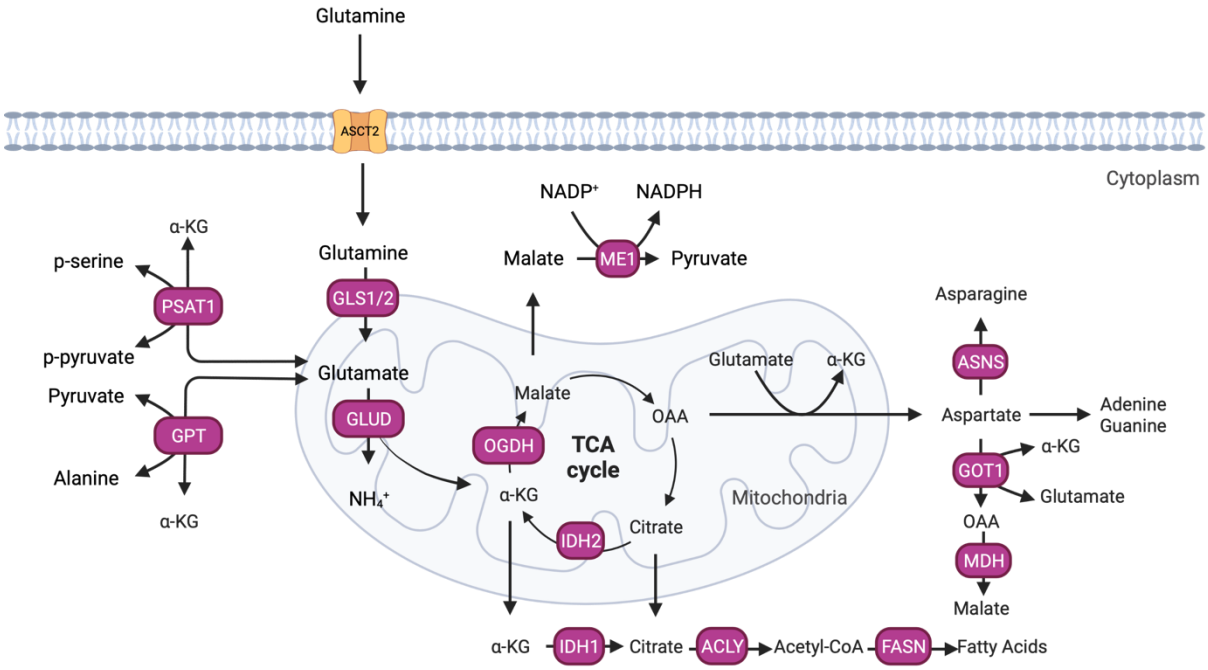

FIGURE 1.11. Glutamine anaplerosis into the TCA Cycle. Glutamine is taken up via ASCT2 and is converted into glutamate. Glutamate is metabolized to αKG by GLUD or transaminases. The TCA cycle metabolite malate can be exported out of the cytoplasm to generate NADPH and pyruvate through the activity of the malic enzyme. OAA can be converted back to aspartate, which supports asparagine generation, and nucleotide synthesis. Citrate can be exported out of the mitochondria for *de novo* fatty acid synthesis. Abbreviations: ACLY, ATP–citrate lyase; ASNS, asparagine synthetase; GLS/GLS2, glutaminase/glutaminase 2; FASN, fatty acid synthetase; GLUD, glutamate dehydrogenase; GOT, glutamate–oxaloacetate transaminase; GPT, glutamate–pyruvate transaminase; IDH, isocitrate dehydrogenase; MDH, malate dehydrogenase; ME, malic enzyme; OAA, oxaloacetate; OGDH, oxoglutarate dehydrogenase; PSAT, phosphoserine transaminase; TCA, tricarboxylic acid; αKG, αketoglutarate. Adapted from [242]. *(Created with BioRender)*

1.4.3 Serine serves as a precursor for anabolic processes

Serine is a crucial NEAA which is involved in the anabolism of macromolecules including phospholipids, ATP, and nucleic acids. As a result, rapidly proliferating cells such as cancer cells are highly dependent on serine, often upregulating pathways involved in uptake and synthesis. Cells acquire serine through four main pathways (**FIGURE 1.12**): 1) uptake from the extracellular environment, 2) degradation from cellular proteins, 3) transamination via glycine, and 4) *de novo* synthesis from glucose and glutamate [251]. Serine is taken up by cells through membrane transporters such as the sodium-independent

neutral amino acid exchanger SLC7A10/SLC3A2 on nerve cells, or SLC1A4/SLC1A5 which are expressed outside the nervous system. As the main transporters of serine, SLC1A4/SLC1A5 are frequently upregulated in serine-dependent tumour cells [252-254]. Serine can also be produced through the degradation of intracellular and extracellular misfolded or deactivated proteins in the lysosome [252].

Moreover, serine can be synthesized through the serine synthesis pathway (SSP), which begins with the glycolytic intermediate 3-PG. 3-PG is converted to 3-hydroxypyruvate in a reaction catalysed by the enzyme phosphoglycerate dehydrogenase (PHGDH). Subsequently, phosphoserine aminotransferase (PSAT1) catalyses the transamination reaction of 3-hydroxypyruvate (3-PHP) with glutamate resulting in the production of phosphoserine (3-PS) and αKG. Phosphoserine is subsequently dephosphorylated by phosphoserine phosphatase (PSPH) to produce serine [255]. Finally, serine can also be mutually converted into glycine by serine hydroxymethyltransferases (SHMTs), in the cytoplasm by SHMT1, or in mitochondria by SHMT2. SHMTs link the SSP and one-carbon metabolism [256]. One-carbon metabolism encompasses a complex network of biochemical reactions functioning to provide 1C units for the synthesis of DNA, polyamines, amino acids, creatine, and phospholipids [257]. Recently, Kiweler *et al.* demonstrated increased glucose-derived serine synthesis and subsequent downstream catabolism of serine via mitochondrial 1C metabolism in breast cancer cells [258]. Interestingly, the study demonstrated that inhibition of PHGDH by BI-4916 reduces cancer cell migration without affecting tumour growth. This demonstrates that mitochondrial 1C metabolism provides a growth advantage to cancer cells by supporting their motility potential independent of proliferation, proving that 1C metabolism has a specific role in promoting cancer cell migration [258].

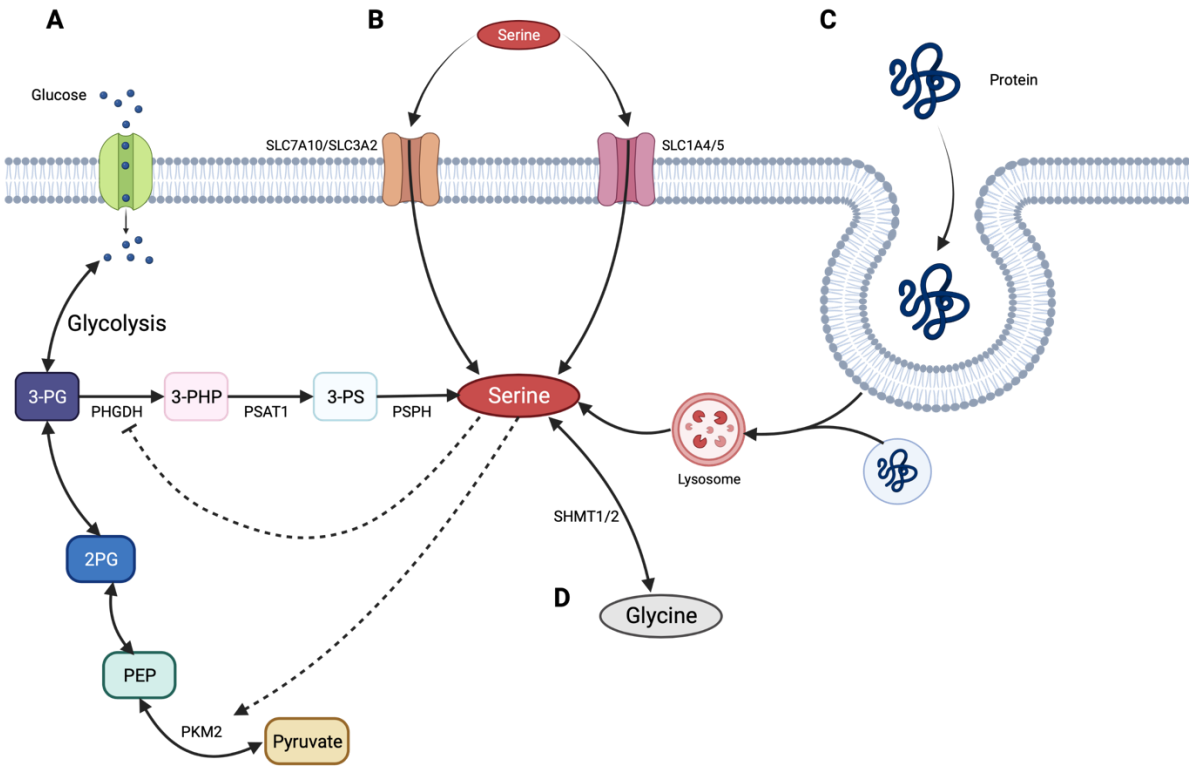

FIGURE 1.12. Sources of serine. Serine can be generated *de novo* through the serine synthesis pathway (SSP) (**A**). First, 3-phosphoglycerate (3-PG) produced by glycolysis or gluconeogenesis is oxidised to 3-phosphohydroxypyruvate (3-PHP) by phosphoglycerate dehydrogenase (PHGDH); subsequently, 3-PHP takes part in a transamination reaction with glutamate producing 3-phosphoserine (3-PS) catalysed by phosphoserine aminotransferase 1 (PSAT1); finally, 3-PS is dephosphorylated by phosphoserine phosphatase (PSPH) to produce. Serine directly binds and promotes allosteric activation of the glycolytic enzyme M2 isoform of pyruvate kinase (PKM2), by contrast, PHGDH can be inhibited by serine. Serine can be taken up by cells through the transporters SLC7A10/SLC3A2 (in nerve cells) and SLC1A4/SLC1A5 (in other cells) in the cell membrane (**B**) or produced by the degradation of serine-containing deactivated or misfolded proteins in the lysosome (**C**). Lastly, serine can be synthesised from glycine via the catalysis of serine hydroxymethyltransferase (SHMT1/2) (**D**). Adapted from [252]. *(Created with BioRender)*

The first link between cancer and serine biosynthesis was suggested by Davis *et al.* who observed higher PHGDH activity in rat hepatoma cell lines versus normal rat liver cells, and of those, those with the highest PHGDH activity proliferated the fastest [259]. A subsequent study supported this notion by demonstrating increased SSP flux in a range of tumours, with increased PHGDH activity correlating with tumour growth rate in the majority of cases [255]. Snell *et al.* hypothesised that the link between serine metabolism and nucleotide synthesis underpinned cancer cell dependency on serine [255]. PHDGH expression has since been found to be amplified in a range of human cancers and cell lines, most notably in melanoma and breast cancer [260, 261]. High PHGDH expression is associated with specific subtypes of cancer. For instance, Locasale *et al.* demonstrated that PHGDH copy number gain

is more frequently found in triple-negative breast cancers versus other breast cancer subtypes [260]. Furthermore, higher PHGDH and PSAT protein expression is associated with a shorter time to relapse, a shorter OS, a higher tumour grade, and increased expression of proliferative markers in metastatic oestrogen receptor-positive (ER+) breast cancer cells [262]. Interestingly, depriving serine-dependent cancer cells of serine triggers activation of the SSP suppresses aerobic glycolysis, and consequently increases TCA cycle flux in a process mediated by p53 [263]. This study highlighted that transient p53-p21 activation and cell cycle arrest promoted cell survival *in vitro*, directing depleted serine stores to glutathione synthesis, and preserving cellular antioxidant capacity. Cells which lacked p53 failed to respond to serine depletion, which led to increased oxidative stress, reduced viability, and severely impaired proliferation [263]. Further research to identify the conditions driving PHGDH amplification and dependence on SSP flux is required, however, the inhibition of serine metabolism has been, and is being, extensively investigated and has the potential to treat different cancers including melanomas, cervical cancer, and colorectal cancer [260, 264, 265].

1.4.4 Therapeutically targeting PHGDH

While targeting cancer cell proliferation with PHGDH inhibitors is a promising therapeutic avenue, there are currently no drugs approved by the FDA or EMA. Several inhibitors are being optimised with the hope of entering clinical trials in the future [266]. For instance, Mullarky *et al*. identified CBR-5884, a PHGDH small-molecule inhibitor by high-throughput screening a library of 800,000 compounds [266, 267]. CBR-5884 is a weak and selective PHGDH inhibitor (IC50 of 33 ± 12 mM), that disrupts the enzymes tetrameric state in favour of the dimeric conformation [267]. Furthermore, Pacold *et al.* identified the PHGDH inhibitor NCT-503 (IC50 of 2.5 ± 0.6 mM) [268]. Despite showing improved inhibition versus CBR-5884, and promising anti-cancer activity *in vitro*, neither demonstrated potency against PHGDH *in vivo* [267, 268]. Moreover, Wang *et al.* discovered PKUMDL-WQ-2101 and PKUMDL-WQ-2201, novel non-NAD^+ competing allosteric inhibitors of PHGDH with an IC50 of 28.1 ± 1.3 µM [269]. PKUMDL-WQ-2101 and PKUMDL-WQ-2201 functioned to inhibit PHGDH activity by forming hydrogen-bond networks in the enzymes' active site which stabilized PHGDH in the inactive conformation, by restricting the movement of the rigid domains and preventing the active sites from closing [269]. Both molecules suppressed tumour growth in mice [269]. Guo J *et al.* discovered that Azacoccone E, a natural compound, is a non-competitive inhibitor of PHGDH with an IC50 of 9.8 ± 4.3 µM [270] [271]. Azacoccone E has been shown to selectively inhibit PHGDH-expressing cancer cell proliferation, though, its antitumour mechanism is yet to be elucidated [271]. Moreover, another natural compound from dietary tomatillos, Ixocarpalactone A (Iox A), discovered by Zheng *et al.* inhibits PHGDH activity with an IC50 of 1.66 ± 0.28 µM. Iox A selectively suppressed the proliferation

of high PHGDH-amplified cancer cell lines, and controlled tumour growth in a xenograft mouse model with low toxic effects [269, 272].

These compounds demonstrate that targeting PHGDH is a viable therapeutic strategy, and as such PHGDH inhibition is being investigated for future clinical testing. Moreover, novel methods of PHGDH inhibition are being explored. For instance, a number of indole amide compounds have been shown to inhibit PHGDH with low nanomolar potencies [273]. While targeting the metabolic vulnerabilities of cancer is an attractive therapeutic strategy, it comes with its limitations, including the likelihood of impeding normal cellular function. Most metabolic pathways rewired in cancer cells also play key roles in normal cells, as such inhibition can be associated with unmanageable toxicities. More targeted approaches such as site-specific delivery systems will likely be key to overcoming these limitations.

1.5 Aims and objectives

MLH1-deficient cells demonstrate a mitochondrial phenotype characterised by reduced oxidative phosphorylation, reduced mtDNA copy number and Complex I inhibition. Preliminary data from our lab has demonstrated that targeting mitochondrial function may be a potential therapeutic strategy for the treatment of MLH1-deficient endometrial tumours, however, MLH1's role in mitochondrial metabolism is not fully understood. Therefore, the main aims of this PhD were to:

1. Investigate how MLH1 loss influences cellular metabolism in MLH1-proficient and deficient EC lines
2. Understand whether altered metabolism in MLH1-deficient EC can be therapeutically targeted

2.0 Materials and Methods

2.1 Cell Culture

2.1.1 Cell lines

The human non-malignant breast epithelial MCF10A cells were grown in Dulbecco's modified Eagle's medium (DMEM) F12 (Sigma-Aldrich) supplemented with 5% horse serum, 20ng/mL EGF, 0.5μg/mL Hydrocortisone, 100ng/mL Cholera Toxin, 10μg/mL Insulin and 1% penicillin/streptomycin (Invitrogen). AN3CA, RKO, KLE, MFE-280 and Ishikawa cell lines were grown in DMEM, 10% foetal bovine serum (FBS; Invitrogen) and 100U/ml penicillin and 100μg/ml streptomycin. For metabolic manipulation where indicated, MFE-280 and Ishikawa paired cell lines were grown Plasmax™ cell culture medium, supplemented with 10% FBS and 1% p/s.

TABLE 2.1. Cell lines

Origin	Species	Cell line	MLH1 Status
Endometrial	Human	RKO	MLH1-deficient (methylated)
Endometrial	Human	AN3CA	MLH1-deficient (methylated)
Endometrial	Human	KLE	MLH1-proficient
Endometrial	Human	MFE-280	MLH1-proficient
Endometrial	Human	MFE-280 gCTRL	MLH1-proficient
Endometrial	Human	MFE-280 K/O 1	MLH1-deficient
Endometrial	Human	MFE-280 K/O 2	MLH1-deficient
Endometrial	Human	Ishikawa EV	MLH1-deficient
Endometrial	Human	Ishikawa MLH1	MLH1-proficient

2.1.2 Cell culture methods

All cells were cultured at 37°C in a humidified atmosphere containing 5% carbon dioxide in T75 flasks. Cell stocks were kept frozen in FBS supplemented with 10% dimethyl sulfoxide (DMSO) in -80°C and liquid nitrogen. Cells were grown for a maximum of 10 passages, except for the MFE-280 clones where indicated. All cell lines were routinely mycoplasma tested and authenticated on the basis of STR profile, viability, and morphological inspection. Table 2.1 indicates the characteristics of the cell lines. Cells were passaged at a ratio of 1:10-1:15 once they reached a confluence of 70%-90%. The cells were washed in phosphate buffered saline (PBS) and then incubated at 37°C with 2mls of 1x trypsin-EDTA (Gibco®, Life Technologies). Once the cells detached from the flask, the trypsin-EDTA was quenched with the addition of 4mls of fresh media. Cells were collected and pelleted by centrifugation for 3 min at 1200 rpm. Media was aspirated and cells were resuspended in fresh media and used for either plating experiments or seeding in T75 flasks for further experiments.

2.1.3 Cell seeding conditions

All experiments were seeded in 96, 24, 12 or 6-well plates (Corning) depending on the experiment and performed in at least duplicate. Cell number was quantified using the BioRad Countess II automated cell counter (Life Technologies), where 10µl of cell suspension was added to each chamber of a dual chamber counting slide (BioRad). Cells were then seeded in plates with fresh media at the appropriate density depending on cell type, the plate used and the experiment, as detailed throughout.

2.2 Small Interfering RNA (siRNA) Transfections

2.2.1 Reverse siRNA transfections for cell viability experiments

In order to determine the cell viability upon ablating a specific gene, siRNA transfection was employed. A total of $2.5x10^3$ Ishikawa cells or $10x10^3$ MFE-280 cells were seeded in 96 well plates for transfection experiments intended for cell viability analysis. Transfection was performed 24 hours later with a 2µM stock of indicated siRNAs (TABLE 2.2), using OptiMEM (Sigma) and Lipofectamine RNAimax transfection reagent (Invitrogen), according to the manufacturer's instructions (TABLE 2.3). Cells were transfected with a non-targeting siRNA alongside and analysed as a control for each experiment. Approximately 24 hours later, fresh cultured medium was added to the cells.

TABLE 2.2. siRNA Specifications

siRNA	Target Sequence (5'→ 3')	Manufacturer
siCTRL - AllStars Negative Control	Proprietary	Qiagen
siMLH1_4	CAGTGGATTGATTATAAATAA	Qiagen
siMLH1_6	GTGGCTCATGTTACTATTACA	Qiagen
siMLH1_smart pool (siMLH1_SP)	GAAUUGGAUGUGAGGAUA GGCAUUAGUUUCUCAGUUA GAAAACAGCUGAUGGAAAG GAAGAUGAUUCCCGAAAGG	Dharmacon
siPHGDH_5	N/A	Qiagen

TABLE 2.3. siRNA Transfection with RNAimax for Cell Viability Experiments

Component	Volume per Reaction For 25nM 96 well (µl per ml)
OptiMEM	24.75
siRNA *(*2µM)	2.5
Lipofectamine RNAimax	0.25

2.2.2 Reverse siRNA transfections for RNA and protein extraction

Transfections intended for total RNA and/or protein extractions were performed in 6-well plates, with a total of $2x10^6$ cells seeded. Transfection was performed 24 hours later with a 20 µM stock of indicated siRNAs (TABLE 2.2), using OptiMEM (Sigma) and Lipofectamine RNAimax transfection reagent (Invitrogen), according to the manufacturer's instructions (TABLE 2.4). Cells were transfected with a non-targeting siRNA alongside and analysed as a control for each experiment. Approximately 24 hours later, fresh cultured medium was added to the cells. To check knockdown efficiency and for downstream analysis, cells were lysed 48 post transfections.

TABLE 2.4. siRNA Transfection with RNAimax for RNA/Protein Extraction

Component	Volume per Reaction for 25nM 6 well (µl per ml)
OptiMEM	250
siRNA (20µM)	2.5
Lipofectamine RNAimax	5

2.3 Small Molecule Inhibitor Treatment

Drug response studies were performed in a 96-well plate format unless otherwise stated. Cells were plated as described in section 1.3 in 100µl growth medium. The next day, 100µl per well of fresh growth medium containing double the concentration of the respective drug than desired was added to the cells. Cells were incubated with the respective drug for indicated times, before carrying out respective cell survival analysis. A complete list of small molecule inhibitors and other chemicals used to treat cells in this study are outlined in **TABLE 2.5**.

TABLE 2.5. Chemical Inhibitors, Small Molecules and Supplements used for Cell Treatments (N/A = purchased as solution)

Reagent	Supplier	Solvent	Description
2-Deoxy-D-Glucose	Sigma-Aldrich	H_2O	Glucose analog (glycolysis inhibitor)
Antimycin A	Sigma-Aldrich	C_2H_6O	Mitochondrial ETC complex III inhibitor
Rotenone	Sigma-Aldrich	C_2H_6O	Mitochondrial ETC complex I inhibitor
Oligomycin A	Sigma-Aldrich	DMSO	ATPase inhibitor
Sodium Pyruvate	Sigma-Aldrich	N/A	Carbohydrate source
Glutamine	Sigma-Aldrich	N/A	Non-essential amino acid
Dimethyl 2-oxoglutarate (DMK)	Sigma-Aldrich	N/A	TCA cycle intermediate
Glucose	Sigma-Aldrich	H_2O	Monosaccharide
Galactose	Sigma-Aldrich	H_2O	Monosaccharide
L-DON	Sigma-Aldrich	H_2O	Glutaminase inhibitor
CB-839	Sigma-Aldrich	DMSO	GLS1 inhibitor
GNE-140	Sigma-Aldrich	DMSO	LDH inhibitor
CPI-613	Sigma-Aldrich	DMSO	PDH inhibitor
GSK2837808A	Merck Millipore	DMSO	LDH inhibitor
PKUMDL	Sigma-Aldrich	DMSO	PHGDH inhibitor
NCT-502	Cayman Chemical	DMSO	PHGDH inhibitor
FX11	Merck Millipore	DMSO	LDHA inhibitor
Metformin	Sigma-Aldrich	H_2O	Gluconeogenic inhibitor
CBR-5884	Sigma-Aldrich	DMSO	PHGDH inhibitor
DMSO	Sigma-Aldrich	N/A	Chemical solvent

2.4 Cell Survival Assays

2.4.1 Cell Titer-Glo (CTG) cell viability assay

The Cell Titer-Glo (CTG) luminescent viability assay (Promega) was used to analyse cell viability diluted 1:4 in PBS following manufacturer's instructions. CTG assays were performed to evaluate cell viability following drug treatments, or to quantify the effect of gene ablation via siRNA transfection. Briefly, media was aspirated from plates and 100µL of diluted CTG reagent was added to each well. Next, the plate was shaken at >1000rpm for 2 minutes before incubating at room temperature for 10 minutes, protected from light. Luminescence emission (emission filter: 3600) was analysed on a FLUOstar Omega plate reader (BMG LABTECH). Luminescence data was normalised to the control conditions to calculate survival fractions.

2.4.2 Clonogenic assay

Clonogenic assays were performed in 6-well plates, with cells were seeded at a density of 500 cells per well in 2mL of medium. Cells were treated with respective drugs, at indicated concentrations every 5 days. On day 10 Cells were fixed and stained with crystal violet which contains formaldehyde (0.05% w/v Crystal Violet (Sigma), 1% Formaldehyde, 1% methanol (Fisher Scientific) in 1x PBS) for 30 minutes at room temperature on a plate shaker. The plates were then washed with running water and air-dried overnight. Colonies were counted manually, and the survival fraction was calculated by normalising to untreated conditions.

2.4.3 Incucyte cell proliferation assay

Cells were seeded in 96-well plates in 100µl of relevant cell culture medium ($2.5x10^3$ Ishikawa cells and $10x10^3$ MFE-280 Cells). Cells were treated with respective drugs at indicated concentrations. Cell proliferation was measured using the Incucyte S3™ or Incucyte ZOOM™ live cell imaging systems (Essen BioScience, MI USA). These systems measure cell proliferation by analysing the occupied area (percentage confluence) of cell images over time.

Images were taken every 3 hours after the first treatment. The percentage confluency of all wells at each time point was quantified by the Incucyte Analysis Software (Essen BioScience, MI USA). The data were normalised to percentage confluence of respective wells at Time 0, followed by normalisation to the control conditions at each time point.

2.5 Nucleic Acid Manipulations

2.5.1 RNA extraction

RNA was isolated from cells using the RNeasy kit (Qiagen) following manufacturer's instructions and quantified using a Nanodrop spectrophotometer (ThermoFisher). Firstly, media was aspirated, and cells were washed with 1x PBS. Cells were subsequently lysed in 350µL RLT (Qiagen) and scraped on ice. 350µL of 70% ethanol was then added to the lysates, before collecting lysate solution was and applied it to an RNeasy Mini spin column (Qiagen) placed in a 2mL collection tube. The column was centrifuged for 15 seconds at 8000 x g and the flow through was discarded. Subsequently 700µL Buffer RW1 (Qiagen) was added to the spin column. The column was re-centrifuged for 15 seconds at 8000 x g and flow through discarded. Next, using 500µL Buffer RPE (Qiagen) the column membrane was washed twice with and centrifuged for 15 seconds at 8000 x g and 2 minutes at 8000 x g respectively. Finally, the empty column was centrifuged at full speed for 1 minute to dry the membrane. RNA was eluted into an Eppendorf tube by adding 30µL RNAase free water (Qiagen) directly to the membrane and centrifuging for 1 minute at 8000 x g. RNA was quantified on a NanoDrop Spectrophotometer (Thermo Scientific) and stored at -80°C.

2.5.2 Reverse transcription

The High-Capacity cDNA Reverse Transcription Kit (Applied Biosystems) was used to reverse transcribe 1µg of RNA (made up to 10µL in H_2O), according to manufacturer's instructions (**TABLE 2.6**). The reverse transcription master mix was prepared on ice and 10µL was added to 10µL of RNA in PCR tubes and mixed by pipetting. Sealed tubes were centrifuged briefly and loaded onto the Veriti Dx thermocycler (Applied Biosystems). Thermocycling was performed as follows – 25°C for 10 mins, 37°C for 120 mins, 85°C for 5 secs. cDNAs were diluted 1:5 in H_2O and stored at -20°C.

TABLE 2.6. Reverse Transcription 2X Master Mix

Component	Volume per Reaction (µL)
10XRT Buffer	2.0
25XdNTPs (100mM)	0.8
10XRT Random Primers	2.0
Multiscribe Reverse Transcriptase	1.0
Nuclease-free H_2O	4.2

2.5.3 Quantitative real time qPCR (RT-qPCR)

Quantitative PCR (qPCR) was performed using TaqMan Universal PCR Master Mix (Applied Biosystems) following **TABLE 2.7** and analysed on a QuantStudio5 Flex System (ThermoFisher) with QuantStudio Real-Time PCR Software v1.7.1 (ThermoFisher). Duplicates were performed for each reaction and contained gene-specific FAM- or VIC-labelled probes (Applied Biosystems). Thermocycling was performed as follows; 50°C for 2 minutes, holding stage of 95°C for 10 minutes and 40 amplification cycles of 95°C 15 seconds, 60°C for 1 minute.

TABLE 2.7. Quantitative PCR Reaction Mix

Component	Volume per Reaction (µL)
TaqMan Universal PCR Master Mix	5.0
Labelled Probe	0.5
Nuclease-free H_2O	4.0
cDNA	0.5

2.5.4 RT-qPCR analysis

The comparative CT (ΔΔCT) method was used for analysing RT-qPCR data. Gene expression was normalised to the housekeeping gene (GAPDH or **β**-actin) as indicated. Target mRNA was normalised (ΔCT) to the housekeeping gene by subtracting the cycle threshold (Ct) of the β-actin sample, for instance, from the cycle threshold (Ct) of each target gene of interest, for each sample. The expression level of each target gene was determined relative to the MLH1-proficient cell line. ΔΔCT = ΔCT MLH1-deficient - ΔCT MLH1-proficient. This was expressed as a fold change in gene expression using the formula: Fold change = $2^{-\Delta\Delta CT}$.

2.6 Protein Manipulations

2.6.1 Protein extraction

Protein was extracted and prepared on ice. Briefly, media was aspirated from cells in plates, and cells were washed with 1xPBS. Cells were lysed using RIPA lysis buffer (150mM sodium chloride, 1% NP-40, 0.5% sodium deoxycholate, 0.1% sodium dodecyl sulphate (SDS), 50mM Tris (pH 8.0), supplemented with protease inhibitors (Roche)) depending on well size and confluency of the cells. The plates were placed on ice for 15 minutes to facilitate protein lysis, before scraping and transfer to microcentrifuge tubes. The tubes were incubated on ice for 15 minutes before centrifugation at 12000 rpm at 4^{o}C for 20 minutes. Supernatants were collected and transferred to a fresh microcentrifuge tube. Protein was stored at -80^{o}C.

2.6.2 Protein quantification

Protein lysates were quantified using the Bradford protein assay (Sigma). 5µL protein was added to a 96 well flat bottom clear plate in duplicates per sample. A standard curve of serially diluted bovine serum albumin (BSA) (0, 0.1, 0.25, 0.5, 1, 1.5 mg/mL) was also included in duplicates Alongside the protein samples. Subsequently, 250µL Bradford Reagent (Sigma) was added to the samples and mixed by pipetting. After incubation for 10 minutes in the dark, absorbance at 630nm was recorded on the FLUOstar Omega plate reader (BMG LABTECH), and protein concentration was calculated following the BSA standard curve.

2.6.3 Western blotting

A total of 30-50µg of protein lysates were prepared for electrophoresis with 1xNuPage Loading Dye buffer (Invitrogen) and 1:4 dithiothreitol (DTT) to a final volume of 20µl for 15-well gels and 30µl for 10-well gels. Protein samples were denatured at 95^{o}C for 5 minutes, cooled on ice, then centrifuged at 10,000rpm for 30 seconds. Equivalent amounts of protein were electrophoresed on 4-12% NuPAGE^{TM} Bis-Tris precast protein gels (Invitrogen) for 90 minutes at 135V in 1xNUPAGE MOPS SDS running buffer (Invitrogen) and transferred electrophoretically to nitrocellulose membrane (ThermoScientific) at 30V for 90 minutes in 10% methanol 1xTris-Glycine transfer buffer. Membranes were blocked for 1 hour in 5% non-fat dried milk (0.1% TBS-Tween) prior to incubation overnight at 4^{o}C in primary antibody (**TABLE 2.8**). Membranes were washed 3x in 0.1% TBS-Tween before probing with the correct secondary antibody. Membranes were washed as before then visualised by chemiluminescent detection using Supersignal West Pico Chemiluminescent Substrate (ThermoScientific), digitally using a ChemiDoc (BioRad, or by traditional x-ray film. Immunoblotting for β-Tubulin, Vinculin or β-Actin was performed as a loading control.

TABLE 2.8. Antibody Specification

Antibody	Species	Dilution	Solution	Incubation	Manufacturer
β-Tubulin	Mouse	1:5,000	5% Milk	1hr RT	Cell Signalling
β-Actin	Rabbit	1:5,000	5% BSA	1hr RT	Cell Signalling
MLH1	Mouse	1:1,000	5% Milk	12hr 4°C	Cell Signalling
PMS2	Rabbit	1:1,000	5% BSA	12hr 4°C	Santa Cruz
GPX1	Rabbit	1:1,000	5% BSA	12hr 4°C	Cell Signalling
NDUFB8	Mouse	1:1,000	5% BSA	12hr 4°C	Abcam
GOT1	Rabbit	1:1,000	5% Milk	12hr 4°C	Cell Signalling
ASCT2	Rabbit	1:1,000	5% Milk	12hr 4°C	Abcam
Cytochrome C	Mouse	1:1,000	5% BSA	12hr 4°C	Cell Signalling
NRF2	Rabbit	1:1,000	5% BSA	12hr 4°C	Cell Signalling
PDH	Rabbit	1:1,000	5% BSA	12hr 4°C	Cell Signalling
LDHA	Rabbit	1:1,000	5% Milk	12hr 4°C	Cell Signalling
Total-OXPHOS	Mouse	1:500	5% Milk	12hr 4°C	Abcam
PHGDH	Rabbit	1:1,000	5% BSA	12hr 4°C	Cell Signalling
PSAT1	Rabbit	1:1,000	5% BSA	12hr 4°C	ThermoFisher
PSPH	Rabbit	1:1,000	5% BSA	12hr 4°C	ThermoFisher
Anti-Mouse	Goat	1:5,000	5% Milk	1hr RT	Dako
Anti-Rabbit	Goat	1:5,000	5% Milk	1hr RT	Dako

2.6.4 Protein densitometry

ImageJ was used to quantify the intensity of bands for the proteins of interest in each sample. The analysis did not account for band intensity and could be made more quantitative by considering intensity and saturation. A box was drawn around the bands using the select tool to generate a histogram. Using the straight-line tool, each peak was separated. ImageJ quantified the area of peaks for each band of the western blot. The area of protein of interest was normalised to the relative loading control. The expression of each protein was subsequently normalised to control samples (untreated, siCTRL, or MLH1-proficient), such that the relative expression for the control samples was 1.

2.7 Metabolic Manipulations

2.7.1 Metabolomic sample preparation and extraction

Due to the sensitivity of the LC/MS equipment, all reagents/solvent used for the sample extraction and preparation were at least LC/MS grade. $2x10^5$ cells per well were plated in 6-well plates on day

0, with an extra well per condition for cell counting, and left to grown overnight. On day 1, media was replaced with flux medium (**TABLE 2.9**) according to the experiment:

TABLE 2.9. Composition of Flux Medias

Experiment	Media	Labelled Metabolite	Other Supplements
Glucose Tracing DMEM	DMEM, no Glucose	D-Glucose U-13C6 (2g/L)	10% FBS, 1% P/S
Glucose Tracing RPMI	RPMI, no Glucose	D-Glucose U-13C6 (2g/L)	10% FBS, 1% P/S
Glutamine Tracing DMEM	DMEM, no Glutamine	L-Glutamine 13C5 (4mM)	10% FBS, 1% P/S

On day 2, the cell number of the spare well for each condition was determined as described in section 1.3. Subsequently, medium was aspirated from the experimental wells, and plates placed on ice. They were then washed 3x with 1mL per well of PBS and aspirated carefully.

Prior to the extraction, the extraction buffer was composed as follows and stored at -20°C:

- 50% Methanol
- 30% Acetonitrile
- 20% Ultrapure Water
- 50 ng/mL HEPES

Each condition was incubated in extraction buffer on a cold bath of dry-ice and methanol for 15 minutes at a ratio of 1mL per 1,000,000 cells. Subsequently, cells were scraped, and cell suspension collected in 1.5mL Eppendorf tubes, before mixing in a thermomixer set at 4°C and the maximum speed for 15 minutes. After the agitation, samples were incubated at -20°C for at least 2h. Subsequently, samples were centrifuged for 10 minutes at 4°C, at maximum rpm, and the supernatant was collected in new tubes. These underwent a further centrifugation step for 10min at 4°C at maximum rpm to remove insoluble debris. The supernatant was then transferred into auto sampler vials and stored at -80°C until further analysis.

2.7.2 Metabolomics Analysis

2.7.3 Measurements of oxygen consumption rate (OCR) and extracellular acidification rate (ECAR)

Oxygen consumption and lactate secretion are physiological symptoms associated with active cellular metabolism. The Seahorse Bioscience Extracellular Flux (XF) Analyser is a tool used to evaluate cellular oxygen consumption rate (OCR) and extracellular acidification rates (ECAR) the latter of which provides an indication of glycolytic activity.

Cells were plated in a 96-well XF Cell Culture Microplates (Seahorse Bioscience) in 100µL culture medium the day before assaying. The number of cells plated was calculated with the aim to achieve 80-90% confluency the following day. Cells were grown overnight (37°C, 5% CO_2). Meanwhile, the XF sensor cartridge (Seahorse Bioscience) was hydrated in 200µl per well XF Calibrant solution (pH 7.4) (Seahorse Bioscience) over night at 37°C, 0% CO_2.

The following day, assay medium was freshly prepared by supplementing plain XF Assay Medium (Seahorse Bioscience) with the nutrients required. 10x drug concentrations were also prepared in this medium was distributed to the appropriate injection ports on the XF sensor cartridge for injection during the assay. The sensor cartridge was then calibrated in the XF Analyser, during which time the cells were washed in assay medium, replenished with 175µl, and incubated at 37°C for ≥ 30 minutes at 0% CO_2 to deacidify the medium. Once calibration was complete, the XF Cell Culture Microplate was inserted into the XF analyser for flux analysis. The composition of assay medium used for the different assays and respective treatments are listed in **TABLE 2.10** and a standard flux analysis protocol is depicted in **TABLE 2.11**.

TABLE 2.10. Media composition and drug concentrations for OCR/ECAR

Assay	Glycolysis	Spare Respiratory Capacity
Medium	XF Assay medium modified DMEM (no glucose, 2mM Glutamax)	
Supplements	2mM Glutamine	10mM Glucose 1mM Sodium Pyruvate 2mM Glutamine
Drugs added (in order)	10mM Glucose 1µM Oligomycin 50mM 2-DG	1µM Oligomycin 0.5µM FCCP 1µM Rotenone/ 1µM Antimycin A

TABLE 2.11. Standard Seahorse Bioanalyzer protocol for 3 injections

Command	Time (minutes)
Equilibrate	~15
Mix	3
Wait	1
Measure	4
Mix	3
Wait	1
Measure	4
Mix	3
Wait	1
Measure	4
Mix	3
Wait	1
Measure	4
Injection Port A	
Mix	3
Wait	1
Measure	4
Mix	3
Wait	1
Measure	4
Mix	3
Wait	1
Measure	4
Injection Port B	
Mix	3
Wait	1
Measure	4
Mix	3
Wait	1
Measure	4
Mix	3
Wait	1
Measure	4
Injection Port C	
Mix	3
Wait	1
Measure	4
Mix	3
Wait	1
Measure	4
Mix	3
Wait	1
Measure	4
End Protocol	

2.7.4 Determination of Complex I activity

Assay Principle

The Complex I Activity ELISA assay (Abcam) was used to measure Complex I activity. The assay utilises a pre-coated microplate with capture antibodies specific to Complex I. Samples were prepared as per the protocol and loaded into the pre-coated microplate wells. After the target is immobilised the activity of Complex I is determined by measuring the oxidation of NADH to NAD^+ and the simultaneous reduction of the provided dye (ε=25.9/mm/well) resulting in an increased absorbance at OD=450nm. The activity of Complex I measured in this assay is independent of ubiquinone.

Sample Preparation

$1x10^6$ cells were plated in $25cm^2$ plate until they reached 80-90% confluence. A cell pellet was obtained as described above. The cell pellet for each cell line was resuspended in 200µl of ice-cold PBS. Protein was extracted by adding 10X non-ionic native detergent solution (n-dodecyl-b-d-maltoside) provided in the kit to a final dilution of 1:10, which fully lyses mitochondrial membranes. Samples were incubated on ice for 30 minutes, then centrifuged for 20 minutes at 4°C at 16000rcf. The supernatant was collected, and protein concentration determined using the Bradford (sigma) protein assay. The samples were diluted in the provided incubation to a concentration of 200µg/200µl.

Experimental Procedure

Equal amounts of protein (200µg) were loaded in the pre-coated 96 well microplate (containing the enzyme NADH dehydrogenase) provided with the kit. Only incubation buffer was added (200µl) for the background wells. The plate was then incubated at room temperature for 3 hours. To remove the contents of the plate, the plate was blotted onto a paper towel face down. 300µl of 1x wash buffer was next added to each well and removed by blotting onto a paper towel. The wash steps were repeated three times, and assay solution prepared as per **TABLE 2.13**. 200µl of assay solution was added to each well and the microplate placed in the plate reader (FLUOstar Omega) using program in **TABLE 2.12** to measure the oxidation of NADH to NAD^+.

Table 2.12. Complex I Activity Program

Program	Setting
Wavelength	450nm
Interval between readings	1 minute
Temperature	Room temperature
Shaking	Shake between readings

TABLE 2.13. Assay solution.

No. of strips (8 well/ strip)	1x Buffer (ml)	20x NADH (µl)	100x Dye (µl)
1	1.57	84	17

2.7.5 Nutrient supplementations

2D Stripped-DMEM Supplementations

$2x10^3$ cells, washed 3x with 1xPBS, were seeded in 96-well plates. Media was supplemented to a final volume of 200µl. DMEM (containing no glucose, no glutamine, and no phenol red) was supplemented accordingly with Glucose (25mM), Glutamine (4mM) and Acetate (1mM). Cell viability and proliferation was measured on day 7.

3D Stripped-DMEM Supplementations

$5x10^3$ cells, washed 3x with 1xPBS, were seeded in ultra-low attachment 96-well plates. Media was supplemented accordingly with Glucose (25mM), Glutamine (4mM) and Acetate (1mM), and plates were centrifuged at 1000g for 10 minutes (4°C). Cell viability was measured on day 5.

Galactose-DMEM Supplementations

Growth rates in galactose were determined by seeding *$5x10^3$* cells in 96-well plates in pentaplicate in DMEM or DMEM without glucose containing 4.5mg/ml galactose, supplemented with 6mM extra glutamine, 6mM galactose and 6mM DMK. Well confluence was measured on day 3 using the Incucyte S3 live cell imaging system.

Plasmax™ Media Supplementation

$2.5x10^3$ Ishikawa cells and $10x10^6$ MFE-280 cells, cultured in Plasmax™, were seeded in 96-well plates. Media was supplemented to a final volume of 200µl. Plasmax™ was supplemented accordingly to contain metabolite levels equivalent to DMEM for Glucose (25mM), Glutamine (4mM), Pyruvate (1mM) and Serine (0.4mM). Proliferation was measured every 3 hours for a total of 3 days, and cell viability measured at the endpoint.

2.8 Migration Assays

2.8.1 Scratch wound assay

Cells were seeded at a density of 20-$40x10^3$ cells per well in a 96-well plate and grown overnight to form a uniform monolayer. Medium was changed the following day for 0% serum Medium O/N prior to performing the experiment. Using the WoundMaker™ (Essen BioScience) reproducible scratches were created in each well. Once scratched, the medium was aspirated and 100µL of fresh medium (1% FBS to prevent cell death) was added to each well. The plate was then placed into the Incucyte ZOOM™ apparatus (Essen BioScience, MI USA) and images of cell spreading were recorded every 2 hours for a total duration of 72 hours. The Incucyte ZOOM™ apparatus automatically calculates cell

confluence within the wound region over time and compares it to the initial wound created by the WoundMaker™.

2.9 CRISPR-Cas9 Gene Editing

A total of $6x10^4$ MFE-280 cells were seeded in a 24-well plate. After 24 hours, cells were transfected following **TABLE 2.14** with guide RNA (gRNA) targeting the MLH1 gene, and a non-targeting control gRNA (**TABLE 2.15**), TracrRNA and Cas9 puro plasmid in the presence of OptiMEM and RNAiMax lipofectamine transfection reagent, in antibiotic free media. Media was changed after 24 hours. Transfected cells were selected using 1µg/mL Puromycin, 48 and 72 hours after transfection. Puromycin-free media was added 96 hours post transfection. Once confluent, cells were trypsinised and 200 cells were plated in $20cm^2$ plates for single cell colony selection to isolate individual clones from the pooled population. Individual clones were grown and harvested for knockout efficiency.

TABLE 2.14. CRISPR specifications

Component	Control	gRNA
Cas9	10µl **puro** plasmid	10µl **puro** plasmid
TracrRNA	2.5µl	2.5µl
Edit-R crRNA targeting MLH1	/	1.25µl
Edit-R crCTRL non-targeting control	1.25ul	/
Optimem	83.25µl	83.25µl
RNAiMax	3µl	3µl
Antibiotic free medium	400µl	400µl
Total	**500µl**	**500µl**

TABLE 2.15. CRISPR-cas9 gRNAs

gRNA	Sequence	Brand
gCTRL (Edit-R crCTRL non-targeting control #2)	Proprietary	Dharmacon
gMLH1_1 (Edit-R crRNA targeting MLH1)	ATCTGTACGAACCATCTGGT	Dharmacon
gMLH1_3 (Edit-R crRNA targeting MLH1)	TACCTCACCTCGAAAGCCAT	Dharmacon

2.10 Verification of CRISPR-cas9 Gene Editing

2.10.1 DNA extraction

DNA was extracted from the cells using DNeasy Blood & Tissue Kit (Qiagen) following manufacturer's instructions. Cultured MFE-280 cells were trypsinised, centrifuged and the cell pellet was resuspended in 200µL PBS and 20µL proteinase K. Subsequently, 200µL Buffer AL was added and mixed by vortexing. This was followed by the addition of 200µL 100% ethanol and vortexing. The mixture was then pipetted into a DNeasy Mini spin column placed within a 2mL collection tube and centrifuged for

1 minute at 8000 x g. Flow through was discarded and collection tube replaced. Subsequently, 500µL Buffer AW1 was added and centrifuged for 1 minute at 8000 x g. Flow through was discarded and collection tube replaced again and 500µL Buffer AW2 was added and centrifuged for 3 minutes at 20,000 x g. Flow through was discarded and DNA was eluted from the membrane into an Eppendorf tube by adding 200µL Buffer AE directly to the membrane and centrifuging for 1 minute at 8000 x g. DNA was quantified on a NanoDrop Spectrophotometer (Thermo Scientific). DNA was stored at -20°C.

2.10.2 DNA sequencing

MFE-280 DNA underwent Illumina NextSeq 500 WGS of the two loci of MLH1 for CRISPR-Cas9 knockout validation. Sequencing was performed and interpreted by the Genome Centre (Barts and the London School of Medicine and Dentistry, Queen Mary University of London, London).

2.11.0 RNA Sequencing

RNA was extracted using the RNeasy Mini Kit (Qiagen) (described in section 5.1). The concentration and quality of RNA was measured using the Nanodrop 2000 Spectrophotometer. 1000ng of RNA per sample was provided for RNA sequencing analysis to the Welcome Trust Centre for Human Genetics (WTCHG, Oxford, UK). Library preparation was performed using the poly(A) capture of the mRNA. Sequencing was strand-specific, with 150bp read length and mean coverage of 35 million paired-end reads per sample. Alignment to the reference genome GRCh38 (hg38) was carried out as part of the WTCHG pipeline. Data were downloaded as fastq and bam files. Number of reads aligned to the exonic region of each gene were counted using HTSeq based on Ensembl annotation [274]. Only genes that achieved at least one read count per million reads (CPM) in at least 25% of the samples were kept. This led to 16,246 filtered genes in total, 14,112 of which were protein coding genes. Differential expression analysis was performed using DESeq2. Enrichment score (ES), normalised enrichment score (NES), Nominal P value (NOM p-val.) and False Discovery Rate (FDR q val.) were obtained in each gene set enrichment analysis. The following contrasts were made Ishikawa EV vs. IshikawaMLH1 and MFE-280 K/O 1 vs. MFE-280 gCTRL. Differentially expressed genes thresholded with p adjusted value <0.05.

2.12 Statistical Data Analysis

Data is illustrated, unless otherwise stated, as mean ± standard error of the mean (SEM) of ≥ n=3 replicates. If data was from n=1 or n=2, the data is shown as mean ± standard deviation (SD) of technical replicates. Statistical analysis was carried out using GraphPad Prism 9, test as indicated throughout. A p-value of <0.05 was considered to be significant (* p<0.05, ** p<0.0021, *** p<0.0002, **** p<0.0001).

3.0 Results – Generation and Characterisation of MLH1-deficient Cell Models

3.1 Cell models

3.1.1 Generation of MLH1 knock-out MFE-280 cell models

In order to understand the interplay between MLH1 loss in endometrial cancer (EC) and the mitochondrial phenotype previously identified in the lab [175] we used CRISPR-Cas9 to generate two MLH1 knock-out (K/O) MFE-280 cell lines. MFE-280 cells are a type I EC cell line that was originally derived from a primary endometrial carcinoma [275]. We chose these cell lines as they have a functioning MMR pathway and low microsatellite instability. MFE-280 cells have wildtype (WT) PTEN and KRAS, however, have a splice site mutation in TP53 and harbour PI3K/AKT pathway alterations [276]. We used the Dharmacon Edit-R system, which is comprised of a crRNA, the Cas9 plasmid and tracrRNA. Using two predesigned Edit-R Human MLH1 crRNA from Dharmacon we transfected the cells as described in section 2.9. MFE-280 wildtype cells were transfected with the non-targeting control crRNA (gCTRL) and the two MLH1 crRNA (MLH1_1 or MLH1_3) alone or in combination. We obtained a mixed population of cells from each transfection and assessed these for a reduction in expression of MLH1 before single cell selection. We observed that the pool transfected with both crRNA targeting MLH1 had the greatest reduction of MLH1 expression **(FIGURE 3.1 A)**, suggesting that this pool had the greatest number of MFE-280 K/O cells within the population. This pool underwent single cell selection to isolate single MFE-280 MLH1 K/O cells

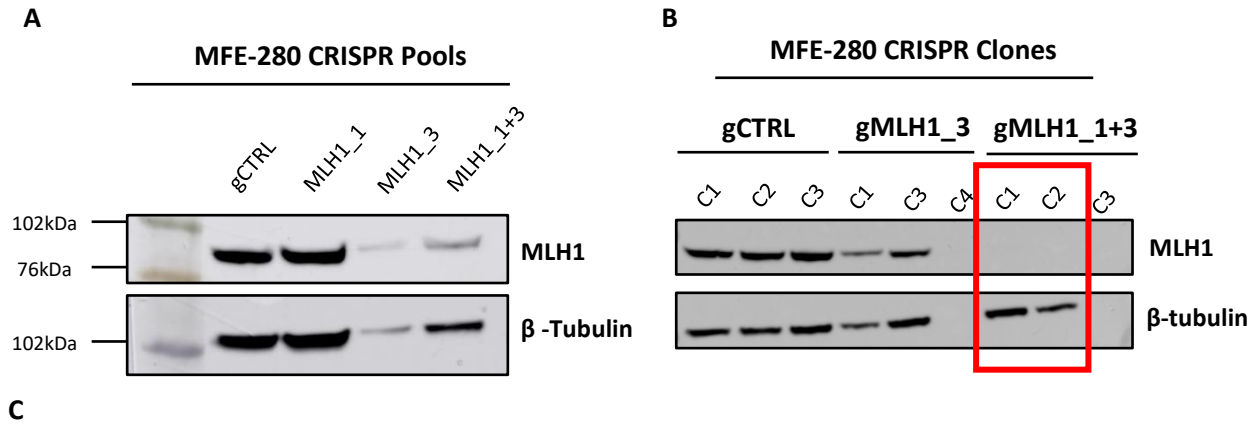

C

Grep sequencing reads for MFE-280 CRISPR-generated cell lines

Sample ID/ Target	MLH1-F1	MLH1-R1	MLH1-F3	MLH1-R3
gCTRL C1	19568	425	11764	12407
K/O 1	0	0	0	0
K/O 2	0	0	0	0

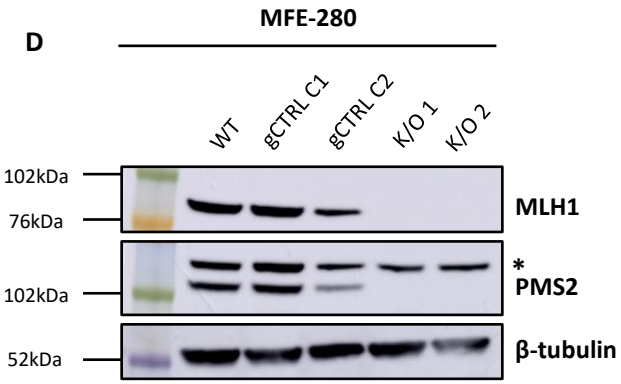

FIGURE 3.1. CRISPR-Cas9 generated MLH1 knockout MFE-280 clones

A. MFE-280 cells were transfected with either non-targeting crRNA or two different crRNA targeting MLH1 (MLH1_1; MLH1_3) either alone or in combination. Western blot analysis of whole cell lysates isolated from MFE-280 CRISPR-Cas9 pools, probed using anti-MLH1 and anti-β-tubulin antibodies. β-tubulin was used as a loading control.

B. Following single cell selection of MLH1 targeting crRNAs, western blot analysis was performed on whole cell lysates isolated from 6 potential MFE-280 MLH1 K/O CRISPR clones and probed using anti-MLH1 and anti-β-tubulin antibodies. β-tubulin was used as a loading control. We identified two MFE-280 MLH1 K/O clones indicated by the red box.

C. MFE-280 MLH1 knockout clones (K/O 1; K/O 2) underwent Next Generation Sequencing for genotyping. Data were analysed by the simple Grep method, used to count how many times the sequence of interest (forward and reverse gRNA) appears in the sequencing data for each clone. Raw Grep data shown. 0=sequence not detected and confirms gene knockout. Red=no expression, green=high expression.

D. Subsequent western blot analysis was performed on whole cell lysates isolated from MFE-280 MLH1 K/O 1 and K/O 2 CRISPR clones, and probed using anti-MLH1, anti-PMS2 and anti-β-tubulin antibodies to confirm K/O. β-tubulin was used as a loading control.

Following single-cell selection, we selected 6 clones and analysed MLH1 expression by western blot. We successfully obtained two clones which showed no expression of MLH1 **(FIGURE 3.1 B)**. To confirm they were mutated at the gRNA sites; DNA was harvested for these clones and analysed by targeted sequencing in the Genome Centre at QMUL. Using the Grep method, the number of reads which aligned to the target sequence was counted for each sample **(FIGURE 3.1 C)**. This table indicates that MFE-280 gCTRL cells contain a high number of sequencing reads for both forward and reverse primers, however, each of the suspected K/O clones contains none. This confirms that MFE-280 K/O 1 and MFE-280 K/O 2 were deficient for MLH1 expression. As an additional confirmation, we blotted the MFE-280 MLH1 K/O 1 and MLH1 K/O 2 clones for PMS2 which is known to have decreased expression in MLH1-deficient cells. As expected, we observed reduced PMS2 expression in both MFE-280 MLH1 K/O 1 and MLH1 K/O 2 clones, further validating that these cell lines are MLH1-deficient **(FIGURE 3.1 D)**.

3.1.2 Generation of Ishikawa paired cell model

Our second cell model for studying the influence of MLH1 loss on mitochondrial metabolism in EC was generated using Ishikawa cells. Ishikawa cells are a well-differentiated, commonly used type I EC cell line that was originally derived from a primary endometrial carcinoma [277]. Ishikawa cells harbour no detectable mutation in the MLH1 gene, nor is the MLH1 promoter methylated [278], however, they do not express the MLH1 protein, and do exhibit a high level of microsatellite instability [276]. The absence of MLH1 could be attributed to an overexpression of miR-155 which Valeri *et al*. has demonstrated down-regulates core MMR proteins, including MLH1 [279]. In addition Ishikawa cells have a PTEN deletion, missense mutation in TP53 and harbour alterations in their PI3K/Akt signalling pathways [276]. Our isogenic MLH1-proficient Ishikawa cell model was generated by stably overexpressing MLH1 in these MLH1-deficient cells. Overexpression of single genes in mammalian cells is widely used in molecular biology to investigate protein function. Ishikawa cells were transfected with either an empty myc-tagged plasmid (empty vector – EV), or the MLH1-myc-tagged plasmid (MLH1). These populations of cells were selected for those containing the plasmid by treatment with the selection marker, G418 until a stable population of MLH1-expressing cells was generated **(FIGURE 3.2)**. It's important to note that the reintroduction of MLH1 might not be adequate to fully restore the MMR pathway in Ishikawa cells, highlighting a limitation of this cellular model. To address this, utilizing an assay as demonstrated by Gu et al., to determine activity, would have been beneficial [280].

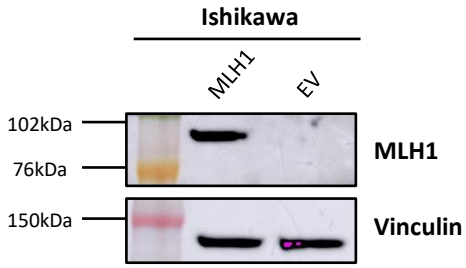

FIGURE 3.2. Generation of Ishikawa paired cell model. Cells were transfected with either an empty myc-tagged plasmid (empty vector – EV), or an MLH1-myc-tagged plasmid (MLH1) and selected with G418 to generate pools of EV or MLH1-transfected cells. Protein lysates were isolated and western blot analysis was performed. Membranes were probed using anti-MLH1 and anti-vinculin antibodies. Vinculin was used as a loading control.

3.2 Characterisation of MLH1-deficient cell models

3.2.1 MLH1 loss does not impact cellular proliferation rate

Before proceeding with functional studies to investigate the role of MLH1 loss in EC, we first investigated whether the MLH1-proficient and deficient cell models have a differential proliferation rate. To do this we used both the Incucyte Live-cell analysis system, as well as the Cell Titer Glo viability assay. Cell proliferation was monitored using the Incucyte Live-cell imaging system, by monitoring the occupied area (% confluence) of cell images photographed every 3 hours, over a period of 5 days. We calculated the proliferation rate for each cell line by comparing the confluence of the cells at each time point, over time, normalised to the confluence recorded at the initial time point. Our data indicates that the re-expression of MLH1 in the Ishikawa (MLH1-deficient) cell line, does not significantly impact proliferation over this time course (**FIGURE 3.3 A**). Interestingly, the loss of MLH1 in MFE-280 cells did significantly ($p<0.0001$) impact cell proliferation. MFE-280 K/O 1 and K/O 2 grow significantly slower over 5 days compared to the gCTRL cells (**FIGURE 3.3 C**). It is important to note that Ishikawa cells proliferate markedly faster than the MFE-280 cells (**FIGURE 3.3**). These differences in proliferation are taken into consideration in subsequent small molecule inhibitor experiments by normalising the confluence measured at each time point, to the confluence measured in the untreated wells, at those equivalent time points.

Next, we assessed cell viability which is another useful assay for indicating the cell proliferation rate using the Cell Titer-Glo (CTG) assay. This assay measures the number of viable cells in culture by quantifying the amount of ATP present, an indicator of metabolically active cells. Experiments were initiated with the same cell density and the Ishikawa and MFE-280 cells were cultured for 1, 7 and 14

days. Cell viability was analysed and normalised to the viability measured on day 1 to give an indication of their rate of proliferation. Our data indicates that there were no significant differences in the proliferation rate of MLH1-proficient and deficient Ishikawa cells (**FIGURE 3.3 B**), which was consistent with our Incucyte data. However, this data implies that there are also no significant differences in the proliferation rate of MFE-280 K/O cells compared to gCTRL cells (**FIGURE 3.3 D**). It is important to note, however, that CTG and Incucyte are functionally distinct. CTG (Promega) determines the number of viable cells in culture based on the quantification of ATP, an indicator of metabolically active cells. Incucyte Live-cell analysis is a non-invasive, image-based measurement of cell growth based on area (confluence) or cell number (count) metrics, and can be visually verified via images and movies [281]. Given that MLH1-deficient cells have a metabolic phenotype and CTG measures metabolically active cells, this could influence the analysis.

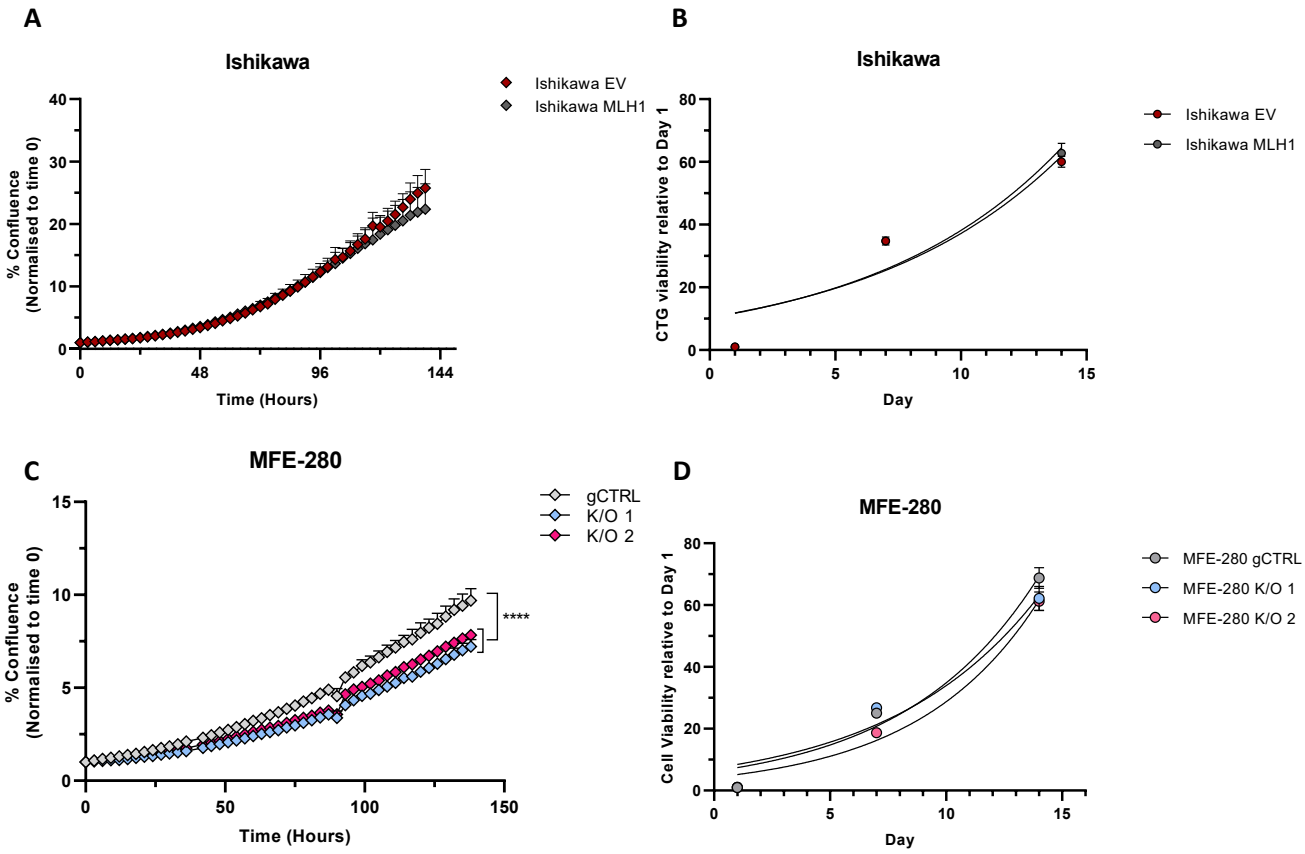

FIGURE 3.3. MLH1 loss does not affect confluence or metabolic activity *in vitro*. Cell growth of MLH1-deficient and proficient Ishikawa **(A)** or MFE-280 **(C)** cells measured at day 1, day 7 and day 14. Plotted relative to day 1. No asterix = not significant. Cell viability measured using the Incucyte Live-cell imaging software. Percentage (%) confluence determined over 6 days, imaged every 3 hours for Ishikawa (n=4) **(B)** and MFE-280 (n=2) **(D)** cells.

3.2.2 MLH1 loss does not impact the migratory potential of cell models *in vitro*

To further characterise our isogenic MLH1 EC cell models, we investigated whether MLH1 loss resulted in a differential cell migratory potential in an *in vitro* setting. For this we used the scratch wound assay, which is a well-developed method for measuring cell migration *in vitro* [282] . We cultured each cell line at a density such that a cell monolayer was formed and as described in section 2.1.3 and made uniform scratches on day 1. Using the Incucyte Live-cell imaging system, the rate of wound closure was calculated by measuring the width of the wound (µm), as detected by the Incucyte analysis software, every 3 hours for 72 hours.

Our data indicates that there was no significant difference in the rate of wound healing in either the MFE-280, or Ishikawa paired cell lines in the absence of MLH1. After 72 hours, Ishikawa EV and Ishikawa MLH1 (**FIGURE 3.4 D-F**) have completely re-established cell-cell contacts and 'healed' the wound. Interestingly, at 72 hours the MFE-280 gCTRL and K/O cells have not completely healed (**FIGURE 3.4 C**). The rate of wound closure for the MFE-280 cells is significantly slower than the Ishikawa cells, which could be attributed to the differences observed in proliferation rate (**FIGURE 3.4 A,B**). This assay gives an indication of how cells might migrate *in vivo* however there are obviously a large number of factors that would further influence the migratory potential of cancer cells *in vivo* which are not represented in this *in vitro* assay [282].

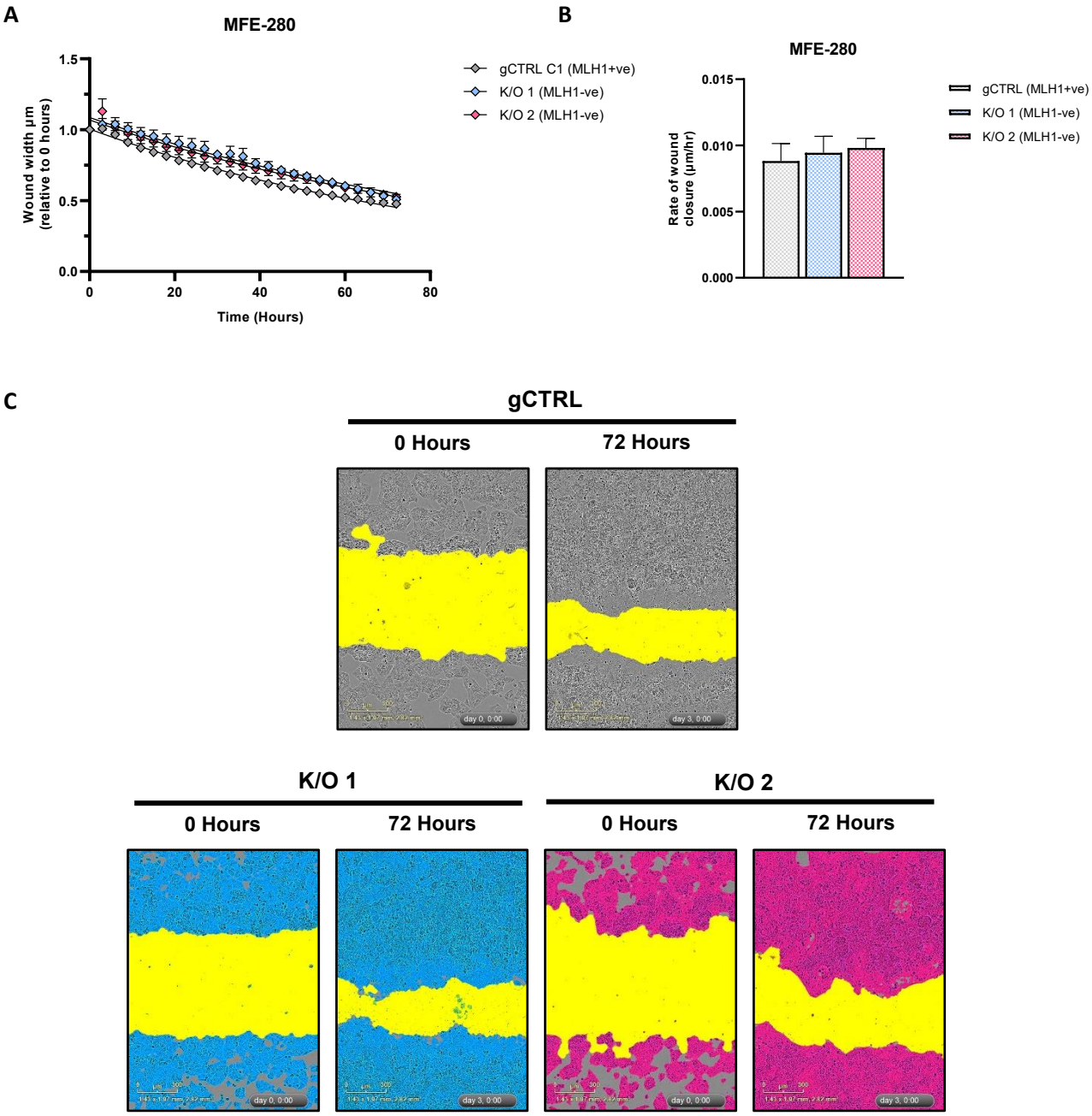
A
MFE-280
Wound width µm (relative to 0 hours)
1.5
1.0
0.5
0.0
0
20
40
60
80
Time (Hours)
gCTRL C1 (MLH1+ve)
K/O 1 (MLH1-ve)
K/O 2 (MLH1-ve)
B
MFE-280
Rate of wound closure (µm/hr)
0.015
0.010
0.005
0.000
gCTRL (MLH1+ve)
K/O 1 (MLH1-ve)
K/O 2 (MLH1-ve)
C
gCTRL
0 Hours
72 Hours
K/O 1
0 Hours
72 Hours
K/O 2
0 Hours
72 Hours

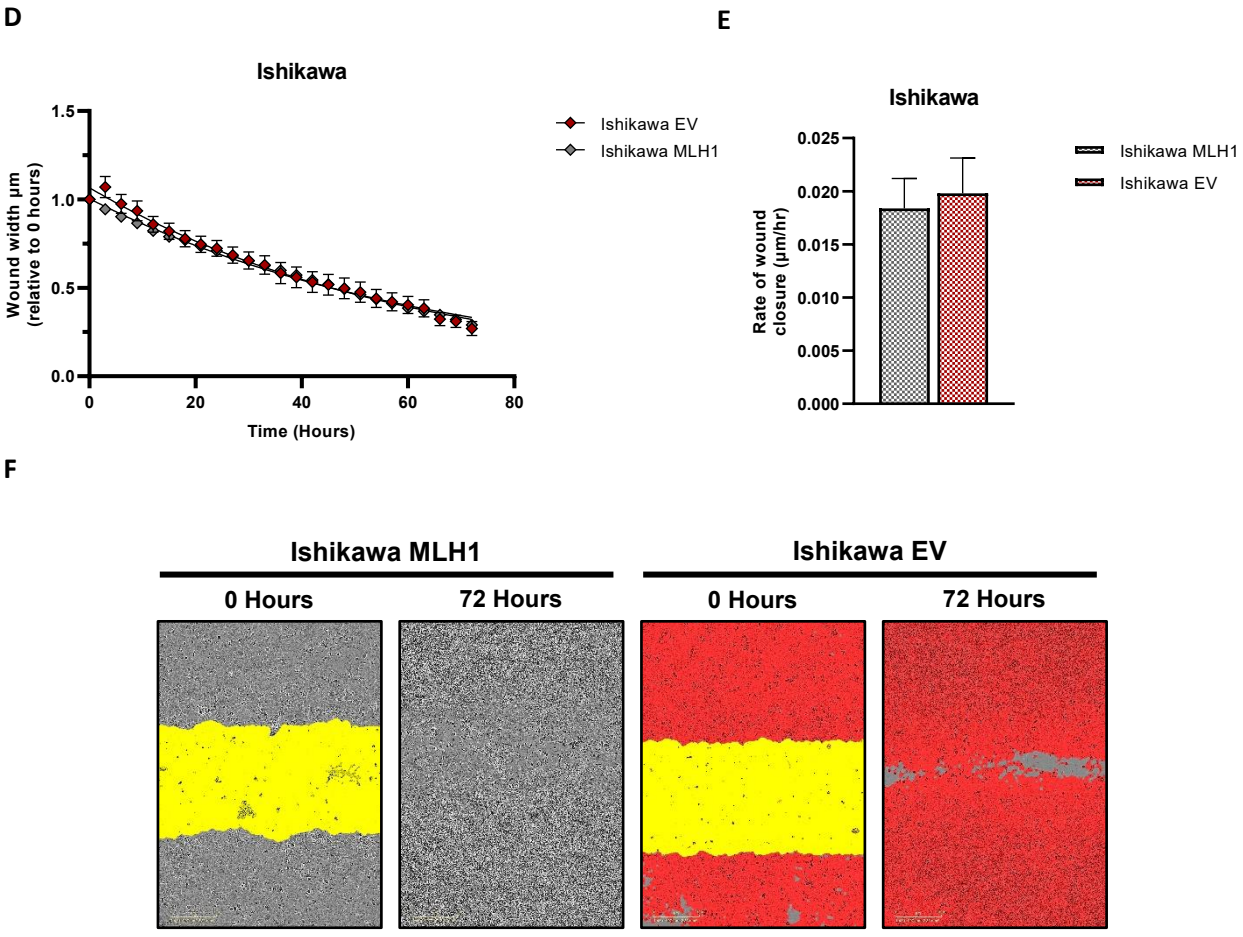

FIGURE 3.4. MLH1-loss has no impact on the migratory potential of cell *in vitro.* Graphs represent 3 independent experiments, indicating wound width (µm) per hour over 3 days, measured using the Incucyte zoom live-cell imaging software (**A, D)**. Rate of wound closure was calculated for MFE-280 (**B**) and Ishikawa (**D**) cells. Representative images taken from 1 experiment and 1 technical repeat, indicating wound (yellow) at 0 hours and 72 hours for MFE-280 **(C)** and Ishikawa **(F)** cells.

3.3 Investigating the mitochondrial function in MLH1-deficient cells

3.3.1 MLH1 loss results in an altered expression of proteins involved in the electron transport chain (ETC)

ATP in non-cancerous cells is primarily generated by mitochondrial OXPHOS [220]. Otto Warburg first described the a glycolytic phenotype in cancerous cells, whereby they rapidly uptake glucose for aerobic glycolysis as a source of ATP [283]. Warburg originally proposed that this phenotype was due to an impairment in mitochondrial OXPHOS, however this view has been challenged since, with studies demonstrating that mitochondrial OXPHOS defects are not always present in spontaneous tumours [220]. Previous research has demonstrated that the loss of MLH1 is associated with a reduced expression of in OXPHOS complex I [175], thus I wanted to determine whether this was also the case in our two MLH1-deficient EC cell models.

Firstly, to determine mitochondrial function, we initially investigated OXPHOS since this is one of the main functions of the mitochondria. We harvested protein from our MLH1-proficient and deficient cell lines and performed western blotting to determine the expression of the five OXPHOS complexes by probing with an OXPHOS antibody cocktail. In the Ishikawa EV cells we observe a significant reduction in expression of Complex I ($p=0.01$), VI ($p=0.0009$) and V ($p=0.04$) (**FIGURE 3.5 A**). Complex I is responsible for the first step of the ETC, and oxidises NADH, transferring electrons to Ubiquinone (Coenzyme Q), a lipid soluble electron carrier embedded in the inner mitochondrial membrane [284]. Complex IV of the ETC, also known as cytochrome c oxidase, functions to transfer electrons from cytochrome c to oxygen, forming water and contributing to the formation of the proton gradient. Complex IV is responsible for the final and rate-limiting regulatory step of OXPHOS [285]. Interestingly, Ishikawa cells also display a small reduction in expression of Complex II or succinate dehydr, although not significant, which is involved in the citric acid cycle. Complex II oxidises succinate to fumarate and acts as the second independent entrance point for electrons into the respiratory chain [286].

We next investigated whether these observations were consistent in our MFE-280 MLH1-deficient cell model. Interestingly, our MLH1 K/O clones appear to have significantly reduced expression of all ETC complexes, except for Complex I (**FIGURE 3.5 C**). This may be because these are two diverse cell models and may potentially harbour other mutations that may affect the expression of these proteins. Moreover, Complex I consists of 45 subunits, so it is possible that mutations could be in any of other subunits.

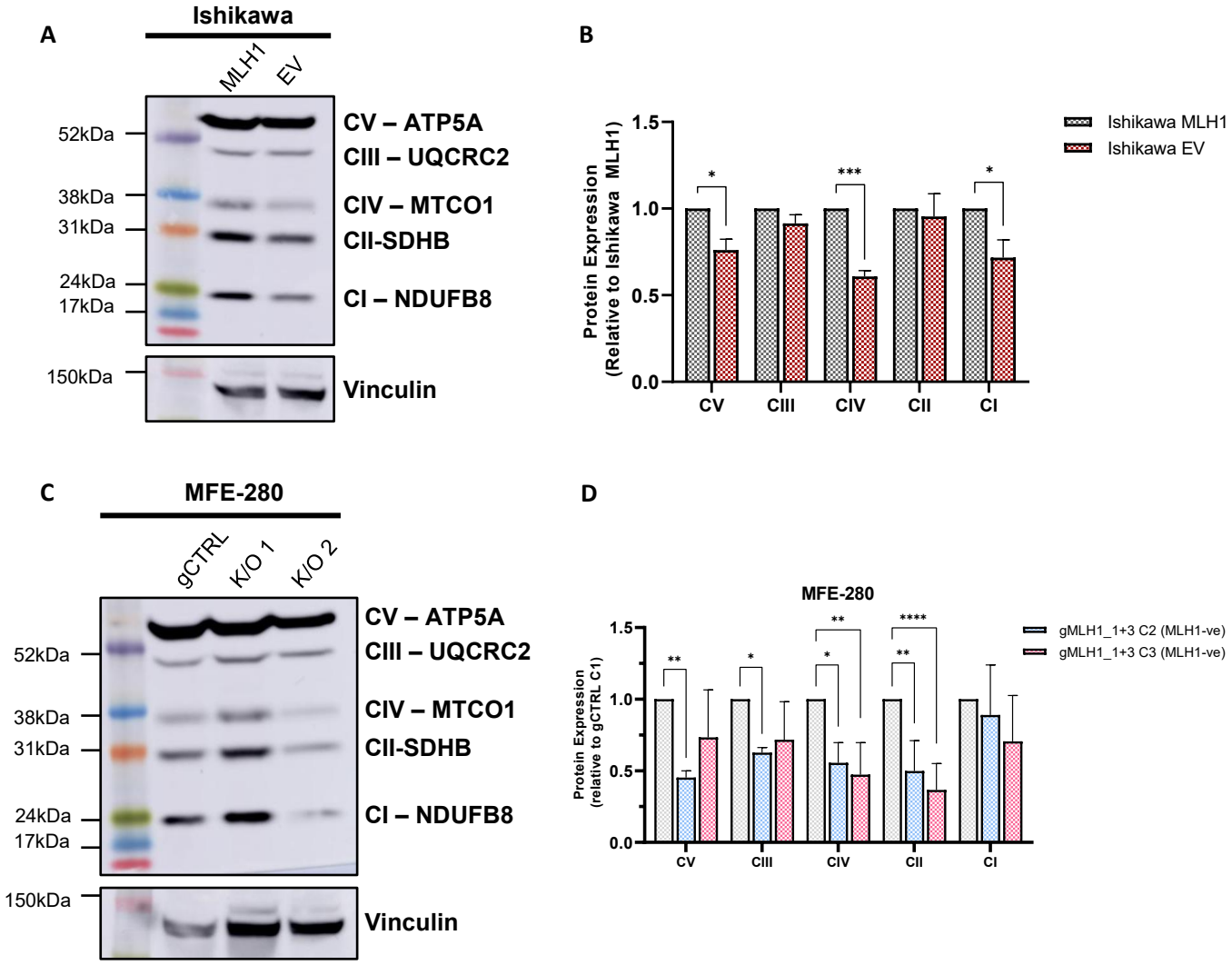

FIGURE 3.5. Altered expression of protein complexes involved in OXPHOS in MLH1-deficient cells. Western blot analysis of protein isolated from MLH1-proficient and MLH1-deficient Ishikawa **(A)** and MFE-280 **(C)** cells. Protein was extracted Ishikawa EV, Ishikawa MLH1, MFE-280 gCTRL, K/O 1, or K/O 2, and expression analysed using anti-total OXPHOS and anti-vinculin. Vinculin was used as a loading control. Protein levels were compared to respective MLH1-proficient cells Ishikawa MLH1 **(B)** and MFE-280 gCTRL **(D)**, estimated by band densitometry, normalised to vinculin as the control. Error bars represent mean with SEM of at least 3 independent experiments. No asterix = not significant. **P*<0.05, ***P*<0.01, ****P*<0.001, *****P*<0.0001.

3.3.2 MLH1-deficient MFE-280 cells have reduced expression of proteins involved in the antioxidant response

To further investigate the deficiencies in Complex I, we analysed the gene expression of two mitochondrial-encoded Complex I core subunits mitochondrial encoded subunits 2 and 5 (MTND2 and MTND5) (**FIGURE 3.6 A,B**). MTND2 and MTND5 expression serves as an indicator of cellular antioxidant response by reflecting alterations in mitochondrial function and ROS generation. In the MFE-280 MLH1-deficient clones, we observed a significant reduction in MTND2 ($p<0.0001$) but not in MTND5, whereas in the Ishikawa MLH1-deficient cells we observed a reduction in both mitochondrial encoded subunits (**FIGURE 3.6 A**). Subsequently, as it has previously been demonstrated that MLH1-deficient cells are sensitive to certain ROS-inducing agent [175], we measured the gene expression and protein levels of the antioxidant response enzyme glutathione peroxidase 1 (GPX1). In the MFE-280 MLH1, K/O clones we observed a significant reduction in the expression of GPX1 protein ($p<0.0001$) and mRNA levels ($p<0.0001$ K/O 1; $p=0.053$ K/O 2), in comparison to the MFE280 gCTRL cells (**FIGURE 3.6 B**). We did not observe this decreased expression of GPX1 in the MLH1-deficient Ishikawa cells at the protein level, however, despite identifying that they have a significant reduction ($p=0.0016$) in GPX1 mRNA levels compared to its MLH1-proficient counterpart (**FIGURE 3.7 A**). The quantitative relationship between RNA and protein is fundamental to biology but is not yet fully understood. This unexpected correlation between a reduced mRNA expression level that is not observed at the protein level could be attributed to proteins having very different half-lives due to varied protein synthesis and degradation. Protein turnover can vary significantly within cells due, as cells control the rates of degradation or synthesis of a given protein [287, 288]. To validate the reduction in the mRNA expression of GPX1 observed in the MFE-280 MLH1 K/O cells, we carried out a short-term siRNA transfection of MFE-280 wildtype cells using either a non-targeting Control siRNA or two different siRNA targeting MLH1. Our data indicates that we do not require a complete loss of MLH1 protein to see this reduction in GPX1. Knockdown of MLH1 resulted in an approximately 50% reduction in GPX1 mRNA levels in the MFE-280 cells relative to the siCTRL treated cells (**FIGURE 3.6 C**), a similar reduction to that observed in the MLH1 K/O clones relative to the gCTRL (**FIGURE 3.7 A**)

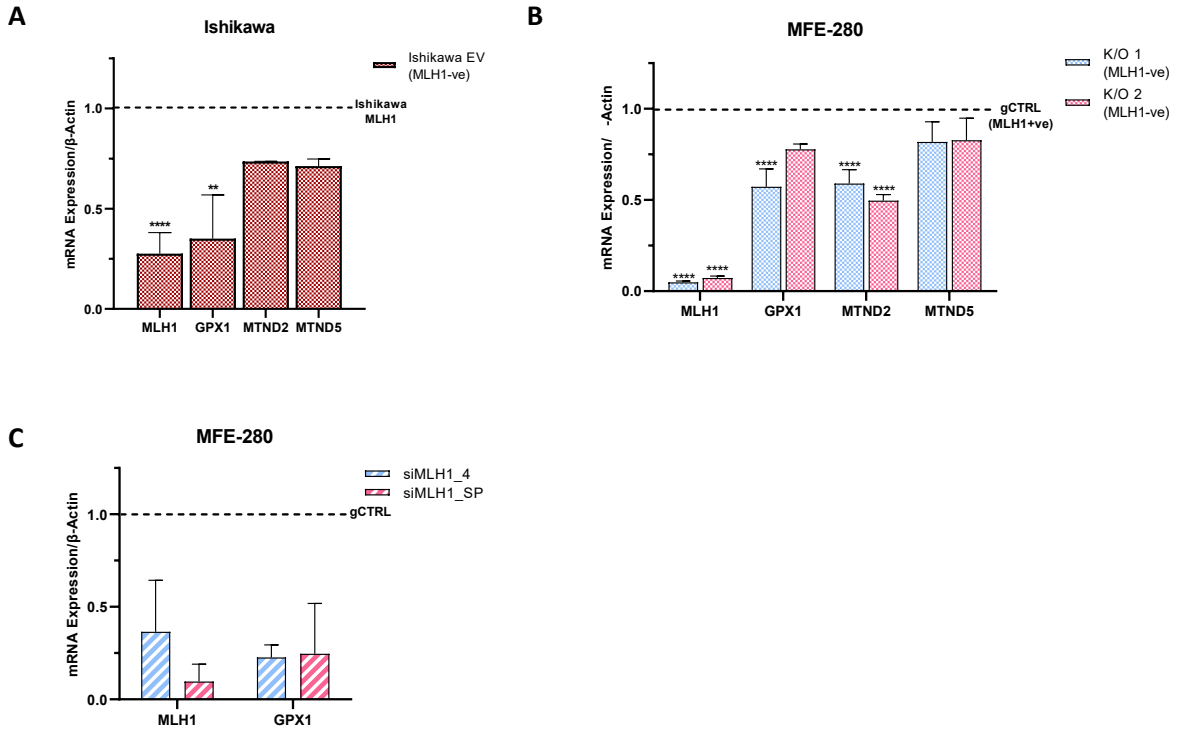

FIGURE 3.6. MLH1-deficient Ishikawa and MFE-280 cells have reduced mRNA expression levels of GPX1 and MTND2. qRT-PCR analysis of RNA extracted from Ishikawa **(A)**, MFE-280 (**B)**, or MFE-280 wildtype cells, transfected with two different siRNA targeting MLH1 **(C)** cells. mRNA expression was measured for MLH1, antioxidant response gene GPX1, mitochondrial encoded complex I subunits MT-ND2 and MT-ND5. Error bars represent mean with standard error of mean for at least 3 independent experiments. *p<0.05, **p<0.01, ***p<0.001, ****p<0.0001.

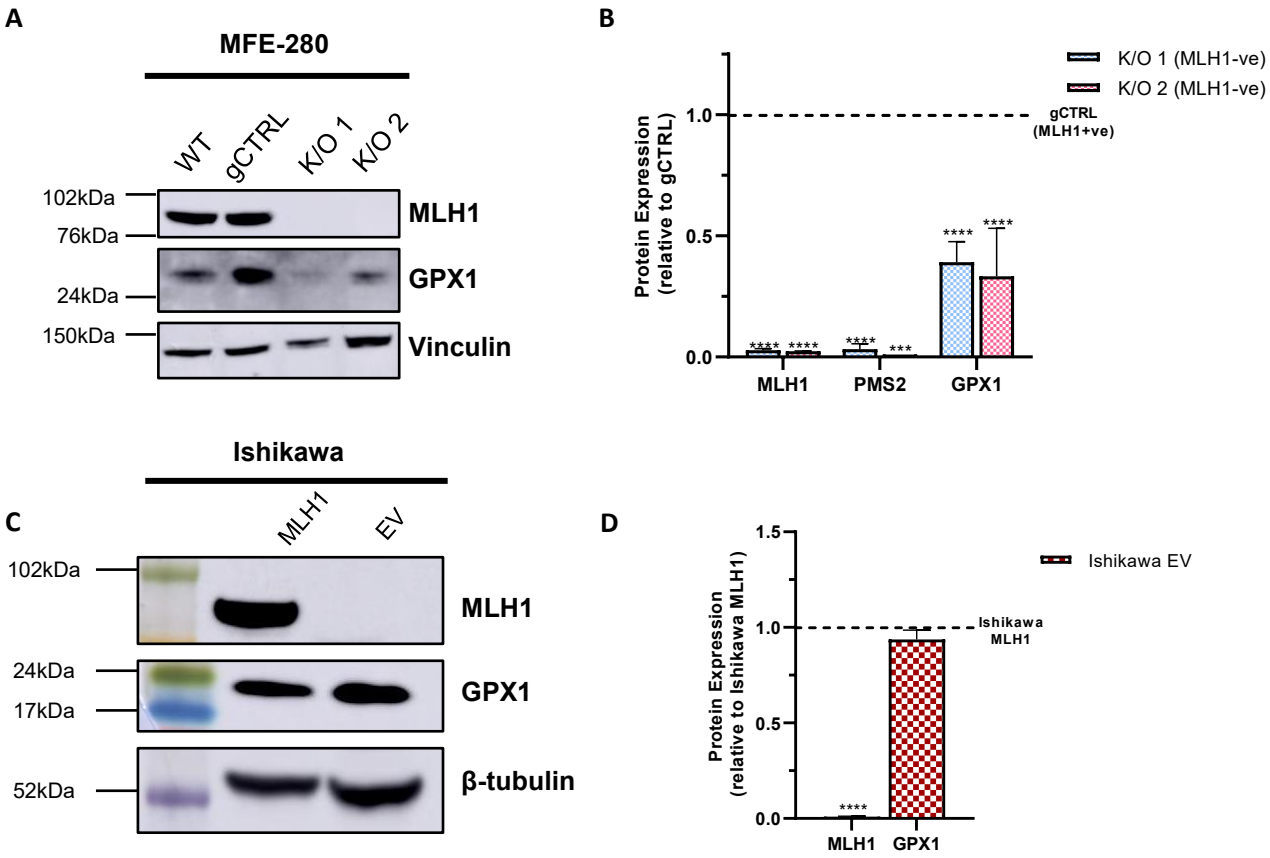

FIGURE 3.7. MLH1-deficient MFE-280 cells, but not Ishikawa cells have a reduced expression of the anti-oxidant response protein GPX1. Western blot analysis of protein isolated from MFE-280 gCTRL, K/O 1 and K/O 2 **(A)** or Ishikawa EV and MLH1 (**C)** cells. Protein was extracted and expression analysed using anti-GPX1 antibody. Vinculin or β-tubulin expression was used as a loading control, as indicated. Protein levels compared to MLH1-proficient control MFE-280 **(B)** or Ishikawa **(D)** cells estimated by band densitometry normalised to loading control. Error bars represent mean with SEM of at least 3 independent experiments. *p<0.05, **p<0.01, ***p<0.001, ****P<0.0001. No asterix = not significant.

3.3.3 Reduced Complex I activity was observed in MLH1-deficient Ishikawa cells, but not MLH1-deficient MFE-280 cells

Thus far, we have observed reduced expression of a number of OXPHOS complexes in both MLH1-deficient cell models which is consistent with previous findings [175] and validates loss of MLH1 results in a perturbed mitochondrial metabolism. Our results do not indicate whether MLH1 loss specifically dives this differential response to antioxidant stress, given the differences we observed in the expression of OXPHOS subunits between our MLH1-deficient cell models. Though, it is important to highlight that the two cell models we used have a diverse genetic makeup and have 'lost' MLH1 in different ways. To further validate our observations, we measured the Complex I activity in the absence of MLH1, as it is a more biologically relevant assay for providing insight into the mitochondrial function of these cells. The Complex I assay is an ELISA assay, which measures the oxidation of NADH to NAD^+, in turn leading to a reduction of a dye and increased absorbance at OD 450nm. We measured the baseline complex I activity in the MLH1-deficient Ishikawa-EV and the MLH1-proficient Ishikawa-MLH1 cells and observed a significant reduction ($p=0.0276$) of Complex I activity in the absence of MLH1, consistent with the labs previous findings (**FIGURE 1.9**; [175]). Next, we analysed baseline complex I activity in our other MLH1-deficient EC cell model, MFE-280 gCTRL and MLH1 K/O cells. Interestingly, we observed differences in complex I activity in our two MLH1 K/O clones (**FIGURE 3.8 C**). There was no significant difference in the Complex I activity of the MLH1 K/O 2 cells, relative to both wildtype and gCTRL MFE-280 cells, however, MLH1 K/O 1 cells had a higher complex I activity in comparison to the MLH1-proficient controls (**FIGURE 3.8 C**). This result is perhaps unsurprising given previous data whereby we demonstrated that Complex I protein expression is not reduced in MLH1-deficient MFE-280 clones (**FIGURE 3.5 C**), whilst we observed reduced complex I protein expression in the Ishikawa MLH1-deficient cells (**FIGURE 3.5 A)**. Given that loss of MLH1 can give rise to a mutator phenotype, we next investigated whether we would observe differences in complex I activity in the MFE-280 MLH1 K/O cells over time with the accumulation of additional mutations. To this end, we cultured the MFE280 gCTRL and MLH1 K/O cells for a period of 12 weeks and measured and compared the activity of Complex I at Week 0, Week 4, and Week 12 (**FIGURE 3.8 E**). Our data illustrates that there are no significant changes in complex I activity between the weeks when comparing the MLH1-deficient and – proficient cell lines (**FIGURE 3.8. E**). The differences we observe between MLH1-deficient cell lines may be due to the fact that each of the cell lines investigated (MFE-280; Ishikawa) have a diverse genetic makeup which may influence the baseline complex I activity in these cells, despite the loss of MLH1.

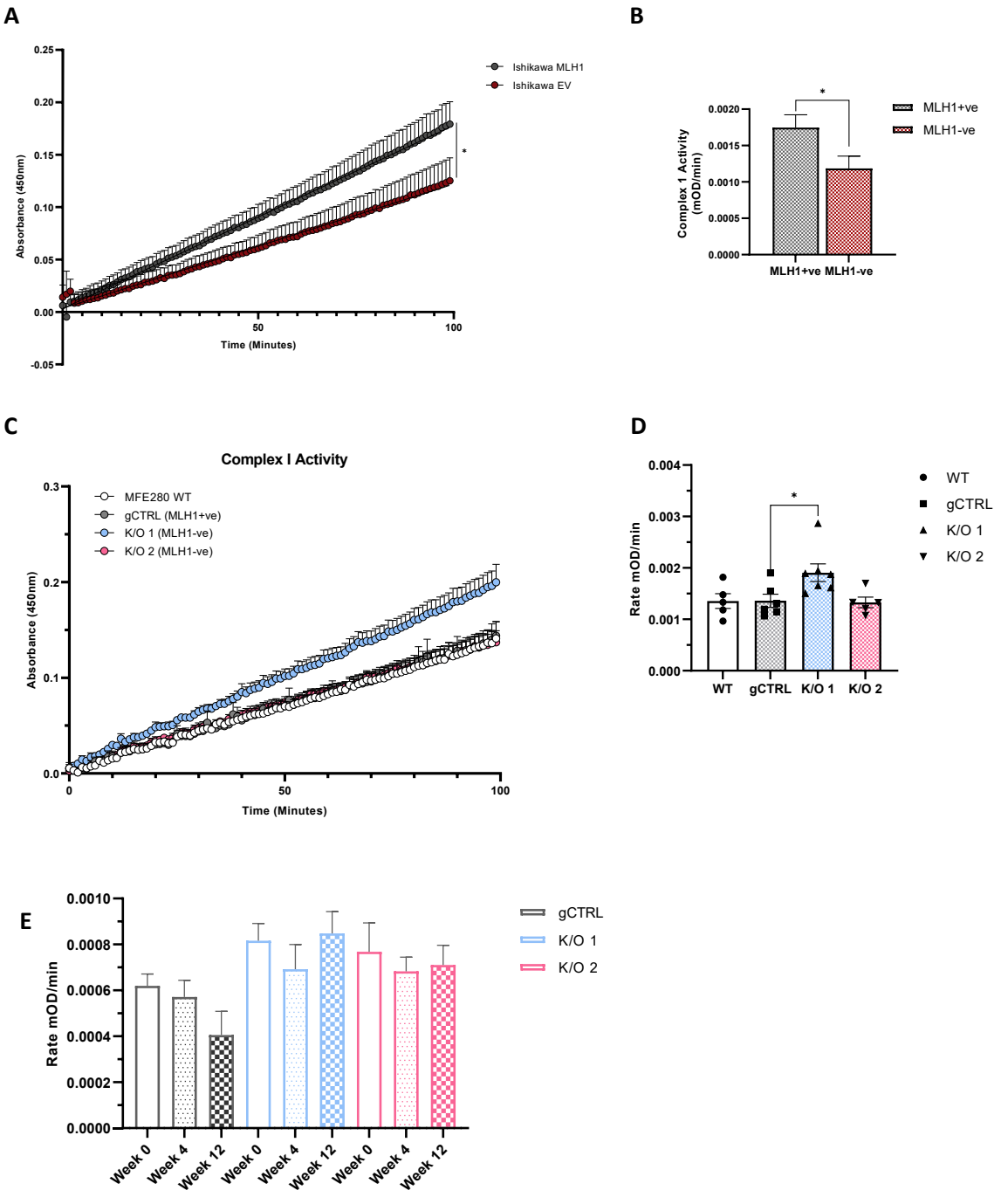

FIGURE 3.8. MLH1-deficient Ishikawa cells, but not MFE-280 cells, have a reduced complex I activity in comparison to MLH1-proficient cells. Complex I activity was measured using an ELISA assay in our panel of MLH1-proficient and deficient EC cell lines. Equal amounts of protein were incubated to determine the activity of Complex I by measuring the oxidation of NADH to NAD^+ and the simultaneous reduction of a dye leading to increased absorbance at 450 nm, over time. The graph shown here is a representation of the consistent differences seen in 3 individual experiments with technical duplicates for Ishikawa (**A**) and MFE-280 **(C)** cells. The activity of Complex I was determined by using the average of duplicates performed in three independent experiments for Ishikawa (**B**) and MFE-280 **(D)** cells. MFE-280 K/O cells were passaged over 12 weeks to see whether the activity of Complex I changed with adaption to loss of MLH1. No significant changes in Complex I activity were observed **(E)**.

3.4 Profiling of MLH1-deficient cell models for nutrient utilisation

3.4.1 No differences in respiration in MLH1-deficient cell models

Thus far we have identified variable changes in expression and activity of Complex I in our panel of MLH1-deficient EC cell lines. Subsequently, we wanted to validate whether OXPHOS and mitochondrial metabolism in general were altered upon MLH1-deficiency using the Seahorse XF analyser, as had previously been observed [175]. The Seahorse XF analyser measures the rate of oxygen consumption in each sample providing a measure of oxidative phosphorylation. The basal OCR, when no drugs are added, represents a measure of basal oxidative phosphorylation. Following basal measurements, oligomycin which inhibits ATP synthase (complex V), is injected to decrease electron flow through the ETC, resulting a reduction in mitochondrial respiration or OCR. This decrease in OCR is linked to cellular ATP production. Upon addition of the uncoupling agent, carbonyl cyanide-p-trifluoromethoxy phenylhydrazone (FCCP), a measure of the cells maximal respiratory capacity is estimated. When the basal OCR is subtracted from the maximal respiration, a measure of spare respiratory capacity (SRC) is obtained. The SRC reflects the cells' ability to respond to stress and increased energy demands. Rotenone and antimycin A are finally injected to inhibit mitochondrial function and result in a decrease in OCR, providing an estimate of non-mitochondrial respiration. We used the XF analyser to measure the difference in OCR between our MLH1-deficient and proficient cell models (**FIGURE 3.9**). Although we observed a consistent trend in our results with Ishikawa EV MLH1-deficient cells having a reduced basal OCR, reduced maximal respiratory capacity and reduced SRC, in comparison to the MLH1-proficient cells, these differences were not statistically significant (**FIGURE 3.9**). This was also true for our MLH1-deficient MFE-280 cells with no significant differences in OCR **(FIGURE 3.9 A)**, basal respiration **(FIGURE 3.9 B)**, maximal respiration **(FIGURE 3.9 C)**, and spare respiratory capacity **(FIGURE 3.9 D)** observed upon MLH1 loss in this model.

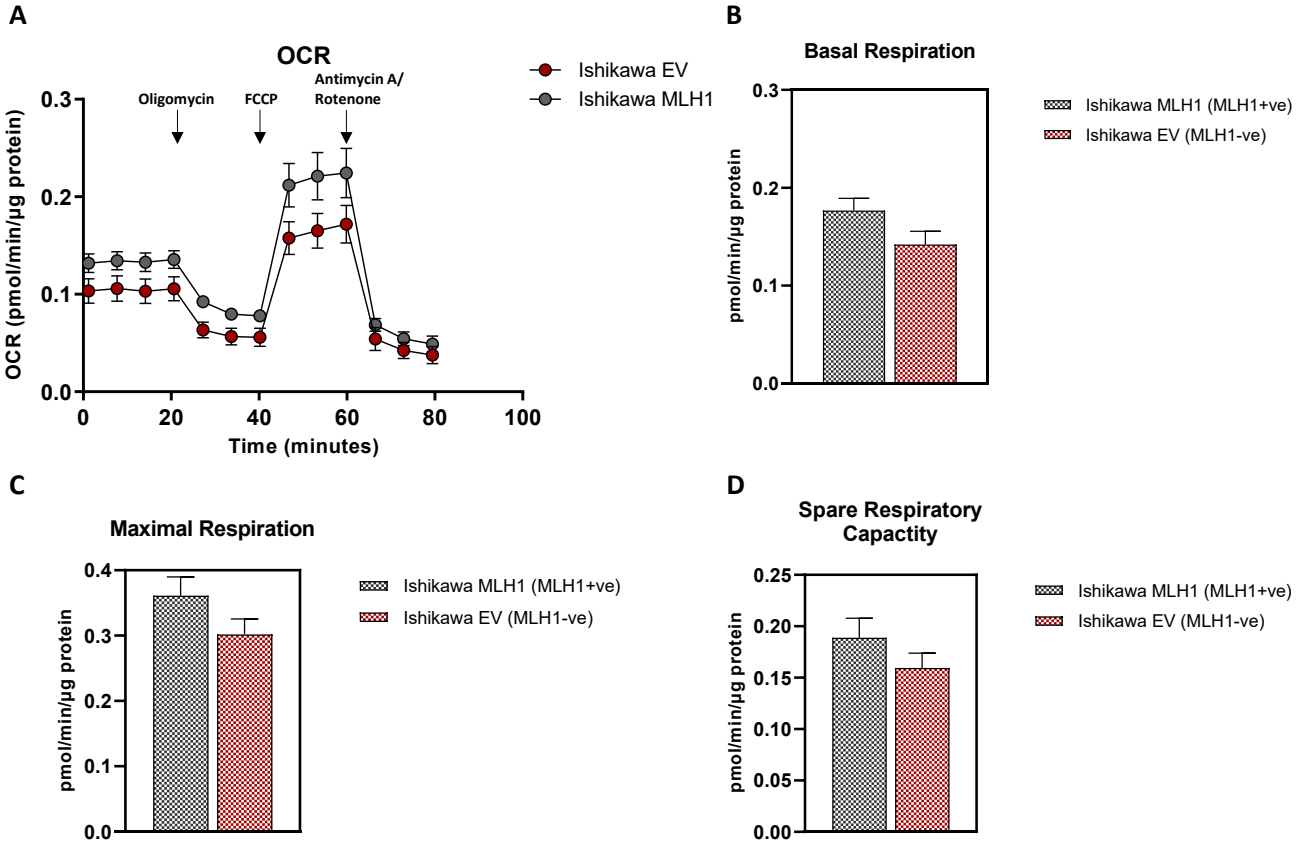

FIGURE 3.9. MLH1 loss did not result in significant changes in cellular respiration in EC cell models. The Seahorse XF extracellular flux analyser was used to measure OCR (pMoles/min/µg protein), indicative of OXPHOS in MLH1-proficient (Ishikawa MLH1) and deficient (Ishikawa EV) cells. **A** is representative of 1 experiment, with at least 5 technical repeats. Error bars represent standard deviation. After establishing a baseline, oligomycin (2µM), FCCP (0.5µM), rotenone (1µM) and antimycin (1µM) were sequentially added as indicated by the arrows. **B** The basal OCR was calculated using the difference between the mean of time points in baseline and in oligomycin treatment (baseline minus oligomycin OCR). **C** The maximal respiratory capacity weas calculated as (FCCP rate minus non-mitochondrial respiration) **D** The spare respiratory capacity was calculated as (OCR following FCCP—baseline OCR). Mitochondrial key parameters including basal respiration, maximal respiration, and spare respiratory capacity were calculated with error bars representing the mean with standard error of mean of at least 3 independent experiments with 5 or more technical repeats. No asterix = not significant.

3.4.2 Increased glycolytic capacity in MLH1-deficient Ishikawa cells

In addition to analysing the OCR within cells, the Seahorse XF analyser can also assess the glycolytic capacity of cells *in vitro*. Therefore, we next assessed the glycolytic profile of our Ishikawa MLH1-proficient and deficient EC cell models (**FIGURE 3.10**). ECAR provides a readout for cellular proton secretion. Proton secretion is a good indication of the export of lactate produced from glucose through glycolysis. Ishikawa EV and Ishikawa MLH1 cells were plated in a Seahorse XF^{96} well plate, and after 24 hours they were starved of glucose for one hour prior to starting the assay. Basal ECAR was measured using the Seahorse XF analyser upon the addition of glucose to stimulate glycolysis. The subsequent treatment with ATP synthase inhibitor oligomycin determines the maximal glycolytic capacity of the cells by inhibiting complex V and shutting down OXPHOS. Lastly, cells were treated with 2-deoxyglucose (2DG), a competitive inhibitor of glucose which functions to shut down glycolysis, to determine the non-glycolytic acidification rate of the cells (**FIGURE 3.10. A**). Our results indicate that the Ishikawa EV, MLH1-deficient cells had a significantly increased glycolytic capacity (p=0.018) and glycolytic reserve (p=0.0018), although no changes in basal glycolysis were observed (**FIGURE 3.10 B-D**).

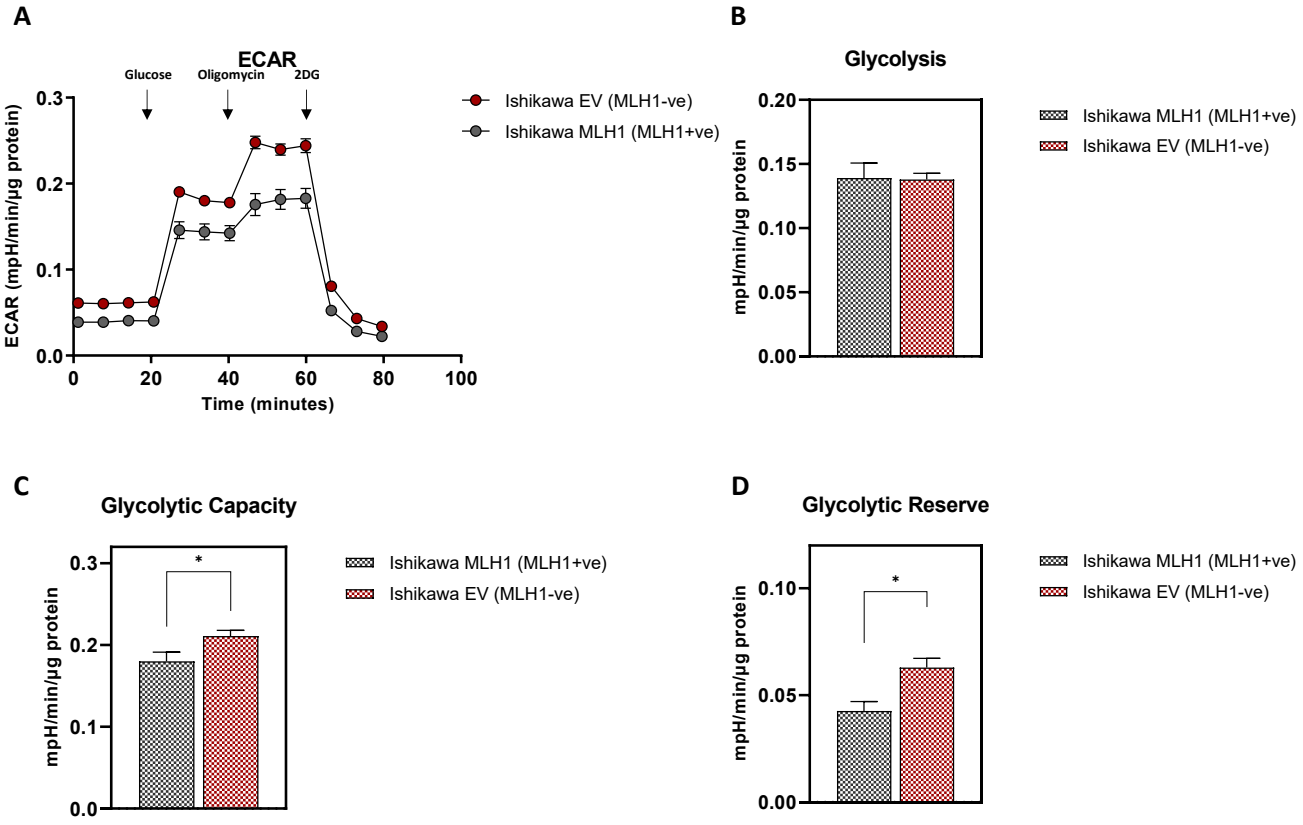

FIGURE 3.10. MLH1-deficient Ishikawa cells have an increased glycolytic capacity and glycolytic reserve. The extracellular acidification rate (ECAR) was measured using a Seahorse XF extracellular flux analyser to quantify ECAR (pMoles/min/µg protein), which is indicative of glycolysis, for Ishikawa EV and MLH1 cells. Ishikawa EV and MLH1 cells were glucose starved for one hour before treated with 10mM D-glucose, oligomycin 2µM, and 2-Deoxyglucose (2-DG) 50mM, as indicated by the arrows. **A** is representative of 1 experiment, with at least 5 technical repeats. Error bars represent standard deviation. Glycolysis (**B**) is estimated upon the addition of saturating amounts of glucose. Glycolytic capacity (**C**) is the maximum ECAR rate reached by a cell following the addition of oligomycin which inhibits complex V effectively shutting down OXPHOS. The glycolytic reserve (**D**) was estimated by calculating the difference in ECAR between glucose and oligomycin injections. Non-glycolytic acidification was estimated upon the addition of 2-DG which is a competitive inhibitor of glucose and functions to shut down glycolysis. The bar charts of mitochondrial key parameters represent mean with standard error of mean of at least 3 independent experiments with 5 or more technical repeats. No asterix = not significant. *p<0.05.

3.4.3 MLH1-deficient cells depend on glutamine metabolism, in the absence of glucose

Studies have demonstrated that cells with mutations in their mtDNA, and OXPHOS dysfunction, can rewire their metabolism to compensate for energy defects, particularly the metabolism of amino acids, which feed into the TCA cycle [249]. Cancer cells are well-known to be highly glycolytic, as initially described by Otto Warburg. However, in addition to glucose dependency, some cancer cells display an increased dependence on extracellular glutamine, despite glutamine being a non-essential amino acid. Glutamine provides precursors for protein and nucleotide synthesis through donation of nitrogen and carbon [289]. Studies have shown that in glucose-deficient conditions, OXPHOS defective cells are not able to grow. Galactose is poorly utilised for glycolysis, yielding no net ATP. Given that we have observed an OXPHOS dysfunction upon MLH1 loss in our cells, we assessed whether our cells exhibited a similar phenotype with dependency on glutamine anaplerosis to support proliferation in the absence of glucose. To do this we cultured Ishikawa EV and MLH1 cells in glucose-free media, supplemented with 25mM Galactose. Since galactose is poorly utilised for glycolysis, glutamine becomes an essential energy source in these conditions (**FIGURE 3.11 A**). Interestingly, our data indicates that both Ishikawa EV and Ishikawa MLH1 cells proliferated at approximately half the rate in media without glucose but with galactose (GAL-DMEM), compared to their respective proliferation in full media (DMEM). Interestingly, supplementation with 6mM extra glutamine and 6mM dimethyl 2-oxoglutarate (DMK) (α-ketoglutarate; α-KG) had no effect on the proliferation of both cell lines in these conditions. The addition of 6mM glutamate, however, restored the rate proliferation of Ishikawa EV cells but not Ishikawa MLH1 cells (**FIGURE 3.11 B**). Under certain circumstances, glutamine may not be able to restore proliferation in the same way as glutamate as GLS1, the enzyme responsible for converting glutamine to glutamate, is the rate-limiting step for glutamine utilization and as such is prone to saturation [290]. Our data indicates that EC cells require glucose to proliferate efficiently but this reliance could be compensated for by the addition of glutamate in MLH1-deficient cells only.

We carried out the same experiment, culturing our MFE-280 gCTRL and MLH1 K/O cells in media without glucose, supplementing them in turn as before with 6mM extra glutamine, glucose and DMK (αKG). Both cell lines, regardless of MLH1 status, proliferated at the same rate in the presence and absence of glucose (**FIGURE 3.11 C**). We observed as previously (**FIGURE 3.3 A**) that MFE-280 MLH1 K/O cells proliferate slower than the gCTRL cells (**FIGURE 3.3 D**). Upon addition of 6mM glutamine, glutamate and α-KG, there was no significant change in proliferation in the MLH1 K/O cells. MFE-280 gCTRL cells also did not proliferate differently upon the addition of glutamine, glutamate, or α-KG (**FIGURE 3.11 C**). Our results imply that MFE-280 cell lines, in the absence or presence of MLH1, are not dependent on glutamine anaplerosis to generate ATP and support proliferation. These data

further suggests that MFE-280 cells do not have defective OXPHOS capabilities upon loss of MLH1 and is consistent with our previous data that demonstrates that MFE-280 MLH1 K/O cells do not have a reduction in Complex I activity (**FIGURE 3.8 C**) or expression (**FIGURE 3.5 A**) relative to the gCTRL cells. To explain this observation, we hypothesized that MFE-280 K/O cells could have an increased number of mitochondria. Previous studies have demonstrated that glycolytic suppression drives an increase in the number of mitochondria, measured by mitochondrial DNA content (cytochrome c oxidase subunit II) as they rely on mitochondrial OXPHOS for survival when glycolysis is supressed [291].

A

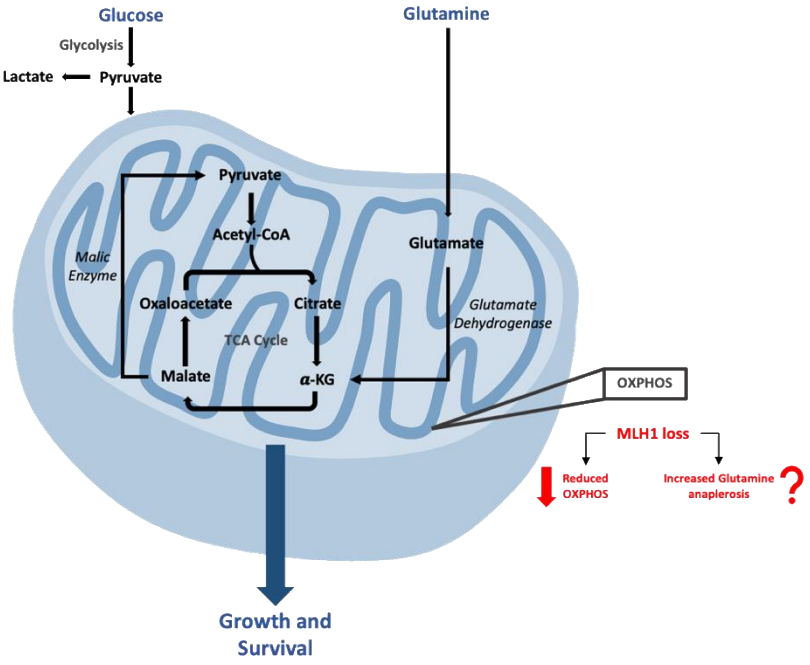

B

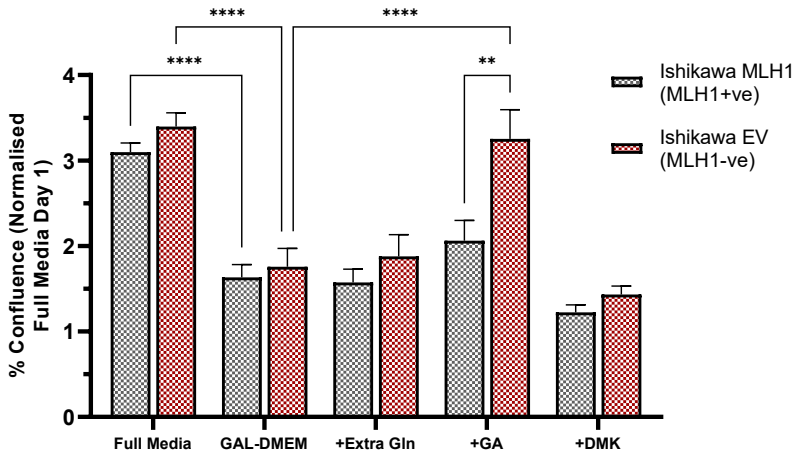

C

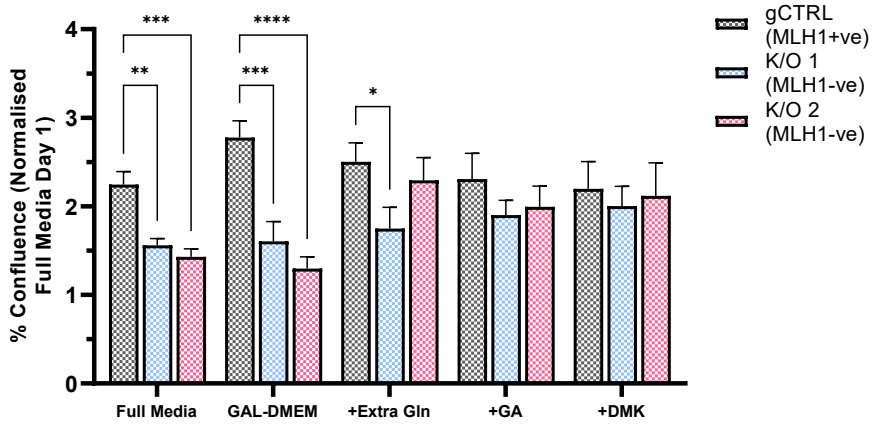

Figure legend on the next page.

FIGURE 3.11. Addition of glutamine, galactose and α-KG failed to rescue the proliferation rate of MFE-280 K/O cells. Schematic diagram of mitochondria (**A**) indicating the interplay between key metabolic pathways required for cell growth and survival including, Glycolysis, TCA cycle and Oxidative Phosphorylation (OXPHOS). MLH1 loss leads to reduced oxidative phosphorylation and potentially an increase in glutamine anaplerosis depending on the level of OXPHOS impairment. Percentage confluence of Ishikawa cells (**B**) and MFE-280 cells (**C**) grown in normal media (glucose-DMEM), media with 4.5mg/ml galactose no glucose (GAL-DMEM), and GAL-DMEM supplemented with 6mM extra glutamine (+Gln), 6mM glutamate (+GA) and 6mM DMK (+DMK). Percentage confluence was measured using the Incucyte S3 over 3 days and normalised to full media Day 1. Error bars represent mean with standard error of mean of at least 3 independent experiments. Statistical significance was determined using a TWO-WAY ANOVA with posthoc Holm-Sidak multiple Comparisons Test to MLH1-proficient control. *p<0.05, **p<0.01, ***p<0.001, ****p<0.0001. No asterix = not significant.

To further characterise the extent of glutamine dependency in our MLH1-deficient cell model we investigated the transcriptional and protein expression of key enzymes in glutamine anaplerosis. First, we assessed the potential contribution of the neutral amino acid transporter ASCT2, which plays a key role in glutamine uptake in rapidly proliferating cells [249]. We further investigated the expression of ASCT2 to glutamine uptake in our MLH1-deficient cell models by western blot analysis. To do this we isolated protein from our MLH1-deficient and proficient Ishikawa and MFE-280 cells and performed western blotting to assess the protein expression levels. Our data indicates that there was a significant upregulation of ASCT2 in the MFE-280 MLH1 K/O 2 cells (p=0.0021) relative to the gCTRL. There is also an increased trend in the MFE-280 MLH1 K/O 1 cells, although this observed difference was not significant (**FIGURE 3.12 A/B**). Interestingly, we observed no differences in ASCT2 protein expression level in the Ishikawa EV cells compared to the Ishikawa MLH1 expressing cells (**FIGURE 3.12 C/D**).

We also assessed the relative levels of transcripts encoding the cytosolic form of glutamate-oxaloacetate transaminase (GOT1). We isolated RNA from MHL1-deficient and -proficient Ishikawa and MFE-280 cells and assessed the RNA expression of the GOT1 gene by qRT-PCR analysis. Our data indicated a ~1.5-fold increase in expression of GOT1 mRNA levels in the MFE-280 MLH1 K/O cells relative to the gCTRL (**FIGURE 3.12 E**). There was no significant upregulation of GOT1 expression in the Ishikawa EV cells relative to Ishikawa MLH1 cells (**FIGURE 3.12 F**). We did not observe an increase in GOT1 protein expression in either isogenic MLH1 EC cell models suggesting that the increased mRNA was not translated to increased protein expression (**FIGURE 3.12 C/D**).

Next, we investigated whether nutrient stress conditions have a differential effect on the MLH1-proficient and deficient cell lines, by comparing their cell viability and rate of proliferation in media stripped of supplements i.e., containing no glucose, glutamine, or acetate. For this experiment, all cell lines were seeded in stripped media in 96-well plates, before being supplemented with glucose, glutamine, or acetate at the indicated concentrations, individually or in combination (**FIGURE 3.13 A**).

Cells were cultured with or without indicated nutrients for 3 days and cell viability was measured by CTG analysis. We did not observe many differences in cell viability, at day 3, however, we observed a significant reduction ($p<0.0001$) in cell viability and proliferation of the Ishikawa EV cells relative to the Ishikawa MLH1-expressing cells, in the absence of glutamine (**FIGURE 3.13 A/B**). There were no significant differences in cell viability between the MFE-280 gCTRL and K/O 1 cell lines in all growth conditions, however, the absence of a combination of glutamine, glucose and acetate reduced the cell viability of K/O 2 cell line. The differences we observed between K/O 1 and K/O 2 cell lines across nutrient stress conditions implies that these observations cannot be solely attributed to MLH1 loss, and it is likely that there are other unknown mutations contributing to the phenotype.

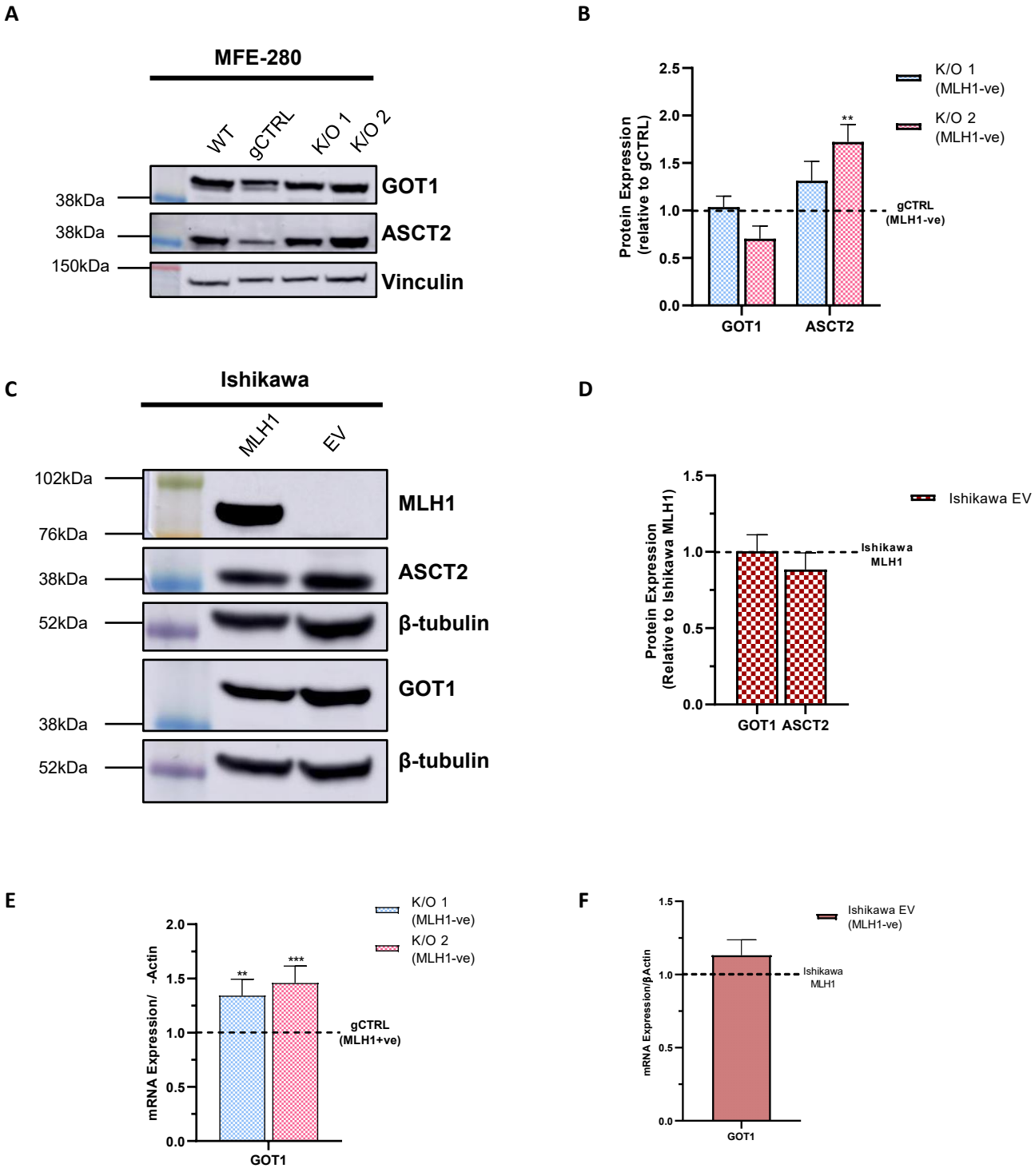

FIGURE 3.12. Variable expression of genes involved in amino acid metabolism in MLH1-deficient cell lines. Western blot analysis of protein isolated from MFE-280 **(A)** or Ishikawa **(C)** cells. Protein was extracted and expression analysed using anti-GOT1 or ant-ASCT2. Vinculin or β-tubulin was used as a loading control. Protein levels compared to MLH1-proficient control MFE-280 **(B)** or Ishikawa **(D)** cells estimated by band densitometry normalised to loading control. qRT-PCR analysis of RNA extracted from MFE-280 K/O **(E)** cells or Ishikawa **(F)**. mRNA expression was measured for GOT1. Error bars represent mean with SEM of at least 3 independent experiments. *p<0.05, **p<0.01, ***p<0.001, ****P<0.0001. No asterix = not significant.

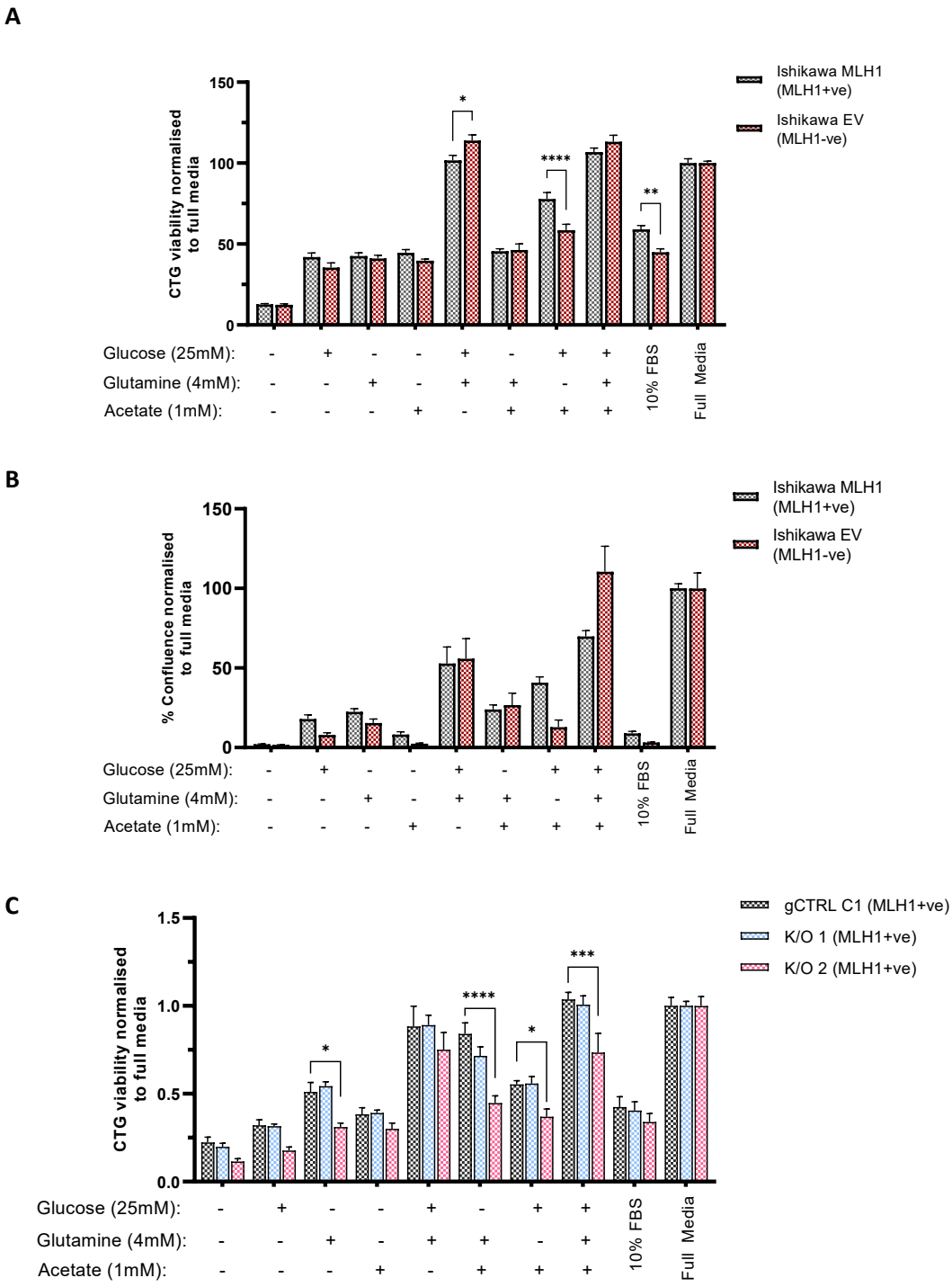

FIGURE 3.13. MLH1-deficient Ishikawa cells are less viable glutamine-deprived conditions. Cell viability was analysed with CTG at day 5 for Ishikawa EV, Ishikawa MLH1 **(A),** and MFE-280 **(C)** cells supplemented with Glucose (25mM), Glutamine (4mM) and Acetate (1mM). Percentage confluence was also measured for Ishikawa EV and MLH1 cells with the same supplements, using the Incucyte live-cell imaging platform (**B)** (normalised to full media, DMEM). Error bars represent mean with standard error of mean for at least 3 independent experiments. Statistical significance was determined using a TWO-WAY ANOVA with posthoc Holm-Sidak multiple Comparisons Test to MLH1-proficient control. *p<0.05, **p<0.01, ***p<0.001, ****p<0.0001. No asterix = not significant.

3.5 Transcriptomic analysis of MLH1-deficient cell models

Our data thus far suggests that MLH1-deficient cells can differentially express a number of mitochondrial and metabolic genes, potentially to proliferate. To gain a more global understanding of how MLH1 loss can influence gene expression in EC cells, we performed RNA sequencing on RNA extracted from the MFE-280 MLH1 K/O 1, MFE-280 gCTRL, Ishikawa EV and Ishikawa MLH1 cells.

3.5.1 Unsupervised clustering of RNA sequencing data

Initially, we performed unsupervised clustering of the different samples based on the gene expression profile of all detected genes. We carried out hierarchical cluster analysis (**FIGURE 3.14 A**), correlation heatmap (**FIGURE 14 B**) based on Pearson's correlation matrix, and principal component analysis (PCA) (**FIGURE 14 C**). PCA uses linear combinations of gene expression to define the new set of unrelated variables. Overall, there was a tight clustering of biological replicates in all sample groups (**FIGURE 3.14 A/B**). The correlation heat map indicates that the overall gene expression of Ishikawa MLH1 and Ishikawa EV is not strikingly different, whereas we observe clear differences in gene expression between the MFE-280 gCTRL and MLH1 K/O cell lines (**FIGURE 3.14 B**). Additionally, we observed a tight clustering between Ishikawa EV and Ishikawa MLH1 samples, whereas MFE-280 gCTRL and MLH1 K/O 1 have clear variation between the groups. The variation between these groups is described in PC2 (**FIGURE 3.14 C**), which accounts for 19% of the total variation within the data set. The PCA plot indicates that the largest amount of variation is observed between the Ishikawa and MFE-280 cell models, regardless of MLH1 status. This is a variation of 61%, illustrated in PC1 (**FIGURE 3.14 C**). Additionally, we investigated the distribution of overall gene expression in our samples (**FIGURE 3.14 D**). We observed minimal differences in the median and interquartile range between biological replicates and sample groups. Interquartile range gives an indication of the gene expression in the respective samples, whereas the median provides information on the regulation of those genes.

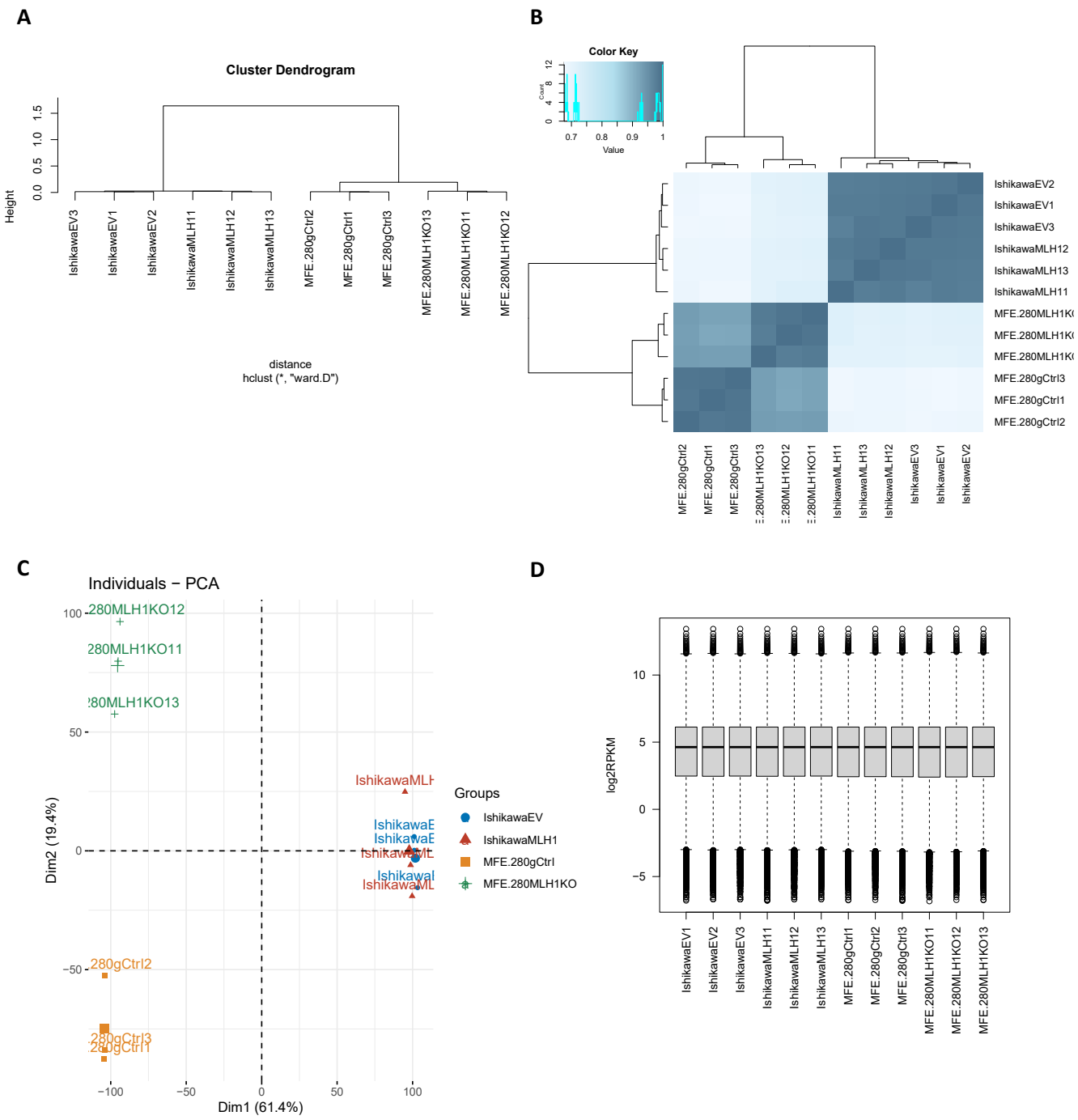

FIGURE 3.14. Unsupervised clustering of MLH1-deficient cell models. Unsupervised clustering of all genes by hierarchical cluster analysis **(A)**. Unsupervised clustering of all genes by correlation, heat map based on Pearson's correlation matrix **(B)**. Unsupervised clustering by principal component analysis **(C)**. Exploratory boxplot indicating the distribution of overall gene expression **(D)**.

3.5.2 Differential gene expression analysis of MLH1-deficient versus MLH1-proficient EC cells

Differential expression analysis was performed as described in section 2.11. A MA plot was generated as part of the differential analysis pipeline to illustrate the comparison between the respective MLH1-proficient and deficient cell lines. The MA plots show log2FC versus mean normalised counts for each gene in the contrast. Each dot represents a gene. The genes coloured in blue are those that were significantly up or downregulated in the contrast (Ishikawa EV vs. Ishikawa MLH1). Our data indicates that there are fewer genes differentially expressed between the Ishikawa EV and Ishikawa MLH1 cell lines (**FIGURE 3.15 A**) compared to the MFE-280 gCTRL and K/O 1 cell lines (**FIGURE 3.15 B**).

We used each respective MLH1-proficient cells as the control to compare the differential gene expression upon MLH1 loss (**TABLE 3.1**) and calculated the number of genes that were up or downregulated. In total, 3899 genes were significantly upregulated in MFE-280 K/O 1 versus MFE-280 gCTRL cells (padj. < 0.05) with a log2FC > 0 in expression. In total, 3740 genes were significantly downregulated in MFE-280 K/O 1 versus MFE-280 gCTRL cells (padj. < 0.05) with a log2FC < 0 in expression. In total, 217 genes were significantly upregulated in the Ishikawa EV versus Ishikawa MLH1 cells (padj. < 0.05) with a log2FC > 0 in expression. In total, 382 genes were significantly downregulated in in Ishikawa EV versus Ishikawa MLH1 (padj. < 0.05) with a log2FC < 0 in expression.

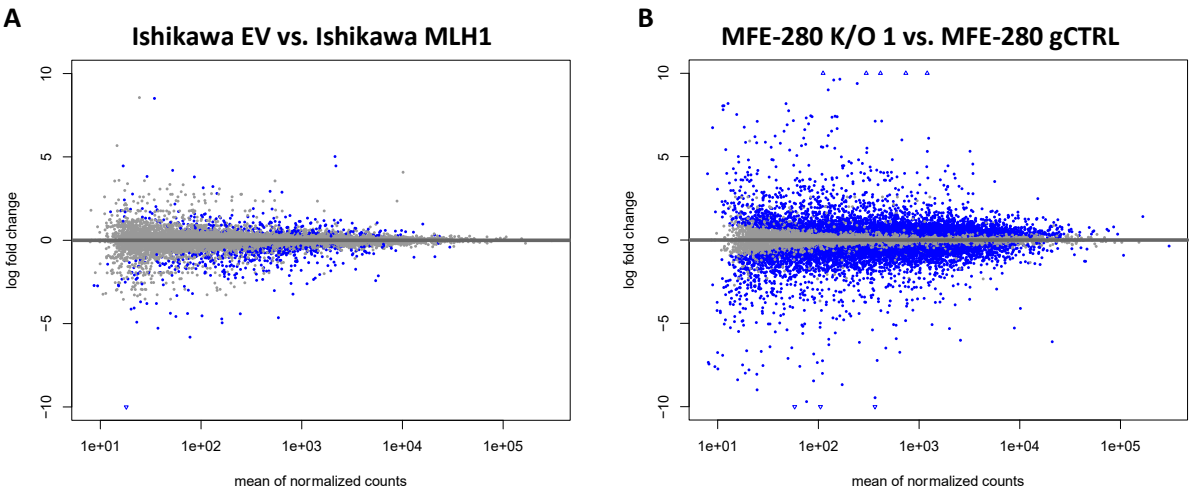

FIGURE 3.15. MA plots demonstrating the number of differentially expressed genes in each MLH1-deficient cell model. Differential expression (DE) analysis was performed in DESeq2 using the wald test. MA plots from DE analysis indicate log2foldchange versus mean normalised counts for each gene in the contrast. The blue genes are those with a *padj*<0.05 for MLH1-deficient Ishikawa **(A)** and MFE-280 **(B)** cells.

TABLE 3.1. Number of differentially expressed genes in MLH1-deficient cell models

	Ishikawa EV vs. Ishikawa MLH1	MFE-280 K/O 1 vs. MFE-280 gCTRL
padj<=0.05 & log2FC > 0 (Upregulated in MLH1-defient)	217	3899
padj<=0.05 & log2FC < 0 (Downregulated in MLH1-deficient)	382	3740

Furthermore, we analysed the correlation of the gene expression fold changes between MLH1-deficient and MLH1-proficient cells to identify overlaps in differentially expressed protein-coding genes (padj. <= 0.05 and $\log_2$FC > 1) (**FIGURE 3.16**). We identified 8 upregulated and 33 down regulated genes in common in the MLH1-deficient Ishikawa EV cells and the MFE280 MLH1 KO*1 cells.

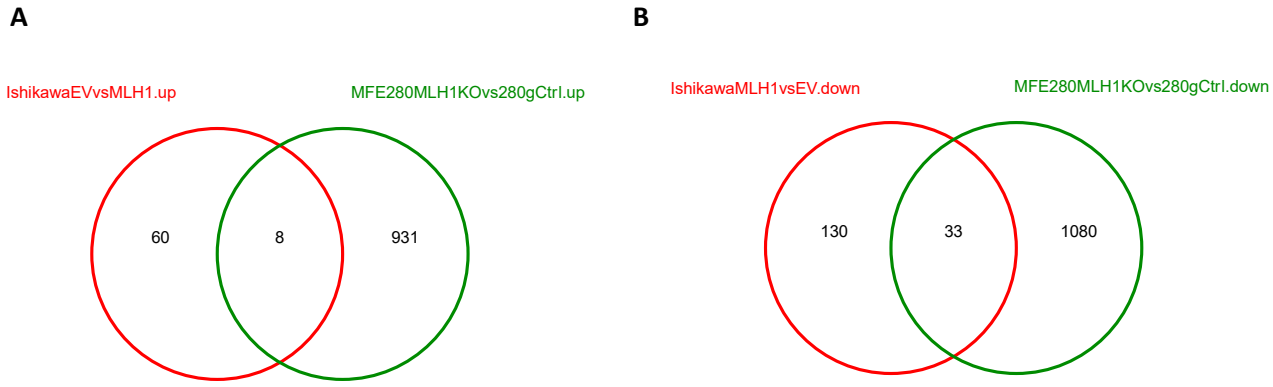

FIGURE 3.16. Correlation of gene expression in MLH1-deficient cell models. Analysis of the significantly upregulated genes in the MLH1-deficient cells **(A)** and significantly downregulated genes in the MLH1-deficient cells **(B)**. Overlaps of differentially expressed protein-coding gene indicated in Venn diagrams. padj$\leq$ 0.05 and $\log_2$FC>1.

3.5.3 Identification of differentially expressed pathways in MLH1-deficient MFE-280 cells

We next performed gene set enrichment analysis using Gene Pattern with ranked DESeq2 Wald statistic of all the genes. The analysis was performed for whole canonical pathways and gene ontology biological processes [292]. Ranked t-statistic is useful for determining the statistical significance of the mean rank of log fold change in gene expression, between two sample groups where standard errors were moderated across genes. Extracting biological meaning from mRNA expression profiles is challenging. A common approach involves focussing on a handful of statistically significant differentially expressed genes, however analysing single genes may miss important effects on pathways. Cellular processes often affect sets of genes acting in concert [293]. We identified pathways that were up and downregulated in the different MLH1-deficient cell models, as well as those that were common between both. The enrichment score (ES), normalised enrichment score (NES), p value (p-val) and adjusted p-value (p-adj) were reported for each gene set. We analysed the NES and p-adj value, which illustrates the statistical significance of the enrichment score for each gene set. Here, I have discussed the top 5 pathways which are up and downregulated in each MLH1-deficient cell model. In addition, I discuss the effect of MLH1 deficiency on the expression of genes involved in MMR, OXPHOS, Glycolysis and Gluconeogenesis, and the TCA cycle.

Our data showed the following canonical pathways and gene ontologies (as determined by the Gene Pattern software) were downregulated to the greatest extent in MFE-280 K/O 1 cells. 1) miRNA targets in extracellular matrix (ECM) and membrane receptors, 2) Regulation of phospholipase C activity, 3) Regulation of morphogenesis of an epithelium, 4) Cell migration and invasion through P75NTR, 5) Mesenchymal to epithelial transition (**TABLE 3.2**). Aberrant miRNA activities are prevalent in diverse tumour types, though how they regulate cancerous processes is not always clear. Increasing evidence has demonstrated that cells deficient for miRNA biogenesis have abnormal cell cycle checkpoints and DNA repair [294], with studies implicating many miRNAs such as miR-24, miR-21, miR-146, miR-421 and miR-373, in the DDR [295]. Our data suggests there is a previously unidentified link between MLH1 loss in EC cells and the regulation of miRNA targets in the ECM. Furthermore, the regulation of phospholipase C was the second most downregulated pathway. Phospholipases are a family of phospholipid metabolising enzymes that catalyse the breakdown of phospholipids into biologically active lipid mediators which control several physiological cell functions. Phospholipases are categorised into four groups based on the type of reaction they catalyse. Phospholipase C's (PLC) have been extensively studied in cancer however their regulatory roles in the oncogenic process are not fully understood [296]. Though there no association has been identified between MLH1 deficiency in

EC and PLC activity or expression, PLC's have been implicated in the DNA damage repose. For instance, PLCε expression facilitates DNA repair in bladder cancer by regulating ATM/EXO1 signalling [297].

Moreover, a study has demonstrated that loss of PLC-β3 leads to the development of neuroendocrine tumours [298], and transfecting PLCB3 to a human endocrine pancreatic tumour cell line induced the activation of the human mismatch repair protein 3 gene [298]. More recently, Ghosh *et al*. demonstrated PD-L1 physically binds with and enhances activation of PLC-γ1 by EGFR, and once stimulated PLC-γ1 activates calcium flux, Rho GTPases, and protein kinase C, collectively promoting an aggressive phenotype in NSCLC [299]. Given there is a strong correlation between PD-L1 expression and MMR deficiency in EC [300, 301] this could provide an explanation for the more aggressive phenotype observed in MLH1 deficient EC.

Interestingly, all five of these pathways are linked to the maintenance of cellular integrity or are involved in the regulation of cellular processes determining cell motility, cell transformation, differentiation, and cell growth. Tissues are dynamically structured by bidirectional communication between resident cells and the extracellular matrix (ECM). The ECM is a major structural component of the tumour microenvironment and is comprised of a network of biochemically distinct components including fibrous proteins, glycoproteins, proteoglycans, and polysaccharides [302]. The structure of the ECM is highly dynamic and is continuously remodelled with components being deposited, degraded or modified [303]. Previous studies have linked oxidative stress and DNA damage to changes in the expression of extracellular matrix components. The interplay between oxidative stress and DNA damage, and ECM remodelling is bidirectional and mutations in ECM components can also trigger oxidative stress and induce DNA damage [304]. Moreover, mutations in genes encoding ECM components or molecules that bridge the ECM to the cytoskeleton lead to mitochondrial dysfunction, a driving force for ROS accumulation [304]. These data implies that there may be a direct link between loss of MLH1 and the downregulation of pathways involved in ECM homeostasis. Future studies are required to characterise the intermediates involved, and the link between MMR-deficiency and ECM remodelling.

TABLE 3.2. Top 5 downregulated pathways in the MFE-280 K/O cells

Pathway	Size	ES	NES	p-val	p-adj
miRNA targets in ECM and membrane receptors	17	-0.76884	-2.14212	0.000109	0.00463
Regulation of phospholipase C activity	30	-0.67373	-2.10412	3.82E-05	0.003
Regulation of morphogenesis of an epithelium	45	-0.60367	-2.06443	4.68E-05	0.003136
Cell migration and invasion through $p75^{NTR}$	28	-0.66091	-2.05127	0.000328	0.00929
Mesenchymal to epithelial transition	16	-0.76032	-2.03704	0.00022	0.0093

Our data showed the following canonical pathways and gene ontologies (as determined by the Gene Pattern software) were upregulated to the greatest extent in MFE-280 MLH1 K/O 1 cells. 1) The role of GTSE1 in G2/M progression after G2 checkpoint, 2) Separation of sister chromatids, 3) APC/C:Cdh1 mediated degradation of Cdc20 and other APC/C:Cdh1 targeted proteins in late mitosis/early G1, 4) APC/C mediated degradation of cell cycle proteins, 5) Mitochondrial translational termination (**TABLE 3.3**). Interestingly, the top four upregulated pathways are involved in the mediation of components directly involved in the cell cycle, or regulation of cell cycle progression itself. Previous studies have demonstrated a role for MMR in signalling cell cycle arrest. These demonstrate how MMR proteins recognise and signal DNA damage cell cycle arrest and apoptosis, and highlight how MMR-deficient cells are defective in cell cycle arrest in response to multiple types of DNA damaging agents [61]. Furthermore, there is an upregulation in mitochondrial translation termination. Mitochondrial protein translation abnormalities are associated with a wide range of diseases, including cancer, cardiovascular diseases, and nervous system diseases. Mitochondrial translation includes initiation, elongation, termination, and ribosome-recycling stages [302]. Mammalian mitochondrial ribosomes synthesise proteins essential for ATP production via OXPHOS in a process requiring a series of mitochondrial factors. These include two initiation factors, three elongation factors, a release factor, and two ribosome recycling factors which are all necessary for mitochondrial translation. Deficiency or mutation in any of these factors leads to abnormal mitochondrial translation and a series of metabolic disorders [302, 305]. These data demonstrates that MLH1-deficient cells harbour mitochondrial defects that may affect their ability to generate ATP, which is consistent with our hypothesis and preliminary data.

TABLE 3.3. Top 5 upregulated pathways in the MFE-280 K/O cells

Pathway	Size	ES	NES	p-val	p-adj
The role of GTSE1 in G2/M progression after G2 checkpoint	70	0.630588	2.386666	4.63E-09	2.06E-06
Separation of sister chromatids	78	0.579524	2.21736	1.34E-07	0.000159
APC/C:Cdh1 mediated degradation of Cdc20 and other APC/C:Cdh1 targeted proteins in late mitosis/early G1	181	0.502716	2.19286	3.25E-10	1.93E-07
APC/C mediated degradation of cell cycle proteins	72	0.568668	2.173506	9.38E-07	0.000149
Mitochondrial translational termination	86	0.550528	2.153028	9.66E-07	0.000149

3.5.4 Identification of differentially expressed pathways in the MLH1-deficient Ishikawa EV cells

We carried out a similar analysis for our MLH1-deficient Ishikawa EV cell model and our data showed the following canonical pathways and gene ontologies (as determined by the Gene Pattern software) were downregulated to the greatest extent in Ishikawa EV cells compared to Ishikawa MLH1 expressing cells. 1) Calcium dependent cell-cell adhesion via plasma membrane cell adhesion molecules, 2) Endocrine hormone secretion, 3) Negative regulation of axon extension involved in axon guidance, 4) Positive regulation of stress fibre assembly, 5) Neuron projection extension involved in neuron projection guidance (**TABLE 3.4**). Interestingly, four out of five of these pathways are involved in cell migration, or regulating cellular response to a stimulus. The most downregulated pathway 'Calcium dependent cell-cell adhesion via plasma membrane cell adhesion molecules', involves the attachment of one cell to another via adhesion molecules that require the presence of calcium for the interaction. Maintenance of normal cell-cell adhesion and cell-ECM interactions are important for maintaining homeostasis in normal tissues. Cell adhesion molecules mediate these distinct interactions and can be classified into four main groups: cadherins, integrins, selectins and immunoglobins. These molecules are mostly transmembrane receptor proteins widely express by particular immune cells [306]. Though not previously reported on, this result suggests downregulation of calcium dependent cell-cell adhesion may be a consequence of MLH1 loss in EC. In vertebrates, mitochondria act as Ca^{2+} storage sites [307]. Park *et al.* demonstrated the main driving force for mitochondrial Ca^{2+} uptake is the mitochondrial membrane potential generated by the activity of the ETC [307]. Altered ETC activity has been associated with reduced mitochondrial Ca^{2+} accumulation. Jana *et al.* demonstrated that knockdown of both complex I assembly factor NDUFAF3 and complex II catalytic subunit SDHA reduce mitochondrial Ca^{2+} fluxes and mitochondrial respiration [308]. If the reduced complex I activity in MLH1-deficient Ishikawa cells significantly reduces Ca^{2+} flux, this could provide an explanation for the downregulation of this pathway.

Moreover, 'Negative regulation of axon extension involved in axon guidance' is involved in any process that stops, prevents, or reduces the frequency, rate or extent of axon extension involved in axon guidance. Axon guidance molecules regulate cell migration and apoptosis in normal and tumorigenic tissues. Previous studies have demonstrated that specific axon guidance molecules play an important role in tumourigenesis [309]. Though there has been no specific link with MLH1 loss, mitochondria play a key role in meeting axonal energy demand by generating ATP through oxidative phosphorylation, supplying the majority of energy required [310]. Mitochondria generate ~93% of ATP in presynaptic terminals, whereas glycolysis contributes the remaining 7% [311], hence Sobieski *et al*. found that simultaneous inhibition of both glycolysis and OXPHOS results in the complete inhibition of evoked synaptic transmission [312]. Given that Ishikawa EV cells have a reduction in OXPHOS this could explain why there is a deregulation of this pathway in this cell line.

Furthermore, 'positive regulation of stress fibre assembly', describes any process that activates or increases the frequency, rate, or extent of the assembly of a stress fibre, a bundle of microfilaments, and other proteins found in fibroblasts. The formation of stress fibres is characteristic of mesenchymal-migrating cells. Studies demonstrate that this stress fibre assembly regulates mesenchymal cell migration, depending on the stress fibre subtype [313], however, no studies have described a link between MMR deficiency or reduced OXPHOS and the assembly of these fibres. Our data evidences a novel association that should be explored further in both EC and other cancers. Overall, the gene expression analysis in Ishikawa EV cells suggests that in the absence of MLH1 there is a downregulation of pathways involved in cellular and tissue homeostasis, which could be a direct or indirect consequence of MMR deficiency.

TABLE 3.4. Top 5 downregulated pathways in the Ishikawa MLH1-deficient cells.

Pathway	Size	ES	NES	p-val	p-adj
Calcium dependent cell-cell adhesion via plasma membrane cell adhesion molecules	27	-0.7487637	-2.1525996	9.53E-06	0.00336458
Endocrine hormone secretion	28	-0.7196809	-2.1047569	1.63E-05	0.0048158
Negative regulation of axon extension involved in axon guidance	25	-0.7242761	-2.0646834	0.00010931	0.01765821
Positive regulation of stress fibre assembly	45	-0.6463909	-2.0575523	2.69E-05	0.00735289
Neuron projection extension involved in neuron projection guidance	34	-0.6742011	-2.0218359	0.0001655	0.01930114

Furthermore, we looked at the significantly upregulated pathways in our Ishikawa cell model and our data showed the following canonical pathways and gene ontologies (as determined by the Gene Pattern software) were upregulated to the greatest extent in Ishikawa EV cells. 1) Axoneme assembly, 2) Cilium movement, 3) Microtubule bundle formation, 4) PPAR alpha pathway, 5) Cilium or flagellum dependent cell motility (**TABLE 3.5**). Interestingly four of these pathways are related to cellular motility and/ or microtubule formation. 'Axoneme assembly', refers to the assembly and the organisation of an axoneme, the bundle of microtubules and associated proteins that forms the core of the cilia in eukaryotic cells, and is responsible for their movements. 'Cilium movement' describes the self-propelled movement of a cilium. 'Microtubule bundle formation' is the process that results in a parallel arrangement of microtubules in the formation centrioles. Microtubules are highly dynamic, and are involved in cell movement, intracellular trafficking, and mitosis. Changes in microtubule stability have been reported in a range of cancers, and are often associated with poor prognosis and chemotherapeutic resistance [314]. Moreover, 'Cilium or flagellum dependent motility' which describes cell motility due to movement of eukaryotic cilia or bacterial-type or archaeal-type flagella, was also upregulated in the MLH1-deficient Ishikawa cells. Cilia and flagella are microtubule-based organelles and play important roles in tissue patterning in development, and inherited mutations affecting core ciliary components lead to a group of syndromes known as ciliopathies [315]. Though not specifically linked to MMR, a study by Ma *et al.* demonstrated DNA double strand breaks (DSBs) actively promoted microtubule dynamics, which they titled the DSB-induced microtubule dynamics stress response, and lead to genomic instability [316]. Our data suggests MMR deficiency caused by MLH1 loss, could have a similar effect on microtubule dynamics, however, more research is required to characterise this relationship.

Furthermore, the 'PPAR alpha pathway' is upregulated in MLH1-deficient Ishikawa cells. Peroxisome proliferator-activated receptors (PPARs) are nuclear hormone receptors that are activated by fatty acids and their derivatives [317]. PPARs function to clear circulating or cellular lipids via the regulation of gene expression involved in lipid metabolism in liver and skeletal muscle. There are three subtypes of PPARs, PPARα, PPARβ/δ and PPARγ. PPARβ/δ is involved in lipid oxidation and cell proliferation, whereas PPARγ promotes adipocyte differentiation to enhance blood glucose uptake, whereas PPARα is involved with the transcriptional regulation of genes involved in beta-oxidation, metabolism, and fatty acid transport [318]. Moreover, upon activation, PPARα restricts mitochondrial OXPHOS and increases the production of ROS causing the accumulation and exacerbation of oxidative stress in the mitochondria. This increases the oxidation of fatty acids while potentially inhibiting glycolysis, further reducing ATP production [318]. Upregulated PPARα signalling could provide an explanation for the reduced OXPHOS observed in MLH1-deficient Ishikawa cells. Overall, the pathway analysis data implies that MLH1-deficient Ishikawa cells upregulate pathways involved in cellular migration and cell motility. Furthermore, the upregulation of PPARα pathway which plays a key role in metabolism implies a link between MMR deficiency and metabolism which warrants further investigations.

TABLE 3.5. Top 5 upregulated pathways in the Ishikawa MLH1-deficient cells

Pathway	Size	ES	NES	p-val	p-adj
Axoneme assembly	48	0.66109776	2.39469886	3.14E-07	0.00041776
Cilium movement	85	0.57365979	2.29443315	2.20E-08	7.81E-05
Microtubule bundle formation	78	0.5688663	2.26344121	3.53E-07	0.00041776
PPAR alpha pathway	17	0.7745926	2.1489542	2.77E-05	0.02138365
Cilium or flagellum dependent cell motility	63	0.55382885	2.11257926	8.61E-06	0.00336458

3.5.5 Differential expression of genes in Ishikawa EV cells that are in involved OXPHOS, glycolysis, gluconeogenesis, and the TCA cycle

Given that our main interest in studying MLH1 loss in these two *in vitro* cell models was to investigate the link between MMR deficiency and cellular metabolism, we specifically studied the expression of genes involved in OXPHOS, glycolysis, gluconeogenesis, and the TCA cycle. The differential analysis included genes involved each indicated pathway as per the gene sets derived from the WikiPathways database. The enrichment analysis of the MMR pathway indicated that MLH1 loss does not significantly influence the MMR pathway as a whole, as both of our MLH1-deficient cell models do not show a significant change in expression upon MLH1 loss. The NES for MFE-280 K/O 1 versus gCTRL was -1.3 with a padj value of 0.3 and for Ishikawa EV versus Ishikawa MLH1 was 0.5 with a padj value of 1. The log fold changes for the specific genes that were included in the core enrichment analysis are indicated in **FIGURE 3.17**. The most significantly downregulated genes upon MLH1 loss in MFE-280 cells are PMS2 and POLD1 (padj. < 0.0001). It is not unsurprising that PMS2 expression is reduced upon loss of MLH1 as previous studies have demonstrated that PMS2 is destabilized when MLH1 is degraded [319-322]. However, mutations in polymerase δ (POLD1) which is one of the main enzymes that replicate eukaryotic DNA along with POLE are quite rare in EC [323, 324]. Given there is no information in the literature that demonstrates a link between MLH1 loss and POLD1 reduced expression or destabilization, our data may be the first to implicate a relationship in EC.

Moreover, the expression of other key members of the MMR pathway such as MSH2, MSH6, MSH3 and PMS1 are unchanged. Moreover, RFC4 (padj. < 0.0001) and RFC5 (padj. < 0.0002) are the two most significantly upregulated genes. Though RFC4 and RFC5 have not been linked to loss of MLH1 in the literature, Zhang *et al.* have recently demonstrated that RFC4 is upregulated during the transition from higher-grade squamous intraepithelial lesions to cervical squamous cell carcinoma (SCC) and has been proposed as an independent prognostic biomarker for SCC [325]. It is possible that this is the first identified link between MLH1 loss and increased RFC expression in EC, though in other cancers it is associated with poor prognosis. This demonstrates that loss of MLH1 results in a significant downregulation of a step of the MMR pathway but does not significantly influence the expression of all genes across the pathway. Interestingly, in the Ishikawa MLH1-deficient cells there are no significant differences in gene expression across the gene set for the MMR pathway. It is important to remember how these models were generated and how they differ, however, we did not observe a significant reduction in MLH1 RNA expression particularly in Ishikawa EV cells, though it is undoubtedly observed at protein level (**FIGURE 3.2**). Ishikawa cells harbour no detectable mutation in the MLH1 gene, nor is the MLH1 promoter methylated [278]. The differences in gene expression we observed in both of our EC cell models suggests that the driving factor for protein has an impact on the resulting

phenotype. This offers an explanation as to why we observed different mitochondrial phenotypes in MLH1-deificent cell lines (Ishikawa EV and MFE-280 K/Os).

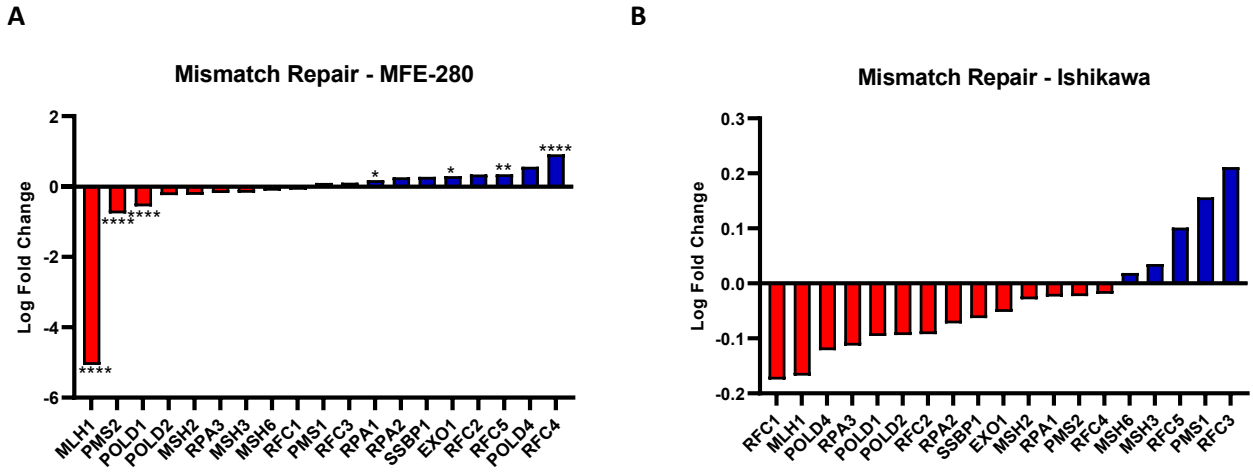

FIGURE 3.17. Gene set enrichment analysis for the mismatch repair pathway. Gene set enrichment analysis was performed for the mismatch repair pathway on Gene Pattern using ranked t-statistic of genes involved in the pathway, derived from Gene Ontology pathway database. Log fold change of the gene expression for those involved in the pathway is illustrated for MFE-280 MLH1-defcient cells **(A)** and Ishikawa MLH1-deficient cells **(B)**. **padj*<0.05, ***padj*<0.0021, ****padj*<0.0002, *****padj*<0.0001.

3.5.6 Genes involved in OXPHOS were upregulated in MFE-280 K/O cells

Next, we looked at the differential analysis of genes involved in the mitochondrial electron transport system as per the gene set derived from the WikiPathways database. From the enrichment analysis, the mitochondrial ETC system is significantly upregulated upon MLH1 loss in our MFE-280 cells, however, no significant differences are observed in our Ishikawa cell model. The NES for MFE-280 K/O 1 versus gCTRL was 2.03 with a padj value of 0.0005 and for Ishikawa EV versus Ishikawa MLH1 was 0.6 with a padj value of 1. The log fold changes for the specific genes that were included in the core enrichment analysis are indicated in **FIGURE 3.18.** Interestingly, although we hypothesised that upon MLH1 loss we would observe a mitochondrial phenotype characterised by reduced OXPHOS and a reduced capacity to respond to increased energy demands, this RNA-seq data supports the contrary. In the MLH1-deficient MFE-280 cells, the expression of genes involved in the mitochondrial electron transport system were increased above a threshold (FDR-adjusted p value <0.05 and NES >0) resulting in a statistically significant upregulation of the whole pathway. These data provides an explanation for our results which indicated that MLH1 loss in MFE-280 cells is not associated with a reduced complex I activity despite reduced expression of the OXPHOS complex II-V. Once again, in the Ishikawa MLH1-deficient cells there are no significant differences in gene expression across the gene set for the ETC system in mitochondria, despite observing a reduction in complex I expression and activity. This may imply that a process is occurring post transcriptionally to cause this phenotype.

A

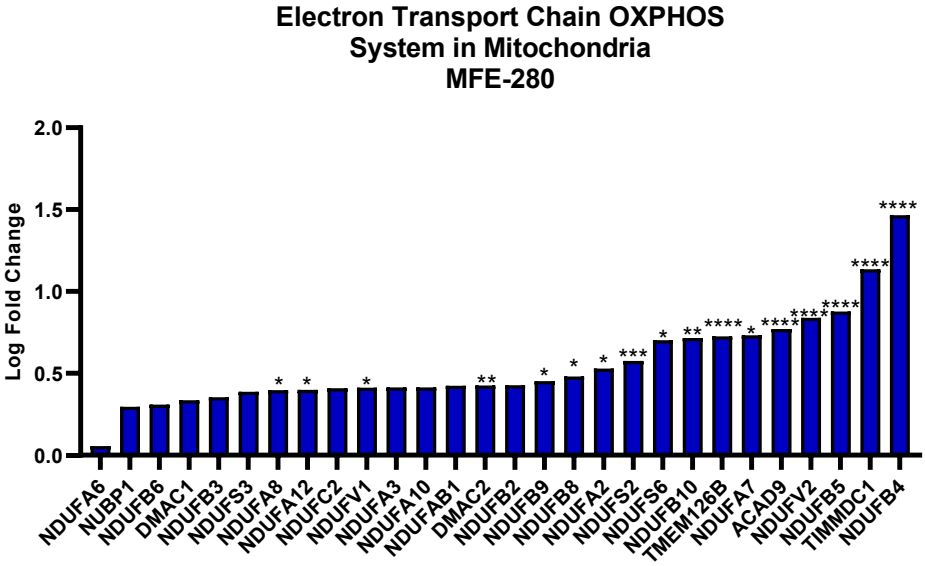

B

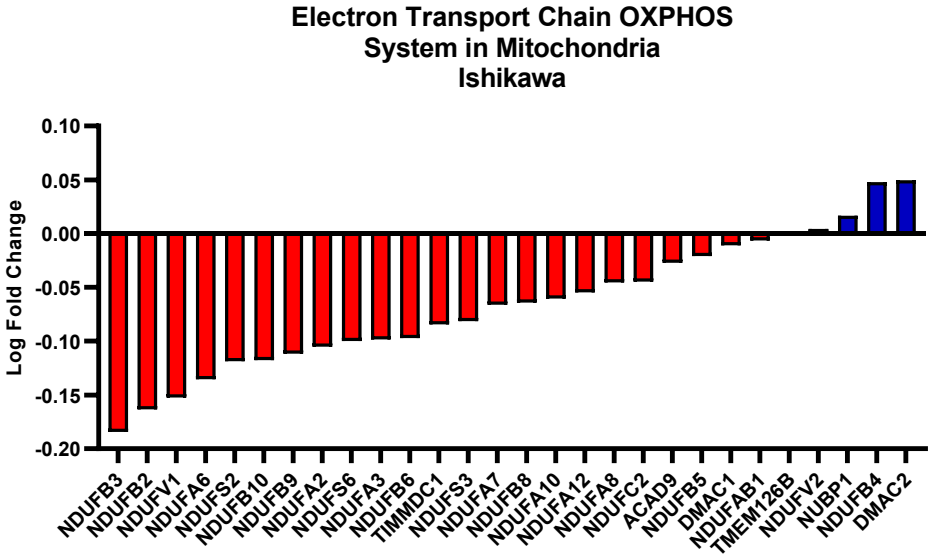

FIGURE 3.18. Gene set enrichment analysis for mitochondrial electron transport chain system. Gene set enrichment analysis was performed for the ETC pathway on Gene Pattern using ranked t-statistic of genes involved in the pathway, derived from Gene Ontology pathway database. Log fold change of the gene expression for those involved in the pathway is illustrated for MFE-280 MLH1-defcient cells **(A)** and Ishikawa MLH1-deficient cells **(B)**. **padj*<0.05, ***padj*<0.0021, ****padj*<0.0002, *****padj*<0.0001.

3.5.7 Several genes involved in Glycolysis and Gluconeogenesis were upregulated in our MLH1-deficient cell models

Next, we looked at the differential expression of genes involved in glycolysis and gluconeogenesis as per the gene set derived from the WikiPathways database. The enrichment analysis showed no significant differences in the glycolysis and gluconeogenesis pathway upon MLH1 loss in our MFE-280 and Ishikawa cell models. The NES for MFE-280 K/O 1 versus gCTRL was 1.37 with a padj value of 0.31 and for Ishikawa EV versus Ishikawa MLH1 was 1.15 with a padj value of 0.7. The log fold changes for the specific genes that were included in the core enrichment analysis are indicated in **FIGURE 3.19.** Here, loss of MLH1 results in a significant downregulation of certain genes involved in the glycolytic pathway. Notably, solute carrier family 2 facilitated glucose transporter member 1 (SLC2A1) (padj. < 0.0001) which provides instructions for producing the glucose transporter protein GLUT1. This protein is embedded in the outer membrane of surrounding cells and is responsible for the uptake of glucose into cells. Additionally, DLAT and PDHA1 (padj. <0.0001) encode components of the multi-enzyme pyruvate dehydrogenase complex (PDC). PDC resides in the inner mitochondrial membrane and catalyses the conversion of pyruvate to acetyl coenzyme A. The metabolism of pyruvate is the start of a series of reactions in the production of ATP, the cells main energy source. Alongside, there is a significant decrease in the expression of PCK1 (padj. < 0.0001), which is the rate-limiting enzyme of gluconeogenesis converting oxaloacetate and GTP into phosphoenolpyruvate and CO_2. Altering glucose metabolism provides cancer cells with a metabolic advantage and flexibility to fuel their biosynthetic requirements. A downregulation of PCK1 is associated with poor prognosis with studies having shown that PCK1 negatively regulates cell cycle progression by activating AMPK and delaying G1 to S phase transition [326]. In both our MLH1-deficient cell models we observe a significant upregulation in the expression of phosphofructokinase platelet (PFKP) (padj. <0.0001 MFE-280 MLH1 K/O1; padj. = 0.041), the platelet isoform of phosphofructokinase-1 (PFK-1), which functions as an important mediator of cell metabolism. Accumulating evidence has demonstrated that PFKP plays a crucial role in promoting aerobic glycolysis and lactate production in breast cancer cells, thereby stimulating cancer cell proliferation and metastasis [327]. As a result, there is accumulating interest in investigating whether PFKP could be used as a diagnostic marker or a drug target in cancer therapy. PFKP catalyses the irreversible conversion of fructose-6-phosphate to fructose-1,6-bisphosphate and is the first rate-limiting step in glycolysis. Though a causative link between PFKP expression and EC has not been published in the literature, a study by Fan *et al.* has illustrated how breast cancer is characterised by high PFKP expression and poor prognosis [327]. Given accumulating evidence suggests PFKP promotes aerobic glycolysis, cancer cell proliferation and metastasis in breast cancer, we hypothesise similar could be occurring in EC [327]. Interestingly, the Ishikawa cells have an upregulation in SLC2A1 expression (padj. < 0.0001), a key regulator of glycolysis. High expression of

SLC2AL and LDHA have been implemented in early carcinogenesis and tumour progression in cancer [328]. Consequently, our data points towards a relationship between MLH1 loss and altered glucose metabolism, however, loss of MLH1 does not uniformly affect the expression of all genes involved in the metabolic pathway across both cell models.

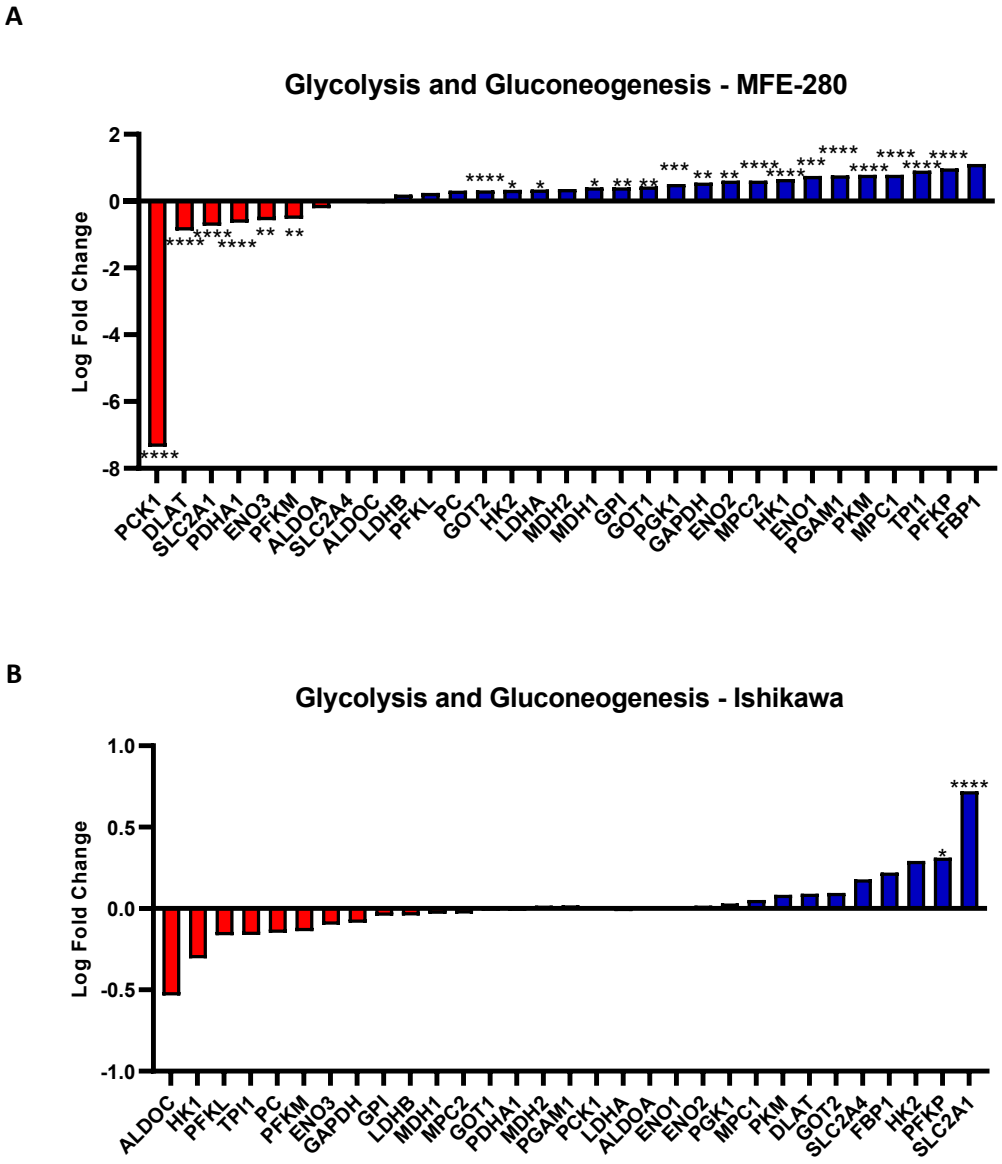

FIGURE 3.19. Gene set enrichment analysis for glycolysis and gluconeogenesis metabolic pathway. Gene set enrichment analysis was performed for the glycolysis and gluconeogenesis on Gene Pattern using ranked t-statistic of genes involved in the pathway, derived from Gene Ontology pathway database. Log fold change of the gene expression for those involved in the pathway is illustrated for MFE-280 MLH1-defcient cells **(A)** and Ishikawa MLH1-deficient cells **(B)**. **padj*<0.05, ***padj*<0.0021, ****padj*<0.0002, *****padj*<0.0001.

3.5.8 Genes involved in the TCA cycle were upregulated in our MLH1-deficient cell models

Next, we looked at the differential analysis of genes involved in the TCA cycle as per the gene set derived from the WikiPathways database. Gene enrichment analysis showed no significant differences in the TCA cycle upon MLH1 loss in our MFE-280 or Ishikawa cell models. The NES for MFE-280 K/O 1 versus gCTRL was 1.43 with a padj value of 0.29 and for Ishikawa EV versus Ishikawa MLH1 was 1.25 with a padj value of 0.65. The log fold changes for the specific genes that were included in the core enrichment analysis is indicated in **FIGURE 3.20.** Notably, MFE-280 MLH1-deficient cells have a significant downregulation in the expression of SDHD (padj. <0.0001), a tumour suppressor responsible for synthesising one of the four subunits of the succinate dehydrogenase (SDH) enzyme. Within the mitochondria, the SDH enzyme links both OXPHOS and the TCA cycle. In the TCA cycle, SDH converts succinate to fumarate, in the process of releasing electrons which are transferred through SDH subunits to the OXPHOS pathway, required to produce ATP. The most significantly upregulated genes in MFE-280 K/O 1 cells were IDH2 (padj. = 0.0006) and SDHB (padj. < 0.0001). Isocitrate dehydrogenase 2 (IDH2) is the mitochondrial enzyme that catalyses the metabolic conversion of isocitrate to α-KG in the TCA cycle. Overexpression of IDH2 is an indicator of poor outcome in lung cancer through the stimulation of the Warburg effect to maintain cancer cells through hypoxia inducible factor 1 α (HIF1 α) [329]. SDHB encodes another subunit of the SDH enzyme. Interestingly, SDHB downregulation is a predisposing factor of aerobic glycolysis and cancer progression [330]. Moreover, the MLH1-deficient Ishikawa cells have an increased expression of the SUCLA2 gene (padj. < 0.0001) which encodes the ATP-forming beta subunit of TCA cycle enzyme, succinate-CoA ligase. This enzyme is most active in tissues that require large amounts of energy [331]. Some studies have demonstrated that succinate-CoA ligase interacts with nucleoside diphosphate kinase, to produce and maintain the building blocks of mtDNA, which is essential for normal energy production within cells [332, 333].

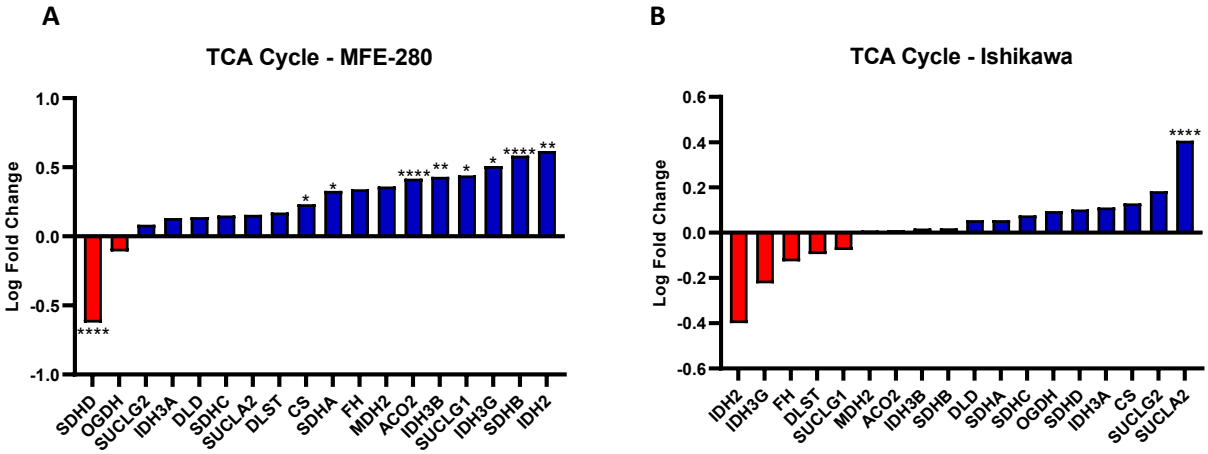

FIGURE 3.20. Gene set enrichment analysis for the TCA cycle. Gene set enrichment analysis was performed for the TCA pathway on Gene Pattern using ranked t-statistic of genes involved in the pathway, derived from Gene Ontology pathway database. Log fold change of the gene expression for those involved in the pathway is illustrated for MFE-280 MLH1-defcient cells **(A)** and Ishikawa MLH1-deficient cells **(B)**. **padj*<0.05, ***padj*<0.0021, ****padj*<0.0002, *****padj*<0.0001.

3.6 Conclusion

In conclusion, we successfully generated two distinct MLH1-deficient EC cell models to use *in vitro* to investigate whether MLH1 loss influences cellular metabolism. MFE-280 cells underwent CRISPR-cas9 gene editing to introduce a mutation into the MLH1 gene and generate two distinct MLH1 K/O MFE-280 cell lines. In MLH1-deficient Ishikawa cells, we stably introduced an MLH1 expressing plasmid to generate our second isogenically paired cell line. These five cell lines were subsequently used to investigate whether MLH1 loss is the driver of a specific metabolic phenotype in an EC setting. As it has been demonstrated that MLH1 loss is associated with a perturbed mitochondrial metabolism [175], we investigated whether this was the case in both of our models. Interestingly, we identified that while MLH1-deficiency does influence cellular metabolism in both models, the specific effects are not uniform. In the absence of MLH1, Ishikawa cells display a reduction in Complex I expression and activity, alongside a likely increased dependency on glutamine anaplerosis. In the MLH1-deficient MFE-280 cell lines, we observe the opposite, particularly in K/O 1, which harbours an increased Complex I activity and an upregulation in expression of genes involved in mitochondrial metabolism and OXPHOS, determined via RNAseq. This information implies that MLH1 loss may not be the sole driver of metabolic rewiring in this setting or could highlight the drawbacks of using *in vitro* cell models for studying metabolism. It would be interesting to profile the expression of metabolic genes in MLH1-deficient endometrial tumours to see what whether there is a correlation in patient data. Additionally, generating more MLH1-deficient pairs of cell lines would help us understand whether these changes

are MLH1-specific, EC-specific, or both. Moreover, there are better assays for investigating metabolic rewiring *in vitro* such as, stable isotope tracing of glucose and glutamine.

4.0 Results – Investigating the Metabolic Flux of MLH1-deficient and -proficient Ishikawa EC Cells using Stable Isotope Tracing

4.1 Quantification of Differential Changes in Metabolite Levels upon MLH1 Loss through Labelled Glutamine Tracing

4.1.1 MLH1-deficient Ishikawa cells have differential levels of metabolites involved in the glycolysis, the TCA cycle, and the urea cycle

To investigate whether MLH1-deficient EC cells have a distinct metabolic signature, we carried out a targeted metabolomics study, looking at specific metabolic intermediates of glycolysis, TCA cycle, glutaminolysis, urea cycle and both essential and nonessential amino acids. Ishikawa EV and MLH1 cells were cultured for 24 hours in DMEM medium, supplemented with 2mM ^{13}C-glutamine, before being harvested for metabolite extraction (~85% confluence on harvest). Five technical replicates were performed for accuracy. Metabolites were extracted in a solution composed of 50% methanol, 30% acetonitrile, 20% ultrapure water and 50ng/ml HEPES. 1ml of extraction solution was added per 1x10^6 cells. Extraction was carried out in a dry ice/methanol bath to maintain the integrity of the metabolites. Dr Valle Morales performed the LC/MS separation and analysis by calculating the ratio of the abundance of each metabolite normalised to total ion count (TIC). Using this data, I determined the fold change of each metabolite in Ishikawa EV and MLH1 cells to determine whether there were any significant differences.

We analysed the levels of ~30 steady state metabolites which are involved in glycolysis, TCA cycle, urea cycle, glutaminolysis and both essential and nonessential amino acids. Additionally, due to the heavy labelling of glutamine generated by culturing our cells in media containing 2mM ^{13}C-glutamine, we also studied whether alterations in glutamine flux occurred in MLH1-deficient cells. Glutamine is a major carbon donor to the metabolites of the TCA cycle. **FIGURE 4.1 A** illustrates the fate of $^{13}C_5$-glutamine in the first round of the TCA cycle. ^{12}C atoms are represented by white circles, whereas ^{13}C-atoms are represented by blue circles. Oxidative metabolism generates M+4 citrate, M+4 succinate, M+4 fumarate, M+4 malate, and M+4 oxaloacetate, whereas reductive carboxylation generates M+5 citrate, M+3 oxaloacetate, M+3 aspartate, M+3 malate, and M+3 fumarate.

The heat maps in **FIGURE 4.1** illustrate the contribution of ^{13}C atoms to each metabolite regardless of isotopic labelling pattern (**FIGURE 4.1. B**), and metabolite abundance at steady state (**FIGURE 4.1. C**), in Ishikawa MLH1 and Ishikawa EV cells. Both heat maps depict the fold change between Ishikawa EV cells versus their isogenically-matched MLH1-proficient Ishikawa cells. We did not identify any striking

differences in specific pathways upon MLH1 loss, when looking at the overall contribution of label to each metabolite. The only significant differences we identified were in succinate and glycine ($p<0.0001$). In MLH1-deficient EV cells, there was a significant increase in incorporation of ^{13}C from glutamine into succinate, and a significant decrease in incorporation of ^{13}C from glutamine into glycine, in MLH1-deficient EV cells (**FIGURE 4.1 B**). Additionally, differential levels of metabolites upon MLH1 loss were identified when looking at steady metabolite levels (**FIGURE 4.2**) (i.e., ratio of abundance of each metabolite/ TIC). Here we observe an increase in the levels of amino acids such as glycine, arginine, isoleucine, leucine, citrulline, in the MLH1-deficient Ishikawa cells, and a decrease in levels of serine, glutamine, malate, and asparagine, along with reductions in TCA cycle intermediates such as glutamate and α-KG (discussed further later in this section). **FIGURE 4.4/4.5** illustrate the differences in the levels of individual isotopomers for each metabolite between Ishikawa EV and MLH1 cells, and the significance of the differences in metabolite abundance.

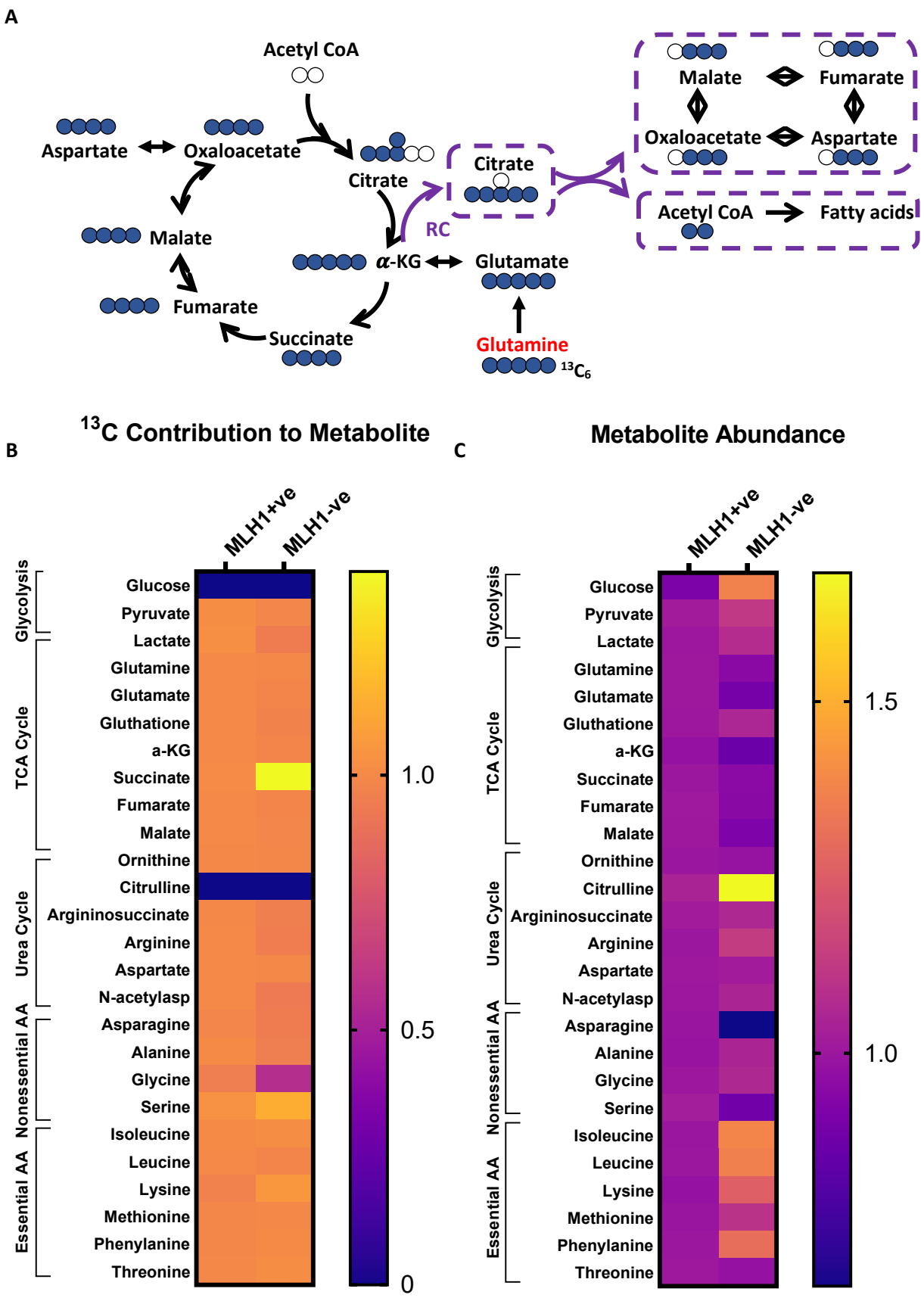

Figure legend on the next page.

FIGURE 4.1. Metabolite abundance and glutamine flux alterations upon MLH1 loss in EC cells. ^{13}C glutamine isotope tracer was used to analyse glutamine metabolism in Ishikawa cells. Ishikawa EV and Ishikawa MLH1 cells were cultured in DMEM with 2mM ^{13}C glutamine. Cells were harvested for metabolite detection. Schematic diagram (**A**) indicates the flux of glutamine through the TCA cycle and beyond, resulting in the incorporation of glutamine tracer into various metabolites. ^{13}C labelled and unlabelled carbons are indicated in blue and white respectively, that would result following one round of the TCA cycle. Purple box indicative of labelled intermediates produced by reductive carboxylation. Heat map (**B**), produced by GraphPad Prism, of total labelled carbon contribution and heat map (**C**), total metabolite abundance. Columns are median-centred, with fold changes compared to MLH1-proficient cells represented by colour (Yellow, higher abundance; Blue, lower abundance). These data highlight that there are minimal differences between the incorporation of label into TCA cycle intermediates suggesting MLH1-deficient do not increase glutamine flux to support proliferation in the absence of proficient OXPHOS.

The analysis of steady state metabolites identified differences in the intermediates of a number of metabolic pathways (**FIGURE 4.2**). Interestingly MLH1-deficient EV cells had significantly less glutamine and glutamate compared to the MLH1-proficient Ishikawa cells. This could be indicative that these cells have upregulated their glutaminolysis pathway and therefore are utilising glutamine and glutamate at a faster rate. Alternatively, it could be that in the absence of MLH1 these cells are less dependent on glutaminolysis to support proliferation and therefore their levels do not need to be sustained. Moreover, Ishikawa EV cells also have less α-KG and Malate, although comparative levels of other TCA cycle intermediates (**FIGURE 4.2**). Under certain circumstances, primary rate limiting step of the TCA cycle is the formation of α-KG by oxidative decarboxylation of isocitrate [249]. Our data could indicate that in the absence of MLH1 this reaction is slower relative to MLH1-proficient cells, or once again that in the absence of MLH1 these cells are more dependent on these intermediates therefore metabolise them at a faster rate. We also observe a reduction in malate levels, alongside an increase in pyruvate levels in Ishikawa EV cells. Malate is exported from the mitochondria and can be recycled to pyruvate catalysed by malic enzyme. This reduction in malate alongside an increase in pyruvate could be due to an increase in this reaction.

Furthermore, we also identified significant changes in the levels of certain essential and nonessential amino acids that were examined after culturing the cells in $^{13}C_5$-glutamine labelled media for 24 hours. Ishikawa MLH1-deficient EV cells had significantly higher levels of citrulline ($p<0.0001$), arginine ($p=0.0226$), glycine ($p=0.0371$), isoleucine ($p<0.0001$), and leucine ($p<0.0001$), relative to Ishikawa MLH1 cells, whereas they have significantly lower levels of asparagine ($p<0.0001$) and serine ($p=0.0082$). Amino acids facilitate the proliferation and survival of cancer cells and are crucial for the synthesis of building blocks, including proteins, nucleic acids, and lipids. For instance, serine is a one-carbon source in nucleotide synthesis and DNA methylation and has been identified to be involved in cancer progression [334]. In the absence of MLH1, Ishikawa EV cells have significantly reduced levels

of serine, but more glycine which indicated that Ishikawa EV cells could potentially be metabolising serine at an increased rate. These data provides further evidence that MLH1-deficient cells have a distinct metabolic signature, though further investigations are required to see whether this phenotype is specific to MLH1 loss in EC or whether these changes are caused by indirect effects.

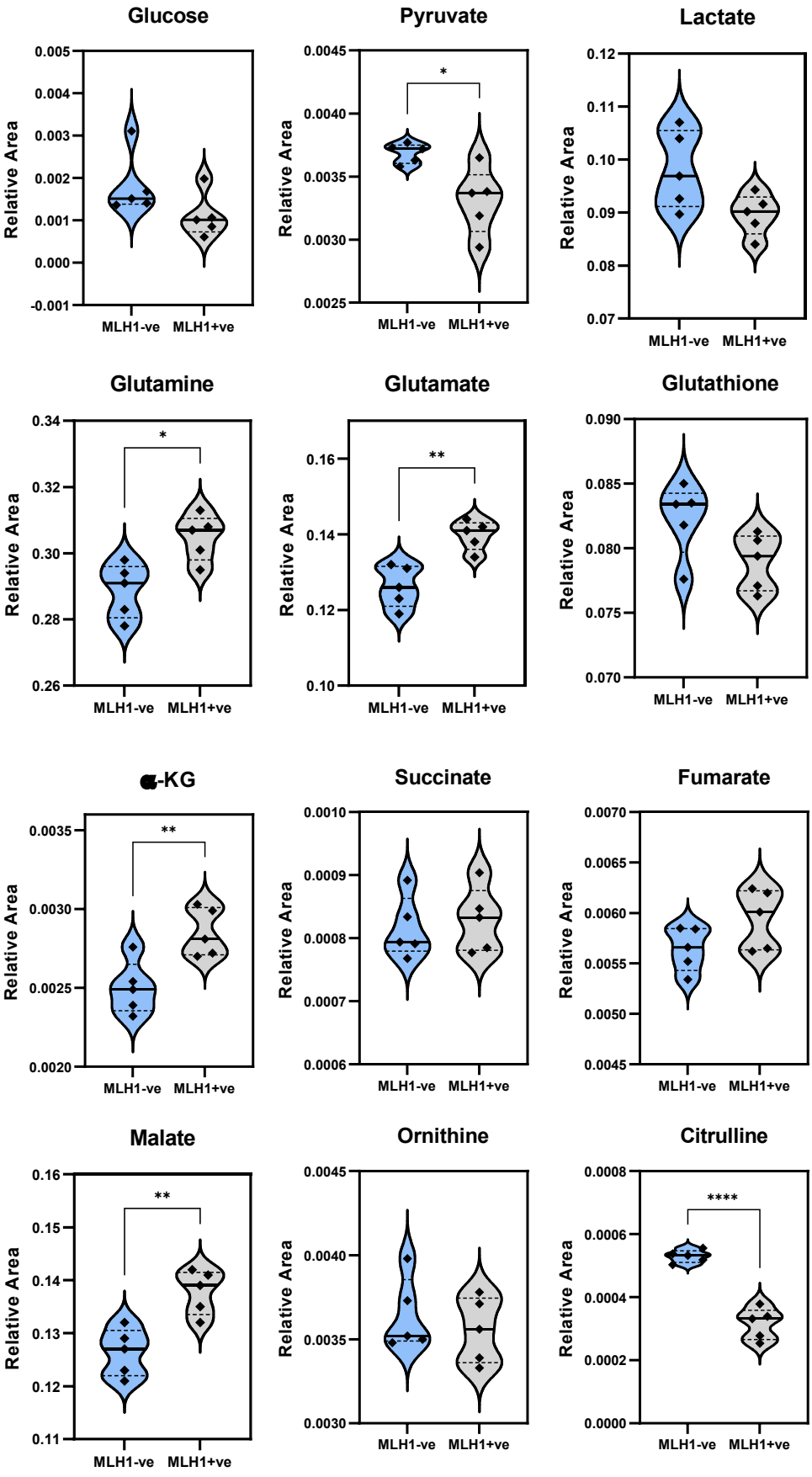

Figure continues…

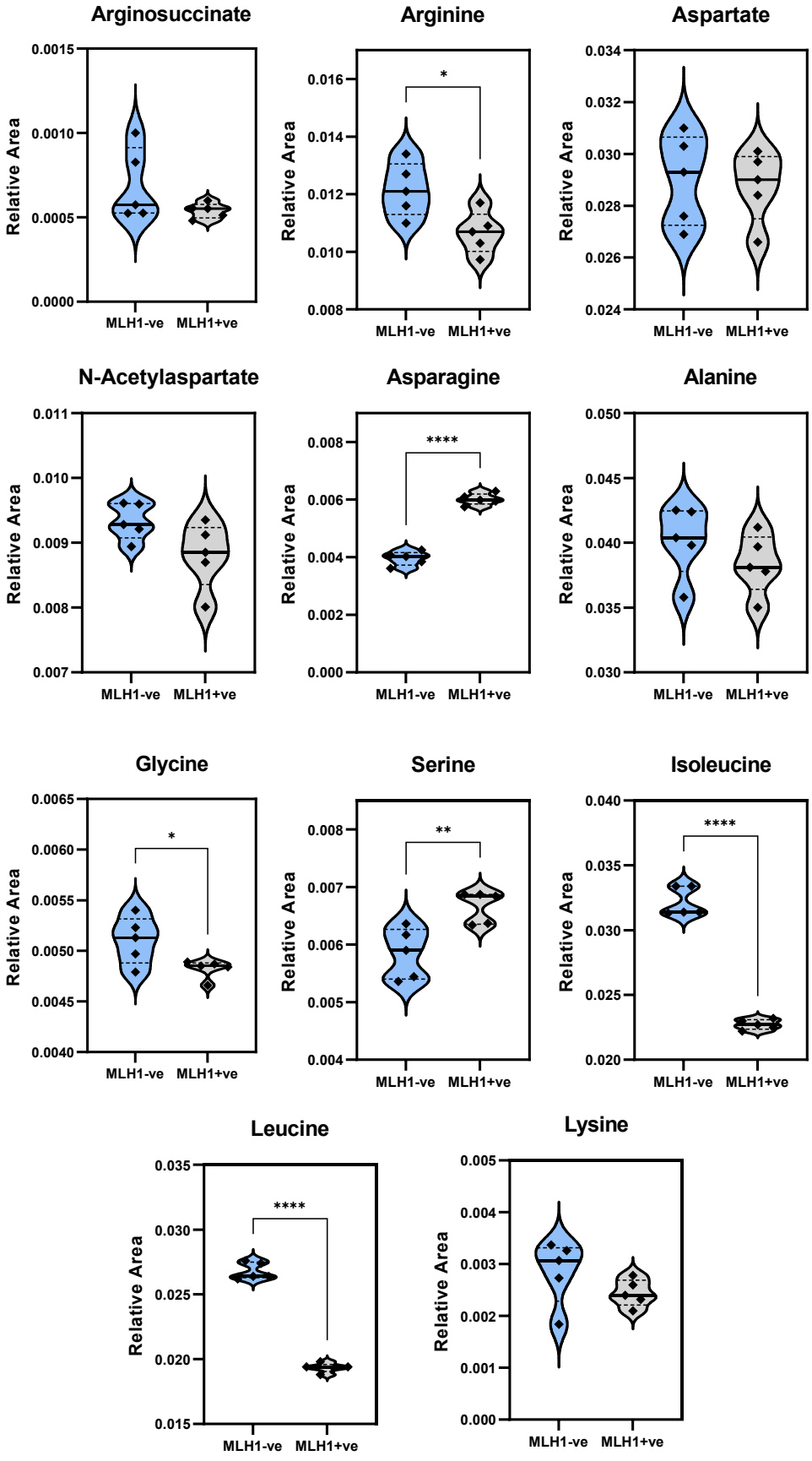

Figure legend on the next page.

FIGURE 4.2. Quantification of metabolites in targeted metabolomics analysis of MLH1-proficient and deficient Ishikawa cells. Graphs represent the relative levels for individual metabolite involved in glycolysis, the TCA cycle, urea cycle, as well as other essential and nonessential amino acids. MLH1 deficient cells have an altered metabolic signature with increased pyruvate and lactate levels implying increased anaerobic activity in the absence of proficient OXPHOS. MLH1-deficient cells also have decreased levels of serine alongside increased levels of glycine, which are crucial amino acids for sustaining one carbon metabolism, and of high clinical relevance. Statistical significance was determined using a multiple t-tests with posthoc Holm-Sidak multiple Comparisons Test to Ishikawa MLH1. *P<0.05, **P<0.01, ***P<0.001, ****P<0.0001. No asterix = not significant.

4.1.2 Metabolic tracing of ^{13}C from glutamine demonstrates that MLH1-deficient Ishikawa cells differentially modulate metabolic pathways

Our targeted metabolomics analysis identified that MLH1-deficient Ishikawa cells differently modulate the metabolism of certain amino acids and metabolic intermediates involved in glutaminolysis and the TCA cycle. To understand more about the metabolic rewiring taking place in MLH1-deficient cells, we performed a metabolic flux analysis using $^{13}C_5$-glutamine. Due to the heavy labelling of glutamine, we were able to detect the fraction of metabolites that incorporated one or more labelled carbons, therefore enabling us to detect metabolites which were synthesised directly from $^{13}C_5$-glutamine. We harvested Ishikawa EV and Ishikawa MLH1 cells for metabolite detection that had been cultured for 24 hours in DMEM supplemented with 2mM of $^{13}C_5$-glutamine. The fractional contribution of glutamine-derived isotopomers was calculated for each metabolite, in each cell line, and statistical comparisons were performed versus Ishikawa MLH1. To put the alterations in metabolite levels into perspective upon MLH1 loss, we have displayed the results as pathways according to known metabolite conversions as described in the literature.

Firstly, the TCA cycle. Glutamine enters the TCA cycle following its conversion to glutamate and subsequently α-KG. In this experiment, one round of oxidative metabolism in the TCA cycle of $^{13}C_5$-glutamine would generate M+4 succinate, malate, aspartate, citrate, and aconitate, due to the incorporation of four 13C atoms in each of these species. In contrast, reductive carboxylation would generate M+5 aconitate and citrate or M+3 oxaloacetate, aspartate, malate, and fumarate. By determining the isotopologue distribution, and the abundance of ^{13}C enrichment in specific metabolic intermediates, we can accurately study whether there are alterations in glutamine metabolism in MLH1-deficient cells. M+5 glutamine accounts for approximately 92% of the total fraction of metabolite in both cell lines. As this is the majority, we can accurately study the downstream incorporation of ^{13}C into metabolites. First, glutamine undergoes deamidation catalyzed by glutaminase, resulting in the conversion of glutamine to glutamate and the release of ammonium. Interestingly, Ishikawa EV cells have significantly less M+5 glutamate compared to Ishikawa MLH1 cells; 81% compared to 84% ($p<0.0001$) (**FIGURE 4.3**). While statistically significant, it is important to

note that statistical significance only indicates that an observed difference or effect is unlikely to have occurred by random chance, however, the magnitude of the observed effect may be too small to have consequences in a biological context. This, accompanied by the data indicating that there is less glutamine and glutamate in Ishikawa EV cells (**FIGURE 4.2**), could suggest that there is a reduced rate of glutamine conversion to glutamate upon MLH1 loss in Ishikawa EV cells, which is unexpected. This trend is also true for M+5 α-KG where the fraction is 83% for Ishikawa EV cells versus 86% for Ishikawa MLH1 ($p<0.0001$). Subsequently, oxidative TCA cycle metabolism would generate M+4 succinate, fumarate, and malate. The M+4 fraction of Ishikawa EV cells is significantly smaller than that for Ishikawa MLH1, further supporting the hypothesis that these cells have reduced oxidative metabolism relative to MLH1-proficient cells. Reductive carboxylation would produce M+3 malate, fumarate, oxaloacetate, and aspartate. Ishikawa EV cells also have significant reductions in these fractions relative to the Ishikawa MLH1-proficient cells (**FIGURE 4.3**). Interestingly, Ishikawa EV cells have significantly more M+3 fraction of α-KG (8% versus 5%; $p<0.0001$) and subsequent M+2 fractions of succinate (6% versus 4%; $p=0.046$), fumarate (7% versus 6%; $p=0.0001$), and malate (8% versus 6%; $p<0.0001$), compared to Ishikawa MLH1 cells. These fractions are generated from subsequent rounds of the TCA cycle and although statistically significant, do not account for a large proportion of labelling in the whole metabolite. As such, it is hard to determine whether these changes are biologically relevant. Nonetheless, we also saw changes in aspartate fractions thus investigated downstream pathways from this metabolite.

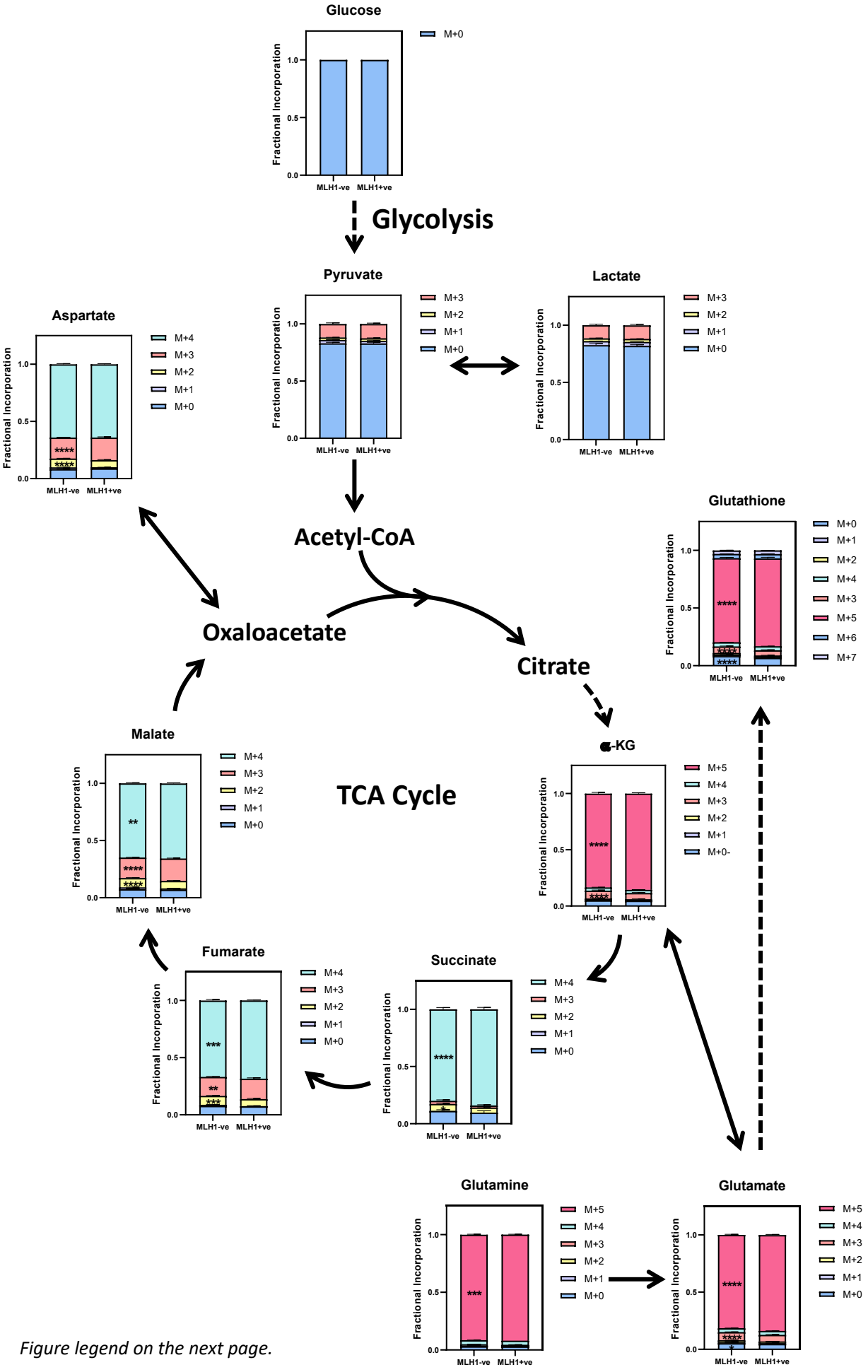

Figure legend on the next page.

FIGURE 4.3. Fractional contribution of labelled glutamine to metabolic intermediates involved in the TCA cycle upon MLH1 loss. Ishikawa EV and MLH1 cells were cultured in DMEM supplemented with 2mM ^{13}C-glutamine. Cells were harvested for metabolite detection. Each metabolite isotopomer is normalised to the total ion content of the sample. Fractional contribution is calculated by adding the fraction of the different 13C-labelled isotopomers and normalising them to the total amount of each metabolite in the sample. Schematic diagram of glutamine metabolism through the TCA cycle, is arranged with graphs according to known metabolite conversions as described in the literature. Statistical significance was determined using multiple t-tests with posthoc Holm-Sidak multiple Comparisons Test to Ishikawa MLH1. **P*<0.05, ***P*<0.01, ****P*<0.001, *****P*<0.0001. No asterix = not significant.

Subsequently, we investigated the aspartate metabolic pathway which connects the TCA cycle (via oxaloacetate), the urea cycle (via arginosuccinate) and the polyamine metabolic pathways (via methionine and dcSAM). Accordingly, the graphs in **FIGURE 4.4** illustrate how these pathways are linked using information from the literature. An essential function of glutamine metabolism is to supply aspartate to the cytosol where it can be used for nucleotide and protein synthesis [335]. We identified that MLH1-deficient cells had higher levels of aspartate (**FIGURE 4.2**) although not statistically significant. Looking at carbon flux we observe labelling in ~92% of aspartate demonstrating that the carbons have stemmed from glutaminolysis and TCA cycle flux of $^{13}C_5$-glutamine. Interestingly, although there was no change in the M+4 isotopologue of aspartate between cell lines, there was statistically less M+3 fraction of Ishikawa EV cells compared to Ishikawa MLH1 cells (18% versus 20%; p<0.0001), and an increase in the M+2 isotopomer (8% versus 6%; p<0.0001; **FIGURE 4.4**). If MLH1 loss was directly affecting aspartate efflux in these cells, we would expect to see changes in the M+4 fraction i.e., the isotopologue generated from the first round of the TCA cycle. Given that MLH1 loss does not affect aspartate levels (**FIGURE 4.2**), taken together, these data implies that MLH1 loss does not directly impact aspartate synthesis. The small reductions in M+2 and M+3 isotopomers could be indicative that the ^{13}C labelled carbon from glutamine is preferentially directed to other metabolic intermediates upon MLH1 loss. Nonetheless, although it is difficult to determine the biological relevance of small changes with metabolic tracing alone, these data further supports the notion that MLH1-deficient cells rewire aspects of their metabolism to support proliferation.

Next, we looked at N-acetyl aspartate (NAA). NAA is a molecule generated from aspartate and acetyl-CoA and is an abundant metabolite detected in the brain. Several studies have demonstrated that the increase of NAA levels in several cancer types has been associated with a worse overall prognosis, as it is thought to have a role in promoting tumour growth [336-340]. In our Ishikawa EV cells, approximately 91% of NAA was labelled, versus 93% for Ishikawa MLH1 cells. This indicates that the majority of incorporation of ^{13}C in NAA comes from $^{13}C_5$-glutamine. Interestingly, we observe the most significant differences in the M+4 isotopologue of NAA (35% EV versus 29% MLH1; p<0.0001). The

majority of M+4 NAA would be generated from M+4 citrate. As well as the altered carbon flux in Ishikawa EV cells, we also observe an increase in the relative levels of aspartate and NAA in MLH1 deficiency, although this difference is not statistically significant (**FIGURE 4.4**).

The other significant difference we observed in this network was the increase in the M+2 fraction of arginosuccinate in MLH1-deficient cells (7% Ishikawa EV versus 5% Ishikawa MLH1; p=0.016) (**FIGURE 4.4**), alongside a decrease in M+3 fraction (19% EV versus 23% MLH1; p=0.0068). Moreover, ~91% of Ishikawa EV is labelled with carbons derived from C^{13} glutamine versus ~94% Ishikawa MLH1. Arginosuccinate synthetase (ASS) catalyses the condensation of citrulline and aspartate to form arginosuccinate, the precursor to arginine. We observe no differences in the abundance of citrulline or arginosuccinate in Ishikawa EV cells (**FIGURE 4.2**), although they have significantly more arginine (**FIGURE 4.2**). Arginine is a major regulator of mitochondrial activities in cancer metabolism and is involved in cellular processes such as proliferation, cell signalling and the synthesis of other amino acids for instance [341]. Interestingly, arginine-deprived cancer cells exhibit mitochondrial dysfunction [342]. A study by Chen *et al.* demonstrated that arginine acts as an epigenetic regulator that modulates histone acetylation resulting in the global upregulation of nuclear-encoded OXPHOS genes, and hence regulates mitochondrial function [343]. MLH1-deficient Ishikawa cells potentially upregulate arginine synthesis to overcome their deficits that result from reduced complex I activity. If further research confirms MLH1-deficient EC cells are dependent on arginine metabolism for survival, this could be therapeutically targeted. Analysis of metabolites further downstream of the aspartate metabolism pathway identified no statistically significant differences in Ishikawa EV cells versus Ishikawa MLH1 cells.

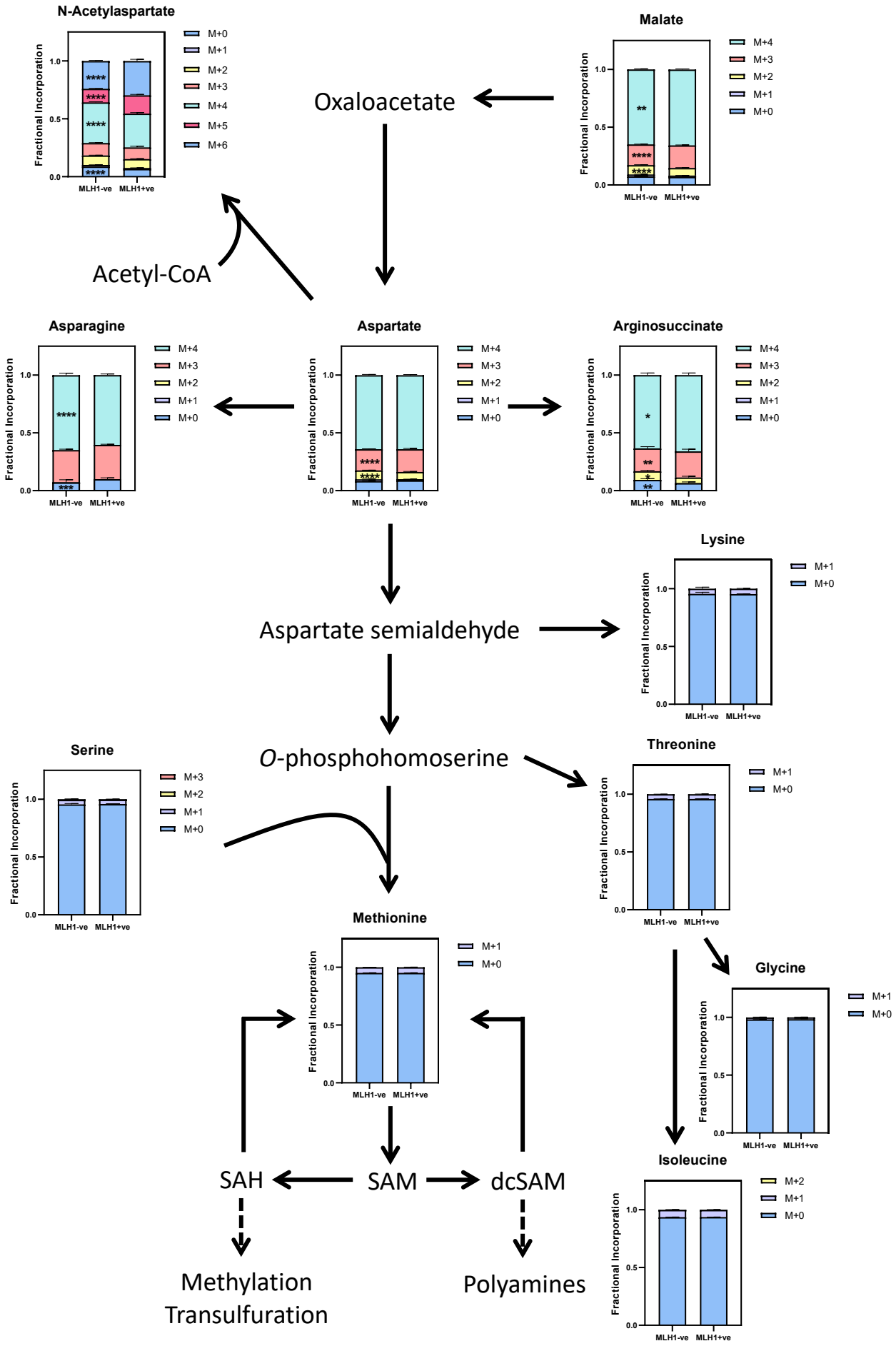

Figure legend on the next page.

FIGURE 4.4. Fractional contribution of labelled glutamine to metabolic intermediates involved in aspartate metabolism. Ishikawa EV and MLH1 cells were cultured in DMEM supplemented with 2mM ^{13}C-glutamine. Cells were harvested for metabolite detection. Each metabolite isotopomer is normalised to the total ion content of the sample. Fractional contribution is calculated by adding the fraction of the different 13C-labelled isotopomers and normalising them to the total amount of each metabolite in the sample. Schematic diagram of how glutamine metabolism fuels aspartate metabolism is arranged with graphs according to known metabolite conversions as described in the literature. Statistical significance was determined using a multiple t-tests with posthoc Holm-Sidak multiple Comparisons Test to Ishikawa MLH1. *P<0.05, **P<0.01, ***P<0.001, ****P<0.0001. No asterix = not significant.

4.2 Quantification of Differential Changes in Metabolite Levels upon MLH1 Loss through Labelled Glucose Tracing

4.2.1 MLH1-deficient Ishikawa cells have differential levels of metabolites involved in the glycolysis, the TCA cycle, and the urea cycle

As we identified that MLH1-deficient Ishikawa cells were more glycolytic, with an increased glycolytic capacity (**FIGURE 3.10 C**) and glycolytic reserve (**FIGURE 3.10 D)** relative to MLH1-proficient Ishikawa MLH1 cells, we were interested in further investigating glucose utilisation in these cells by stable isotope tracing from $^{13}C_6$-glucose. Like the glutamine tracing study, the targeted metabolomics assay identified specific metabolic intermediates of glycolysis, TCA cycle, glutaminolysis, urea cycle and both essential and nonessential amino acids as indicated. Ishikawa EV and MLH1 cells were cultured for 24 hours in DMEM supplemented with 25mM $^{13}C_6$-glucose, before being harvested for metabolite extraction (~85% confluence on harvest). Five technical replicates were performed for accuracy. Metabolites were extracted in a solution composed of 50% methanol, 30% acetonitrile, 20% ultrapure water and 50ng/ml HEPES. 1ml of extraction solution was added per $1x10^6$ cells. Extraction was carried out in a dry ice/methanol bath to maintain the integrity of the metabolites. Dr Valle Morales performed the LC/MS separation and analysis by calculating the ratio of the abundance of each metabolite normalised to TIC. Using these data, I determined the fold change difference of each metabolite in Ishikawa EV and MLH1 cells to determine any significance.

As before we analysed both the levels of metabolic intermediates and glucose flux in MLH1-deficient cells after culturing them for 24 hours in media containing 25mM $^{13}C_6$-glucose, to further understand the metabolic architecture of MLH1-deficient EC cells. Labelled metabolite analysis enabled us to track the synthesis of metabolites derived from glucose. Naturally abundant carbons have an atomic mass of 12 (^{12}C). To label metabolites, we utilised $^{13}C_6$-glucose where all 6 carbons had an atomic mass of 13 (^{13}C). LC/MS analysis detected the increase in metabolic mass of each metabolite and the relative abundance of each isotopomer detected. This enabled us to investigate glucose metabolism in our MLH1-proficient and deficient cell models. We determined the relative abundance of each metabolite and the fractional contribution of labelled glucose to the indicated metabolite. Understanding the fractional contribution of glucose to each metabolite enabled us to identify whether the source of carbon for each metabolite differs in the absence of MLH1. Alongside the targeted metabolomics data, this information is a useful tool for understanding what metabolic rewiring occurs in MLH1-deficient cells.

We harvested samples for metabolite detection that were cultured for 24 hours in DMEM with 25mM $^{13}C_6$-glucose then calculated the fractional contribution of selected metabolites. We investigated metabolites highly dependent on glucose for synthesis i.e., metabolic intermediates of glycolysis or the TCA cycle, as well as derivatives of the TCA cycle. Firstly, we looked at the labelling of glucose before confidently studying the contribution of glucose into other metabolites. We observed a 100% fractional contribution of labelled glucose in both cell lines, demonstrating that all labelled glucose in our study was labelled. Glucose is metabolised in mammalian cells via glycolysis which converts glucose to pyruvate via a series of intermediate metabolites. Pyruvate is a metabolic intermediate with several potential fates including, entry into the TCA within the mitochondrial to produce NADH and $FADH_2$. Alternatively, pyruvate can be converted into lactate in the cytosol by LDH, with the concurrent regeneration of NAD^+ from NADH. An increase in glycolytic flux can increase the rate of ATP production, even though glycolysis is less effective than OXPHOS at generating ATP. Moreover, carbons from 3-phosphoglycerate, another glycolytic metabolite, are used to synthesise serine, glycine, and cysteine which in turn supply one-carbon metabolism. **FIGURE 4.5** illustrates the fate of ^{13}C-glucose during glycolysis and the first round of the TCA cycle. ^{12}C atoms are represented by white circles, whereas ^{13}C-atoms are represented by red circles. Oxidative TCA cycle metabolism whereby M+2 acetyl-CoA is combined with oxaloacetate, generates M+2 citrate, M+2 α-KG, M+2 succinate, M+2 fumarate, M+2 malate, and M+2 oxaloacetate. Oxidative TCA cycle metabolism whereby M+3 pyruvate generates M+3 oxaloacetate in the reaction catalysed by pyruvate carboxylase, generates M+5 citrate, M+3 α-KG, M+3 succinate, M+3 fumarate, and M+3 malate etc.

The heat maps in **FIGURE 4.5** illustrate the contribution of ^{13}C atoms to each metabolite regardless of isotopic labelling pattern (**FIGURE 4.5 B**), and metabolite abundance at steady state (**FIGURE 4.5 C**), in Ishikawa MLH1 and Ishikawa EV cells. Both heat maps depict the fold change between Ishikawa EV cells versus Ishikawa MLH1-proficient cells. We identified a significant increase in the overall contribution of the label from glucose to metabolites involved in glycolysis, TCA cycle, aspartate metabolism and the serine synthesis pathway, in MLH1-deficient cells, in comparison to their isogenic MLH1-proficient Ishikawa cells. In MLH1-deficient EV cells, there was a marked increase in the incorporation of ^{13}C from glucose in several metabolites, most notably in serine and glycine (**FIGURE 4.5 B**), which is discussed further later in this section. We also identified differences between steady metabolite levels (i.e., the ratio of abundance of each metabolite/ TIC) in the Ishikawa EV cells versus Ishikawa MLH1 which are discussed in section 4.2.2. **FIGURE 4.6** illustrates the differences in the levels of specific isotopomers for each metabolite and significant differences in metabolite abundance between MLH1 deficient and proficient Ishikawa cells.

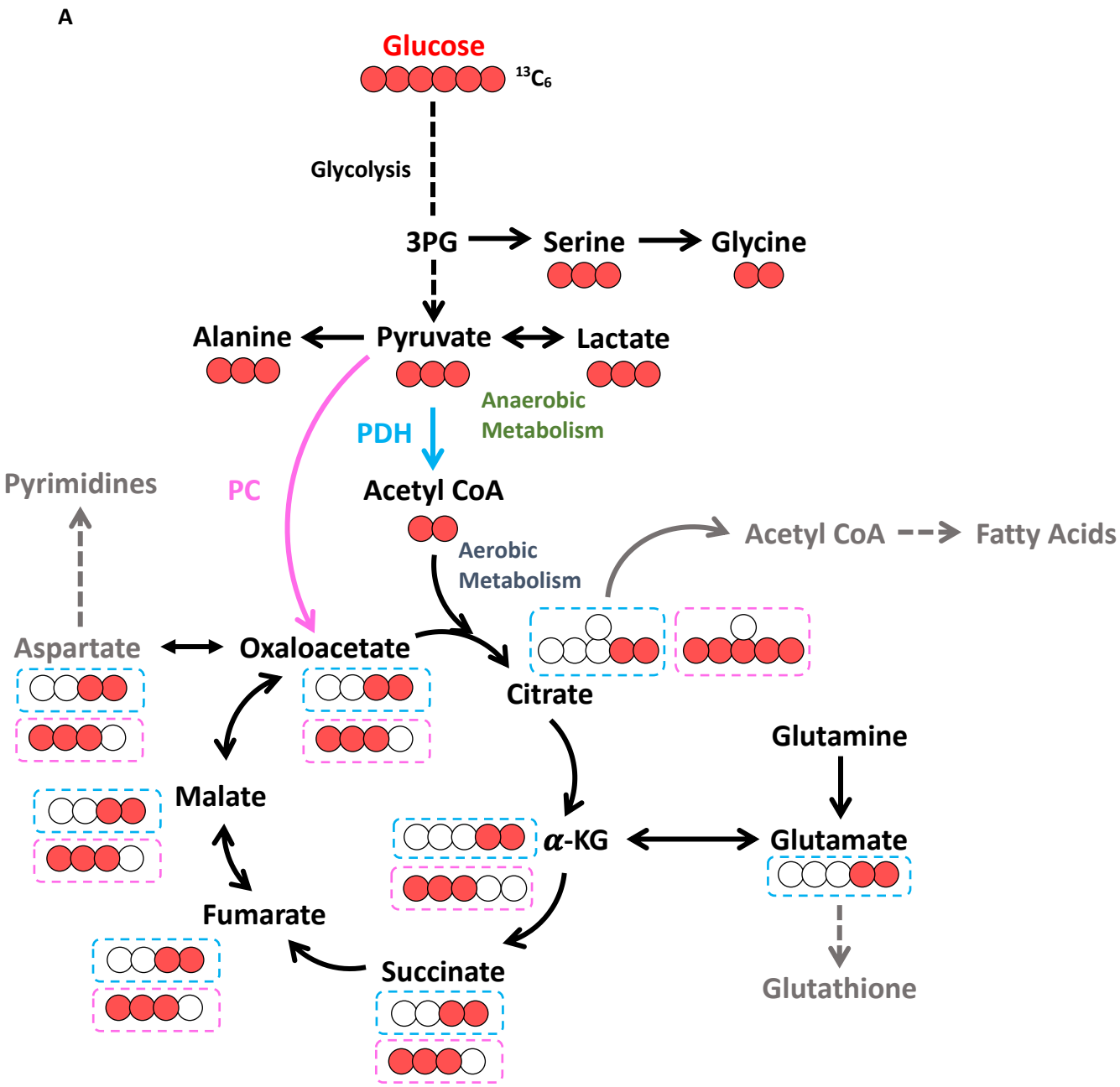

Figure continues…

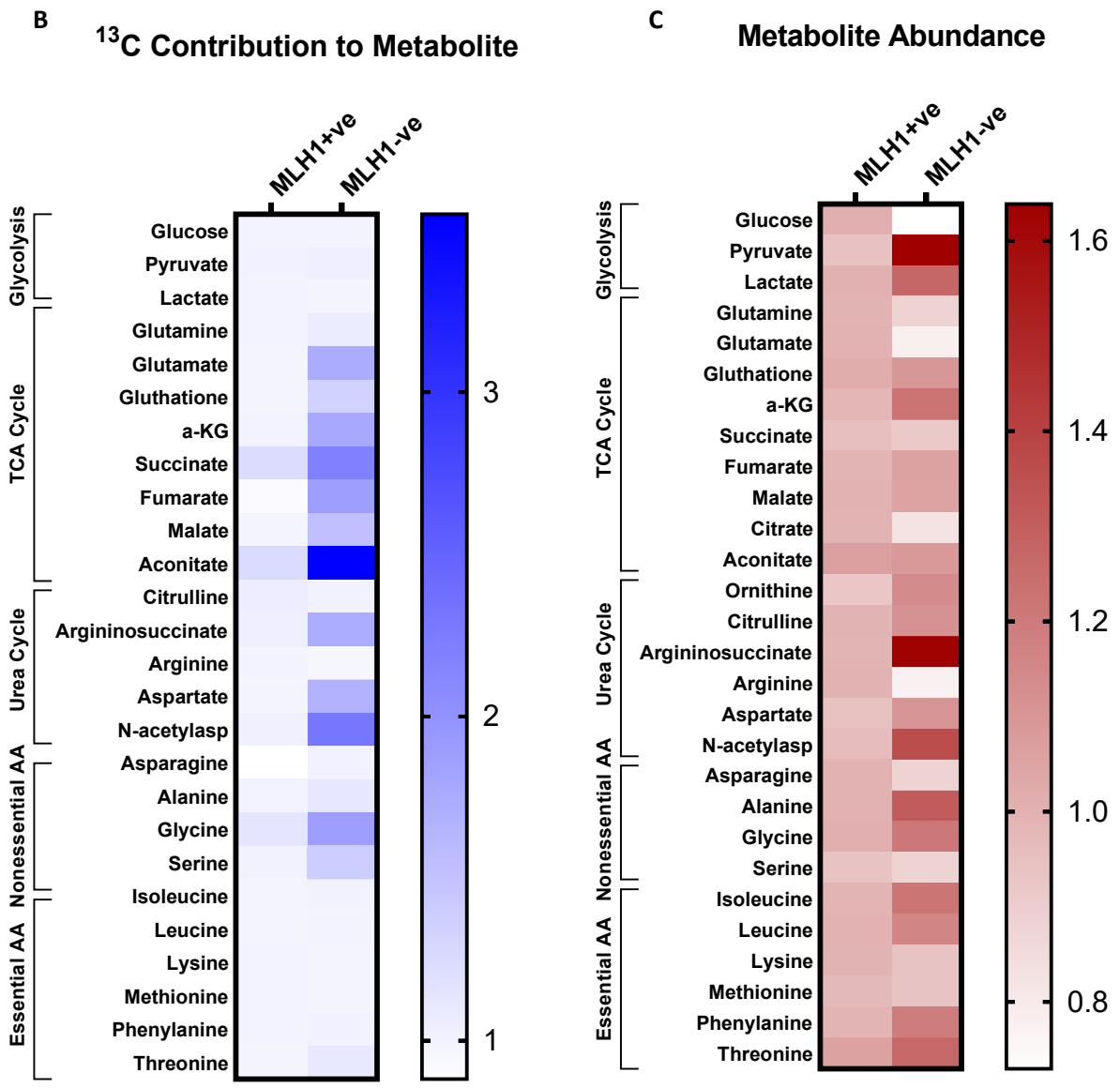

FIGURE 4.5. Metabolite abundance and glucose flux alterations in EC cells. ^{13}C glucose isotope tracer was used to analyse glucose metabolism in Ishikawa cells. Ishikawa EV and Ishikawa MLH1 cells were cultured in DMEM with 2g/L ^{13}C glucose. Cells were harvested for metabolite detection. Schematic diagram (**A**) indicates the flux of glucose through glycolysis and TCA cycle, resulting in the incorporation of glucose tracer into various metabolites. ^{13}C labelled and unlabelled carbons are indicated in red and white respectively, that would result following one round of the TCA cycle. Pink boxes indicative of the labelled metabolites generated following pyruvates conversion to oxaloacetate catalysed by the enzyme pyruvate carboxylase (PC). Blue boxes are indicative of the labelled metabolites generated following the reaction of pyruvate to Acetyl-Co A catalysed by the enzyme pyruvate dehydrogenase (PDH). Heat map (**B**), produced by GraphPad Prism, of total labelled carbon contribution and heat map (**C**) of total metabolite abundance. Columns are median-centred, with fold changes compared to MLH1-proficient cells represented by colour (Dark, higher abundance; Light, lower abundance). Data shows an increased incorporation of label into TCA and Urea cycle intermediates suggesting MLH1-deficient cells are more metabolically active and have a distinct metabolic signature.

The analysis of steady-state metabolites identified differences in levels of intermediates of certain metabolic pathways in MLH1-deficient Ishikawa cells (**FIGURE 4.6**). Upon MLH1 loss we identified significantly reduced levels of glucose ($p=0.0442$), glutamine ($p=0.0017$), glutamate ($p<0.0001$), and arginine ($p<0.0001$), alongside increased levels of pyruvate ($p=0.0056$), lactate ($p<0.0001$), a-KG ($p=0.0052$), glutathione ($p=0.0012$), NAA ($p=0.0008$), arginosuccinate ($p=0.0002$), aspartate ($p=0.0267$), alanine ($p=0.0013$), isoleucine ($p<0.0001$), leucine ($p<0.0001$), and phenylalanine ($p<0.0001$). Notably, MLH1-deficient EV cells had significantly less glucose, alongside significantly more pyruvate and lactate (**FIGURE 4.6**). This could be indicative that in the absence of MLH1 Ishikawa EV cells increase their glycolytic rate to generate more ATP. We also observed increased levels of pyruvate and lactate in our glutamine tracing assay (**FIGURE 4.3**). Given stable isotope metabolites are metabolised by cells in the same way as nonlabelled metabolic precursors, we expected to identify the same trend in levels of glucose between the glucose and glutamine tracing experiments. These differences may be due to unintentional differences in sample preparation between the two assays, i.e., confluency or quench timing. Despite the care taken to ensure consistency in both tracing experiments, the absence of precise replication during sample preparation can result in the incorrect interpretation of collected data. Consequently, analysis of dynamic stable isotope tracing is more representative of the internal metabolic architecture of cells and when used in conjunction with steady-state labelling patterns in downstream metabolites, provides valuable qualitative information as to their origin and relative rates of production. Continuing advances in the field of metabolomics have led to the identification of perhaps an even more informative metabolomics assay that quantifies metabolic fluxes in specific subcellular compartments i.e., in the mitochondria or cytosol. Shlomi *et al.* recently described a spatial-fluxomic approach for mammalian cells, where isotope tracing is followed by rapid subcellular fractionation and quenching of metabolism, then followed by LC/MS-based metabolomics analysis [344]. This method was used to demonstrate that reductive glutamine metabolism is the major producer of cytosolic citrate (rather than glucose oxidation) in HeLa cells, and that succinate dehydrogenase-deficient tumour cells reverse citrate synthase flux to produce oxaloacetate in mitochondria [344]. This assay could be useful to confirm whether the differential glucose metabolism we believe is occurring in MLH1-deficient EC cells alters the levels of pyruvate entering the mitochondria where it is metabolised for eventual entry into the TCA cycle.

Furthermore, Ishikawa EV cells have significantly less glutamine ($p=0.0017$) and glutamate ($p<0.0001$) (**FIGURE 4.6**) compared to Ishikawa MLH1, consistent with data observed in the glutamine tracing assay (**FIGURE 4.3**). Given the importance of glutamine and glutamate for normal and cancer cell growth, these data could suggest that MLH1-deficient Ishikawa cells are more dependent on these

bioenergy substrates to support their proliferation and survival, thus are utilising glutamine and glutamate at a faster rate. On the contrary, these data could imply that Ishikawa EV cells are less reliant on glutaminolysis for energy production relative to Ishikawa MLH1 cells, potentially as they are exploiting an alternative metabolic pathway for ATP production which could imply that it is not as essential for the levels of glutamine and glutamate to be sustained. Furthermore, Ishikawa EV cells also have significantly higher levels of α-KG than MLH1 cells, although comparative levels of other TCA cycle intermediates. These data supports the former hypothesis suggesting that in the absence of MLH1, Ishikawa EV cells increase the rate of glutaminolysis. Further insight can be gained by combining this steady-state data with the dynamic stable isotope tracing data in section 4.2.2. The Ishikawa EV cells have increased M+2 fraction of glutamine ($p=0.0085$)), glutamate ($p<0.0001$), a-KG ($p<0.0001$), and glutathione ($p<0.0001$) versus Ishikawa MLH1, which provides evidence to support that upon MLH1 loss, Ishikawa cells are more metabolically active and increase their rate of glutaminolysis.

Furthermore, we also identified significant changes in several essential and nonessential amino acids. Ishikawa EV cells have markedly higher levels of NAA, arginosuccinate, aspartate, alanine, isoleucine, leucine, phenylalanine, and threonine, versus the Ishikawa MLH1 cells. Whereas they have significantly lower levels of arginine, asparagine, and methionine. In both glutamine and glucose tracing experiments, we observed that MLH1-deficient Ishikawa cells had a significant increase in the levels of isoleucine and leucine versus Ishikawa MLH1 cells. A study by Liang *et al*. demonstrated that BCAAs such as leucine can increase mitochondrial content, promote mitochondrial biogenesis, increase PGC-1α expression, and increase fatty acid oxidation through protein post-translational modification and transcriptional regulation [345, 346]. PGC-1α has emerged as a master regulator of mitochondrial biogenesis and energy expenditure and is important in the adaptive metabolic response, whereas PGC-1β is responsible for basal mitochondrial functions [347]. A recent study by Ghilardi *et al.* highlights that impaired OXPHOS can help control ovarian cancer progression, and this benefit correlates with the expression of PGC-1α and PGC-1β, with high levels of PGC1α/β characteristic of tumours more addicted to OXPHOS metabolism and more susceptible to OXPHOS inhibition [348]. Rashid *et al*. have already demonstrated that MLH1-deficient cancer cells exhibit a reduced expression of the nuclear transcriptional co-activator PGC-1β, along with reduced OXPHOS [175]. Though we did not identify differences in PGC1α/β RNA expression in the MLH1-deficient Ishikawa cells, the increase in leucine we observed is reflective of the perturbed mitochondrial metabolism these cells exhibit, though also is indicative that further research is required to understand whether this metabolic vulnerability can be exploited therapeutically.

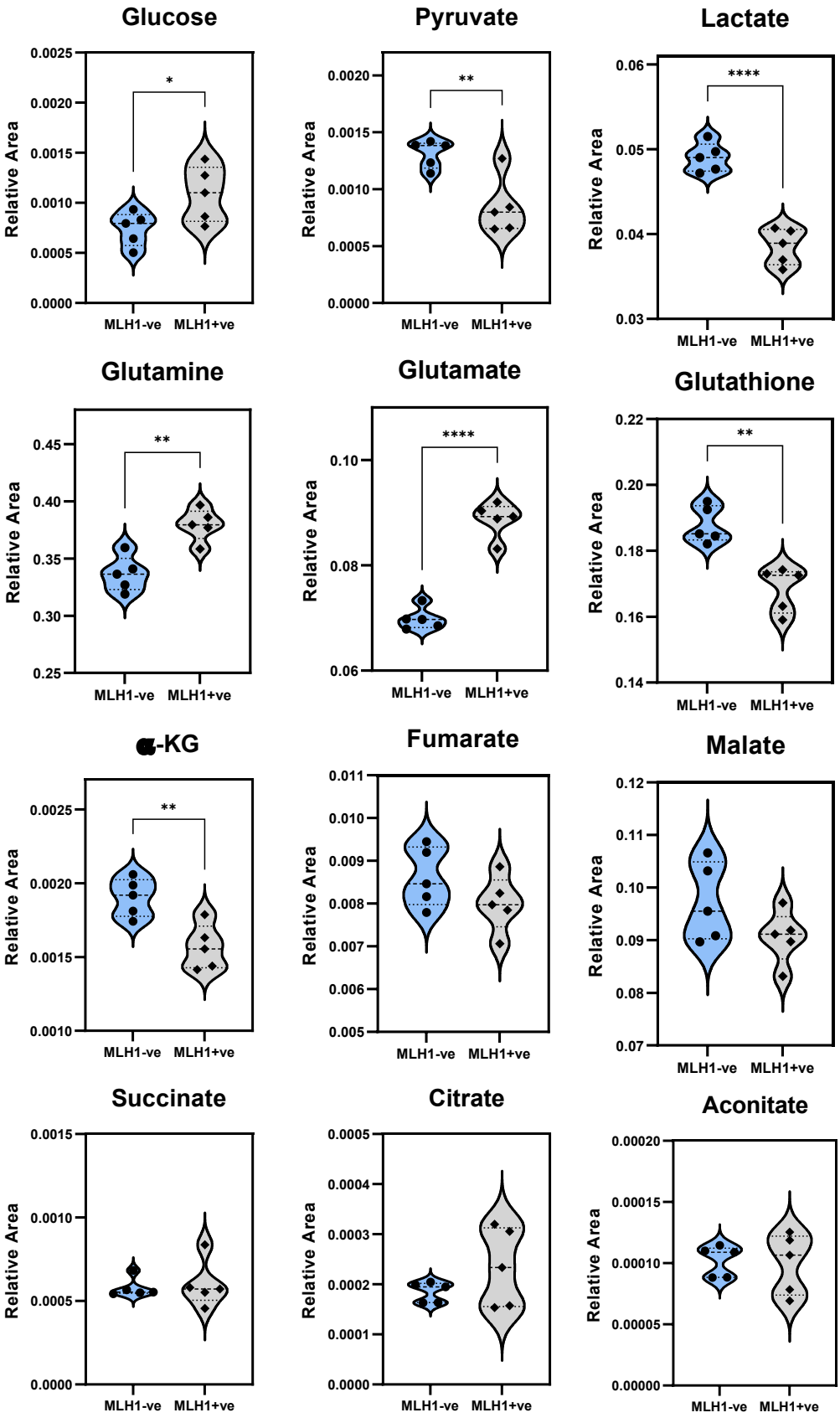
Glucose
Relative Area
0.0025
0.0020
0.0015
0.0010
0.0005
0.0000
*
MLH1-ve
MLH1+ve
Pyruvate
Relative Area
0.0020
0.0015
0.0010
0.0005
0.0000
**
MLH1-ve
MLH1+ve
Lactate
Relative Area
0.06
0.05
0.04
0.03
****
MLH1-ve
MLH1+ve
Glutamine
Relative Area
0.45
0.40
0.35
0.30
0.25
**
MLH1-ve
MLH1+ve
Glutamate
Relative Area
0.10
0.08
0.06
****
MLH1-ve
MLH1+ve
Glutathione
Relative Area
0.22
0.20
0.18
0.16
0.14
**
MLH1-ve
MLH1+ve
-KG
Relative Area
0.0025
0.0020
0.0015
0.0010
**
MLH1-ve
MLH1+ve
Fumarate
Relative Area
0.011
0.010
0.009
0.008
0.007
0.006
0.005
MLH1-ve
MLH1+ve
Malate
Relative Area
0.12
0.11
0.10
0.09
0.08
0.07
MLH1-ve
MLH1+ve
Succinate
Relative Area
0.0015
0.0010
0.0005
0.0000
MLH1-ve
MLH1+ve
Citrate
Relative Area
0.0005
0.0004
0.0003
0.0002
0.0001
0.0000
MLH1-ve
MLH1+ve
Aconitate
Relative Area
0.00020
0.00015
0.00010
0.00005
0.00000
MLH1-ve
MLH1+ve

Figure continues…

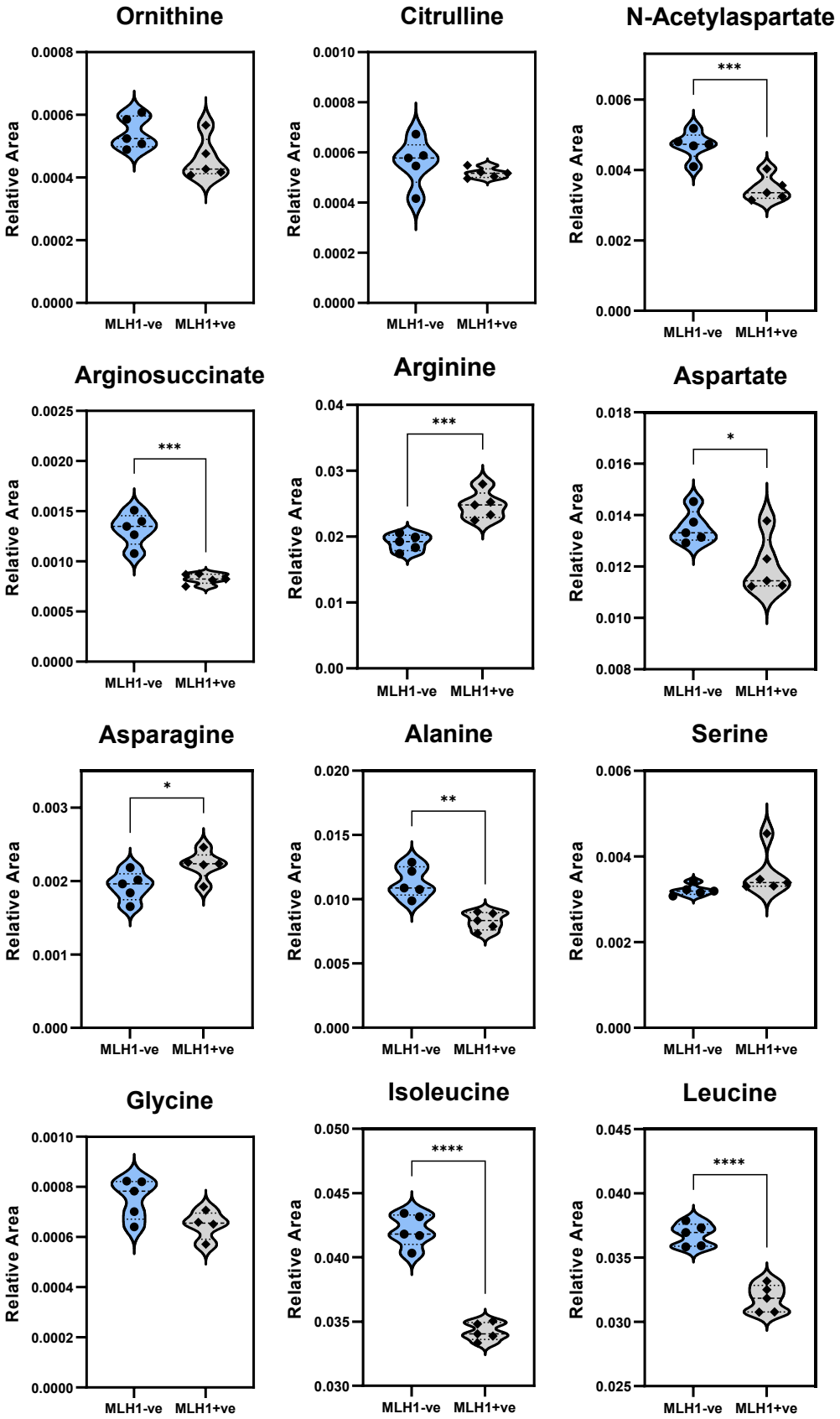

Figure continues…

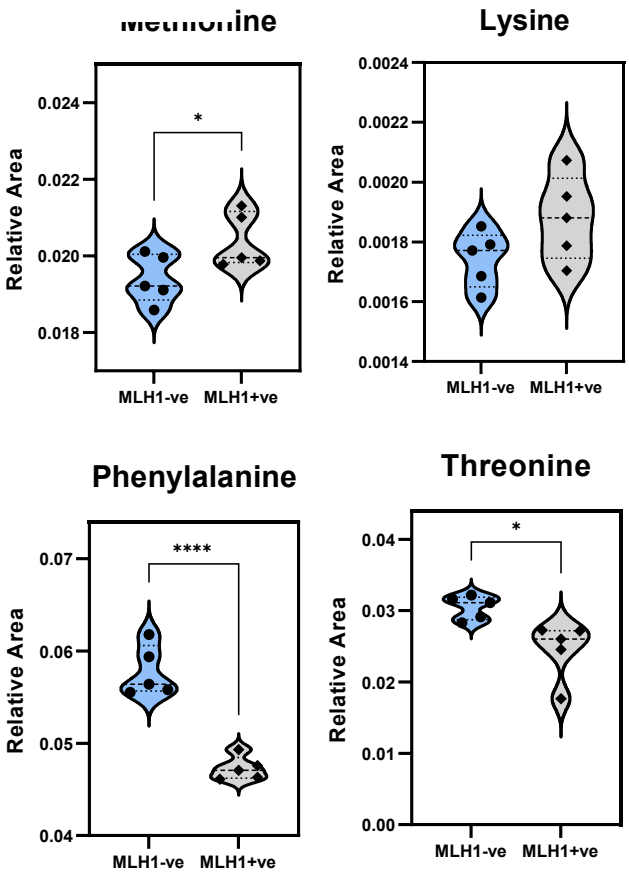

FIGURE 4.6. Quantification of metabolites in targeted metabolomics analysis of MLH1-proficient and deficient Ishikawa cells. Graphs represent the relative levels for individual metabolite involved in glycolysis, the TCA cycle, urea cycle, as well as other essential and nonessential amino acids. MLH1 deficient cells have an altered metabolic signature with increased pyruvate and lactate levels implying increased anaerobic activity in the absence of proficient OXPHOS. Statistical significance was determined using a multiple t-tests with posthoc Holm-Sidak multiple Comparisons Test to Ishikawa MLH1. **P*<0.05, ***P*<0.01, ****P*<0.001, *****P*<0.0001. No asterix = not significant.

4.2.2 Metabolic tracing of ^{13}C from glucose demonstrates that MLH1-deficient Ishikawa cells differentially modulate metabolic pathways

Due to glucose labelling, we were able to identify glucose-derived isotopomers and how many atoms of ^{13}C-glucose were donated by the labelled metabolite. It is therefore possible to discriminate between metabolites derived from ^{13}C-glucose or through other sources of nutrients present in the media. We have illustrated the results according to known metabolite reactions, as described in the literature (**FIGURE 4.7**).

The glycolysis pathway is the first step of glucose metabolism in cells. Once metabolised to 3-phosphoglycerate, glucose transfers 3 labelled carbons to serine resulting in M+3 serine from M+6 Glucose. In our Ishikawa EV cells, approximately 40% of serine comes from glucose, compared to approximately 30% for Ishikawa MLH1 cells. Our Ishikawa EV cells have 16% M+3 labelled serine versus 11% for Ishikawa MLH1 ($p<0.001$). Furthermore, they also have significantly more M+2 labelled glycine 18% for Ishikawa EV versus 9% for Ishikawa MLH1 ($p=0.0017$) (**FIGURE 4.7**). This increased flux implies that in the absence of MLH1, these cells rewire their metabolism to upregulate serine synthesis to support proliferation and survival.

The redox modulator glutathione is generated from glycine, glutamate, and cysteine. Glutathione plays an important role in antioxidant defence, nutrient metabolism, and regulation of numerous cellular processes. Recent studies have implicated glutathione as a player involved in processes such as cell differentiation, proliferation, and immune function to name a few [349]. MLH1-deficient Ishikawa cells have significantly less glutamate ($p<0.0001$) but more glutathione ($p=0.0012$) and no difference in glycine (p=ns) (**FIGURE 4.6**). Despite this observation, approximately only 20% of glycine is labelled, so the largest fraction of this metabolite is taken up from the media and thus not from $^{13}C_6$-glucose. Nonetheless, there is a significant increase in M+2 levels of glycine 18% in Ishikawa EV cells relative to 9% Ishikawa MLH1-proficient cells (**FIGURE 4.7**), further implying that MLH1-deficient Ishikawa cells are more metabolically active. Moreover, Ishikawa EV cells have significantly more M+2 glutathione, 14% compared to 10% in Ishikawa MLH1 cells ($p<0.0001$) (**FIGURE 4.7**). As such, these data demonstrates that there is increased incorporation of labelled carbon in metabolite involved in serine, glycine, and glutathione synthesis in MLH1-deficient cells. Higher levels of glutathione have been identified to promote tumour progression, with increased levels associated with increased metastasis [350]. This could be a contributing factor to the poor prognostic factors including lymphovascular space and deep myometrial invasion observed in MMR-deficient EC [351].

Following glycolysis, $^{13}C_6$-glucose transfers 3 labelled carbons to pyruvate and subsequently lactate. In our cells we observe that ~75% of pyruvate and lactate is M+3 labelled, proving the majority of pyruvate and lactate in these cells comes from glucose metabolism. We don't see any significant differences between the fractional contribution of M+3 between Ishikawa EV and Ishikawa MLH1 cell lines, however (**FIGURE 4.7**). Despite this, Ishikawa EV cells have markedly more pyruvate and lactate compared to Ishikawa MLH1 cells as described in section 4.2.1 (**FIGURE 4.7**). This may be indicative that MLH1-deficient cells are more metabolically active. Lastly, pyruvate can be transaminated to form alanine catalysed by the enzyme alanine transaminase (ALT). This enzyme converts glutamate and pyruvate to α-KG and alanine. Studies in the literature suggest that the role of alanine in cancer metabolism is poorly understood. Some speculate this is due to shortfalls in *in vitro* cell culture medias which we discuss in more detail in section 6.3.1. Alanine is the second most abundant circulating amino acid in human plasma, however, is barely present in most culture medias [352]. This forces most cancer cells in culture to synthesise nearly all their alanine regardless of whether this would normally occur in the tumour microenvironment. Consequently, it is important to consider the possibility of tissue-culture-generated artifacts. Nonetheless, Ishikawa EV cells have significantly more alanine than Ishikawa MLH1 cells (**FIGURE 4.6**), in addition to increased incorporation of labelled carbons from glucose, 68% versus 61% (**FIGURE 4.7**).

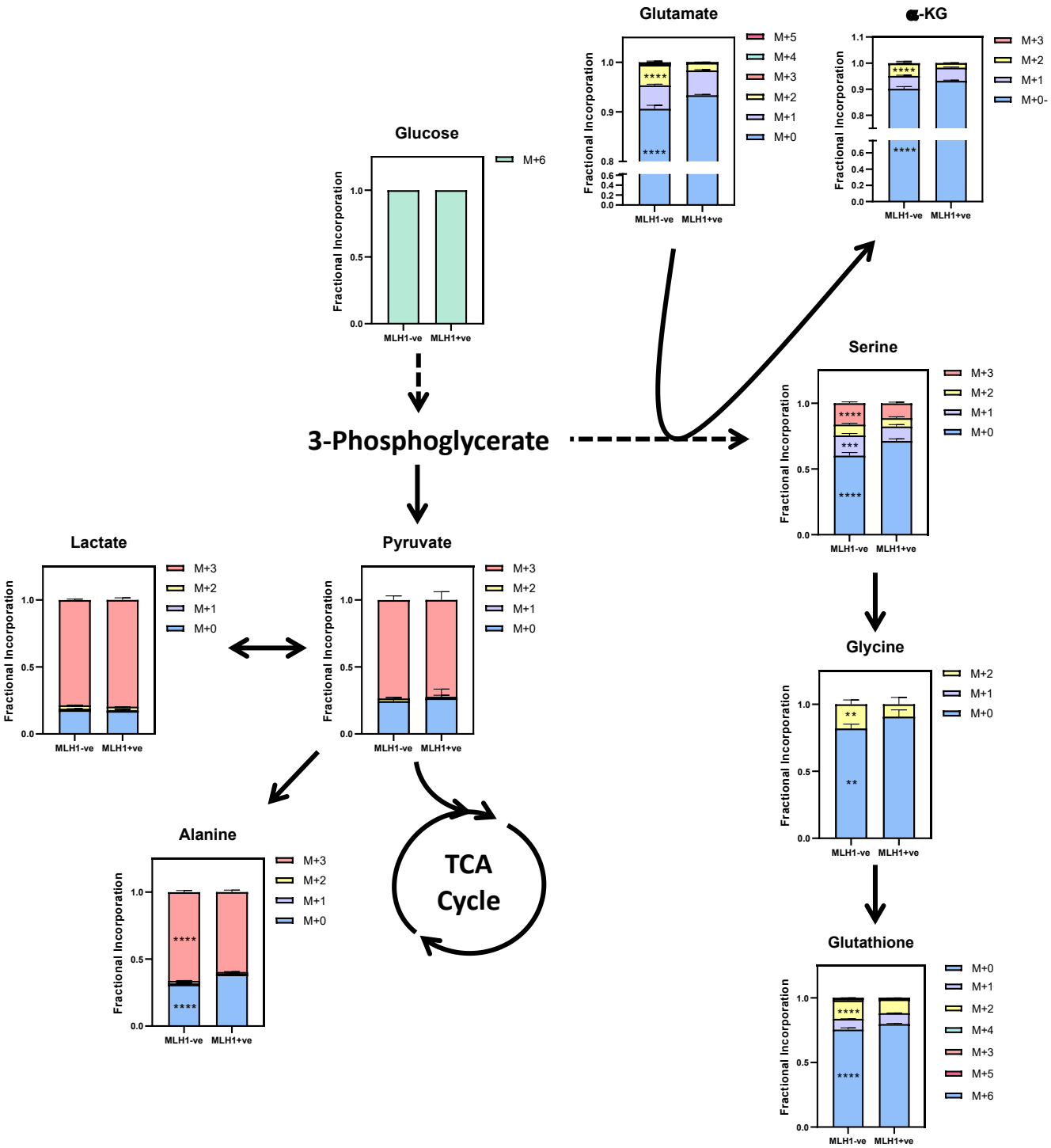

FIGURE 4.7. Fractional contribution of labelled glucose to metabolic intermediates through glycolysis. Ishikawa EV and MLH1 cells were cultured in DMEM supplemented with 25mM ^{13}C-glucose. Cells were harvested for metabolite detection. Each metabolite isotopomer is normalised to the total ion content of the sample. Fractional contribution is calculated by adding the fraction of the different 13C-labelled isotopomers and normalising them to the total amount of each metabolite in the sample. Schematic diagram of glucose metabolism through glycolysis, is arranged with graphs according to known metabolite conversions as described in the literature. Statistical significance was determined using a multiple t-tests with posthoc Holm-Sidak multiple Comparisons Test to Ishikawa MLH1. *P<0.05, **P<0.01, ***P<0.001, ****P<0.0001. No asterix = not significant.

Next, we were interested in studying the impact of MLH1 loss on the incorporation of glucose-derived carbon into the TCA cycle. Studying glucose-derived flux in the TCA cycle was not as easy as glycolysis to investigate. The main precursor of the TCA cycle from glucose metabolism is acetyl-coA, which was not detected in our analysis. Pyruvate can be converted to acetyl-CoA which would result in the acetyl-coA having two labelled carbons in this experimental setting (**FIGURE 4.5**). Subsequently, acetyl-CoA enters the TCA cycle where it is oxidised for energy production. From here, the level of glucose incorporation into TCA cycle intermediates depends on the cycle number. In the first cycle, TCA cycle metabolites incorporate two ^{13}C resulting in M+2 TCA cycle metabolites derived from labelled acetyl-coA (**FIGURE 4.8**). Subsequent rounds of the TCA cycle generate metabolic intermediates with various isotopic labelling patterns and can result in up to M+4 intermediates or M+5 for aconitate, all originally derived from $^{13}C_6$-glucose. Additionally, if M+3 pyruvate is converted to oxaloacetate by pyruvate carboxylase this results in M+3 oxaloacetate feeding the TCA cycle, and subsequently M+3 TCA cycle intermediates in the first round.

Interestingly, the largest contributing fraction of TCA cycle intermediates in this experiment for both MLH1-proficient and deficient cells is unlabelled (M+0) and only ~10% of each metabolite is labelled. This confirms the carbon is coming from glutamine. Nonetheless, we do observe differences between the MLH1-proficient and deficient cells. Firstly, there is significantly less unlabelled (M+0) α-KG (90% versus 93%; $p<0.0001$), succinate (93% versus 96%), fumarate (91% versus 95%), and malate (90% versus 93%) in Ishikawa EV compared to Ishikawa MLH1 cells (**FIGURE 4.8**), however, the glutamine tracing assay is a better way of interrogating the TCA cycle in these cells. This could imply that there is a reduction in the conversion of these metabolites, or that in the absence of MLH1 these cells are less dependent on the TCA cycle. It is possible that they are relying on other metabolic pathways which we also investigate further.

Moreover, in the MLH1-deficient cells, there is a significant increase in M+2 labelled glutamine (0.4% versus 0.1%; $p=0.0085$), glutamate (4% versus 1%; $p<0.0001$), α-KG (4% versus 2%; $p<0.0001$) and glutathione (15% versus 10%; $p<0.0001$). α-KG is an entry point to the TCA cycle via the reversible conversion of glutamate catalysed by glutamate dehydrogenase. Interestingly this coincides with significantly reduced levels of glutamine and glutamate alongside significantly increased levels of α-KG and glutathione in MLH1-deficient cells. This implies that in the absence of MLH1 these cells upregulate glutaminolysis, increasing the conversion of glutamine to glutamate and subsequently α-KG. This would result in higher levels of α-KG. It is important to note that glutamine and lactate account for half of all TCA cycle carbon under fasted conditions [353]. Interestingly there are also

higher levels of M+2 fumarate and malate in Ishikawa EV cells relative to Ishikawa MLH1 (**FIGURE 4.8**). This further implies that there is an increase in TCA cycle flux in this MLH1-deficient model. Though not statistically significant, this change is also appears to be accompanied by higher relative levels of both these intermediates (**FIGURE 4.6**).

Intriguingly, although subsequent TCA cycle rounds would generate M+3 and M+4 metabolic intermediates, these form a very small fraction of each total metabolite regardless of MLH1 status. This suggests that labelled glucose is predominantly fuelling other metabolic pathways, for instance, oxaloacetate gives rise to amino acid aspartate. Our MLH1-deficient Ishikawa cells have significantly more M+2 labelled aspartate (3% versus 1%; $p<0.0001$) (**FIGURE 4.8**); alongside higher relative levels of aspartate (**FIGURE 4.6**) compared to Ishikawa MLH1 cells. Aspartate is a non-essential amino acid, with most of the cellular demand met by internal biosynthesis through the transamination of oxaloacetate by aspartate aminotransferase or amino acid oxidase. As aspartate is derived from oxaloacetate the level of glucose incorporation would be similar to the glucose incorporation from oxaloacetate. Unfortunately, we did not detect oxaloacetate in our assay, however, we detected malate, its precursor. We observe a similar fractional contribution of M+2 malate (4% for Ishikawa EV and 1% for Ishikawa MLH1; $p<0.0001$) to M+2 aspartate (~4% for Ishikawa EV and 1% for Ishikawa MLH1; $p<0.0001$), both significantly more than the fractional contribution of each to Ishikawa MLH1 cells. We investigate aspartate metabolism further in the next section. Nonetheless, the modulation of these metabolite levels implies an increase in glucose flux into the TCA cycle in this MLH1-deficient cell model.

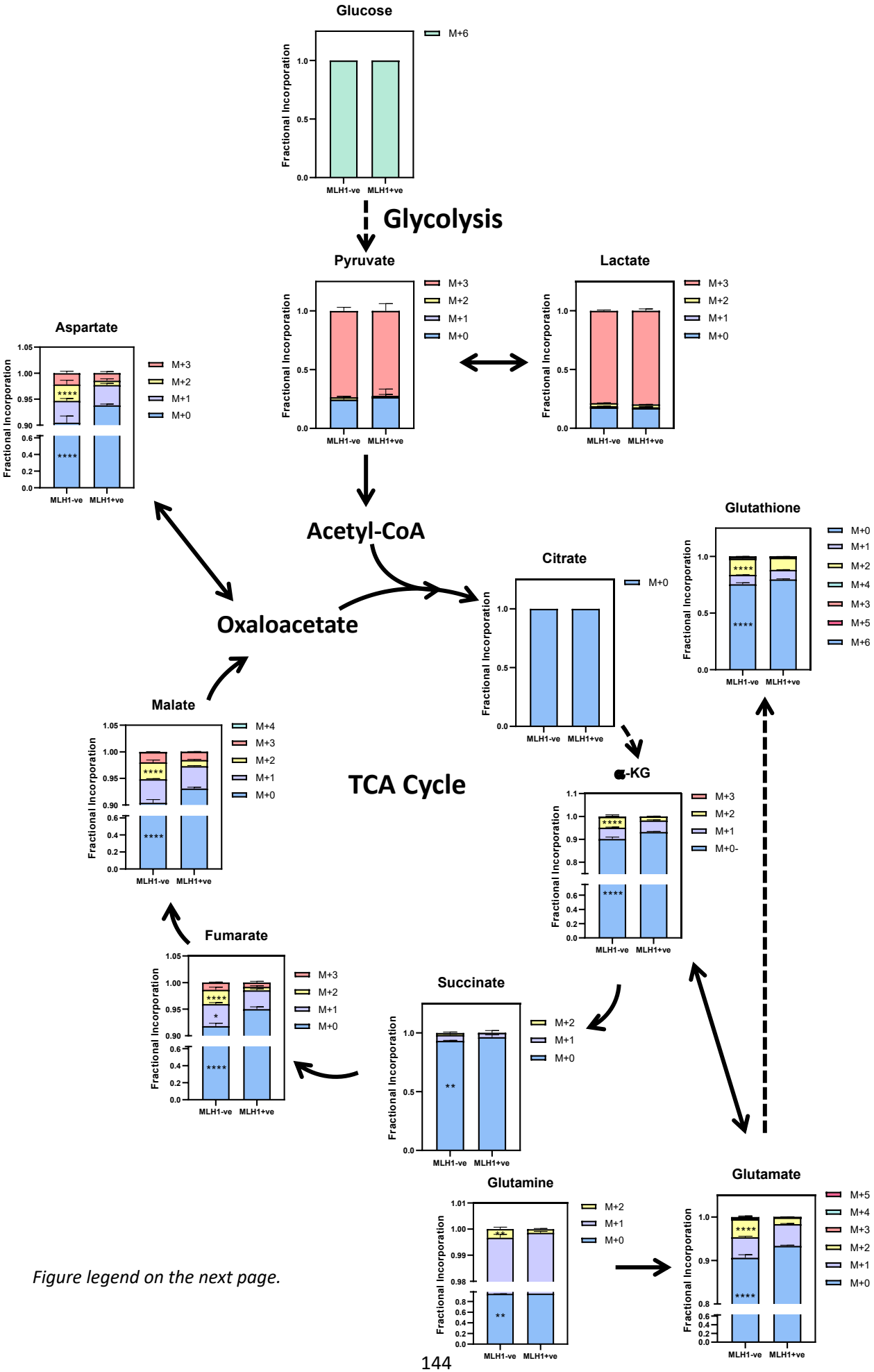

Figure legend on the next page.

FIGURE 4.8. Fractional contribution of labelled glucose to metabolic intermediates involved in the TCA cycle. Ishikawa EV and MLH1 cells were cultured in DMEM supplemented with 25mM ^{13}C-glucose. Cells were harvested for metabolite detection. Each metabolite isotopomer is normalised to the total ion content of the sample. Fractional contribution is calculated by adding the fraction of the different 13C-labelled isotopomers and normalising them to the total amount of each metabolite in the sample. Schematic diagram of glucose metabolism through the TCA cycle, is arranged with graphs according to known metabolite conversions as described in the literature. Statistical significance was determined using a multiple t-tests with posthoc Holm-Sidak multiple Comparisons Test to Ishikawa MLH1. *P<0.05, **P<0.01, ***P<0.001, ****P<0.0001. No asterix = not significant.

We went on to investigate the aspartate metabolic pathway as it links the TCA cycle (via oxaloacetate), the urea cycle (via arginosuccinate) the polyamine metabolic pathways (via methionine and dcSAM), AMP synthesis and the purine nucleotide cycle. Accordingly, the graphs in **FIGURE 4.9** illustrate how these pathways are linked using information from the literature. We identified that MLH1-deficient cells had higher levels of aspartate (**FIGURE 4.6**), as well as an increase in the M+2 isotopomer (**FIGURE 4.9**), relative to Ishikawa MLH1. Next, we looked at N-acetyl aspartate (NAA). NAA is a molecule generated from aspartate and acetyl-CoA and is an abundant metabolite detected in the brain. Several studies have demonstrated that the increase of NAA levels in several cancer types has been associated with a worse overall prognosis, as it is thought to have a role in promoting tumour growth [336-340]. In our Ishikawa EV cells, approximately 28% of NAA was labelled, compared to 15% for Ishikawa MLH1 cells. This is also more than the M+2 fraction of aspartate; 3% aspartate versus 23% NAA for Ishikawa EV and 1% aspartate versus 9% NAA for Ishikawa MLH1). As only a small fraction of aspartate was labelled (10% EV and 7% MLH1), this implies that the majority of incorporation of ^{13}C in NAA comes from the labelled acetyl-CoA. Additionally, we detected very small amounts of M+4 NAA in both cell lines which would be generated from the reaction with M+2 aspartate and M+2 acetyl-CoA. As well as the altered carbon flux in Ishikawa EV cells, we also observe an increase in the relative levels of aspartate and NAA in MLH1-deficient cells (**FIGURE 4.6**).

The other significant difference we observed in this metabolic pathway was in the increase in M+2 fraction of arginosuccinate in MLH1-deficiency; 3% Ishikawa EV versus <1% Ishikawa MLH1 ($p<0.0003$) (**FIGURE 4.9**). This is accompanied by an increase in the abundance of this metabolite (**FIGURE 4.6**). Moreover, ~14% of Ishikawa EV is labelled versus ~10% of Ishikawa MLH1. Arginosuccinate synthetase (ASS) catalyses the condensation of citrulline and aspartate to form arginosuccinate, the precursor to arginine. We observe no differences in the abundance of citrulline although there is significantly less arginine in Ishikawa EV. Additionally, there are no statistically significant differences in any of the isotopomers for either of these metabolites. It will be interesting to further investigate the link between MLH1 loss and arginine metabolism to see whether this could be exploited therapeutically.

Further downstream of aspartate metabolism pathway we saw no statistically significant differences in Ishikawa EV cells compared to Ishikawa MLH1 cells.

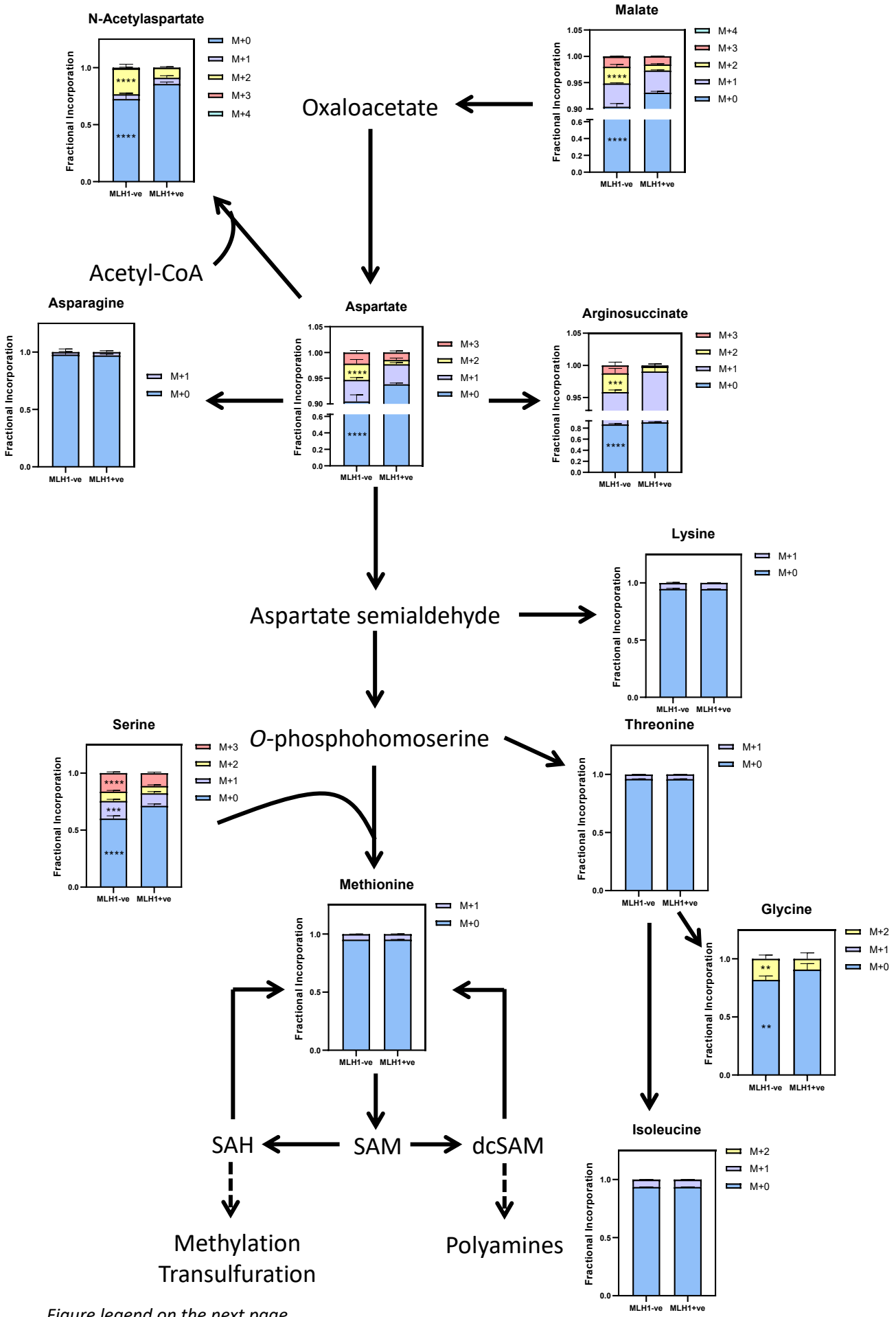

Figure legend on the next page.

FIGURE 4.9. Fractional contribution of labelled glucose to metabolic intermediates involved in aspartate metabolism. Ishikawa EV and MLH1 cells were cultured in DMEM supplemented with 2mM ^{13}C-glucose. Cells were harvested for metabolite detection. Each metabolite isotopomer is normalised to the total ion content of the sample. Fractional contribution is calculated by adding the fraction of the different 13C-labelled isotopomers and normalising them to the total amount of each metabolite in the sample. Schematic diagram of how glycolysis fuels aspartate metabolism is arranged with graphs according to known metabolite conversions as described in the literature. Statistical significance was determined using a multiple t-tests with posthoc Holm-Sidak multiple Comparisons Test to Ishikawa MLH1. *P<0.05, **P<0.01, ***P<0.001, ****P<0.0001. No asterix = not significant.

4.3 Culturing cells in DMEM vs. RPMI influences metabolic pathway dependency *in vitro*

There are limitations to studying cancer metabolism *in vitro*. The more we learn about how cancer cells adapt their metabolic architecture to survive and proliferate in unfavourable conditions, the more research has gone into ensuring we are using the correct assays *in vitro* so we can test hypotheses in a biologically relevant setting. Currently available cell culture medias such as DMEM and RPMI do not accurately reproduce the metabolic environment of tumours. Studies have demonstrated that the nutrient composition of commercial medias can impose metabolic artifacts on cancer cells that when translated *in vivo* are not biologically relevant [354]. Furthermore, Joly *et al*. demonstrated that media compositions can impact metabolic pathway dependencies of cancer cells, and thus influence therapeutically targeted vulnerabilities [355].

As such, we carried out the same targeted metabolomics-based study as discussed above in DMEM media, but this time in RPMI media and analysed the differences in the abundances of metabolites detected and compared our data to the previous results from cells cultured in DMEM. Once again, we investigated metabolites involved in glycolysis, the TCA cycle, the urea cycle, as well as essential and nonessential amino acids. In each experiment, cells were cultured for 24 hours in DMEM supplemented with 25mM $^{13}C_6$-glucose, or RPMI supplemented with ~12mM $^{13}C_6$-glucose, before being harvested for metabolite extraction (~85% confluence on harvest). Five technical replicates were performed for accuracy. Metabolites were extracted in a solution composed of 50% methanol, 30% acetonitrile, 20% ultrapure water and 50ng/ml HEPES. 1ml of extraction solution was added per $1x10^6$ cells. Extraction was carried out in a dry ice/methanol bath to maintain the integrity of the metabolites. Dr Valle Morales performed the LC/MS separation and analysis by calculating the ratio of the abundance of each metabolite normalised to total ion count (TIC). Using these data, I determined the fold change of each metabolite in Ishikawa EV and MLH1 cells to determine any significance.

It is important to note that cells grown in DMEM had increased levels of amino acids and vitamins relative to cells grown in RPMI, up to fourfold in some cases (**TABLE 8.1**). Most strikingly, however, DMEM contains more than double the concentration of glucose than RPMI media (25mM compared to 11.1mM) and approximately double the amount of glutamine (4mM compared to 2.1mM), the two metabolites we have labelled in previous flux experiments. We looked at the levels of specific metabolites in Ishikawa EV and MLH1 cells, cultured in each media. Firstly, we presented the data in a heat map representing the abundance of each metabolite at steady state in both cell lines (**FIGURE 4.10**). The values depict the fold change differences between Ishikawa EV versus MLH1; high values

represented in red, lower values in white. In both medias, there is less glucose detected in Ishikawa EV cells, relative to MLH1 cells. This could be because they are more glycolytic as our flux analysis demonstrates, thus are turning over glucose at a faster rate upon MLH1 loss. Interestingly, cells grown in DMEM had higher levels of pyruvate and lactate in Ishikawa EV cells which is not seen when cells were grown in RPMI. This could be as DMEM has an artificially high concentration of glucose which is favouring a higher rate of glycolysis. The next striking difference we observed between cells grown in the two medias is in the TCA cycle intermediates. In cells grown in RPMI, there was less succinate, fumarate, and malate in Ishikawa EV cells relative to MLH1-expressing cells, however, in cells grown in DMEM, there were minimal differences upon MLH1 loss. Moreover, significant differences in metabolite levels were also observed metabolites involved in the urea cycle. In Ishikawa EV cells cultured in DMEM there is more arginosuccinate, less aspartate and more NAA, relative to Ishikawa MLH1-expressing cells. This trend is not seen when these cells are cultured in RPMI (**FIGURE 4.10**). There is a link between the urea cycle and gluconeogenesis which could explain this response in DMEM. Most excess amino groups are converted into urea through the urea cycle, while their carbon skeletons are used to synthesise other intermediates such as glucose. In media containing supraphysiological concentrations of glucose, the requirement for gluconeogenesis may be reduced, leading to an accumulation of amino acids particularly those involved in the urea cycle.

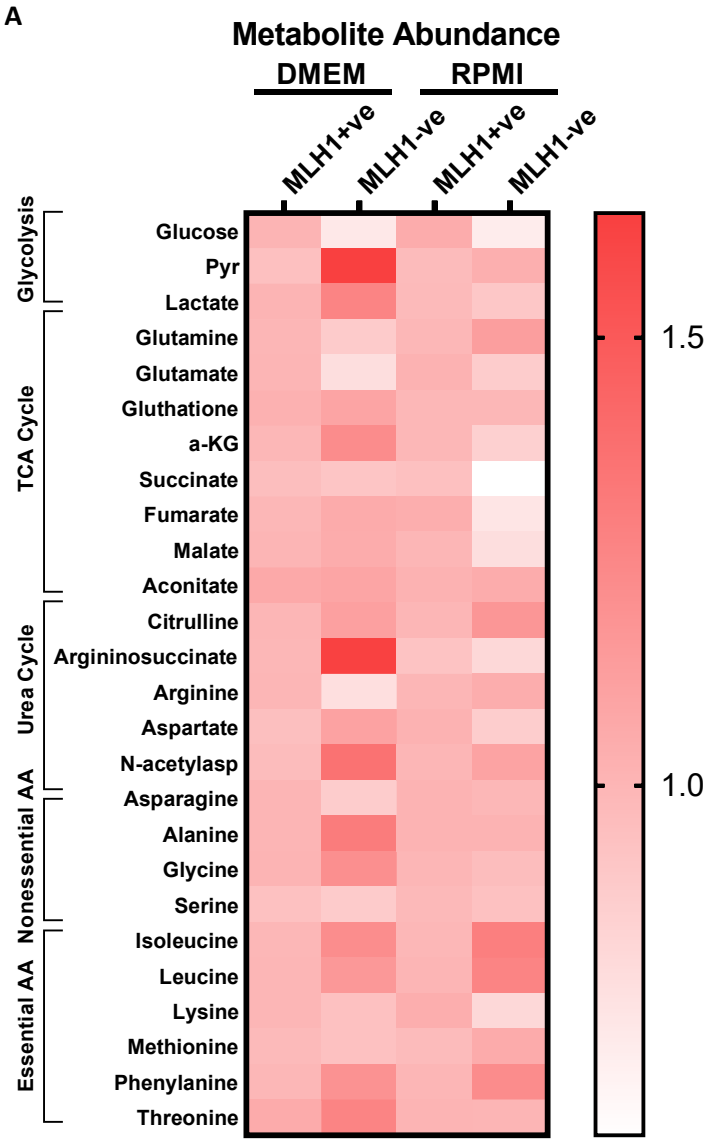

FIGURE 4.10. Ishikawa cells alter their metabolic pathway dependencies when grown in DMEM versus RPMI. Ishikawa EV and MLH1 cells were cultured in DMEM (containing 25mM glucose, 4mM glutamine) or RPMI (containing 11mM glucose, 2mM glutamine). DMEM uniquely contains a higher concentration of amino acids and vitamins. Heat map (**A**), produced by GraphPad Prism, shows the differential levels of metabolites present depending on the condition in which they are grown. Columns are median-centred, with fold changes compared to MLH1-proficient cells and represented by colour (Dark, higher abundance; Light, lower abundance). Ishikawa MLH1 and EV cells display different metabolic signatures depending on the media in which they are grown.

Investigating the metabolite differences between our cell models when they are cultured in different medias highlights one of the limitations of using *in vitro* models with the aim of identifying metabolic vulnerabilities which can be therapeutically targeted. Although this is interesting data, it is perhaps more informative to look at the metabolites with the same trend upon MLH1 loss, regardless of media in which they are cultured. As such, in our analysis we identified that Ishikawa EV cells had significantly

lower levels of glutamate compared to Ishikawa MLH1 cells (**FIGURE 4.11 A**). One explanation could be that MLH1-deficient cells may have increased glutamine anaplerosis, so they are metabolising glutamate to α-KG at a faster rate. Alternatively, these cells may not be relying on the TCA cycle as much, due to an altered pathway dependency in the absence of MLH1, hence do not require the same levels of glutamate as Ishikawa MLH1 cells. Moreover, it is possible that there is a link between MLH1 deficiency and glutaminase activity that would be interesting to explore. Nonetheless, this validates our finding which demonstrated that supplementation with glutamate in GAL-DMEM increases proliferation in Ishikawa EV cells.

Furthermore, Ishikawa EV cells have significantly more leucine ($p<0.0001$ DMEM & RPMI), isoleucine ($p<0.0001$ DMEM & RPMI) and phenylalanine ($p<0.0001$ DMEM; $p=0.0001$ RPMI) compared to Ishikawa MLH1 cells (**FIGURE 4.11 B-D**), all of which are essential amino acids, regardless of which media the cells are cultured in. Leucine and isoleucine play roles in the response to stress, and in energy production however are minimal contributors to enery production in tussue culture. These are branched-chain amino acids (BCAA) that are catabolised to acetyl-CoA and/or succinate-CoA for entry into the TCA cycle. Studies have demonstrated how BCAAs such as leucine and isoleucine, enhance glucose uptake by increasing the expression of glucose transporters GLUT1 and GLUT4 or by influencing the PI3K and PKC signalling pathways [356, 357]. Additionally, accumulating evidence demonstrates that BCAAs are essential nutrients for cancer cell growth and BCAA-specific metabolic enzymes are correlate with aggressive growth and proliferation. It would be interesting to further investigate whether there is a link between the expression of BCAA metabolic enzymes and MLH1 deficiency. Looking at our RNAseq data, we see a significant reduction in the expression of BCAT1 in both our Ishikawa and MFE-280 cell models. The log2Fold change for MLH1-deficient relative to proficient cells is -1.04 for Ishikawa ($p=0.006$), and -0.85 for MFE-280 ($p=0.006$). This enzyme catalyses the reversible transamination of branched-chain alpha-keto acids to branched-chain L-amino acids required for cell growth.

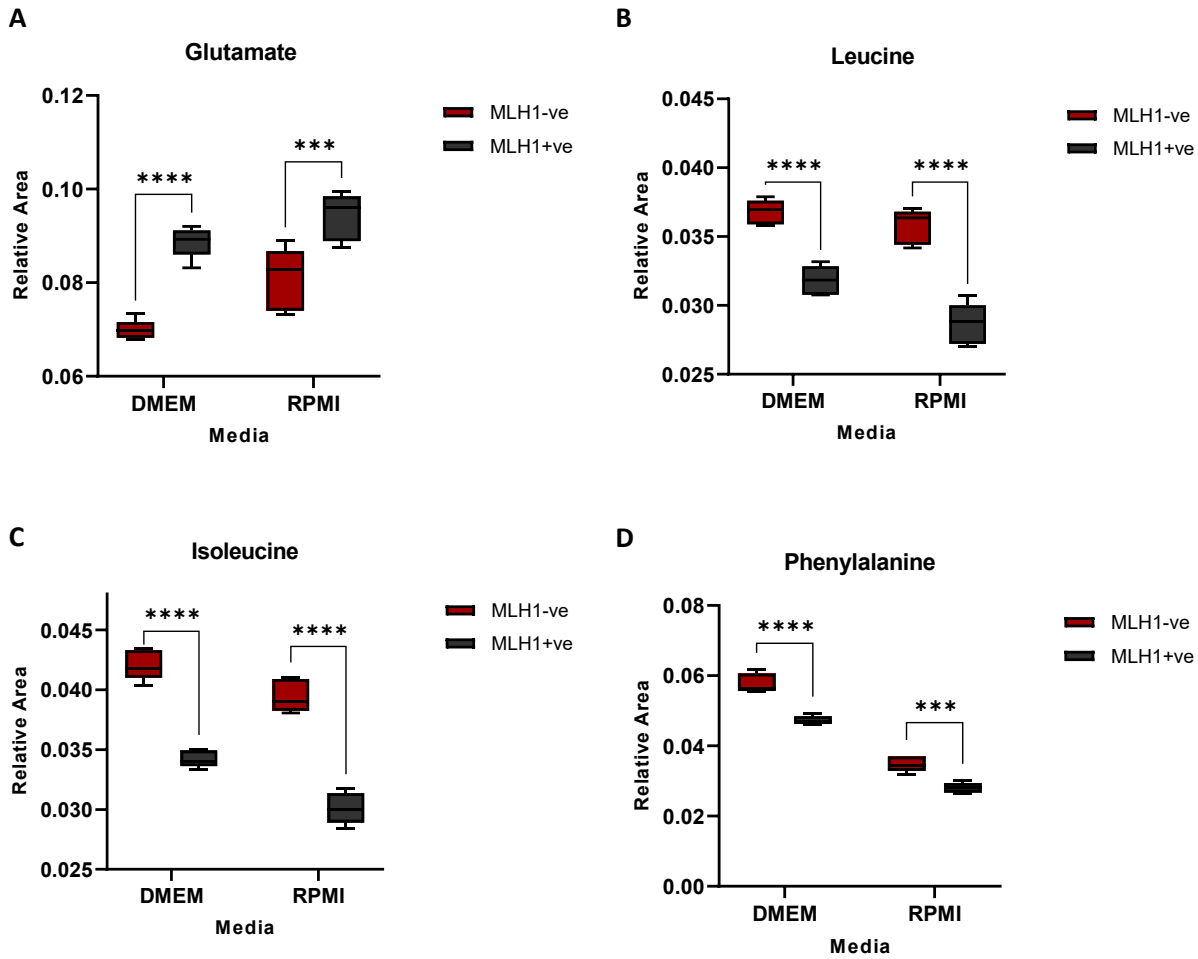

FIGURE 4.11. Quantification of metabolites *in vitro* when in EC cells grown in DMEM versus RPMI media. Ishikawa EV and MLH1 cells were cultured in DMEM (containing 25mM glucose, 4mM glutamine) or RPMI (containing 11mM glucose, 2mM glutamine). Graphs shown are the metabolites with the same differences, regardless of the media in which the cells are grown. The relative levels of Glutamate (**A**), Leucine (**B**), Isoleucine (**C**), and Phenylalanine (**D**). Statistical significance was determined using a TWO-WAY ANOVA with posthoc Holm-Sidak multiple Comparisons Test to Ishikawa MLH1. **P*<0.05, ***P*<0.01, ****P*<0.001, *****P*<0.0001. No asterix = not significant.

Subsequently, to visualise the impact cell culture media has on glycolysis and the TCA cycle, we positioned the graphs relative to the known reactions for each, as indicated by the literature. Firstly, we observe that there are comparable levels of glucose detected in Ishikawa MLH1 cells in both DMEM and RPMI, despite the higher concentration of glucose we know DMEM to possess. Glucose is subsequently metabolised to pyruvate through a series of reactions. The first marked difference we observed was in the levels of pyruvate in cells cultured in RPMI and DMEM. Interestingly, cells cultured in RPMI have strikingly higher levels of pyruvate and subsequently lactate, compared to the cells cultured in DMEM (**FIGURE 4.13**). Moreover, the glycolytic intermediate 3-phosphoglycerate is a precursor to the serine and glycine through the serine synthesis pathway (SSP). Interestingly there are also remarkably lower levels of serine and glycine in cells cultured in DMEM versus RPMI (**FIGURE 4.12**).

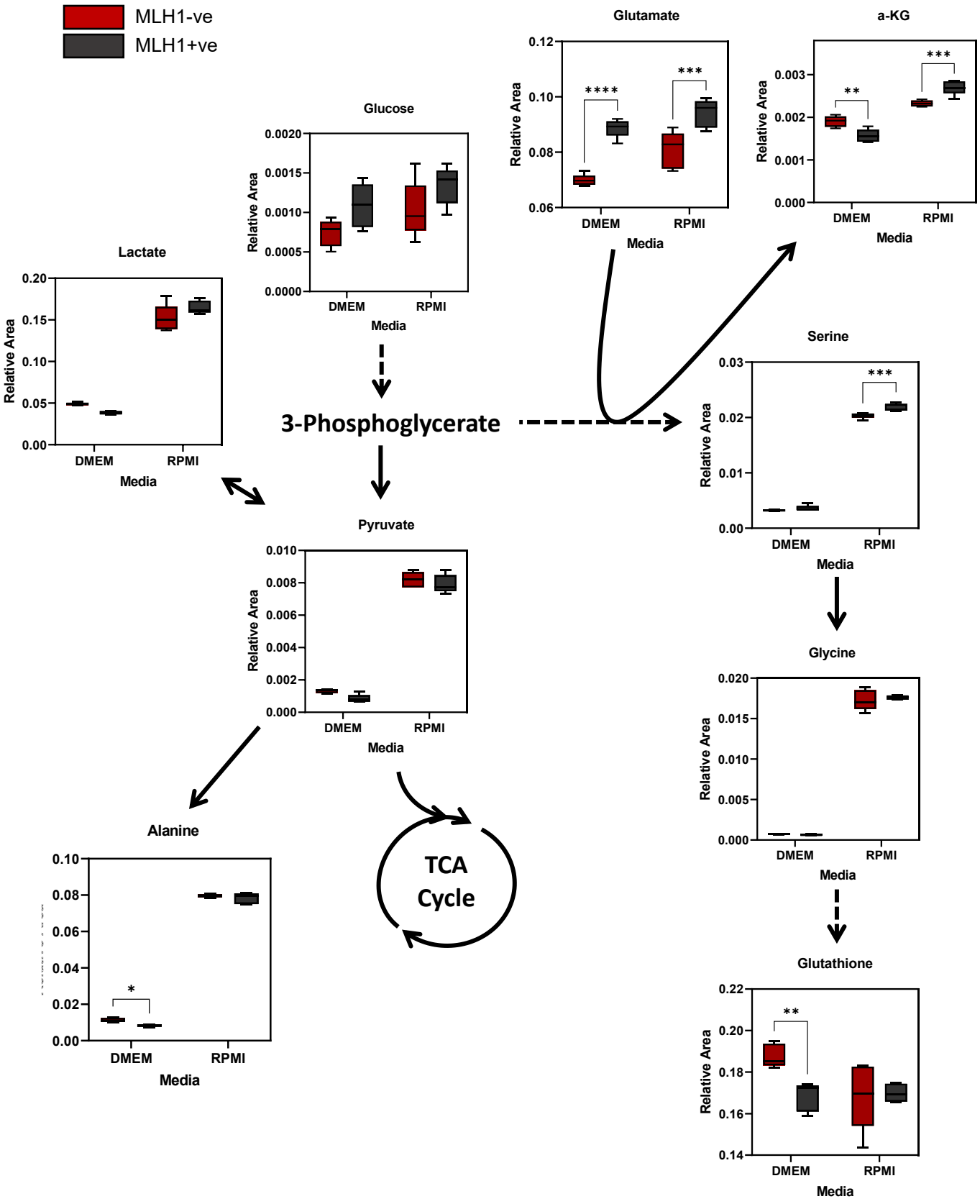

Figure legend on the next page.

FIGURE 4.12. Ishikawa cells alter their metabolic pathway dependencies when grown in DMEM versus RPMI. Ishikawa EV and MLH1 cells were cultured in DMEM (containing 25mM glucose, 4mM glutamine) or RPMI (containing 11mM glucose, 2mM glutamine). DMEM uniquely contains a higher concentration of amino acids and vitamins. Cells were harvested for metabolite detection. Schematic diagram of glucose metabolism through glycolysis and beyond is arranged with graphs according to known metabolite conversions as described in the literature. Ishikawa MLH1 and EV cells display different metabolic signatures depending on the media in which they are grown.

Following glucose metabolism, acetyl-CoA is formed by the oxidative carboxylation of pyruvate catalysed by the pyruvate dehydrogenase complex. Although we observe significantly lower levels of pyruvate in our cells cultured in DMEM relative to those cultured in RPMI, this trend is not replicated throughout all subsequent TCA cycle metabolites (**FIGURE 4. 13**). It is understood that glutamine supplies the greatest proportion of carbons to the TCA cycle. Accordingly, in our Ishikawa EV cells they have significantly more glutamine than those cells grown in RPMI, however despite these cells cultured in both medias have comparable levels of glutamate, α-KG, and succinate. Interestingly, EV cells have more fumarate and malate in DMEM. This could be because the media is richer in nutrients and thus the cells have the precursors required to support the synthesis of these metabolites. Nonetheless, these data demonstrates how culturing cells in different compositions of metabolites *in vitro* impacts the metabolic architecture of Ishikawa cells regardless of MLH1 status. As such, it is necessary to keep this in mind when hypothesising new therapeutic strategies.

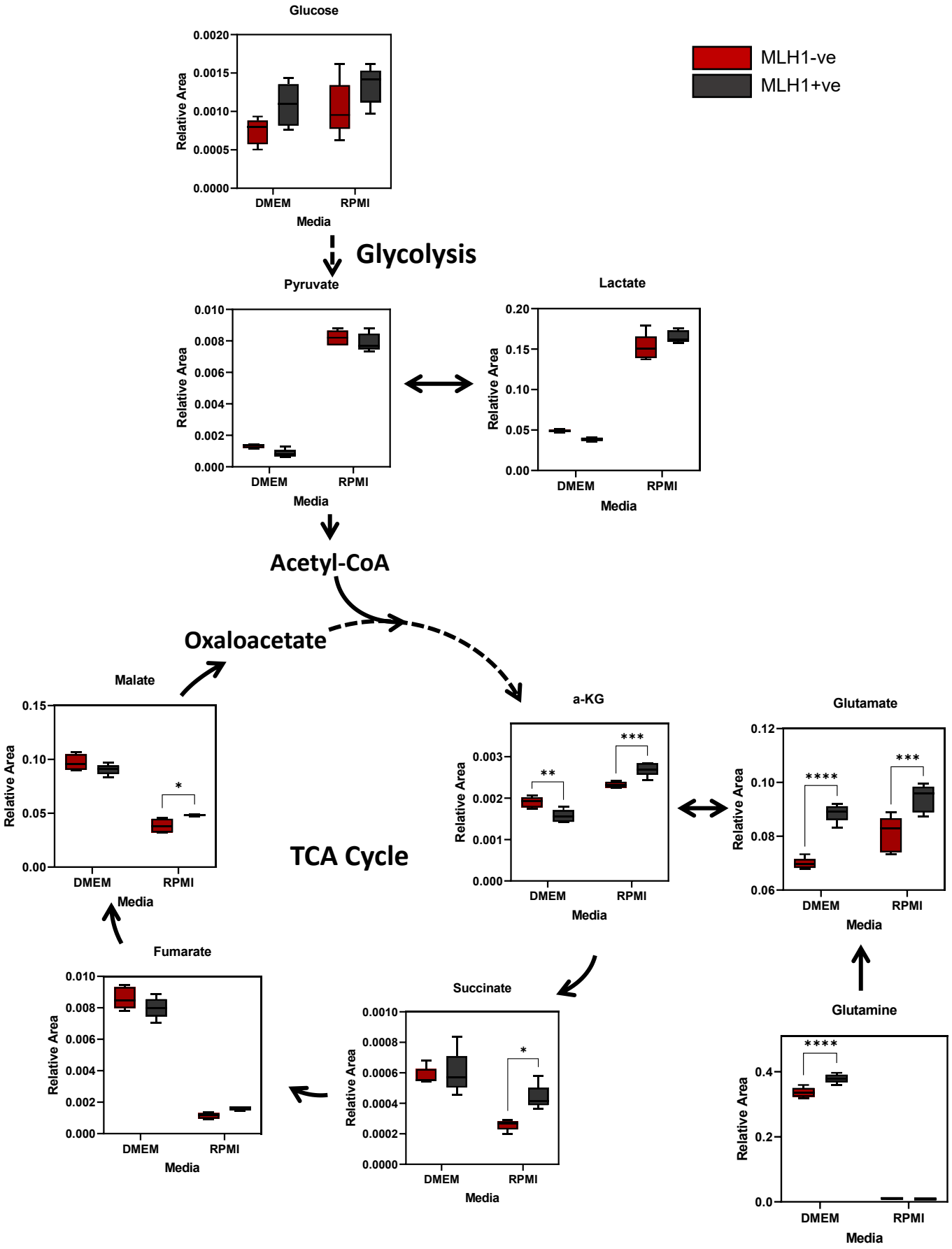

Figure legend on the next page.

FIGURE 4.13. Ishikawa cells have higher relative levels of TCA cycle intermediates when grown in DMEM versus RPMI suggesting an increased dependency on glutamine over glucose. Ishikawa EV and MLH1 cells were cultured in DMEM (containing 25mM glucose, 4mM glutamine) or RPMI (containing 11mM glucose, 2mM glutamine). DMEM uniquely contains a higher concentration of amino acids and vitamins. Cells were harvested for metabolite detection. Schematic diagram of glucose and glutamine metabolism through glycolysis and the TCA cycle, is arranged with graphs according to known metabolite conversions as described in the literature. Ishikawa MLH1 and EV cells display different metabolic signatures depending on the media in which they are grown.

4.4 Conclusion

In conclusion, MLH1-deficient cells have a distinct metabolic architecture compared to their MLH1-proficitent counterparts. These experiments indicated that Ishikawa EV cells were more metabolically active in the absence of MLH1. Paired with our previous data which demonstrated that MLH1-deficient Ishikawa EV cells have reduced OXPHOS capabilities and reduced complex I expression and activity, I hypothesise that this may be how these cells continue to proliferate efficiently. The metabolomics results demonstrate that MLH1-deficient cells may have an increased dependency on anaerobic metabolism and serine synthesis. In the following chapter I investigate the mechanism underlying these observations to see whether we have identified a biologically significant phenotype that may be therapeutically targeted. The difference in results we highlighted between culturing the cells in DMEM and RPMI, however highlights the drawbacks of studying cancer metabolism *in vitro*, and should be taken into consideration. This is discussed further in section 6.3.1.

5.0 Results – Identifying Metabolic Vulnerabilities in MLH1-deficient Endometrial Cancer

5.1 Role of anaerobic metabolism in MLH1-deficiency

5.1.1 Characterising the effect of lactate dehydrogenase and glutaminase inhibition on Ishikawa and MFE-280 MLH1-deficient EC cells

The results from our metabolomics study demonstrated that MLH1-deficient Ishikawa cells were more metabolically active, with a notable increase in anaerobic metabolism relative to their MLH1-proficient counterparts (**FIGURE 4.1**). With the intention of understanding the mechanism driving this phenotype and the possible identification of drug candidates that MLH1-deficient cells are selectively sensitive to, we investigated the effect of several metabolic inhibitors on our cell models, initially focussing on LDH inhibition given our metabolomics analysis indicated MLH1-deficient Ishikawa cells were more glycolytic than their MLH1-proficient counterparts, with increased incorporation of M+3 labelled carbon into pyruvate (**FIGURE 4.3**). Targeting specific metabolic vulnerabilities of cancer cells has been a fast-growing area of cancer research ever since Warburg proposed that cancer cells prefer glycolysis to OXPHOS [217]. In this context, LDH, which converts pyruvate to lactate at the end of glycolysis has been a well-researched cancer therapeutic target. Lactate, produced by tumour cells, contributes to the tumour microenvironment, facilitating tumour invasion and suppressing anticancer immune effectors [358, 359]. Lactate is taken up by stromal cells to either regenerate pyruvate to refuel the cancer cell or be utilised for OXPHOS. Fischer *et al*. demonstrate how high lactic acid concentrations in the tumour environment block the export of lactic acid in T cells thus interrupting their metabolism and function [360]. This system demonstrates how cancerous and non-cancerous cells engage complementary metabolic pathways to sustain cancer cell survival and growth. Recently, Oshima *et al.* demonstrated how LDH inhibition slows tumour growth but redirects pyruvate to support mitochondrial metabolism. Consequently, inhibiting both mitochondrial complex I and LDH in unison suppress the metabolic plasticity of glycolytic tumours *in vivo*, significantly prolonging the inhibitory effect on tumour growth [361].

We commenced by investigating the sensitivity of our MLH1-deficient and proficient EC cell lines to 3-dihydroxy-6-methyl-7-(phenylmethyl)-4-propylnaphthalene-1-carboxylic acid (FX11) treatment. FX11, a gossypol derivative, is an LDH inhibitor which demonstrates a higher selectivity for the forward reaction of LDHA, than for the reverse reaction of LDHB (Ki=8 µM for LDHA, Ki=20 µM for LDHB) [362-364], and has been shown to demonstrate preclinical efficacy in adult cancers [365]. To investigate whether LDHA inhibition has a differential effect on our MLH1-deficient EC cell models, we treated our cells with 20µM of FX11 for 96 hours and monitored cell proliferation over time using the Incucyte

Zoom Live-Cell imaging system. Values were normalised to the percentage confluence at time 0. Furthermore, to remove the potential effect of differential cell line proliferation rates, each treated time point was normalised relative to its respective untreated measurement at the same time point. As a result, the untreated conditions at each time point are equal to 1. Interestingly, our results indicate that that the MLH1-deficient MFE-280 gCTRL cells were more sensitive to LDH inhibition, compared to both MLH1-deficient K/O clones (**FIGURE 5.1 A**). This is in contrast to our Ishikawa cell model where MLH1-deficient Ishikawa EV cells were more sensitive to LDH inhibition (**FIGURE 5.1 B**). We next carried out this experiment over a longer time course (6 days) to determine whether sustained inhibition of LDH had an increased effect on cell proliferation. We again observed that the Ishikawa EV MLH1-deficient cells were more sensitive to FX11 than the Ishikawa MLH1 cells (**FIGURE 5.2 A**) and in contrast, MLH1-proficient MFE-280 cells were more sensitive to FX11 than their MLH1-deficient cells (**FIGURE 5.2 B**). Given that we observed decreased Complex I activity in the Ishikawa EV MLH1-deficient cells, these results may suggest that MLH1-deficient cells may be sensitive to LDH inhibition in a setting where MLH1 loss results is associated with reduced OXPHOS capacity. However, MLH1-deficient MFE-280 cells which we have shown have increased RNA expression of genes involved in mitochondrial metabolism (**FIGURE 3.18**), despite a reduction in expression of OXPHOS complexes as indicated in **FIGURE 3.5**, are not sensitive to LDH inhibition. In fact, these MLH1-deficient EC cells are more resistant relative to the MFE-280 gCTRL cells (**FIGURE 5.1 A, C, D**). These results demonstrate that there are metabolic differences between our two EC cell models that are unlinked to MLH1 loss, highlighting a significant limitation of using *in vitro* techniques to investigate cancer cell metabolism. Nonetheless, given we observed opposite trends in sensitivity to LDH inhibition between our Ishikawa EV and MFE-280 MLH1 K/O clones we deduced that it was likely that lactate metabolism is not the predominant mechanism MLH1-deficient cells rely on to proliferate in the absence of proficient OXPHOS. To further investigate the differences in sensitivity to LDH inhibition we observed between our cell models and validate the importance of lactate metabolism in MLH1-deficient EC cells, additional work is required to ensure that FX11 was sufficiently and comparatively decreasing lactate production in all cell lines. Furthermore, it would be interesting to investigate whether LDH inhibition in combination with Complex I inhibition, prolonged its suppressive effect on cell proliferation in Ishikawa EV cells, and rendered the MLH1-deficient MFE-280 cell lines sensitive.

Next, we investigated the effect of inhibiting glutamine utilising enzymes such as GLS, that catalyses the conversion of glutamine to glutamate. Our metabolomic data demonstrated that MLH1-deficient Ishikawa EV cells have an increased incorporation of ^{13}C from glutamine into TCA intermediates (**FIGURE 4.1**). Glutamine metabolism has been extensively investigated as a potential therapeutic

target for cancer. Rapidly proliferating healthy cells or those under physiological stress have an increased demand for glutamine. As such, we investigated whether our MLH1-deficient EC cell lines were sensitive to the glutamine antagonist 6-diazo-5-oxo-L-norleucine (L-DON). L-DON has been studied for many years as a cancer therapeutic and at low doses has shown promising antitumour activity, however, clinical development ceased when higher doses induced intolerable side effects in phase 1 and 2 clinical trials [366]. Glutamine is the most abundant circulating amino acid, and once taken up by cells is utilised in numerous metabolic processes. Glutamine is hydrolysed to glutamate and ammonia by glutaminase, it is subject to glutamine aminotransferases which catalyse the use of the amino group as a building block for nucleosides, amino acids, and hexosamine sugars, or it can be used to charge tRNA for protein synthesis [366]. Glutamate can be further metabolised to αKG for entry into the TCA cycle. Glutamine-derived glutamate is also vital for maintaining cellular redox status. Many tumours become largely dependent on glutamine to provide carbon and nitrogen building blocks for proliferation [367].

To investigate whether broad inhibition of glutamine-utilising enzymes has a differential effect on our MLH1-deficient Ishikawa EV and MFE-280 MLH1 K/O cell lines, we treated our cells with 5µM of L-DON, which has been shown to inhibit glutamine-utilizing enzymes, including glutaminase, at low micromolar levels [368], for 96 hours and monitored cell proliferation over time using the Incucyte Zoom Live-Cell imaging software. Values were normalised to the percentage confluence at time 0. Furthermore, to remove the potential effect of differential cell line proliferation rates, each treated time point was normalised relative to its respective untreated measurement at the same time point. As a result, the untreated conditions at each time point are equal 1. Our results revealed no differences in sensitivity upon L-DON treatment between the MLH1-proficient and MLH1-deficient MFE-280 cells lines (**FIGURE 5.1 C**). Interestingly, our MLH1-proficient Ishikawa cells are marginally more sensitive (padj. =0.0444) to L-DON inhibition after 48 hours, however, this sensitivity diminishes by 96 hours (**FIGURE 5.1 D**). We proposed that MLH1-deficient Ishikawa EV cells are potentially more adaptable to altering their nutrient uptake and metabolic networks compared to Ishikawa MLH1 cells. Additionally, the metabolomics data demonstrates that Ishikawa EV cells are more metabolically active than Ishikawa MLH1 cells therefore are likely able to compensate at a faster rate. To investigate this sensitivity further, we treated our cells in a similar manner with 5µM of CB-839. CB-839 is selective glutaminase inhibitor that has been associated with reduced growth of lymphomas, breast, renal and pancreatic cancers in pre-clinical studies. Additionally, CB-839 is being investigated in combination with other chemotherapies, in Phase II clinical trials for prostate cancer (i.e., NCT04824937). CB-839 targets the allosteric site of glutaminase, the enzyme responsible for converting glutamine to

glutamate, with high specificity. We observed no difference in sensitivity between our MLH1-proficient and deficient MFE-280 cells once again, however, this time the same is also true for our Ishikawa cell lines which also show no sensitivity (**FIGURE 5.1 E/F**).

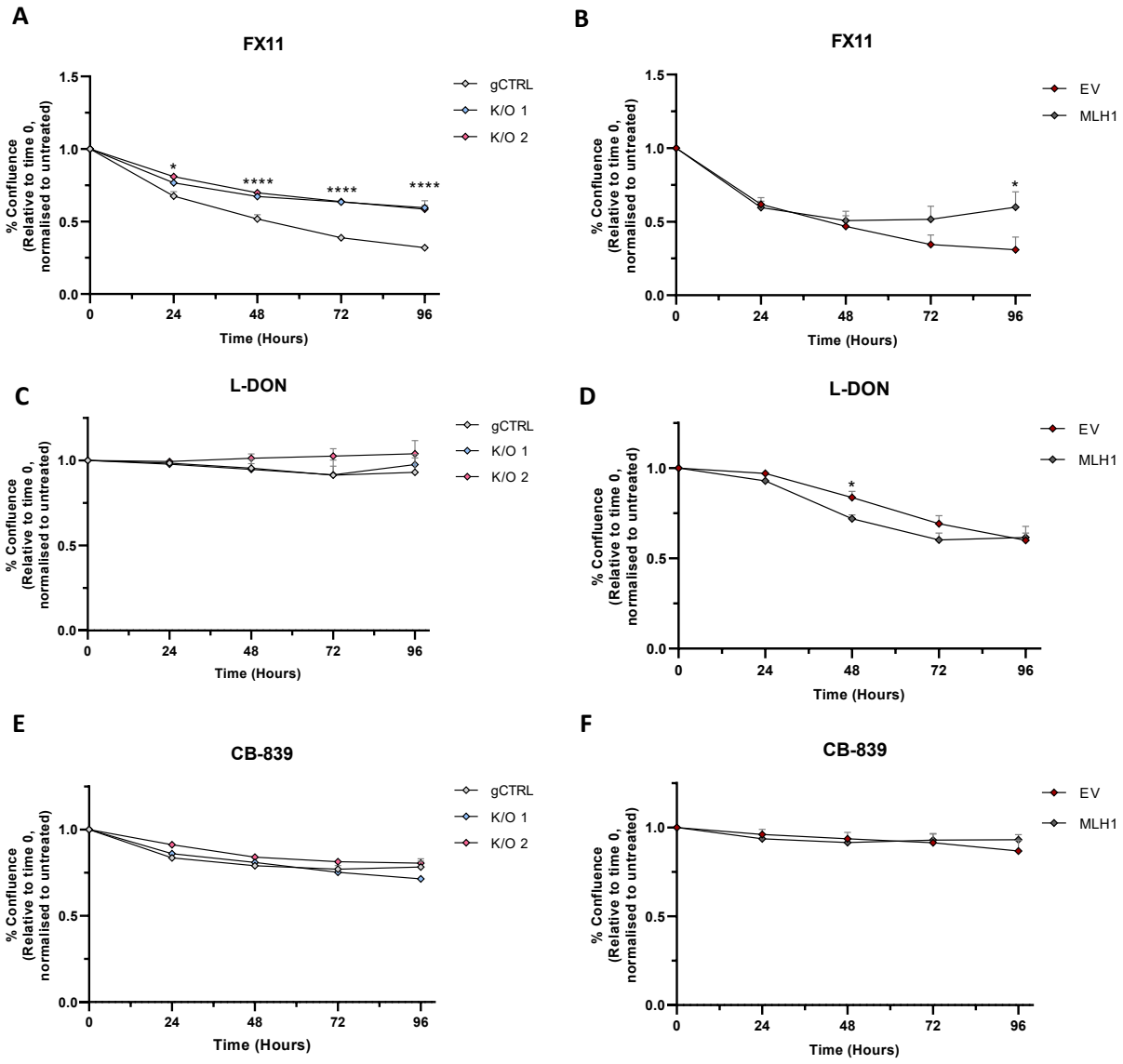

FIGURE 5.1. MLH1-deficient Ishikawa but not MFE-280 MLH1 K/O cells were sensitive to LDH inhibition. MLH1-proficient and deficient Ishikawa and MFE-280 cells were treated with 20µM FX11 **(A, B)**, 5µM L-DON **(C, D)**, and 5µM CB-839 **(E, F)**. The effect of drug treatment on the confluence of cells was measured relative to untreated and normalised to the confluence of each well at time 0, using the Incucyte Zoom Live-Cell imaging software over 3 days. Graph represents 3 independent cultures with 4 technical repeats. Error bars represent standard error of mean. Statistical significance was determined using a TWO-WAY ANOVA with posthoc Holm-Sidak multiple Comparisons Test to Ishikawa MLH1 or MFE-280 gCTRL. *p<0.05, ****p<0.0001. No asterix = not significant.

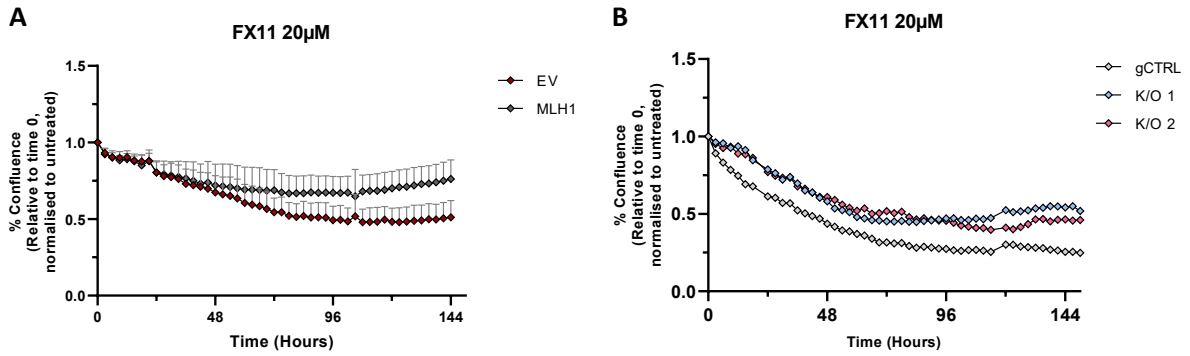

FIGURE 5.2. Monitoring of cell proliferation over time validates that MLH1-deficient Ishikawa but not MFE-280 cells are sensitive to FX11 treatment. MLH1-proficient and deficient Ishikawa **(A)** and MFE-280 **(B)** cells were treated with 20μM FX11 **(A, B)**. The effect of drug treatment on the confluence of cells was measured relative to untreated and normalised to the confluence of each well at time 0, using the Incucyte Zoom Live-Cell imaging software over 6 days. Graph represents 3 independent cultures with at least 4 technical repeats for **(A)** and 1 independent culture with at least 4 technical repeats for **(B)**. Error bars represent standard error of mean. Statistical significance was determined using a TWO-WAY ANOVA with posthoc Holm-Sidak multiple Comparisons Test to Ishikawa MLH1 or MFE-280 gCTRL. No asterix = not significant.

We validated these results using the CTG cell viability assay, treating Ishikawa EV, Ishikawa MLH1, MFE-280 gCTRL, K/O 1, and K/O 2 cell lines with increasing concentrations of FX11, L-DON, CB-839, CPI-613 for 72 hours as indicated (**FIGURE 5.3/4**). Furthermore, we treated our cells with two additional LDH inhibitors GNE-140 and GSK2837808A to investigate whether we observed the same trend in sensitivity between our two MLH1-deficient cell models. GNE-140 and GSK2837808A are selective inhibitors of LDHA and LDHB; GNE-140 has suggested IC50 of 3 nM and 5 nM for each respective enzyme [369], while GSK2837808A has a suggested IC50 of 2.6 nM and 43 nM, respectively [370]. Boudreau *et al.* demonstrated GNE-140 caused growth arrest in highly glycolytic pancreatic cancer cell lines such as MiaPaca2 by inhibiting LDHA/B [371]. Moreover, GSK2837808A has been shown to rapidly inhibit lactate production in multiple cancer cell lines including hepatocellular and breast carcinomas, however, the potency of the inhibitor varied significantly across 30 cancer cell lines investigated [370].

There are limitations to using cell viability-based assays to determine the effect of metabolic inhibition on cell lines because the assay measures the metabolite ATP. Previous studies have demonstrated large variability between a range of viability assays thus this should be taken into consideration [372]. Nonetheless, the CTG analysis of Ishikawa EV and MLH1 cells treated with LDH inhibitors FX11, GNE-140 and GSK2837808A showed trends consistent with proliferation results via Incucyte analysis (**FIGURE 5.3**), whereby the MLH1-deficient Ishikawa EV cells were marginally more sensitive compared

to their MLH1-proficient counterparts (**FIGURE 5.3 A-C**). Additionally, our MLH1-proficient gCTRL cells were more sensitive to FX11 treatment (**FIGURE 5.3 A**), again consistent with the Incucyte cell proliferation data in **FIGURE 5.1**. The MFE-280 MLH1 K/O 2 and MFE-280 gCTRL cells were more sensitive than the MLH1 K/O 1 cells to treatment with GNE-140, with a significant reduction in cell viability as the concentration of the inhibitor increases (**FIGURE 5.4 B**), once again drawing attention to the limitations of creating cell lines from single cells. The MFE-280 cells exhibited a similar trend when treated with GSK2837808A, where MLH1 K/O 1 cells were less sensitive to treatment versus MLH1 K/O 2 and gCTRL cell lines (**FIGURE 5.4 C**), though these were not significant differences.

Interestingly, CTG analysis of the Ishikawa MLH1-deficient and proficient cell lines treated with increasing concentrations of L-DON showed no differences in sensitivity to the drug (**FIGURE 5.3 D**), contrary to the cell proliferation data where Ishikawa MLH1-proficient cells were more sensitive to treatment with L-DON (**FIGURE 5.1 D**). For the MFE-280 cells, despite proliferation data indicating no significant differences in sensitivity to L-DON upon MLH1-loss, using the cell viability assay we observed that the MLH1-proficient MFE-280 gCTRL cells were significantly more sensitive to L-DON treatment when compared to the MFE-280 MLH1 K/O 1 cells, however, this was not observed in the MLH1 K/O 2 cells (**FIGURE 5.4 D**). These results highlight that there are metabolic differences between our MLH1-deficient K/O clones unexplained by MLH1 loss which may be due to the limitations of single-cell selection during the CRISPR process. Rederiving a cell line from a single cell creates a genetic bottleneck, where if a single cell-derived clone captures only a subset of the diversity present within the starting cell population experiments may be confounded [373]. Additionally, creating a genetically edited clonal population from a single cell represents a significant selective pressure which could enrich certain genetic and epigenetic alterations within the clone that promote proliferation [373]. As such it is necessary to investigate multiple independent K/O cell lines to ensure that any unexpected result is not a clonal artefact [373]. Alternatively, perhaps the lack of sensitivity MLH1-deficient MFE-280 K/O 1 cells exhibited to LDH or glutaminase inhibition could be associated with their increased complex I activity (**FIGURE 3.3**), however, to further investigate these findings more MLH1-deficient MFE-280 clones would need to be generated and compared.

Furthermore, we observed no significant differences in cell viability between Ishikawa EV and MLH1 cells treated with glutaminase inhibitor CB-839, though we did observe a slight trend where MLH1-deficient Ishikawa cells were more sensitive at 6.3-12.5 μM (**FIGURE 5.3 E**). We did not observe this trend through cell proliferation analysis using the Incucyte (**FIGURE 5.1 F**) which implied that treatment with CB-839 had no differential effect on Ishikawa EV and MLH1 cells, however, for that

experiment, the cells were only treated with one, slightly lower concentration of 5µM of CB-839. To validate whether these findings are biologically significant, the proliferation of Ishikawa EV and MLH1 cells treated with a higher concentration of CB-839 would need to be investigated.

Moreover, we observed the opposite for MFE-280 cells, whereby MFE-280 gCTRL cells were significantly more sensitive to CB-839 treatment compared to the two MLH1 K/O cell lines (**FIGURE 5.4 E)**, contrary to proliferation data (**FIGURE 5.1 D**), however, this was also performed at only one concentration. Lastly, we investigated whether CPI-613, a pyruvate dehydrogenase (PDH) inhibitor, had a differential effect on our cell lines, as we observed increased steady-state levels of pyruvate (**FIGURE 4.2/6**) and increased incorporation of M+3 labelled carbon into pyruvate in MLH1-deficient Ishikawa EV cells. CPI-613 has been shown to exhibit anticancer activity in pancreatic cancer cells by triggering ROS-associated apoptosis, which is accompanied by increased autophagy and repressed lipid metabolism through activating the AMPK signalling. CPI-613 is a lipoic analogue, which induces tumour suppression by changing the mitochondrial enzyme activity and redox status. It is used as an inhibitor of mitochondrial TCA for cancer treatment as it can specifically target PDH and alpha-ketoglutarate dehydrogenase [374]. CPI-613 is being investigated in phase 1 and 2 clinical trials in combination with other chemotherapies for the treatment of certain pancreatic cancers (i.e., NCT03699319). Though not significant, our data demonstrates our Ishikawa EV cells were slightly more sensitive versus MLH1 cells at relatively high concentrations of 50 and 100µM (**FIGURE 5.3 F**). The MFE-280 gCTRL cell line were more sensitive to treatment with the CPI-613 inhibitor in comparison to the two MLH1 knockout cell lines (**FIGURE 5.4 F).**

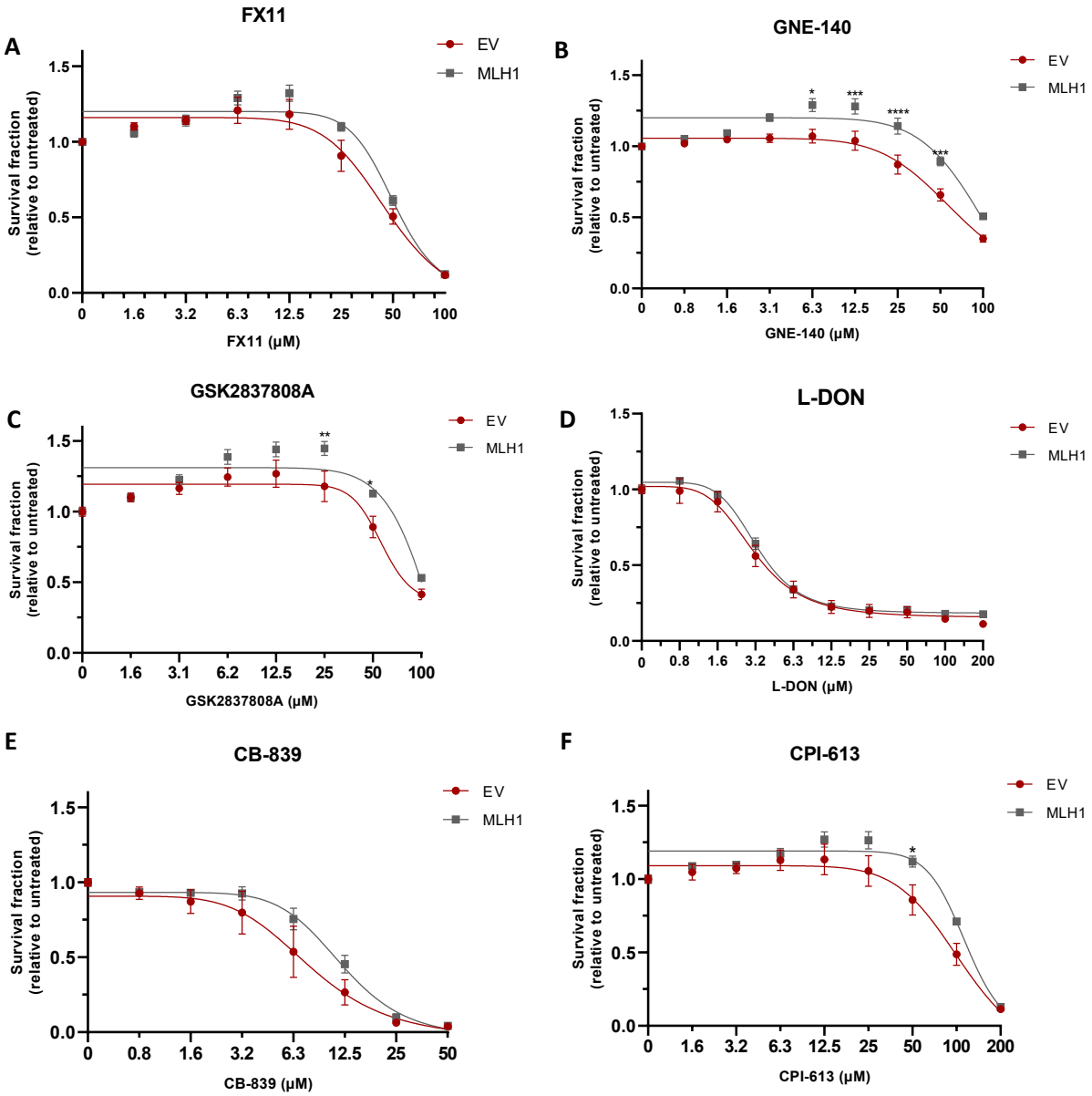

FIGURE 5.3. MLH1-deficient Ishikawa are more sensitive to LDH and PDH inhibition. MLH1-proficient and deficient Ishikawa cells were treated with FX11, GNE-140, L-DON, CB-839 and CPI-613. Short term survival curves are shown under continuous exposure to increasing concentration of drug. After 3 days cell viability was estimated using the ATP assay Cell Titre Glo. Error bars represent mean with standard error of mean of at least 3 independent experiments. Statistical significance was determined using a TWO-WAY ANOVA with posthoc Holm-Sidak multiple Comparisons Test to Ishikawa MLH1. **P*<0.05, ***P*<0.01, ****P*<0.001, *****P*<0.0001. No asterix = not significant.

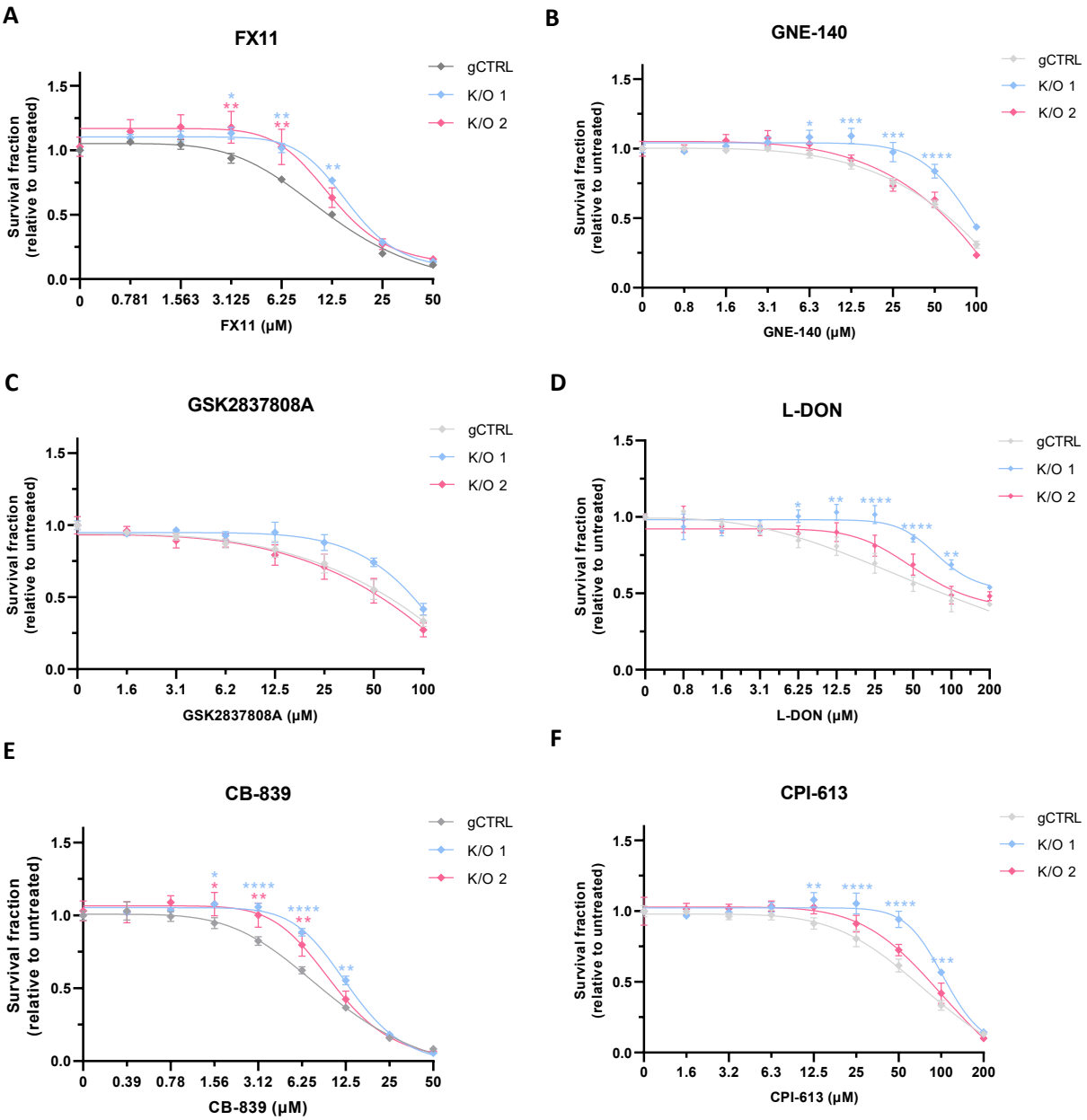

FIGURE 5.4. MLH1-proficient MFE-280 are more sensitive to LDH and PDH inhibition. MLH1-proficient and deficient MFE-280 cells were treated with FX11, GNE-140, L-DON, CB-839 and CPI-613. Short term survival curves are shown under continuous exposure to increasing concentration of drug. After 3 days cell viability was estimated using the ATP assay Cell Titre Glo. Error bars represent mean with standard error of mean of at least 3 independent experiments. Statistical significance was determined using a TWO-WAY ANOVA with posthoc Holm-Sidak multiple Comparisons Test to MFE-280 gCTRL. *P<0.05, **P<0.01, ***P<0.001, ****P<0.0001. No asterix = not significant.

Subsequently, we performed a clonogenic assay as an additional *in vitro* based cell survival assay to determine MLH1-deficient cell response to FX11, GNE-140 and L-DON treatment. The clonogenic assay measures the ability of single cells to proliferate and form clones following treatment and is considered a gold standard assay for detecting the effect a drug is having on cells. Moreover, the clonogenic assay can detect treatment-induced loss of proliferative capacity. In this assay we seeded the Ishikawa EV or MLH1 cells and treated them with increasing concentrations of FX11, GNE-140, L-DON, as indicated. The experimental control was treated with 0.01% DMSO. Cells were treated with respective treatment on day 1 and day 7, and fixed and stained on day 10. Individual colonies were counted using ImageJ and normalised to the untreated condition to calculate the survival fraction. Our data indicates that MLH1-deficient Ishikawa EV cells are more sensitive to LDH inhibition by FX11 (**FIGURE 5.5 A-C**) and GNE-140 (**FIGURE 5.6 A-C**). This is consistent with cell proliferation data from the Incucyte (**FIGURE 5.1 A**). Similarly consistent with previous proliferation data (**FIGURE 5.1 B**), Ishikawa MLH1 cells are more sensitive to L-DON inhibition in the clonogenic assay although this is not statistically significant (**FIGURE 5.7 A-C**). Unfortunately, we were not successful in getting MFE-280 cells to form colonies that could be properly analysed.

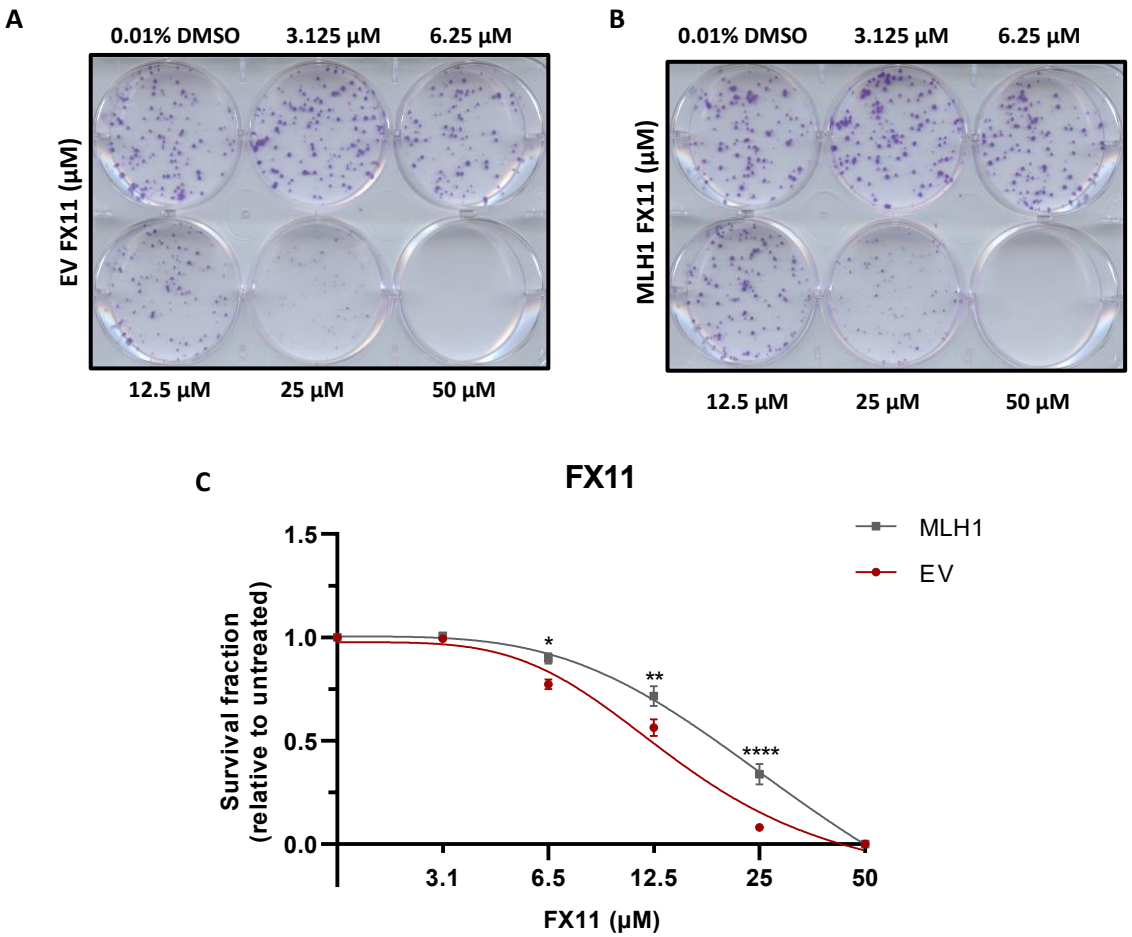

FIGURE 5.5. MLH1-deficient Ishikawa cells are more sensitive to LDH inhibition by FX11 treatment in a colony formation assay. A colony formation assay was performed in MLH1-deficient **(A)** and proficient **(B)** Ishikawa cells that were treated with 0-50µM of FX11. Cells were treated on day 1 and 7 and the images were taken at day 10. Individual colonies were counted using ImageJ cell counter and survival curve was plotted relative to the untreated samples. Error bars represent the standard error of mean for 2 independent cultures with 2 technical repeats. Statistical significance was determined using a TWO-WAY ANOVA with posthoc Holm-Sidak multiple Comparisons Test to Ishikawa MLH1. **P*<0.05, ***P*<0.01, *****P*<0.0001. No asterix = not significant.

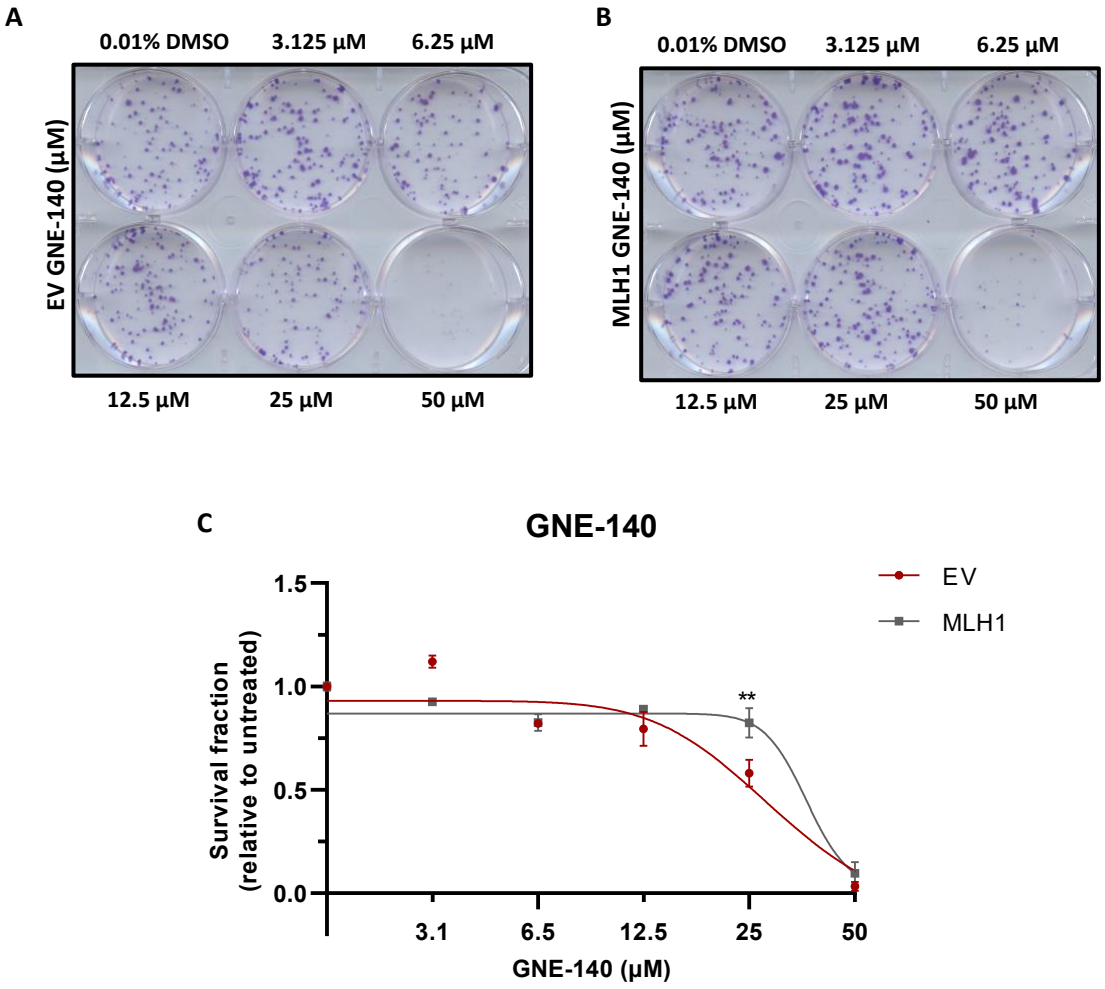

FIGURE 5.6. MLH1-deficient Ishikawa cells are more sensitive to LDH inhibition by GNE-140 treatment. Colony formation assay was performed in MLH1-deficient **(A)** and proficient **(B)** Ishikawa cells that were treated with 0-50µM of GNE-140. Cells were treated on day 1 and 7 and the images taken at day 10. Individual colonies were counted using ImageJ cell counter and survival curve plotted relative to the untreated samples. Error bars represent standard error of mean for 2 independent cultures with 2 technical repeats. Statistical significance was determined using a TWO-WAY ANOVA with posthoc Holm-Sidak multiple Comparisons Test to Ishikawa MLH1. ***P*<0.01. No asterix = not significant.

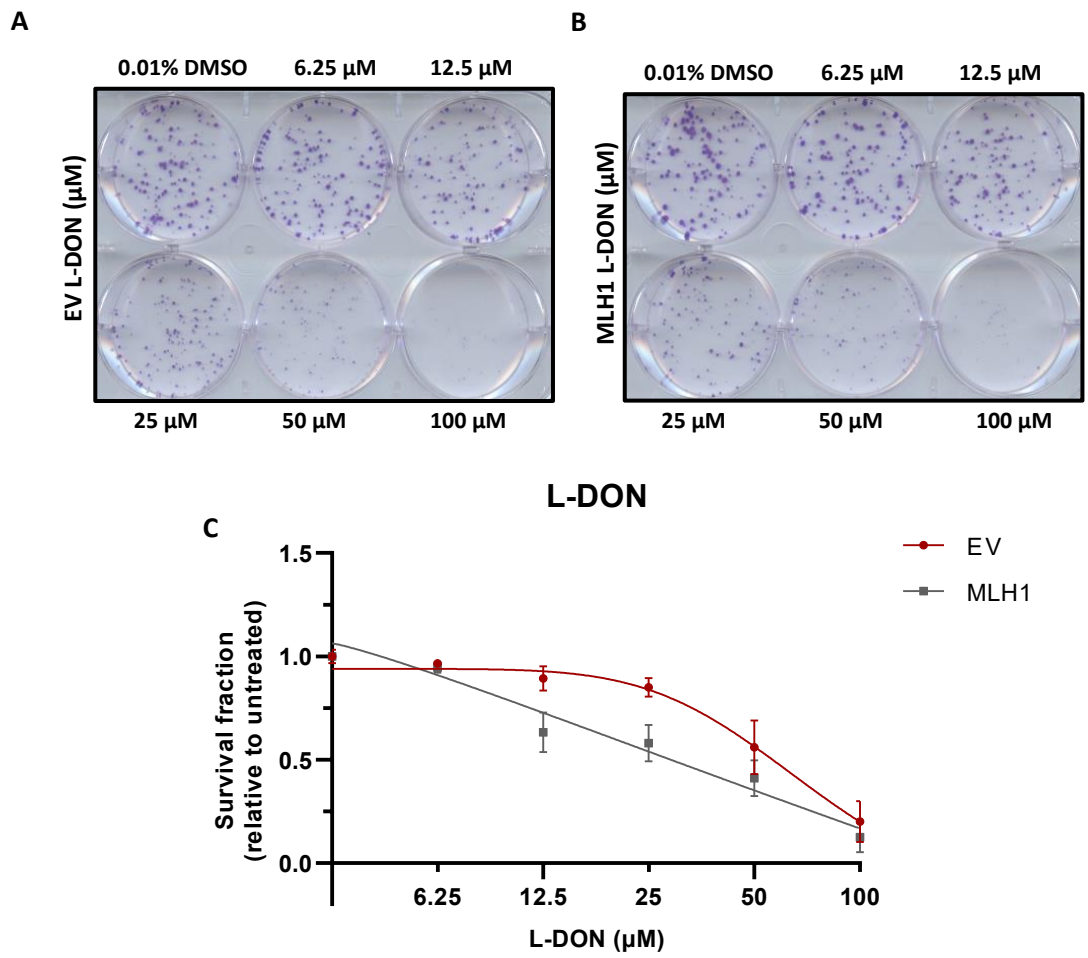

FIGURE 5.7. MLH1-proficient Ishikawa cells are more sensitive to L-DON treatment that inhibits glutamine utilising enzymes. Colony formation assay was performed in MLH1-deficient **(A)** and proficient **(B)** Ishikawa cells that were treated with 0-100 µM of L-DON. Cells were treated on day 1 and 7 and the images taken at day 10. Individual colonies were counted using ImageJ cell counter and survival curve plotted relative to the untreated samples. Error bars represent standard error of mean for 2 independent cultures with 2 technical repeats.

5.1.2 Investigating the effect of culturing Ishikawa and MFE-280 MLH1-deficient EC cell lines in more physiologically relevant media

The importance of metabolic rewiring in cancer cell survival and progression is now widely acknowledged. With this understanding, it was shown that typically used cell culture media such as DMEM or RPMI for *in vitro* experiments, may not accurately reproduce the metabolic environment of tumours *in vivo* [354]. With the aim of reducing the gap between *in vitro* observations and tumour biology, Tardito *et al*. created a complex culture medium composed of more than 50 nutrients and metabolites at the concentration 'normally' found in human blood and directly compared its effects on cultured cells in relation to standard commercial medias **(FIGURE 5.8)** [354]. Tardito *et al*. consulted a publicly available database to define the concentrations of nutrients and metabolites normally present in human blood, using an arbitrary threshold of 2µM. The key differences in concentration of metabolites between the different medias used in this study are highlighted in **TABLE 8.1 Supplementary**. Interestingly, in DMEM glucose and glutamine have significantly higher concentrations of glutamine 4 mM in DMEM versus 0.65 mM in Plasmax, and 25 mM of glucose versus 5.556 mM in each respective media. In Plasmax glucose and glutamine contribute to less than half of the whole pool of nutrients, contrary to DMEM. Furthermore, more than a quarter of the total nutrient availability in Plasmax is made up of components that are not present in DMEM, thus providing alternative sources of nutrients for cells (**FIGURE 8.1**). Interestingly, Tardito's studies demonstrated that the sodium selenite component of Plasmax prevented ferroptosis and thus enhanced the capacity of triple negative breast cancer (TNBC) cells to form colonies, which they were unable to do when cultured in DMEM F-12 [354]. It would have been beneficial to investigate whether MFE-280 cells formed colonies in Plasmax media, enabling them to be incorporated in the clonogenic assay analysis, however, time did not permit.

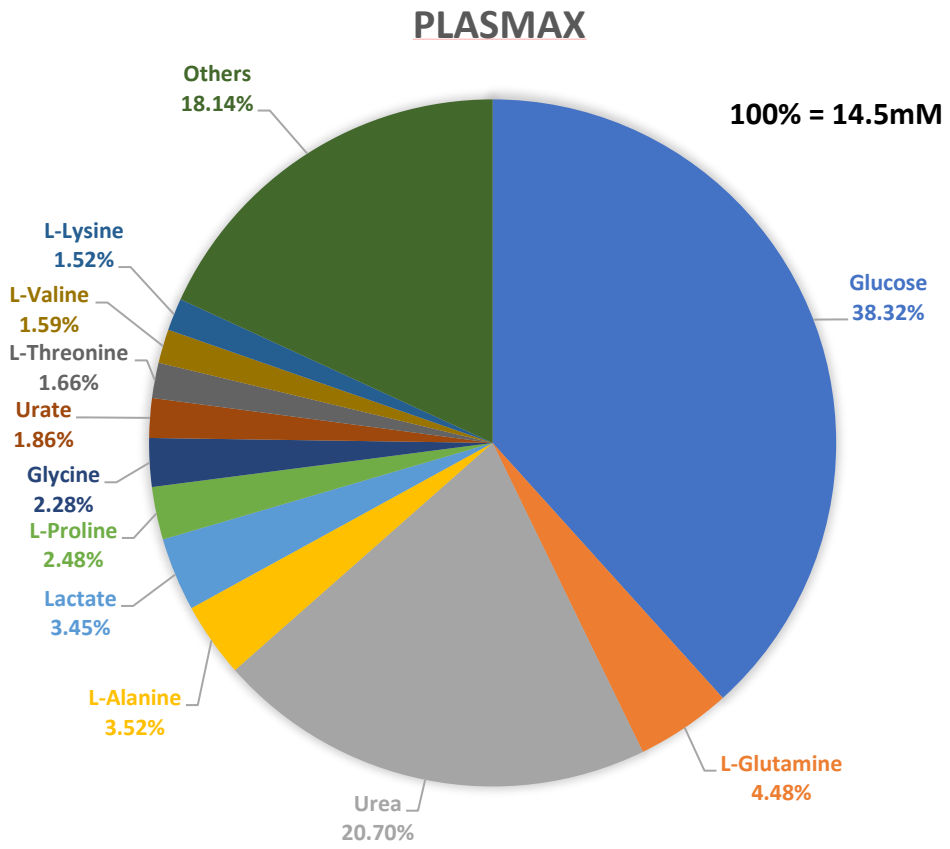

FIGURE 5.8. Plasmax composition. Glucose and glutamine contribute to less than half of the whole pool of nutrients in the physiologically relevant media, Plasmax.

To investigate whether the metabolic effects of the cell culture environment were influencing our results, we performed the following experiments in DMEM, RPMI, and Plasmax for comparison. Initially we compared the cell viability of Ishikawa EV, MLH1, MFE-280 gCTRL, MLH1 K/O 1 and K/O 2 cells cultured in each media over 5 days, to understand whether their rate of proliferation differed in each media. Prior to this, MFE-280 cells and Ishikawa cells were originally cultured in DMEM media. Cells were harvested from their flasks and washed three times with PBS before seeding in 96 wells plates at the densities indicated in section 2.1.2. On day 5, the viability of the cells was measured using the Cell Titer Glo viability assay and each cell line normalised to their respective DMEM cell line (i.e., their viability when grown in RPMI or Plasmax, relative to their viability when grown in their typical media, DMEM). Statistical comparisons were carried out relative to MLH1-proficient cell lines i.e., gCTRL MFE-280 or Ishikawa MLH1.

Our data demonstrated that MFE-280 gCTRL cells grow similarly in all medias (**FIGURE 5.9.A**). MLH1-deficient clones have a reduced viability relative to the gCTRL in RPMI media, however, exhibit similar viability compared to when they are grown in DMEM. We observed statistical differences between the MLH1-proficient and deficient cells when the cells were cultured in Plasmax media. In these conditions, both the MFE-280 MLH1 K/O clones have reduced viability relative to the gCTRL cells, and also to their viability when cultured in Plasmax (**FIGURE 5.9 A**). Of note, Tardito *et al*. found that the breast cancer cell line, MDA-MB-468, trended toward slower proliferation in Plasmax versus DMEM-F12 [354]. They found that Plasmax affected the morphology of these cells, which were flatter, with looser associations between neighbouring cells compared to when they were grown in DMEM-F12 [354]. A change in morphology and interactions with their neighbouring cells could explain provide an explanation for why our MLH1-deficient MFE-280 cells are proliferating slower than the MLH1-proficient MFE-280 gCTRL cells, however, due to time constraints we were not able to investigate these observations further. We performed a similar experiment with our Ishikawa cell lines and observed the opposite effect. MLH1-deficient cell line Ishikawa EV cell viability remained relatively unchanged between DMEM, RPMI and Plasmax, however, there was a reduction in viability of Ishikawa MLH1 cells in Plasmax and RPMI relative to DMEM (**FIGURE 5.9 B**).

Subsequently, we investigated whether there was a relationship between cell viability and the concentration of specific metabolites in the three medias. For this, we plotted the correlation between raw cell viability value and increasing concentrations of Glucose, Pyruvate, Glutamine, Arginine, Cysteine, Methionine, Serine, and Glycine. Statistical comparisons were carried out relative to respective MLH1-proficient cells, at each respective metabolite concentration. Our data for MFE-280 MLH1-deficient cells indicates there is a positive correlation between an increase in metabolite concentration (for those that we investigated), and cell viability, except Glycine. This was not true for MFE-280 gCTRL cells, where the viability of cells was unchanged upon increasing the concentration of each metabolite investigated (**FIGURE 5.10**). These results highlight the cellular plasticity of MLH1-deficient EC cells and how they are influenced by nutrient availability.

Furthermore, we performed the same analysis in our Ishikawa cells, the model that was used for the metabolomics experiments, hence we know they have differential metabolic vulnerabilities. In the same manner, as described above, we investigated the correlation between cell viability and concentration of metabolite for each cell line. Interestingly, we observe a positive correlation between increasing the concentration of each metabolite except glycine, and cell viability in the MLH1-proficient Ishikawa cells (**FIGURE 5.11**). There was no correlation between metabolite concentration

and cell viability in Ishikawa EV cells (**FIGURE 5.11**). This information could be indicative irrespective of the media Ishikawa EV cells are grown in, that in the absence of MLH1, these cells are able to rewire their metabolism to proliferate regardless of nutrient composition. Alternatively, it could suggest that Ishikawa EV cells have a growth disadvantage in the absence of MLH1 which means that despite increasing the concentration of specific metabolites these cells cannot proliferate any faster. Contrastingly, MLH1-proficient Ishikawa cells can grow faster when supplied with additional nutrients. Previous studies have compared the effects of exchange rates of nutrients between cells and media [354]. In both Plasmax and DMEM-F12, glucose was the most consumed metabolite, with lactate being the most abundantly released metabolite. The exchange rates between glucose and lactose were not significantly different, thus the rate of glucose fermentation is independent of extracellular availability. In contrast, cells consumed significantly less glutamine in Plasmax which contains less glutamine than DMEM-F12 (0.65mM versus 2mM respectively). Additionally, there was a positive correlation between metabolite availability and consumption of neutral proteinogenic amino acids and the rate that they were consumed or secreted [354].

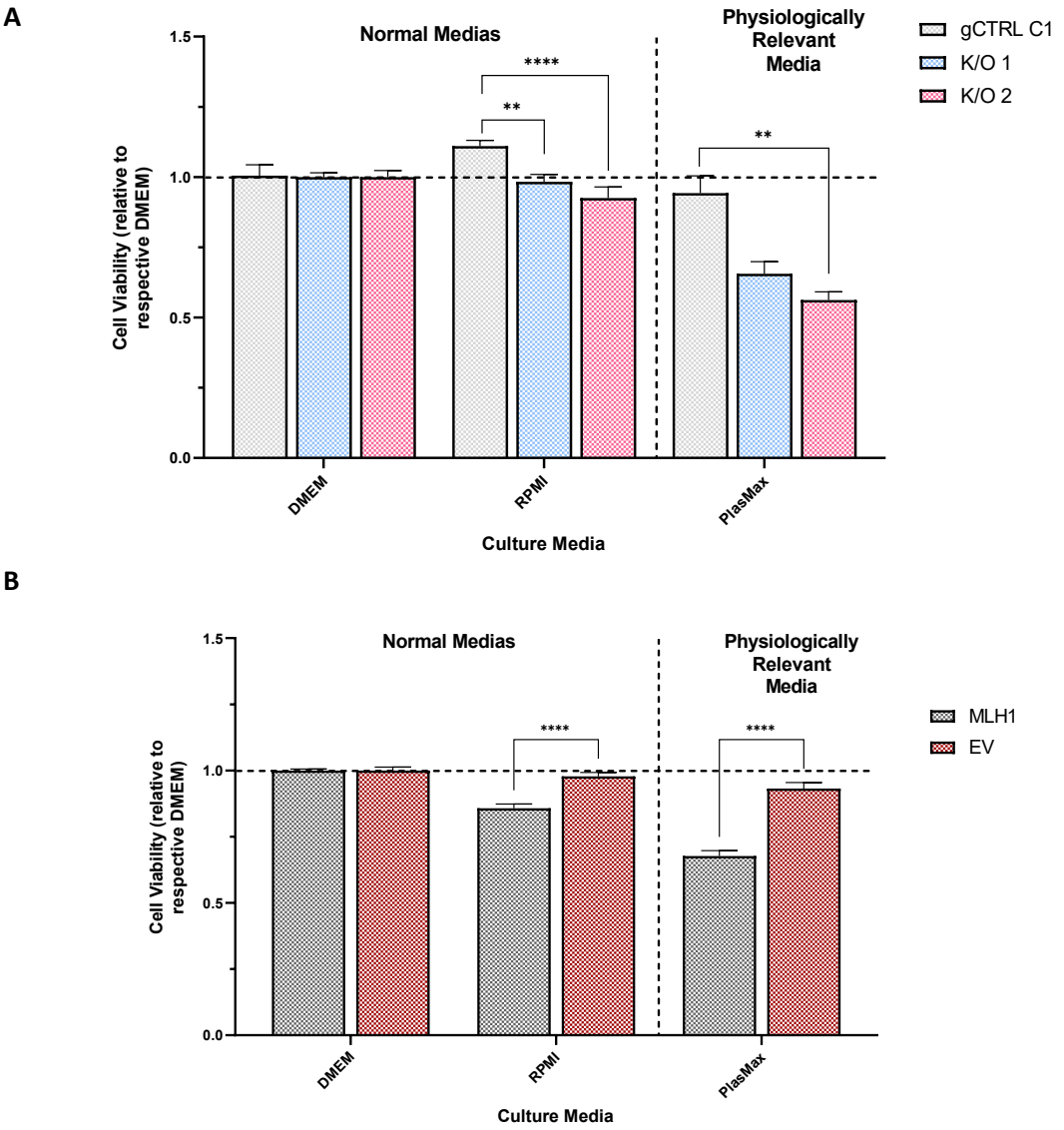

FIGURE 5.9. MLH1-deficient MFE-280 cells are less viable when cultured in RPMI and Plasmax versus their MLH1-proficient counterparts, whereas Ishikawa EV cells are more viable when cultured in RPMI and Plasmax versus their MLH1-proficient counterparts. MFE-280 **(A)** and Ishikawa **(B)** cells were cultured in DMEM, RPMI, or Plasmax for 5 days, and the cell viability was measured using the Cell Titer Glo viability assay. Error bars represent the standard error of mean of at least 3 independent cultures. Statistical significance was determined using a TWO-WAY ANOVA with posthoc Holm-Sidak multiple Comparisons Test to MFE-280 gCTRL or Ishikawa MLH1. *P<0.05, **P<0.01, ***P<0.001, ****P<0.0001. No asterix = not significant.

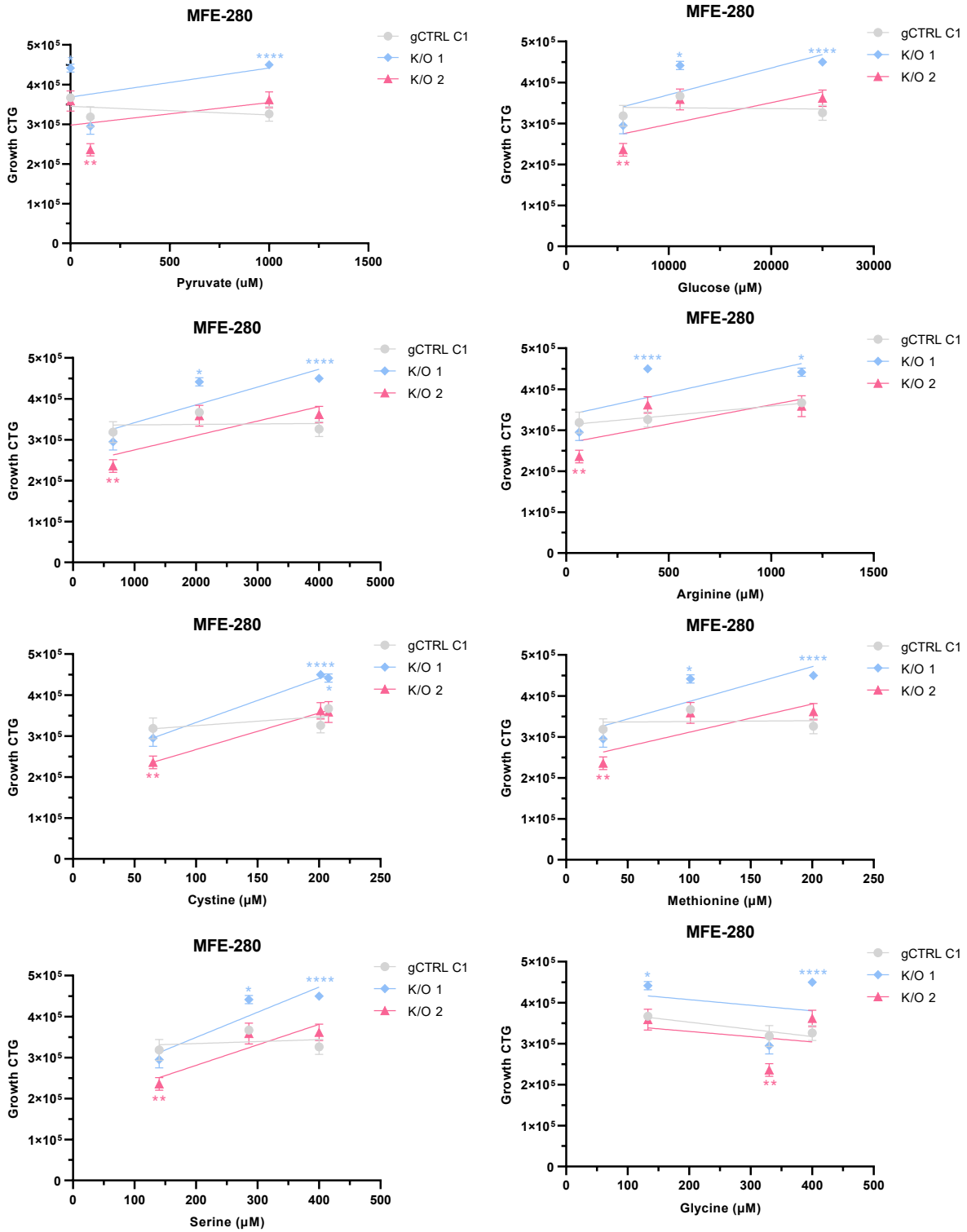

FIGURE 5.10. An increased concentration of pyruvate, glucose, glutamine, arginine, cystine, methionine, and serine result in an increased viability of MFE-280 gCTRL cells. MFE-280 gCTRL, K/O 1 and K/O 2 cells were cultured in DMEM, RPMI, or Plasmax for 5 days and their cell viability measured using the Cell Titer Glo viability assay. Graphs represent the cell viability of each cell line relative to the concentration of metabolite present in the media (as indicated in Supplementary **TABLE 8.1**). Error bars represent standard error of mean of at least 3 independent cultures with at least 4 technical repeats. Statistical significance was determined using a TWO-WAY ANOVA with posthoc Holm-Sidak multiple Comparisons Test to MFE-280 gCTRL. *P<0.05, **P<0.01, ***P<0.001, ****P<0.0001. No asterix = not significant.

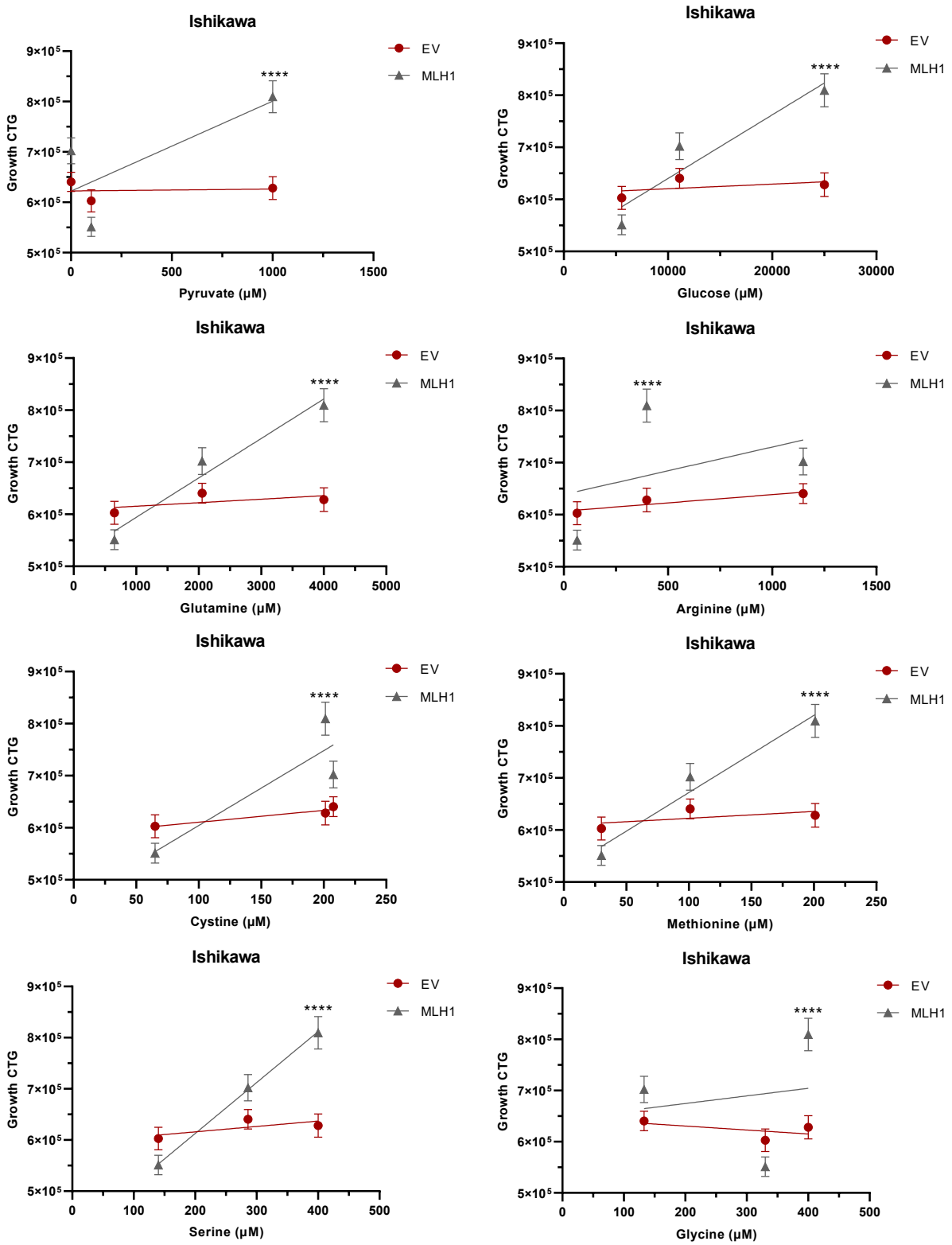

FIGURE 5.11. An increased concentration of pyruvate, glucose, glutamine, arginine, cysteine, methionine, and serine correlates with increased viability of Ishikawa MLH1-proficient cells. Ishikawa EV and MLH1 cells were cultured in DMEM, RPMI, or Plasmax for 5 days and their cell viability was measured using the Cell Titer Glo viability assay. Graphs represent the cell viability of each cell line relative to the concentration of metabolite present in the media (as indicated in Supplementary **TABLE 8.1**). Error bars represent the standard error of mean of at least 3 independent cultures with at least 4 technical repeats. Statistical significance was determined using a TWO-WAY ANOVA with posthoc Holm-Sidak multiple Comparisons Test to Ishikawa MLH1. *P<0.05, **P<0.01, ***P<0.001, ****P<0.0001. No asterix = not significant.

Additionally, we assessed the proliferation of the Ishikawa MLH1-proficient and -deficient cells in each media, using the Incucyte Zoom Live-Cell imaging system (**FIGURE 5.12**). Cells were seeded in DMEM, RPMI, or Plasmax and their proliferation was monitored over 5 days. Percentage confluence for Ishikawa EV and MLH1 cell lines were calculated at each time point in each condition and normalised to each respective percentage confluence at time 0. Our data indicated that in each media there are no significant differences in proliferation between Ishikawa MLH1 and Ishikawa EV cells (**FIGURE 5.12 A/B**)**,** however, while both cell lines grow comparatively in DMEM and RPMI, they do proliferate slightly slower in Plasmax (**FIGURE 5.12 C**). In conclusion, our results demonstrate how each media can significantly influence *in vitro* results, further highlighting the drawbacks of common cell culture techniques for metabolomics investigations.

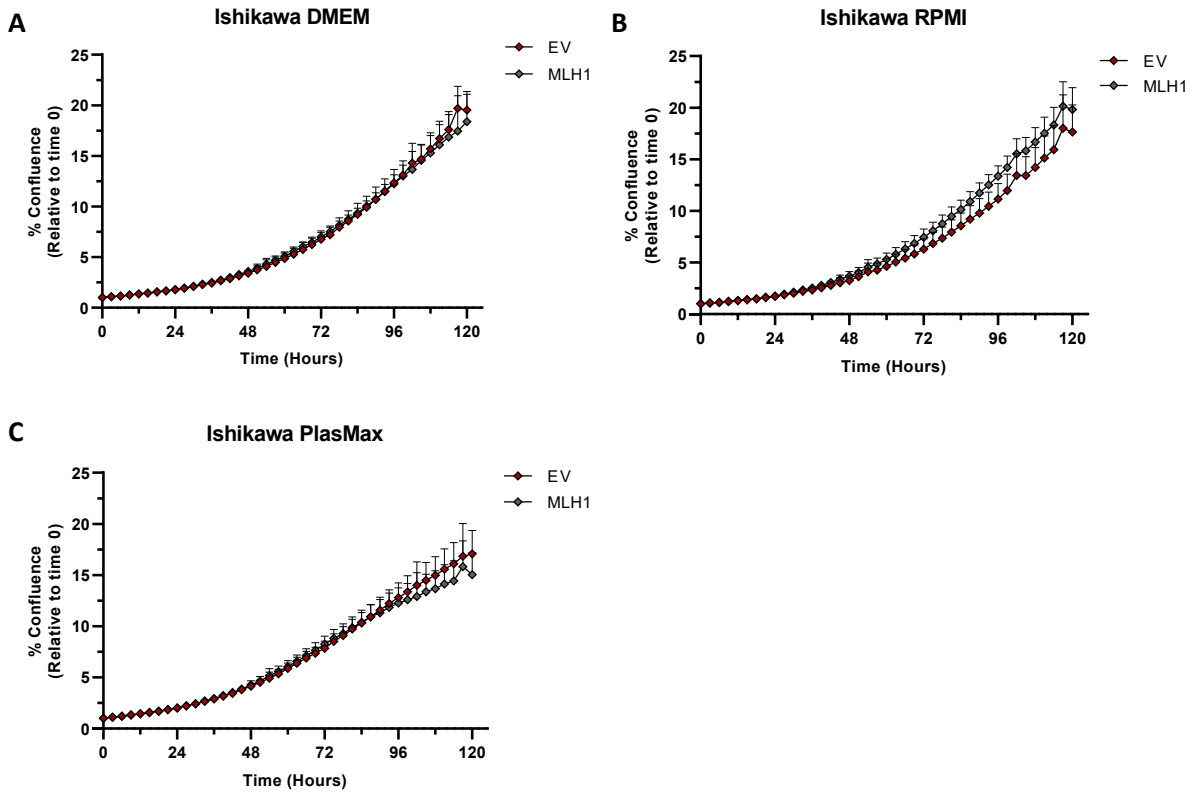

FIGURE 5.12. There is no difference in the rate of proliferation between MLH1-deficient and proficient Ishikawa cells in DMEM, RPMI, or Plasmax. Cells were cultured in DMEM **(A)**, RPMI **(B)**, and Plasmax **(C)**. The effect of each media was calculated by measuring the confluence of each well relative to the confluence of respective wells at time 0, using the Incucyte Zoom Live-Cell imaging software over 5 days. The graph represents 3 independent cultures with at least 4 technical repeats. Error bars represent the standard error of mean.

5.1.3 Characterising the effect of LDH inhibition on MLH1-deficient and proficient cells grown, in DMEM, RPMI and Plasmax media

Given there are considerable differences in nutrient composition between the three medias, and studies have indicated that supraphysiological concentration of metabolites in commercially available metabolites can lead to artificial *in vitro* results, we investigated whether our cell lines had a differential response to metabolic inhibition, depending on the media in which they were cultured [354]. For this experiment we cultured MFE-280 and Ishikawa MLH1-proficient and deficient cells in DMEM, RPMI and Plasmax and treated them with 20µM FX11 for 96 hours, monitoring cell proliferation over time using the Incucyte Zoom Live-Cell imaging system (**FIGURE 5.13**). Values were normalised to the percentage confluence at time 0. Furthermore, to remove the potential effect of differential proliferation rates in each media, each treated time point was normalised relative to its respective untreated measurement at the same time point, in that media. As a result, the untreated conditions at each time point are equal 1. Our results confirm that Ishikawa EV cells show a slight sensitivity to LDH inhibition following GNE-140 treatment, versus Ishikawa MLH1 cells, when cultured in DMEM (**FIGURE 5.13 A**). Interestingly, when cultured in Plasmax, this sensitivity wasn't observed and there were no significant differences in cell proliferation of the Ishikawa EV and MLH1-expressing cells when treated with FX11 in this media (**FIGURE 5.13 C**). Although there are no differences in sensitivity between Ishikawa EV and MLH1 cells treated with FX11 when cultured in in RPMI, in this media both cell lines were more sensitive to the LDH inhibition (**FIGURE 5.13 B**). Graham *et al.* have investigated the metabolic pathway dependencies of cancer cells grown in DMEM versus RPMI. Their work demonstrates that media composition influences cancer cell line metabolic pathway dependence and that future studies of metabolic vulnerabilities should take media composition into consideration [355]. Moreover, Graham *et al.* assessed the essentiality of metabolic pathways in cancer cell lines and identified striking differences between DMEM and RPMI. For instance, cancer cells grown in DMEM were remarkedly more reliant on OXPHOS than cancer cells grown in RPMI. A function of OXPHOS is to enable aspartate synthesis to accept electrons from the electron transport chain [355]. Graham *et al.* went on to investigate whether metabolic pathway activity is correlated with anti-cancer drug sensitivity. They carried out large-scale pharmacologic screens and interestingly uncovered differential responses to compounds depending on the media in which the cells were treated, DMEM versus RPMI. Consequently, it is unsurprising that when grown in DMEM or RPMI, our Ishikawa cells are differentially sensitive to LDH inhibition by FX11. Furthermore, given Plasmax is the only culture media that has lactate in it, inhibiting LDH (to reduce cytosolic lactate levels) when Ishikawa cells MLH1-proficient and -deficient cell lines are cultured in Plasmax may be less consequential, likely as the cells can uptake the lactate required to sustain cell proliferation from the

surrounding medium. Moreover, lactate also serves as a major circulating carbohydrate source which may also influence the metabolic pathway dependencies when Ishikawa cells are grown in this media.

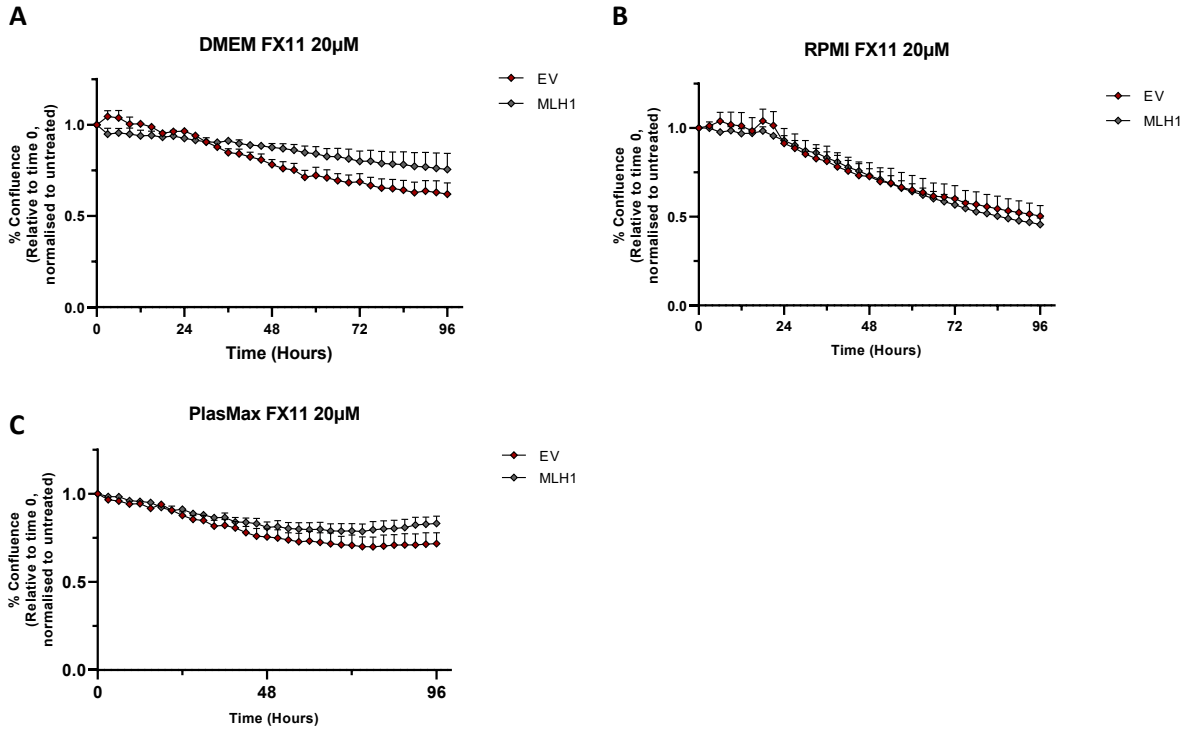

FIGURE 5.13. Sensitivity to FX11 treatment when cultured in DMEM, RPMI, and Plasmax. MLH1-deficient Ishikawa cells are more sensitive to LDH inhibition by 20µM FX11 in DMEM **(A)** but not RPMI **(B)** or Plasmax **(C)**. The effect of drug treatment on the confluence of cells was measured relative to untreated and normalised to the confluence of each well at time 0, using the Incucyte Zoom Live-Cell imaging software over 3 days. Graph represents 3 independent cultures with at least 4 technical repeats. Error bars represent standard error of mean.

Subsequently, we investigated our Ishikawa cells response to GNE-140 inhibition in different medias. Similarly, we cultured our cells in DMEM, RPMI and Plasmax and treated them with 25µM GNE-140 for 96 hours, monitoring cell proliferation over time using the Incucyte Zoom Live-Cell imaging system (**FIGURE 5.14**). Values were normalised to percentage confluence at time 0. Furthermore, to remove the potential effect of differential proliferation rates in each media, each treated time point was normalised relative to its respective untreated measurement at the same time point, in that media. As a result, the untreated conditions at each time point are equal 1. Our results demonstrate when cultured in DMEM, Ishikawa MLH1-deficient EV cells appeared more sensitive to GNE-140 treatment compared to Ishikawa MLH1 cells (**FIGURE 5.14 A**), though not significant. Interestingly, in both RPMI (**FIGURE 5.14 B**) and Plasmax (**FIGURE 5.14 C**), this difference in sensitivity was no longer observed and conversely the Ishikawa MLH1-expressing cells were marginally more sensitive to GNE-140 treatment which could be due to significantly reduced levels of levels of glucose in RPMI and Plasmax

relative to DMEM media. Our results further demonstrate the substantial effect cell culture media has on *in vitro* experiments, and the limitations therefore, when aiming to identify or characterize metabolic inhibitors for targeting cancer cells *in vivo*.

It would be interesting to further investigate the specific metabolites or combination of metabolites that are responsible for altering the sensitivity of these cell lines to LDH inhibition, however, these experiments were not feasible with the timeframe available. As cancer research relies heavily on results obtained *in vitro*, using physiologically relevant models and media will improve the reliability of results and increase the probability of reducibility *in vivo*. Nonetheless, given we observed that MLH1-deficient cells were not selectively sensitive to LDH inhibition in a physiologically relevant media *in vitro*, we turned our attention elsewhere, in the search for metabolic vulnerabilities that could provide information on the metabolic rewiring that occurs upon loss of MLH1 in EC and could be potentially targetable.

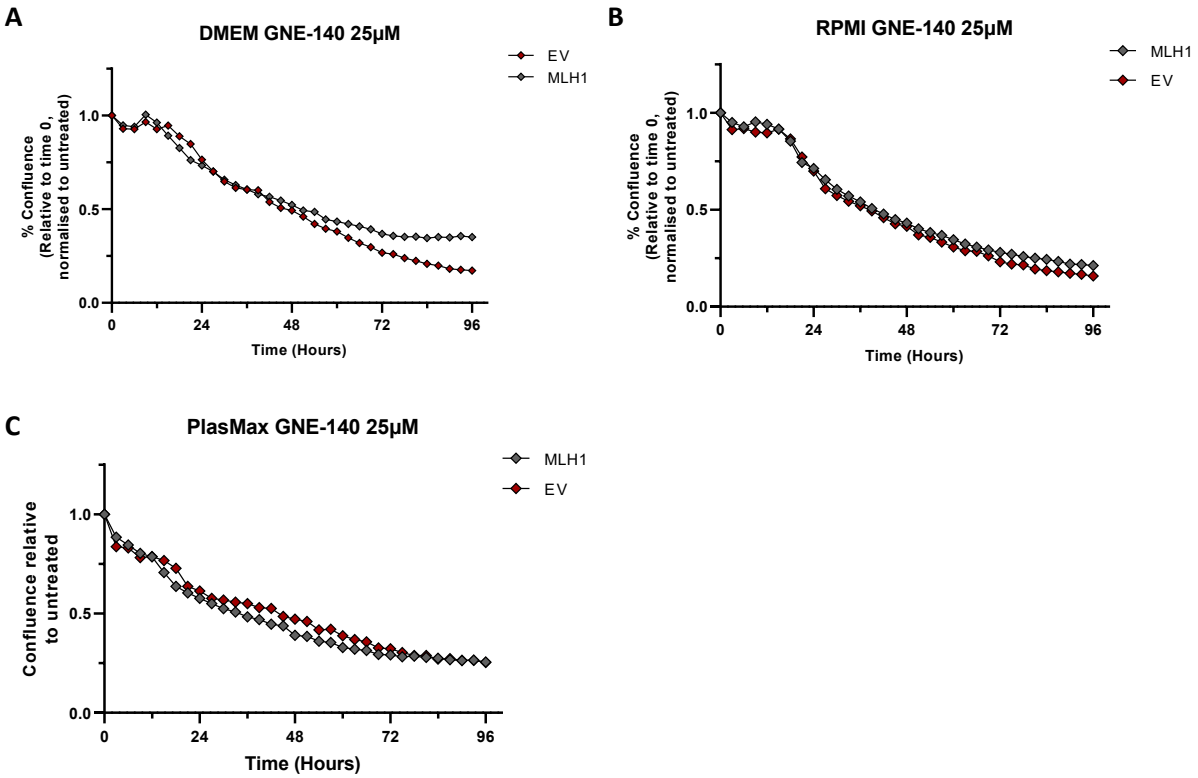

FIGURE 5.14. MLH1-deficient Ishikawa cells are sensitive to GNE-140 treatment when cultured in DMEM but not RPMI or Plasmax. MLH1-deficient Ishikawa cells are more sensitive to LDH inhibition by 25µM GNE-140 in DMEM **(A)** but not RPMI **(B)** or Plasmax **(C)**. The effect of drug treatment on the confluence of cells was measured relative to untreated and normalised to the confluence of each well at time 0, using the Incucyte Zoom Live-Cell imaging software over 3 days. Graph represents 1 independent culture with at least 4 technical repeats.

5.2 Investigating the role of the SSP in MLH1-deficiency

5.2.1 Investigating whether Ishikawa and MFE-280 MLH1-deficient cells differentially express SSP proteins

Our metabolomics study also highlighted a dysregulation of the Serine Synthesis Pathway (SSP) in the MLH1-deficient Ishikawa EV cells. The SSP pathway functions to synthesise serine in a three-step process utilising the glycolytic intermediate 3-phosphoglycerate [256]. Serine, a nonessential amino acid, is a central hub for cancer metabolism, thus it is unsurprising that cancer cells also exploit this metabolic pathway to support their growth and proliferation. Imported serine or serine derived from glycolysis can be converted into glycine to provide carbon units for one-carbon metabolism. One-carbon metabolism comprises several interconnected metabolic pathways that provide one-carbon units for the synthesis of DNA, polyamine, amino acids, creatine, and phospholipids [375]. Depletion of exogenous serine activates this biosynthetic pathway.

Although we identified no significant changes in the abundance of serine and glycine in Ishikawa cells (**FIGURE 4.6**), we identified differences in ^{13}C incorporation in the MLH1-deficient cells (**FIGURE 4.7**) signifying deregulation in the rate or activity of the serine synthesis pathway. We observed increased incorporation of M+2 ^{13}C carbon (originating from ^{13}C glucose) into glycine and increased incorporation of M+1, M+2 and M+3 ^{13}C carbon into serine in the Ishikawa EV cells relative to MLH1 cells (**FIGURE 4.7**). Therefore, we analysed our RNA-seq data and carried out differential analysis of genes involved in glycine, serine, and threonine metabolism as per the gene set derived from the KEGG Pathways database. From the enrichment analysis, this pathway was not significantly deregulated in the absence of MLH1 in either of our cell models. The NES for MFE-280 K/O 1 versus gCTRL was -1.04 with a padj value of 0.65 and for Ishikawa EV versus Ishikawa MLH1 was -0.94 with a padj value of 0.92. The log fold changes for the specific genes that were included in the core enrichment analysis is indicated in **FIGURE 5.15**. Despite there being no significant change in overall pathway, we did identify significant changes in specific genes involved directly in the SSP.

Studies have identified that the reprogramming of serine, glycine and one carbon metabolism is a key feature of many cancer cells and thus metabolic pathways that lead to the synthesis, uptake and use of serine are frequently amplified. The nonessential amino acid, serine, can either be taken up from the circulation or synthesised de novo in three steps catalysed by phosphoglycerate dehydrogenase (PHGDH), PSAT1, and PSPH [376]. From our RNA-seq data, we observed a significant decrease in the serine biosynthesis genes, glycerate kinase (GLYCTK), glycine decarboxylase (GLDC) and PSAT1 (**FIGURE 5.15 A**). Glycerate kinase catalyses the phosphorylation of (R)-glycerate and may be involved in serine degradation and fructose metabolism. Furthermore, GLDC encodes glycine carboxylase

which catalyses the degradation of glycine. Lastly, PSAT1 which encodes phosphoserine aminotransferase, catalyses the reversible conversion of 3-phosphohydroxypyruvate to phosphoserine and of 3-hydroxy-2-oxo-4-phosphonooxybutanoate to phosphohydroxythreonine during serine synthesis. Interestingly, recent work by Choi *et al.* demonstrates that low PSAT1 expression prevents de novo serine biosynthesis and sensitises luminal breast cancer cells to serine and glycine starvation *in vitro* and *in vivo* [377].

We also observed a number of serine metabolism genes that were upregulated upon MLH1 loss in MFE-280 cells including SDS (padj. =0.011), SRR (padj. =0.05) and PHGDH (padj. =0.0012) (**FIGURE 15 A**). SDS encodes serine dehydratase, one of three enzymes involved in metabolizing serine and glycine. Moreover, SRR which encodes serine racemase, catalyses the synthesis of D-serine from L-serine. Lastly, PHGDH which encodes phosphoglycerate dehydrogenase, the enzyme that catalyses the first step in the phosphorylated L-serine biosynthesis pathway, the reversible oxidation of 3-phospho-D-glycerate to 3-phosphonooxypyruvate.

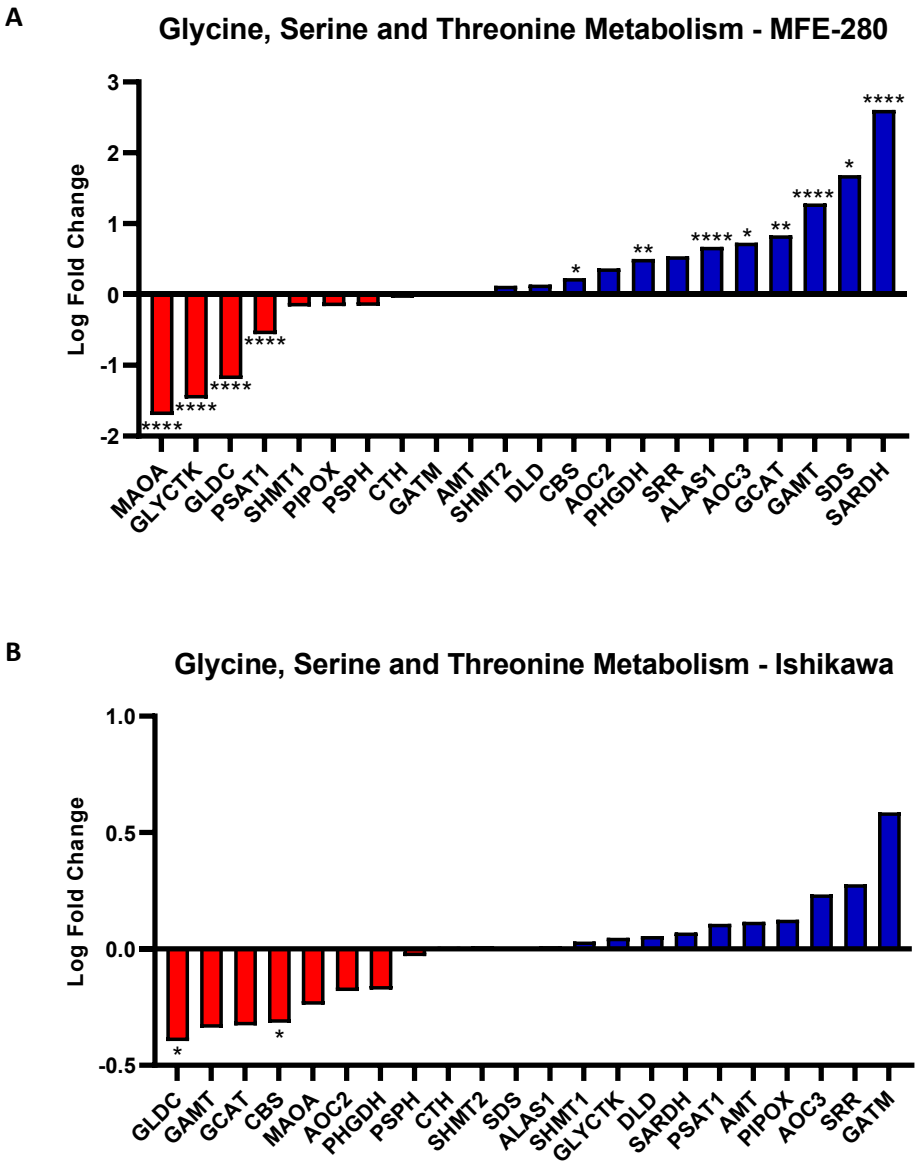

FIGURE 5.15. Gene set enrichment analysis for genes involved in mitochondrial glycine, serine, and threonine metabolism. Gene set enrichment analysis was performed for the glycine, serine and threonine metabolic pathway on Gene Pattern using ranked t-statistic of genes involved in the pathway, derived from Gene Ontology pathway database. Log fold change of the gene expression for those involved in the pathway is illustrated for MFE-280 MLH1-defcient cells **(A)** and Ishikawa MLH1-deficient K/O 1 cells **(B)**. **padj*<0.05, ***padj*<0.0021, ****padj*<0.0002, *****padj*<0.0001.

Given that we saw differential expression of SSP genes at the mRNA level, we went on to investigate whether we identified any differences at protein level in our MLH1-deficient cell models. We harvested protein from our MLH1-proficient and deficient cell lines cultured in DMEM, RPMI and Plasmax and performed western blotting to determine the expression PHGDH, PSPH, and LDH (**FIGURE 5.16**). Firstly, we investigated the expression level of each protein when the cells were cultured in each media with the aim of understanding what was happening at the molecular level to elicit the increased ^{13}C flux in the SSP that we observed in the metabolomics assay. Secondly, if we observed

differences, we were interested in understanding whether these changes were media-specific and thus likely to be influenced by nutrient availability. Interestingly across all the MLH1-proficient and deficient MFE-280 cell lines, we observed a reduced expression of PHGDH and PSAT1 when they are cultured in DMEM, compared to when they are cultured in RPMI or Plasmax (**FIGURE 5.16 A**). This could suggest that in DMEM all these cell lines are less reliant on serine as an energy source, potentially as they have access to an abundance of other nutrients to support their proliferation through alternative metabolic pathways. The same is not true for the expression of LDHA however, there was a higher expression level of LDHA when all MFE-280 cell lines were cultured in DMEM and RPMI relative to when the cells were cultured in Plasmax. It is worth noting here Plasmax is the only media, of the three that we compared, that has lactate present in the media. This reduction in expression highlights how quickly each cell line can alter their metabolic pathway dependencies based on nutrient availability, further supporting how important it is to choose physiologically relevant models in preclinical studies. Next, we compared the expression levels of the same proteins in the MFE-280 gCTRL cells relative to the two MLH1 K/O cell lines (**FIGURE 5.16**). When the cell lines were cultured in DMEM and RPMI, there were no significant differences between the expression of PHGDH or PSPH in gCTRL versus MLH1 K/O 1 and K/O 2 respectively. Interestingly, when they were cultured in the physiologically relevant media Plasmax, there was a significant increase in PHGDH and PSPH expression in both MLH1 K/O cell lines relative to the gCTRL ($p<0.05$ K/O 1; $p<0.001$ K/O 2) (**FIGURE 5.16 B-C**). These comparisons were carried out relative to the expression level of the protein in DMEM. These data highlights that MLH1-deficeint cells can upregulate their SSP pathway activity to sustain growth and proliferation in a physiologically relevant environment.

We went on to investigate whether the alterations in protein expression that we observed in the MFE-280 cell lines was also true in the Ishikawa cell model. Comparatively, we see a small increase in expression of PHGDH, PSAT1 and PSPH when the cells were cultured in RPMI and Plasmax relative to DMEM (**FIGURE 5.17**). Both cell lines have an increased expression of PHGDH and PSPH when cultured in Plasmax relative to DMEM and RPMI, although this change was not statistically significant. Moreover, when we compared the expression levels of each protein in each respective media, taking MLH1-status into consideration, we observed no significant differences between Ishikawa EV and Ishikawa MLH1 cell lines. This is intriguing given the metabolomics study implied that MLH1-deficient EV cells have increased SSP activity based of their incorporation of ^{13}C carbons. The ability to increase the activity of the SSP however, may not be solely controlled by the expression of the three main proteins.

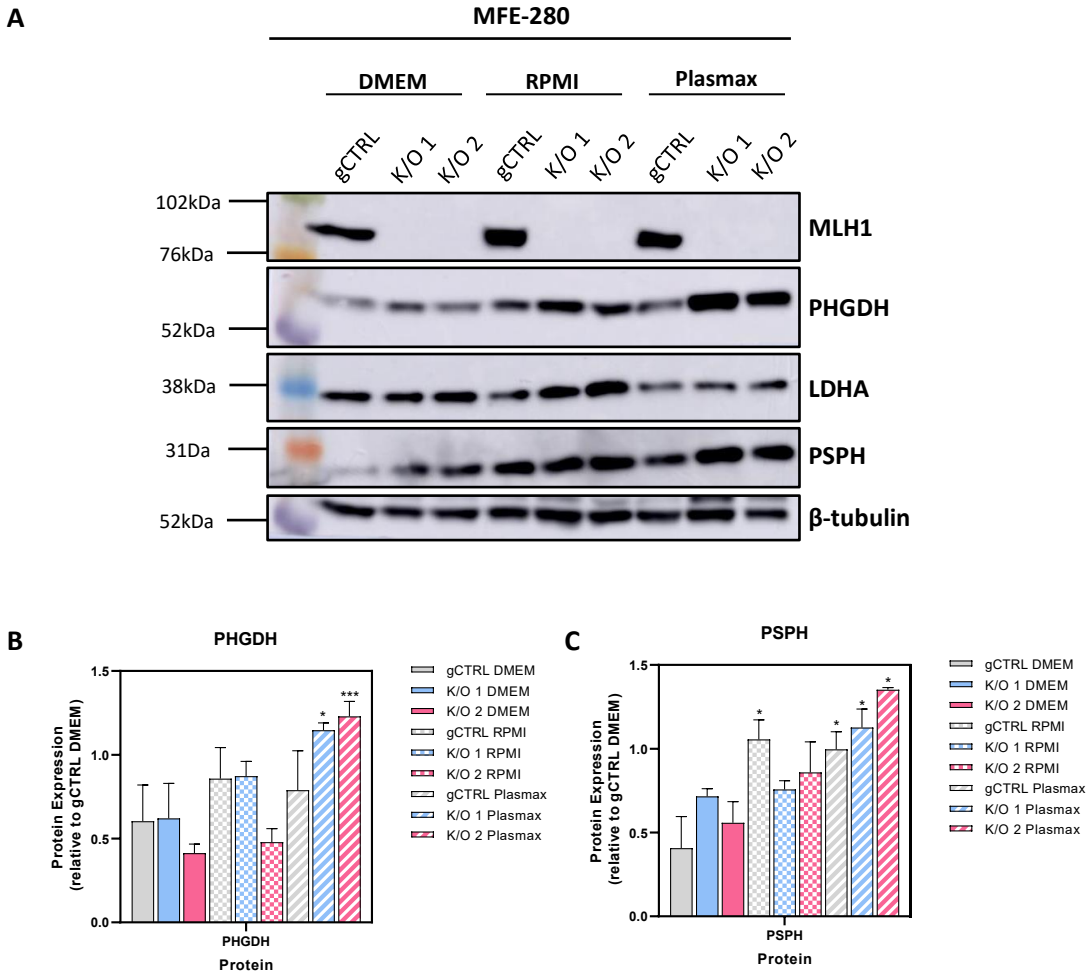

FIGURE 5.16. Increased expression of PHGDH and PSPH upon MLH1 loss in cells grown in Plasmax media. Western blot analysis of protein isolated from MFE-280 gCTRL, K/O 1 and K/O 2 cells cultured in DMEM, RPMI or Plasmax media for 3 days **(A)**. Protein was extracted and expression analysed using anti-PHGDH, anti-PSPH, or anti-LDHA. β-tubulin was used as a loading control. Protein levels compared to MLH1-proficient MFE-280 gCTRL cells for PHGDH **(B)**, or PSAT1 **(C)**, estimated by band densitometry normalised to loading control. Error bars represent mean with SEM of at least 3 independent experiments. Pairwise comparison carried out versus respective protein expression in cells cultured in DMEM. *p<0.05, ***p<0.001. No asterix = not significant.

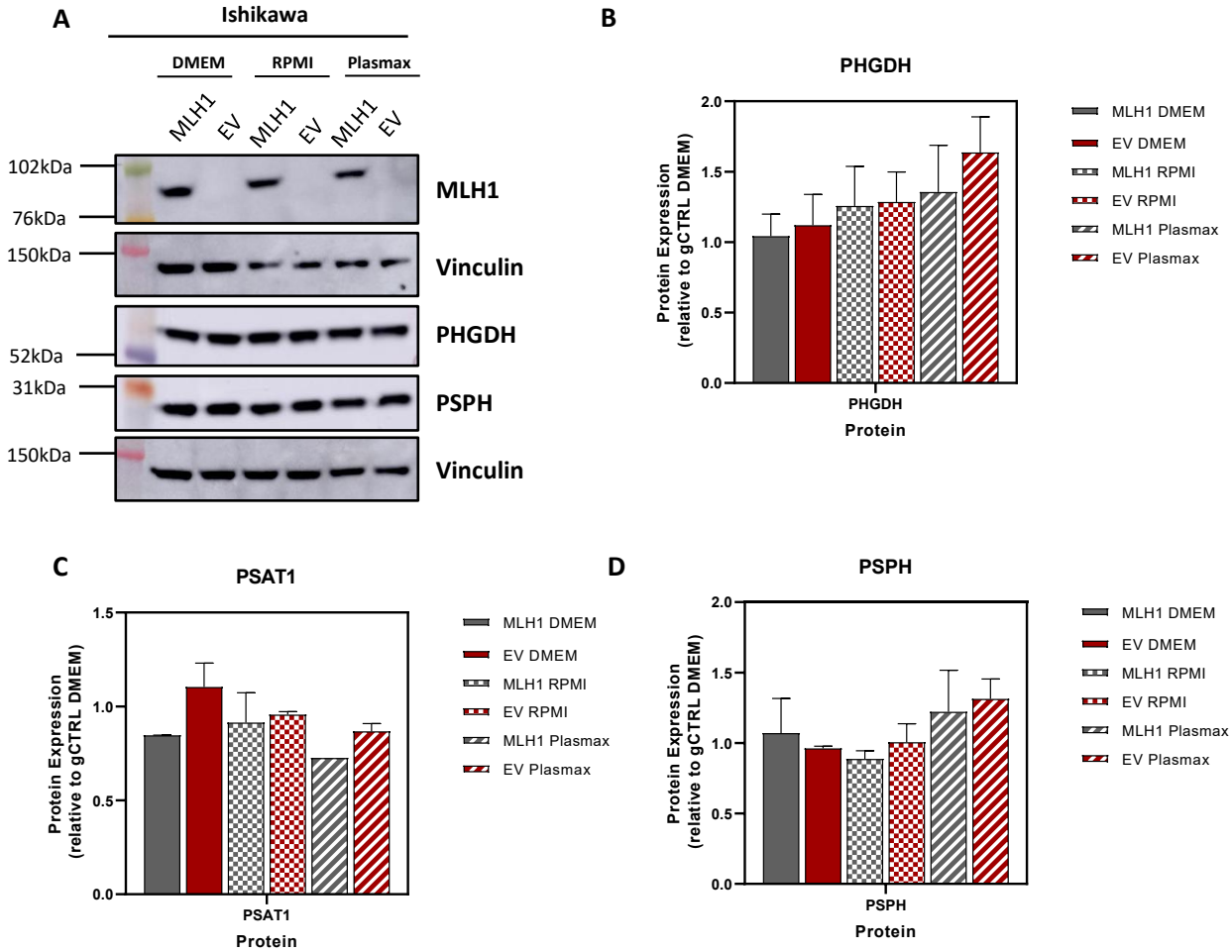

FIGURE 5.17. Increased expression of PHGDH and PSPH in Ishikawa cells grown in Plasmax versus DMEM and RPMI medias. Western blot analysis of protein isolated from Ishikawa EV, and Ishikawa MLH1, cultured in DMEM, RPMI or Plasmax media for 3 days **(A)**. Protein was extracted and expression analysed using anti-PHGDH, anti-PSPH, or anti-PSAT1. Vinculin was used as a loading control. Protein levels compared to MLH1-proficient Ishikawa MLH1 cells for PHGDH **(B)**, or PSAT1 **(C)**, or PSPH **(D)**, estimated by band densitometry normalised to loading control.

5.2.2 Characterising the effect of PHGDH inhibition on MLH1-deficient Ishikawa and MFE-280 cells lines

Given that we observed a dysregulation of the SSP in the MLH1-deficient Ishikawa EV cells in our metabolomic analysis, and increased PHGDH and PSPH expression (**FIGURE 5.16**), we were interested in investigating the effect of SSP inhibition on MLH1-deficient cells. Increased expression of SSP proteins such as PHGDH can be indicative that cells are dependent on the serine biosynthetic pathway for their viability, and have been shown to be upregulated in a wide variety of cancers [378]. Elevated PHGDH expression drives resistance to a variety of chemotherapeutics by modulating metabolic pathways. Understanding the different mechanisms underpinning this resistance, could provide information leading to the design of novel drug combination therapies [378], which could prove beneficial for EC treatment.

To this end, we treated our panel of MLH1-deficient and -proficient EC cells lines with two different PHGDH inhibitors, PKUMDL, and NCT-502 (**FIGURE 5.18**). PKUMDL is a negative allosteric modulator of PHGDH. Previous studies demonstrated that PKUMDL exhibited antitumour activity *in vitro* in breast cancer cells with amplified PHGDH [269]. NCT-502 is another allosteric regulator of PHGDH. Studies have demonstrated that NCT-502 treatment reduced intracellular serine concentration in media lacking serine and glycine [268]. Initially we treated the MFE-280 gCTRL and MLH1 K/O cell lines with a single concentration (35 µM) of each inhibitor, guided by available literature [269]. We plated the MFE-280 gCTRL and MLH1 K/O cell lines in DMEM, RPMI or Plasmax and treated each with 0.01% DMSO, 35 µM of PKUMDL, or 35 µM NCT-502. Cell viability was measured on day 3. Interestingly, our data demonstrates that PKUMDL is a much more potent inhibitor compared to NCT-502. Significantly, we observed that the MLH1 K/O MFE-280 cell lines were more sensitive to PKUMDL treatment when cultured in RPMI or the physiologically relevant media, Plasmax ($p<0.05$) (**FIGURE 5.18 A**). We did not observe any differentially sensitivity upon MLH1 loss upon treatment with NCT-502 (**FIGURE 5.18 B**), therefore we next optimised the concentration of the drugs used.

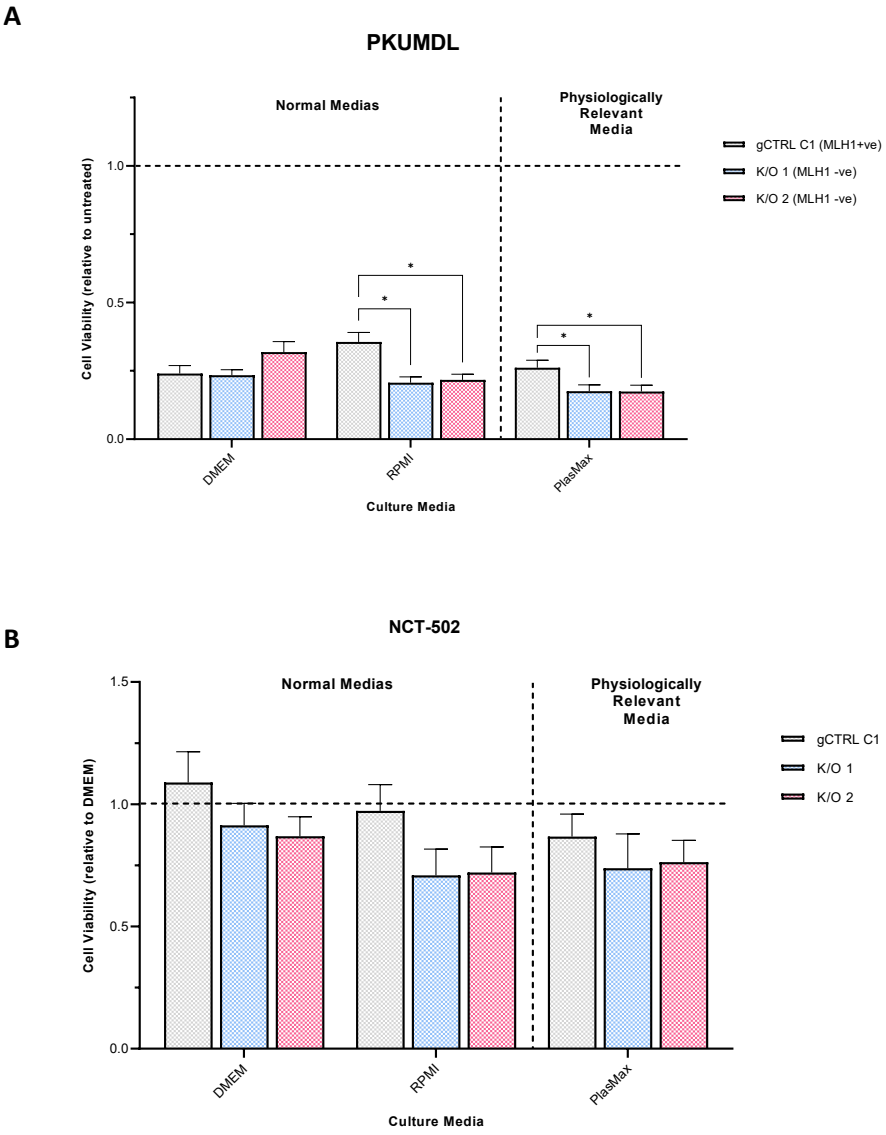

FIGURE 5.18. MLH1-deficient MFE-280 cells are more sensitive to PHGDH inhibition in RPMI and Plasmax media. Ishikawa cells were cultured in DMEM, RPMI or Plasmax media and exposed to 35µM PKUMDL **(A)** and 35µM NCT-502 **(B)**. Cell viability was measured on day 3 using the Cell Titer Glo viability assay and normalised to respective untreated. Graph represents 3 independent cultures with at least 4 technical repeats. Statistical significance was determined using a TWO-WAY ANOVA with posthoc Holm-Sidak multiple Comparisons Test to Ishikawa MLH1. *P<0.05. No asterix = not significant.

We next treated our MFE-280 gCTRL and MLH1 K/O cell lines with increasing concentrations of PKUMDL (0-25 µM) and NCT-502 (0-100 µM) and monitored the effect of each inhibitor on cell proliferation using the Incucyte Zoom Live-Cell imaging system (**FIGURE 5.19 A**). We also measured cell viability using the Cell Titer Glo viability assay after 72 hours, the endpoint of the experiment (**FIGURE 5.19 B**). For this experiment, we used cells that had been cultured continuously in Plasmax for at least 2 weeks, which we hypothesised would ensure the cells had adapted to this physiologically

relevant media. MFE-280 gCTRL and MLH1 K/O cells were seeded on day 0 and treated with increasing concentrations of PKUMDL or NCT-502 on day 1. We measured cell proliferation every 3 hrs, over 72 hours of treatment, and measured cell viability after 72 hrs. Incucyte data was normalised and plotted as follows: values were normalised to percentage confluence at time 0. Furthermore, to remove the potential effect of differential proliferation rates in each media, each treated time point was normalised relative to its respective untreated measurement at the same time point, in that media. As a result, the untreated conditions at each time point are equal to 1. Normalised values were plotted relative to the respective concentration of inhibitor resulting in a dose-response curve reflecting how increasing inhibitor concentrations affect each cell line's proliferation rate. Our results demonstrate that the MLH1-deficient MFE-280 K/O cell lines were significantly more sensitive ($p<0.0001$) to PKUMDL treatment at concentrations as low as ~1 µM (**FIGURE 5.19. A**). This differential sensitivity was observed upon measurement of the cell viability, where values were normalised to respective untreated wells. These data indicates that MFE-280 K/O cells lines were more sensitive to increasing concentrations of PKUMDL compared to the MLH1-proficient gCTRL cells at 0.8, 1.6, 3.1, 6.3 and 12.5 µM (**FIGURE 5.19 B**). **FIGURE 5.19 C** depicts representative images from the Incucyte Zoom software for each cell line at time 0 and 69 hours, either treated with 0.01% DMSO as a control, or 3.13 µM of PKUMDL. The images demonstrate how the MLH1 K/O 1 and K/O 2 cell lines fail to proliferate or proliferate significantly slower when treated with PKUMDL. This is in comparison to the gCTRL cell line, which although also does proliferate slower when treated with PKUMDL compared to 0.01% DMSO, was not as adversely affected by PHGDH inhibition (**FIGURE 5.19**).

We next performed the same experiment treating our MFE280 gCTRL and MLH1 K/O cells with the other serine metabolic inhibitor, NCT-502 (**FIGURE 5.20**). We observed that the MLH1-deficient MFE-280 cells were not as sensitive to this inhibitor compared to PKUMDL, however, we did observe a significant decrease in cell proliferation in the MLH1-deficient cells in comparison to the isogenic MLH1-proficient MFE-280 cells. Specifically, we observed that the MFE-280 K/O 1 cells proliferate significantly slower when treated with 6.25, 12.5 and 25µM of NCT-502 in comparison to the gCTRL cells (**FIGURE 5.20 A**). We observed a similar differential sensitivity in the MLH1 K/O 2 cells relative to gCTRL cells, however, this difference was not statistically significant. We also measured cell viability at the end of the assay and calculated the survival fraction relative to each untreated cell line. In these data we see a small increase in sensitivity in the MLH1 K/O 1 cells compared to the MFE-280 gCTRL cells when treated with 3.12 or 6.25 µM of inhibitor, but no significant changes in the cell viability in the MLH1 K/O 2 cells, relative to the gCTRL cells (**FIGURE 5.20 B**). It is worth noting that cell proliferation is a better measurement than cell viability given we are treating our cells with metabolic inhibitors. The CTG assay measures ATP to estimate cell viability, which could be directly impacted by

PHGDH inhibition for more reasons than the cells are less viable. **FIGURE 5.20 C** depicts representative images from the Incucyte Zoom software for each cell line at time 0 and 69 hours, either treated with 0.01% DMSO as a control, or 6.25 μM of NCT-502.

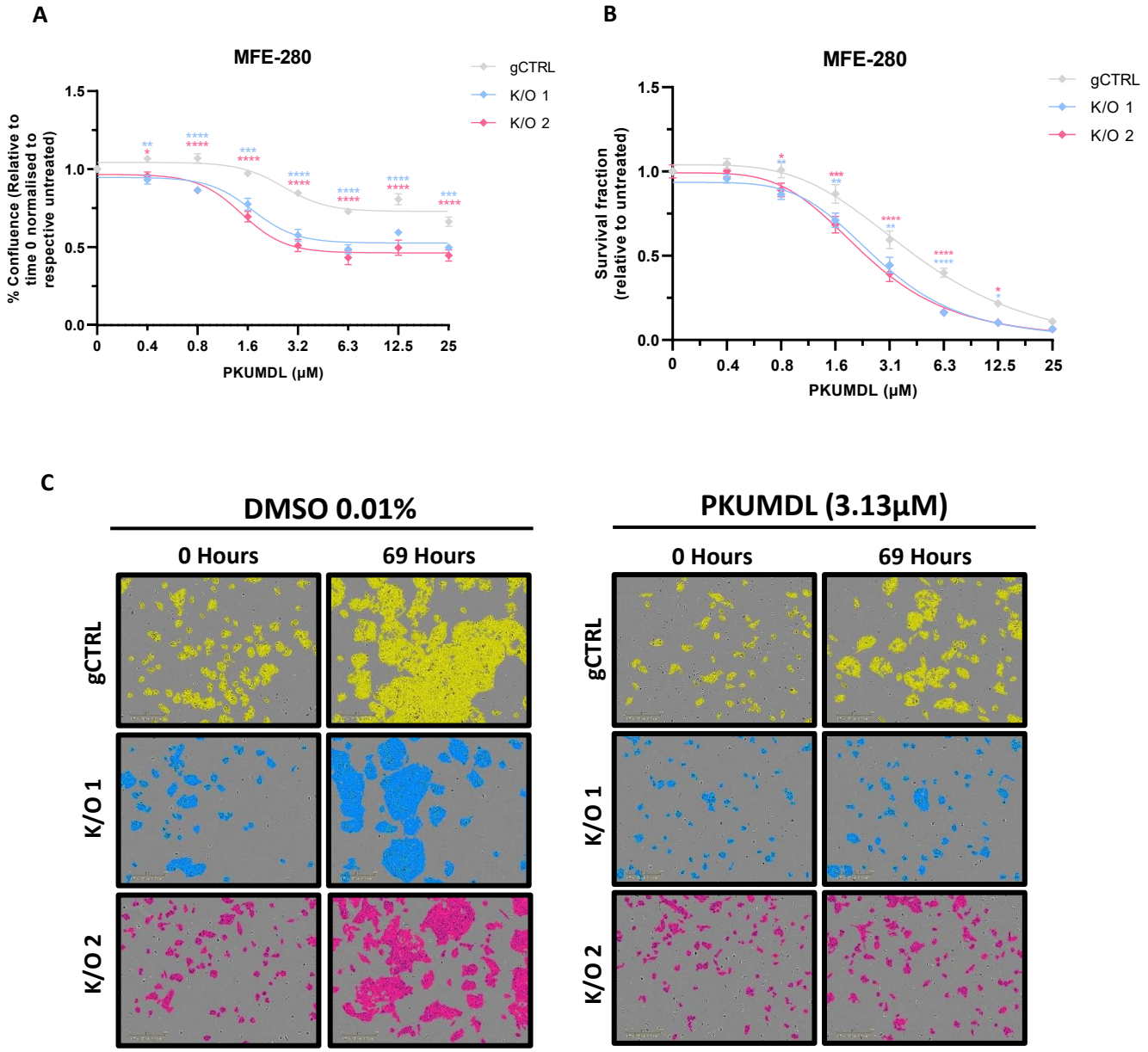

FIGURE 5.19. MLH1-deficient MFE-280 cells are more sensitive to PKUMDL treatment. MLH1-deficient MFE-280 cells are more sensitive to PHGDH inhibition. Cells were cultured in Plasmax media and exposed to increasing concentrations of PKUMDL. The effect of drug treatment on the confluence of cells was measured relative to respective untreated at each time point and normalised to the confluence of each well at time 0, using the Incucyte S3 live-cell imaging software over 3 days **(A)**. Cell viability was measured after 72 hours using the Cell Titer Glo viability assay and normalised to respective untreated **(B)**. Graph represents 3 independent cultures with at least 4 technical repeats. Statistical significance was determined using a TWO-WAY ANOVA with posthoc Holm-Sidak multiple Comparisons Test to Ishikawa MLH1. **P*<0.05, ***P*<0.01, ****P*<0.001, *****P*<0.0001. No asterix = not significant. Representative images taken for each cell line exposed to 0.01% DMSO or 3.13μM PKUMDL **(C)**.

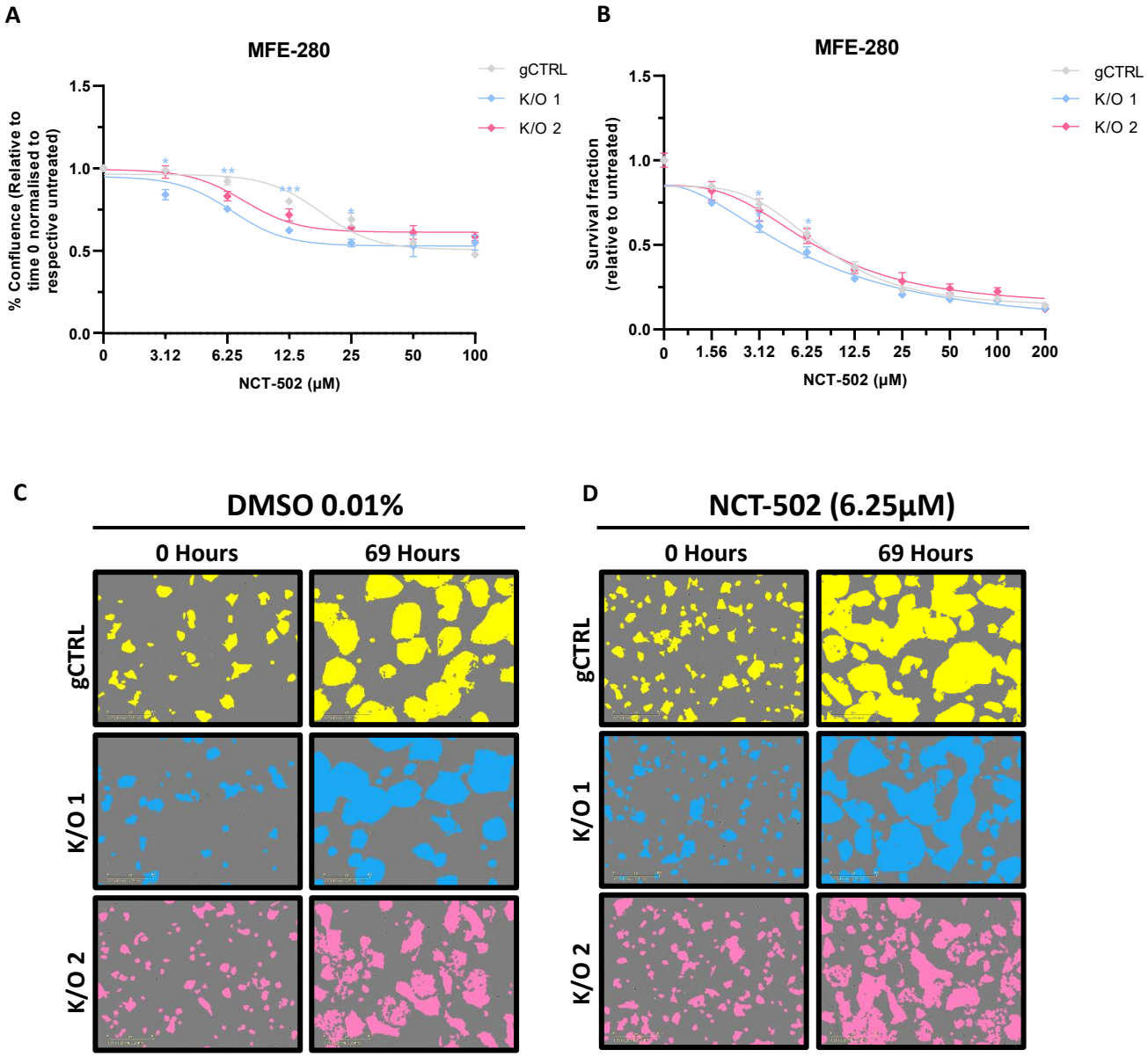

FIGURE 5.20. MLH1-deficient MFE-280 cells are more sensitive to NCT-502 treatment. MLH1-deficient MFE-280 cells are more sensitive to PHGDH inhibition. Cells were cultured in Plasmax media and exposed to increasing concentrations of NCT-502. The effect of drug treatment on the confluence of cells was measured relative to respective untreated at each time point and normalised to the confluence of each well at time 0, using the Incucyte S3 live-cell imaging software over 3 days **(A)**. Cell viability was measured on day 3 using the Cell Titer Glo viability assay and normalised to respective untreated **(B)**. Graph represents 3 independent cultures with at least 4 technical repeats. Statistical significance was determined using a TWO-WAY ANOVA with posthoc Holm-Sidak multiple Comparisons Test to Ishikawa MLH1. *P<0.05, **P<0.01, ***P<0.001. No asterix = not significant. Representative images taken for each cell line exposed to 0.01% DMSO or 6.25μM PKUMDL **(C)**.

We next aimed to validate our findings in our other model of MLH1 deficiency in EC cells, the Ishikawa MLH1-deficient EV cells and Ishikawa MLH1-expressing cells. In the Ishikawa MLH1 isogenic model, we observed that treatment with PKUMDL was a more potent inhibitor compared to NCT-502, however, in this case the MLH1-deficient Ishikawa EV cells were not selectively sensitive to PHGDH inhibition by either inhibitor (**FIGURE 5.21. A-D**). It is possible that MLH1-deficient Ishikawa cells are not sensitive to PHGDH inhibition like the MLH1-deficient MFE-280 cells as they do not have elevated levels of the PHGDH relative to Ishikawa MLH1, as was observed in the MFE-280 model. Moreover, it is worth reemphasising the differences in how these two models have been generated. Ishikawa cells are an MLH1-deficient EC cell line. Our 'wildtype' model Ishikawa MLH1 has been engineered to express a plasmid with the MLH1 protein. Re-expressing MLH1 in MLH1-deficient Ishikawa cells may not be sufficient to reverse the molecular and metabolic changes that occurred because of MLH1 loss in the first place. Consequently, our CRISPR generated MFE-280 model is a better MLH1 K/O model in general, though results will need to be validated to see whether this is cell line or even cell type-specific. It would be beneficial to investigate the response of MLH1-deficient cells to other allosteric or competitive inhibitors of PHGDH such as NCT-503 or CBR-5884 [267, 269, 379, 380].

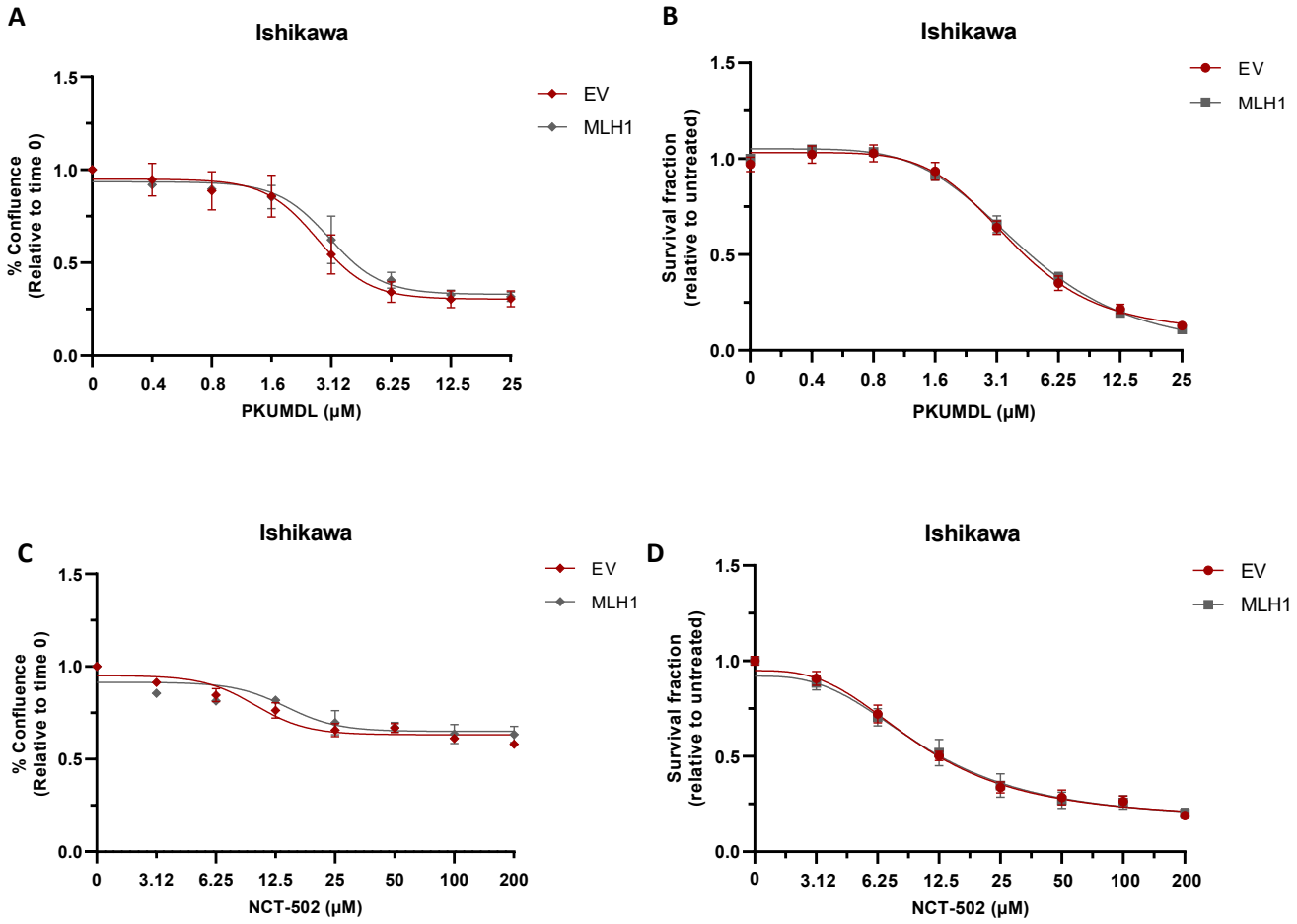

FIGURE 5.21. MLH1-deficient Ishikawa cells are not sensitive to PHGDH inhibition. Ishikawa cells were cultured in Plasmax media and exposed to increasing concentrations of PKUMDL and NCT-502. The effect of drug treatment on the confluence of cells was measured relative to respective untreated at each time point and normalised to the confluence of each well at time 0, using the Incucyte S3 live-cell imaging software over 3 days **(A, C)**. Cell viability was measured on day 3 using the Cell Titer Glo viability assay and normalised to respective untreated **(B, D)**. The graph represents 3 independent cultures with at least 4 technical repeats.

Given that we observed a variable response to PHGDH inhibition across our panel of MLH1-deficient and proficient EC cell lines, we investigated the impact of the serine inhibitor on the expression of the SSP enzymes, PHGDH, PSAT1 and PSPH in the presence and absence of MLH1. To do this we harvested protein from MFE-280 gCTRL and MLH1 K/O cells that were cultured in Plasmax and treated with 0.01% DMSO, 5 μM PKUMDL, or 10 μM NCT-502 for 72 hrs. We performed western blotting to determine the expression levels of PHGDH, PSAT1 and PSPH. The results demonstrate that upon PKUMDL treatment the expression of PHGDH, PSAT1 and PHGDH did not change in the MLH1-proficient gCTRL cells (**FIGURE 5.22. A**). However, when the two MLH1 K/O cell lines are treated with PKUMDL, there was a reduction in the expression of PSAT1 and PSPH (**FIGURE 5.22 A/B**) Statistical comparisons could not be carried out on these data as it represents only two biological repeats. The

same trend was observed when cells were treated with NCT-502. The expression of PHGDH, PSAT1 and PSPH did not change upon treatment with NCT-502 in MLH1-proficient cells. However, when both MLH1 K/O cell lines were treated with NCT-502, we observed a reduction in PSAT1 and PSPH expression (**FIGURE 5.22 A/C**). These differences were more striking in the MLH1 K/O 1 cells compared to MLH1 K/O 2 cells which may explain why MLH1 K/O 1 cells were significantly more sensitive to NCT-502 in **FIGURE 5.22 A** in comparison to the MLH1 K/O 2 cells. The fact that there are less striking expression level changes between the MLH1-proficient and deficient cells upon NCT-502 treatment may suggest why PKUMDL elicited a greater response. To more accurately compare the effectiveness of both inhibitors and their ability to inhibit PHGDH equivocally in each cell line, it would have been beneficial to measure the intracellular levels of serine upon treatment, however unfortunately time did not permit TABLE 5.1 indicated the IC50 for MLH1-proficient and deficient cell lines treated with PKUMDL and NCT-502.

TABLE 5.1. IC50 of MLH1-proficient and deficient cell lines treated with PKUMDL and NCT-502.

Cell Line	Drug (μM)	
	PKUMDL	NCT-502
MFE-280 gCTRL	2.5	2.1
MFE-280 K/O 1	1.5	0.8
MFE-280 K/O 2	1.3	0.8
Ishikawa EV	2.7	1.1
Ishikawa MLH1	3.2	1.5

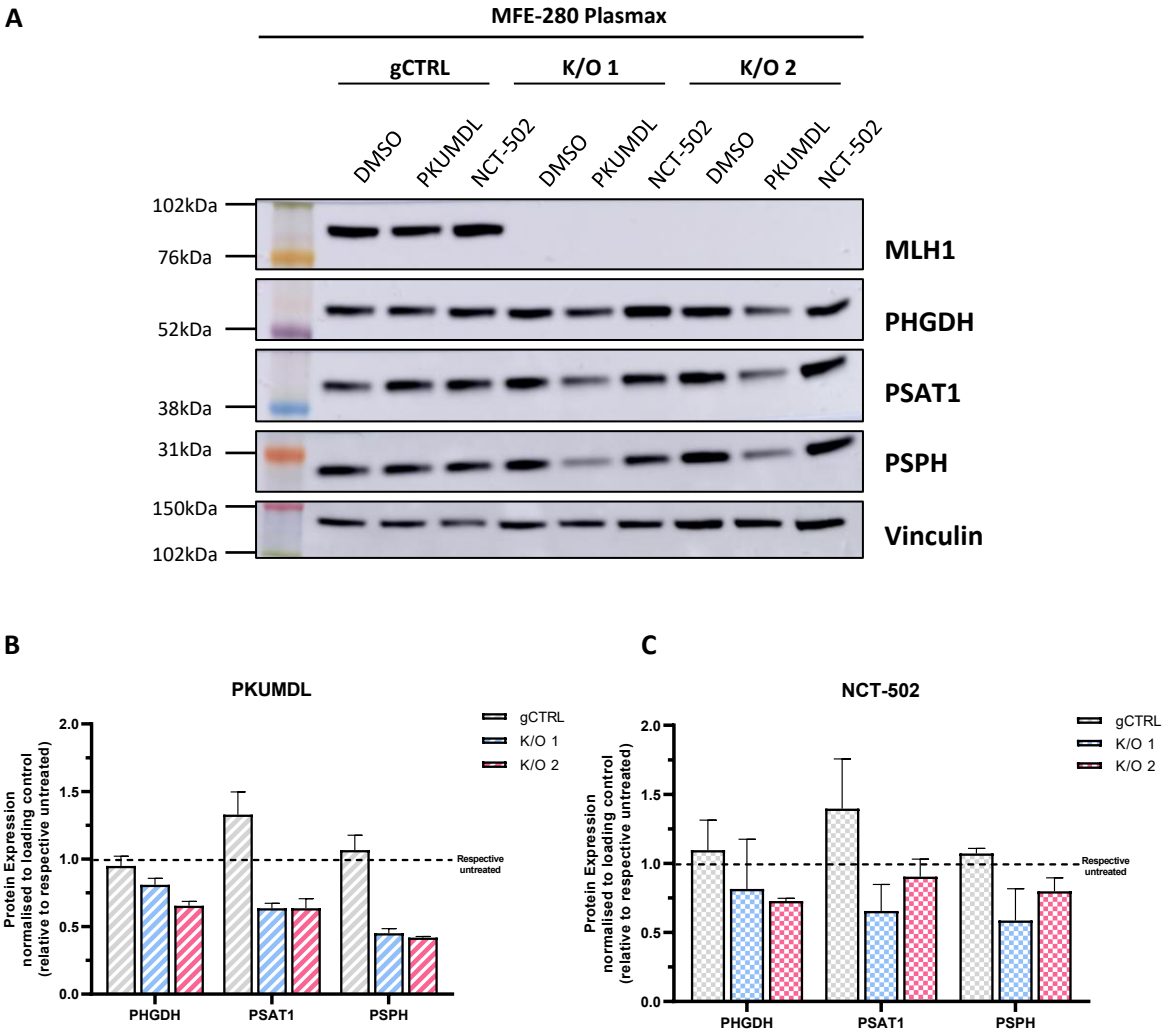

FIGURE 5.22. MLH1-deficient MFE-280 MLH1 K/O cells have a reduced expression of PSAT1 and PSPH upon treatment with PKUMDL (5µM) and NCT-502 (10µM). Western blot analysis of protein isolated from MFE-280 gCTRL, K/O 1 and K/O 2 cells cultured in Plasmax media and treated with PHGDH inhibitors PKUMDL or NCT-502 for 3 days **(A)**. Protein was extracted and expression was analysed using anti-PHGDH, anti-PSPH, or anti-PSAT1. Vinculin was used as a loading control. Protein levels compared to MLH1-proficient MFE-280 gCTRL cells when treated with PKUMDL **(B)**, or NCT-502 **(C)**, estimated by band densitometry normalised to loading control. Error bars represent mean with SD of 2 independent experiments.

To investigate if we saw a similar result upon MLH1 loss in the Ishikawa cell line, we harvested protein from Ishikawa cells that were cultured in Plasmax and treated with 0.01% DMSO, 5 µM PKUMDL, or 10 µM NCT-502 for 72 hours to investigate the effect of PHGDH inhibition on the expression of SSP proteins. We performed western blotting to determine the expression levels of PHGDH, PSAT1 and PSPH. The results demonstrate that upon PKUMDL and NCT-502 treatment the expression of PHGDH, PSAT1 and PHGDH did not change in the MLH1-proficient Ishikawa MLH1 cells (**FIGURE 5.23 A/B**). However, when MLH1-deficient Ishikawa EV cells are treated with PKUMDL, there was an increase in the expression of PSPH. Statistical comparisons could not be carried out on these data as it represents only two biological repeats. The same trend was observed when cells were treated with NCT-502. The expression of PHGDH, PSAT1 and PSPH did not change upon treatment with NCT-502 in MLH1-proficient Ishikawa cells, however, when Ishikawa EV cells were treated with NCT-502, we observed an increase in PSPH expression (**FIGURE 5.23 A/C)**. The different trends that we observed in SSP protein expression levels between our MKLH1-deficient Ishikawa and MFE-280 cell models upon PHGDH inhibition could explain the difference in sensitivity we observe to PHGDH inhibition (**FIGURE 5.19/20**). To further investigate this phenotype and its link to MLH1 loss in EC, these results need to be validated. It would have been beneficial to silence MLH1 in MFE-280 WT cells to investigate whether we observe the same sensitivity and SSP protein expression changes as the MLH1 K/O cell lines, upon PHGDH inhibition, though unfortunately time did not permit. Additionally, it would have been beneficial to perform similar experiments on a panel of MLH1-proficient and deficient cell lines across a range of tissue types to identify if there is an association between MLH1 loss and sensitivity to PHGDH inhibition, whether this phenotype is EC-specific.

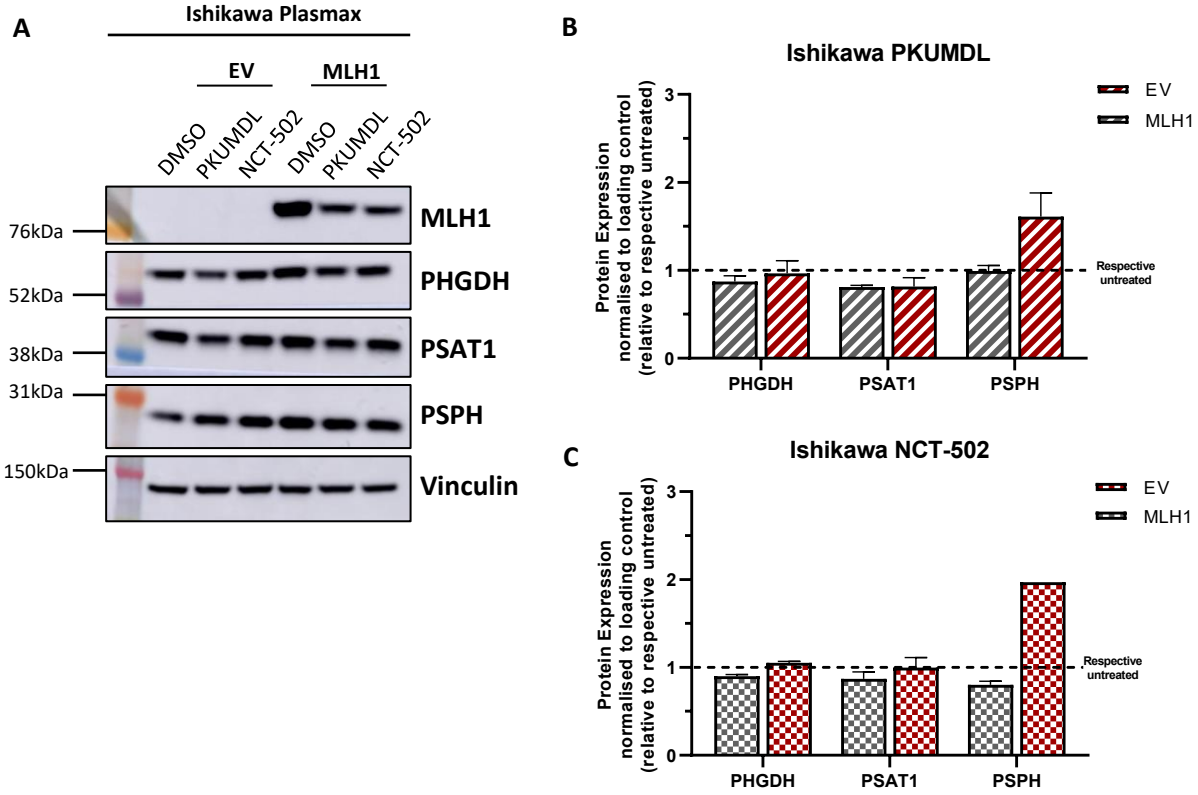

FIGURE 5.23. Ishikawa EV cells have increased expression of PSPH when treated with PHGDH inhibitors (5 µM) and NCT-502 (10 µM). Western blot analysis of protein isolated from Ishikawa EV and MLH1 cells cultured in Plasmax media and treated with PHGDH inhibitors PKUMDL or NCT-502 for 3 days **(A)**. Protein was extracted and expression analysed using anti-PHGDH, anti-PSPH, or anti-PSAT1. Vinculin was used as a loading control. Protein levels compared to MLH1-proficient Ishikawa cells when treated with PKUMDL **(B)**, or NCT-502 **(C)**, estimated by band densitometry normalised to loading control. Error bars represent mean with SD of 2 independent experiments.

5.2.3 Characterising the effect of PHGDH depletion on Ishikawa and MFE-280 MLH1-deficient cells

To better understand how treatment with the serine inhibitors results in a differential sensitivity in MLH1-deficient cells, we investigated the effect of PHGDH depletion using siRNA on MLH1-deficient cells. For this experiment, we cultured Ishikawa EV Ishikawa MLH1, and MFE-280 gCTRL, K/O 1 and K/O 2 cells in DMEM or Plasmax media and transfected each with a non-targeting siRNA control (siCTRL), or an siRNA targeting PHGDH. To ensure any differences observed weren't due to off-target effects, it would have been beneficial to test a range of siRNA targeting PHGDH, however, we were limited by time. After silencing for 72 hours, we harvested protein from each cell line and performed western blotting to measure the expression levels of PHGDH, PSAT1 and PSPH. In both DMEM and Plasmax we observed no difference in the expression levels of PSAT1 and PSPH upon depletion of PHGDH in Ishikawa MLH1 cells (**FIGURE 5.24 A-D**). In Ishikawa EV cells, upon MLH1 depletion, we observed an upregulation in the expression of PSPH in DMEM (**FIGURE 5.24 A/B**) and PSAT1 and PSPH in Plasmax (**FIGURE 5.24 C/D**). This differential response in Plasmax versus DMEM could be attributed to the availability of extracellular serine in each media. Plasmax contains approximately 140 µM of serine, whereas DMEM contains 400 µM of serine. The less significant change observed in DMEM upon PHGDH depletion could be due to alternative metabolic pathway dependencies depending on the media in which the cells are cultured. Moreover, we observe similar protein expression changes upon MLH1 depletion in our MFE-280 cell lines. In both DMEM and Plasmax there is no change in the expression of PSAT1 or PSPH in the gCTRL cells (**FIGURE 5.25 A-D**). Upon PHGDH depletion there is an increase in the expression of PSAT1 in both K/O cell lines cultured in both medias (**FIGURE 5.25 A-D**).

These data indicates that the depletion of PHGDH and pharmacological inhibition of PHGDH instigates a different molecular response. RNA interference-mediated silencing removes the target mRNA from the cell, while pharmacological inhibition blocks the function of a protein therefore the protein is still present. Drug-inhibited PHGDH may lack a certain activity but may still interact with some binding partners and assemble into macromolecular complexes. Moreover, RNA interference usually takes days to take effect, whereas pharmacological inhibition can be immediate. As such, it is not unsurprising that we observe differential protein expression changes when we deplete versus pharmacologically inhibit PHGDH.

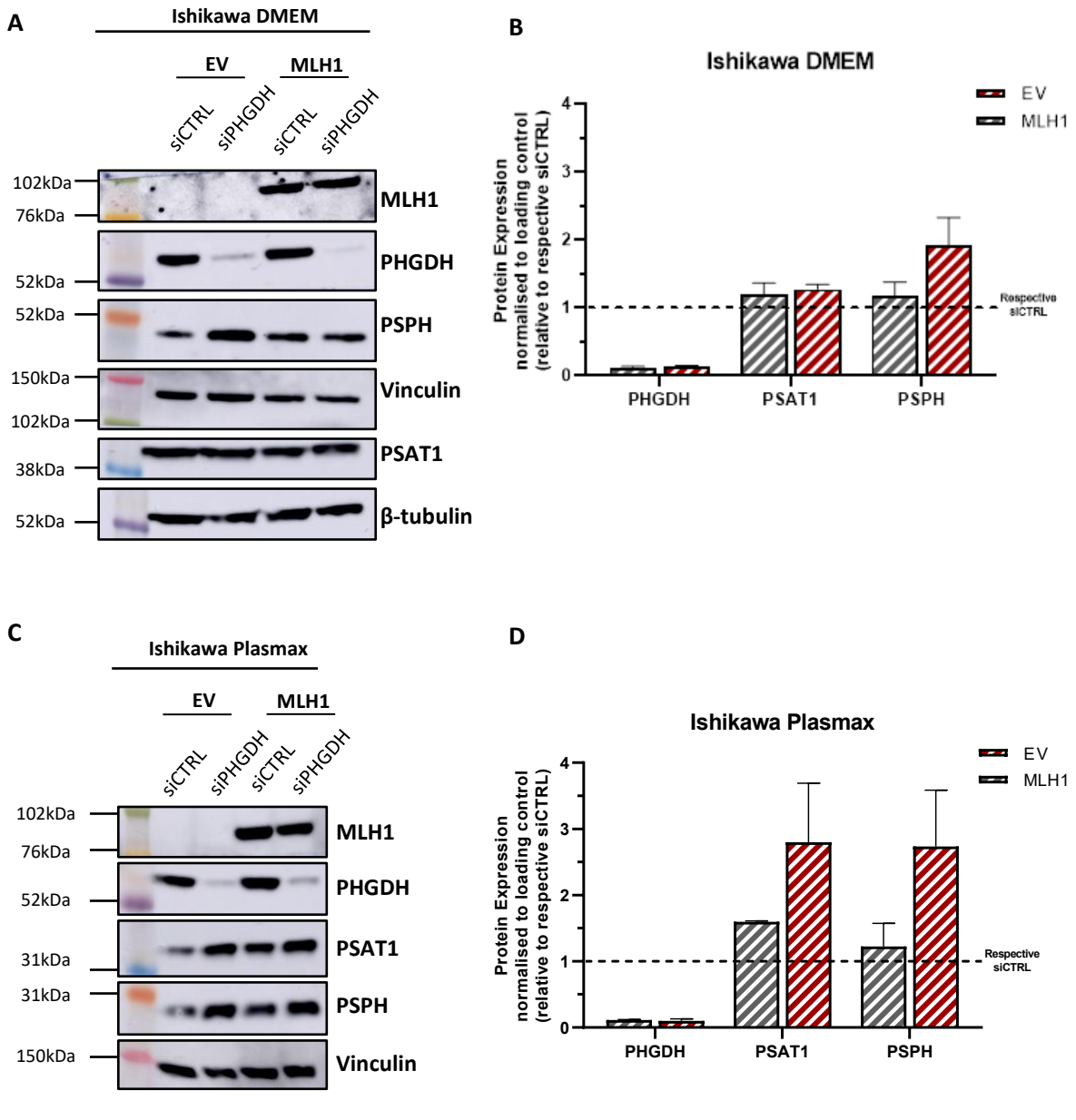

FIGURE 5.24. Increased expression of PSAT1 and PSPH in MLH1-deficient Ishikawa EV cells growing in Plasmax but not DMEM. Western blot analysis of protein isolated from Ishikawa EV and MLH1 cells cultured in DMEM **(A)** or Plasmax **(B)** media and transfected with siRNA targeting PHGDH. Protein was extracted and expression was analysed using anti-PHGDH, anti-PSPH, or anti-PSAT1. Vinculin was used as a loading control. Protein levels compared to MLH1-proficient Ishikawa cells in DMEM **(B)**, or Plasmax **(D)**, estimated by band densitometry normalised to loading control. Error bars represent mean with SEM of 3 independent experiments.

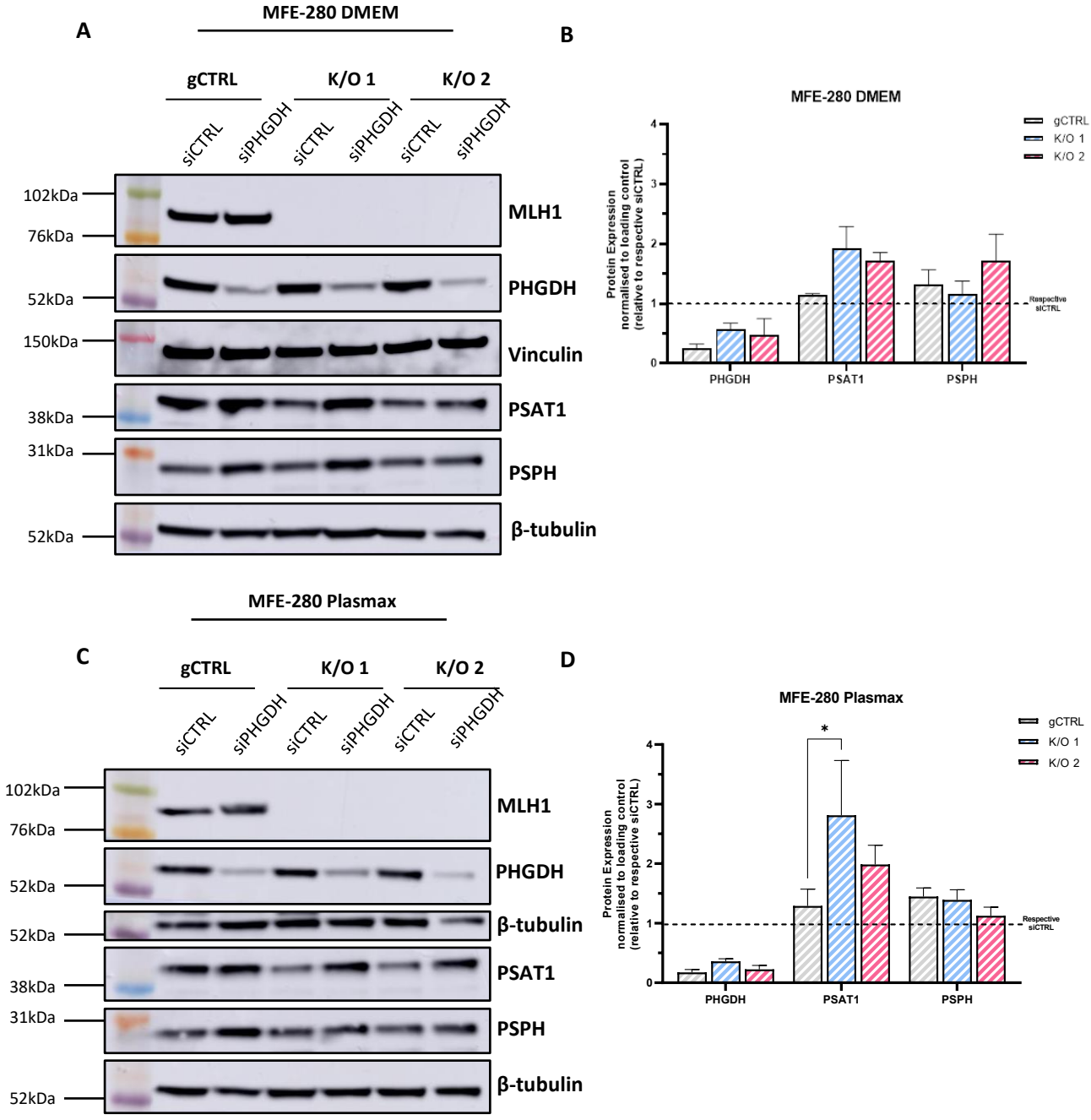

FIGURE 5.25. Increased expression of PSAT1 upon PHGDH depletion in MFE-280 MLH1 K/O cell lines grown in Plasmax. Western blot analysis of protein isolated from gCTRL, K/O 1 and K/O 2 cells cultured in DMEM (A) or Plasmax (B) media and transfected with siRNA targeting PHGDH. Protein was extracted and expression analysed using anti-PHGDH, anti-PSPH, or anti-PSAT1. Vinculin was used as a loading control. Protein levels compared to MLH1-proficient MFE-280 gCTRL cells in DMEM (B), or Plasmax (D), estimated by band densitometry normalised to loading control. Error bars represent mean with SEM of at least 3 independent experiments. *p<0.05. No asterix = not significant.

Lastly, we investigated whether depleting PHDGH using siRNA in our panel of cell lines could influence cell proliferation similar to pharmacological PHGDH inhibition. For this experiment, we seeded Ishikawa and MFE-280 cell lines in DMEM or Plasmax and transfected them for 72 hours with the same siRNA targeting PHGDH. In this experiment, siPLK1 was used as a positive control to indicate transfection efficiency, as PLK1 is an essential gene and its loss results in a significant reduction in cell viability. Cell proliferation was measured using the Incucyte ZOOM Live-Cell imaging system with images taken every 3 hours. Percentage confluence was normalised to time 0 to remove potential differences in cell proliferation, then subsequently normalised back to each respective siCTRL at each time point. Consequently, the siCTRL for each cell line is equal to 1 and not plotted.

The data demonstrates there are no differences between MLH1-proficient and deficient cells upon PHGDH depletion in both Ishikawa and MFE-280 cell models (**FIGURE 5.26 A-D**). I hypothesised that these cells may need time to adapt to the depletion of PHGDH and thus carried out a long-term siRNA experiment and investigated proliferation over 168 hours. These data demonstrates that depleting PHGDH has no effect on cell proliferation regardless of MLH1 status (**FIGURE 5.27 A-D**). If anything, the data indicates that MFE-280 K/O cell lines have a growth advantage upon PHGDH depletion over this longer time course (**FIGURE 5.27 A/C**).

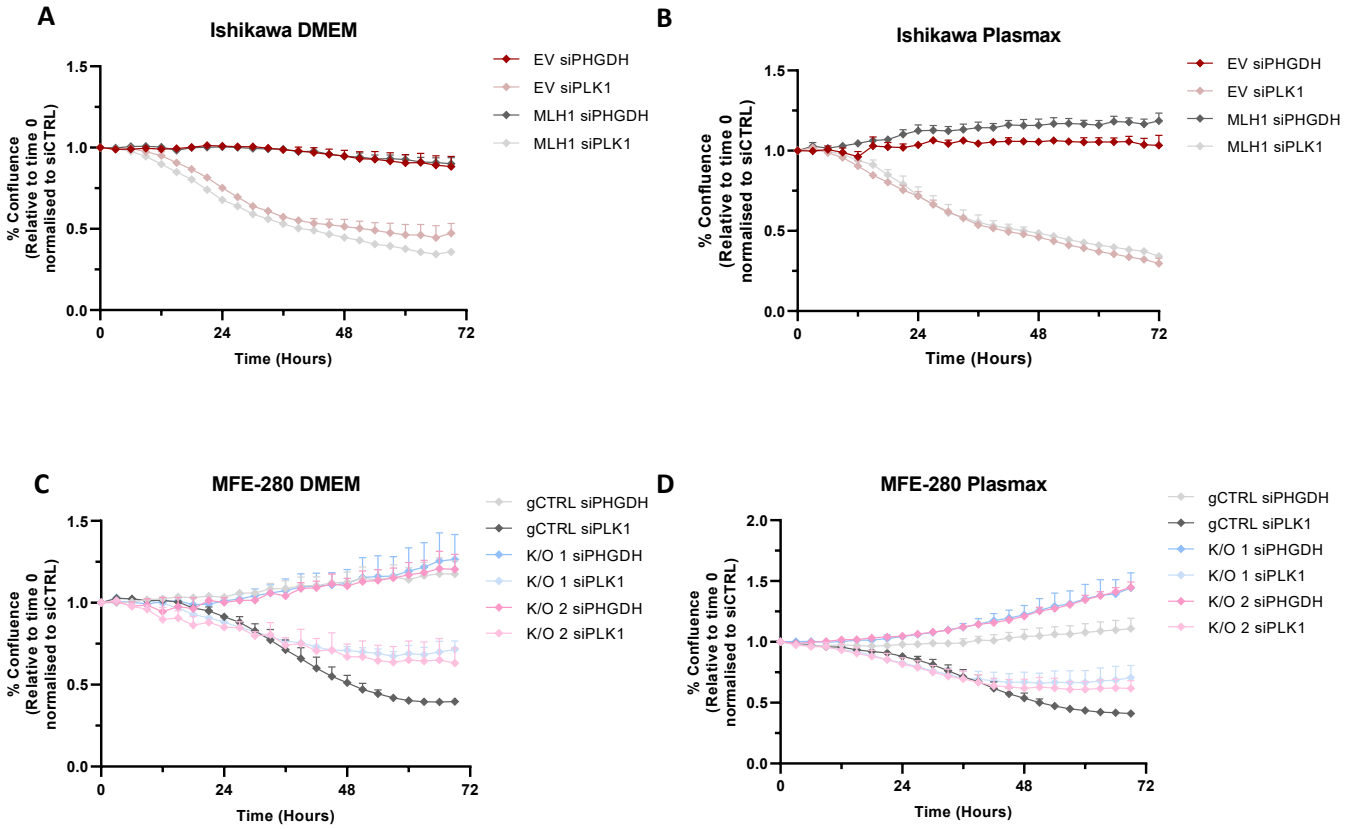

FIGURE 5.26. Depleting PHGDH has no effect on proliferation rate or cell viability of MLH1-deficient Ishikawa or MFE-280 EC cells over 3 days. Ishikawa **(A, B)** and MFE-280 **(C, D)** cells lines were cultured in either DMEM **(A, C)**, or Plasmax **(B, D)**. The effect of PHGDH depletion on the confluence of cells was measured relative to respective siCTRL and normalised to the confluence of each well at time 0, using the Incucyte S3 live-cell imaging software over 72 hours. Graph represents 3 independent cultures with at least 4 technical repeats. Error bars represent SEM.

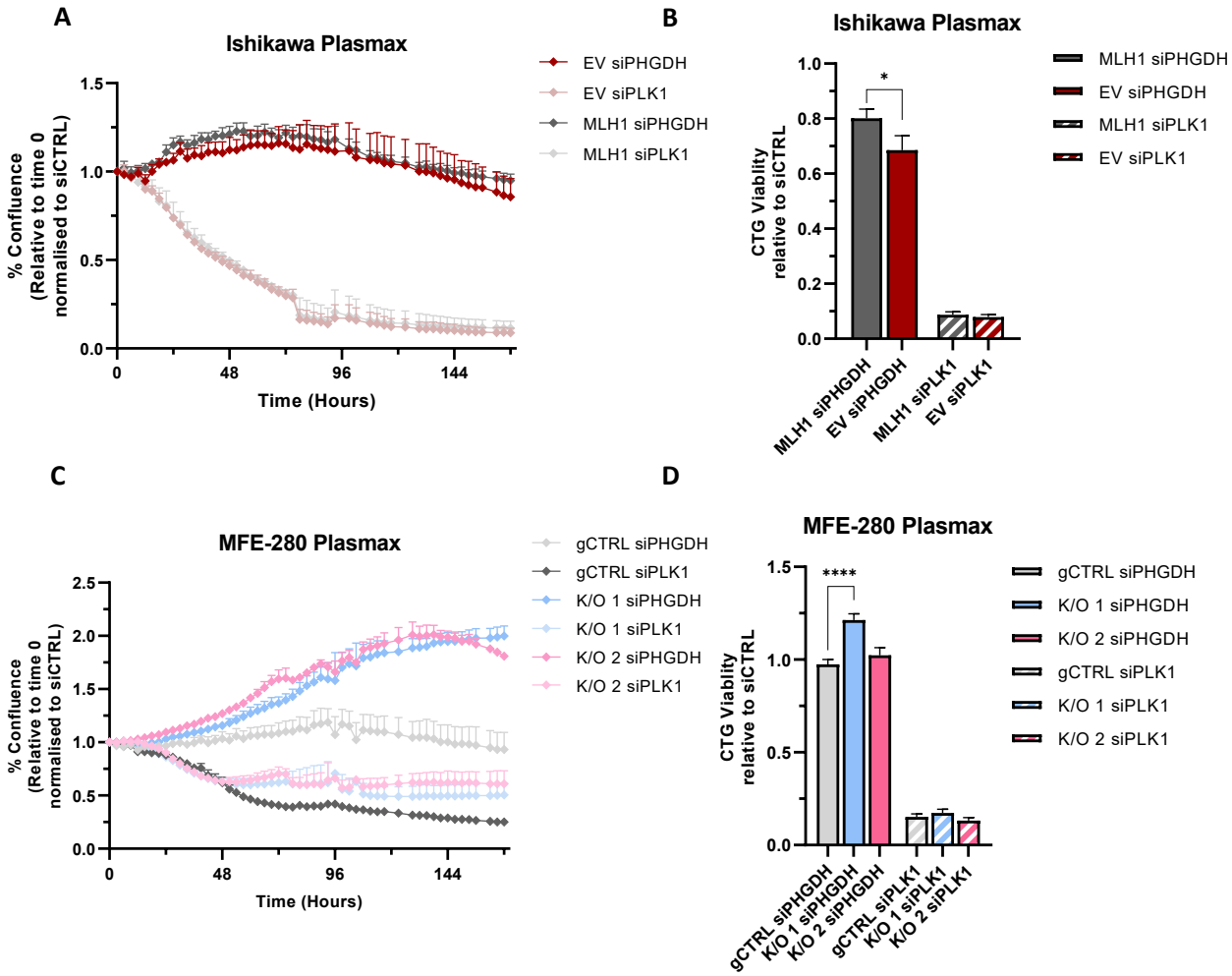

FIGURE 5.27 Depleting PHGDH over 7 days has no effect on the proliferation rate or cell viability of MLH1-deficient Ishikawa or MFE-280 EC cells. Ishikawa **(A)** and MFE-280 **(C)** cells lines were cultured in Plasmax. The effect of PHGDH depletion on each cell line was measured relative to respective siCTRL and normalised to the confluence of each well at time 0, using the Incucyte S3 live-cell imaging software over 7 days. The cell viability was measured on day 7 using the Cell Titer Glo viability assay and normalised respective to siCTRL samples. Graphs represent 3 independent cultures with at least 4 technical repeats. Error bars represent SEM. *p<0.05. ****p<0.0001. No asterix = not significant.

5.3 Conclusion

In conclusion, we have highlighted the importance of selecting physiologically relevant models i.e., the most relevant cell culture media, for *in vitro* studies. Our results initially suggested that MLH1-deficient EC cells may be sensitive to LDH inhibition. This indication arose from metabolomics data which demonstrated that MLH1-deficient cells were more metabolically active and had a noticeable increase in pyruvate and lactate levels relative to the MLH1-proficient control cells. These data however was generated from cells cultured in DMEM, a media that is well renowned to contain supraphysiological concentrations of specific metabolites such as glucose and glutamine, yet to be totally lacking in others. Historically medias were constituted to contain the minimum number of different metabolites to sustain consistent cell proliferation *in vitro*. When we compared the response of each cell line to LDH inhibition for cells cultured in Plasmax versus DMEM, we no longer observed this sensitivity in MLH1-deficient EC cells. In our remaining experiments, we utilised Plasmax to generate a more physiologically relevant setting but also compared inhibitor response to DMEM alongside, where possible. Subsequently, we identified a sensitivity of MFE-280 K/O cell lines to PHGDH inhibition. Although this response was not replicated in Ishikawa cell lines, we observed similar SSP protein expression changes following treatment with PKUMDL and NCT-502 in both cell models. Interestingly, upon depletion of PHGDH via siRNA-mediated silencing, we did not observe the same sensitivity in MLH1-deficient cells. Consequently, between the RNAseq data and preliminary molecular assay results, we have identified that MLH1-deficient cells can rewire their metabolism to support serine synthesis in a setting resembling nutrient availability in the tumour microenvironment. To understand the mechanism underpinning this observed phenotype, alongside investigating whether this observation is biologically relevant, these experiments would need to be validated in a range of cell lines and tumour types. Additionally, it would be interesting to investigate whether there is a link between MLH1 loss and PHGDH expression in patient tumours.

6.0 Discussion

EC is the fourth most common cancer in women and the most common gynaecological malignancy in the developed world [381]. Mortality has decreased over the last decade, as genomic characterisation of EC has led to the identification of subtypes, which has guided treatment decisions and prognosis predictions [18, 381]. Though molecular alterations are frequently found in EC, it is only in recent times that they are being implemented into the treatment strategy for the disease, and there is still room for improvement. Targeted therapy in combination with traditional cytotoxic agents, or novel biologic agents targeting a relevant mutation or phenotype, could help prevent disease recurrence, for which outcomes are poor. For instance, evidence has demonstrated that assessment of molecular alterations can dictate which, and the type of adjuvant therapy patients require, depending on the tumour's genomic profile [382]. Though ongoing trials are investigating targeted therapies in EC, more evidence is needed to understand the mechanism underpinning the four molecular subclasses recognised in the disease: POLE-ultramutated, microsatellite unstable, copy-number low, and copy-number high. In this study we investigated the role of MLH1 loss in EC, a well-documented driver of microsatellite instability, particularly focusing on the identification of metabolic alterations associated with the mutation, to identify vulnerabilities that could be exploited therapeutically.

6.1 MLH1-deficient endometrial cancer

6.1.1 MLH1-loss due to methylation is associated with a more severe disease phenotype

Approximately 20-30% of ECs are MMR-deficient, the majority of which are caused by the dual loss of MLH1 and PMS2 which is destabilised upon the loss of its partner protein [383]. Interestingly, most of these cancers are not caused by a pathogenic mutation in MLH1 but by the hypermethylation of the MLH1 promoter (25%), which tends to be associated with a poorer prognosis [78, 93, 162, 383]. Poor prognostic indicators including high tumour grade, lymph node involvement, metastasis and recurrence have been identified in EEC's [93, 384, 385], which is contrary to CRC, where MMR deficiency tends to be associated with good prognosis [386]. Although several studies have acknowledged the differential phenotype caused by mutative or epigenetic MLH1 loss in EC specifically, the reason why this may be the case is not known. Understanding the mechanisms underpinning MLH1-deficient ECs could ultimately guide treatment approaches and improve survival outcomes.

A study by McMeekin *et al.* demonstrated that epigenetic and 'probable mutations in MMR' were significantly associated with several poor prognostic indicators including higher grade, and more frequent lymphovascular space invasion [164]. Additionally, epigenetic defects were more common

in patients with higher FIGO stage, and though there were no differences in patient outcomes, PFS was worse in those who had epigenetic MMR defects compared with the MMR normal group [164]. Moreover, Cosgrove *et al.* have also demonstrated that epigenetic MMR loss confers a worse prognosis than germline MMR loss, with cases of Endometrioid EC with epigenetic MMR defects associated with significantly reduced recurrence-free survival [93]. This study suggested the possibility of chemoresistance in advanced-stage MMR-deficient patients, explaining the high rate of recurrence observed in the group with advanced epigenetic MMR-deficient EC. This hypothesis is supported by several studies that have highlighted the association between platinum resistance in MMR-deficient cell lines *in vitro* [387-389].

Consistent with these findings, Kaneko *et al.* further demonstrated the poorer prognosis associated with epigenetic MMR-deficient ECs, compared to MMR-proficient and those with suspected Lynch syndrome. In this study, the MLH1 hypermethylated group had a lower percentage of grade I tumours and a higher percentage of stage III/IV tumours compared to the other group's [162]. Although the OS and PFS were significantly better in the MMR-deficient group vs. the MMR-proficient group, OS and PFS of the methylated EC group were significantly worse than those of the group with suspected Lynch syndrome, and of the MMR-deficient group, the methylated group showed worse OS and PFS [162]. More recently, Post *et al*. demonstrated that Lynch syndrome-associated ECs (mostly as a result of germline variants in the MSH6 and PMS2 genes) exhibited a trend towards better recurrence-free survival and higher risk than MLH1-hypermethylated MMR-deficient ECs that were associated with increased rates of metastasis [78].

One explanation for this could be the differential expression of PD-L1 observed in these subgroups. It has been demonstrated that compared to MSS endometrial tumours, MSI-h endometrial tumours exhibit increased PD-L1 expression and neoantigen production which is associated with an increased mutational burden and consequently CD8+ T cell immune infiltration [300]. Moreover, The TME of MLH1-deficient ECs are more immunogenic vs. MLH1-proficient tumours [301]. In a clinical analysis of MLH1-deficient endometrial tumours, Sloan *et al.* identified that ECs caused by mutated- or methylated-MLH1 demonstrated varying PD-L1 expression patterns, with MLH1-mutated ECs expressing increased PD-L1 levels (70%) vs. the MHL1-methylated ECs (33) [301]. Additionally, this study demonstrated that response to immune checkpoint blockade varied depending on the molecular mechanism underpinning MLH1 loss in MLH1-deficient EC patients [301]. Interestingly, however, PD-L1 positivity in tumour cells but not immune cells is associated with a favourable prognosis in patients with high-risk EC [390]. Although little information is available in the literature

about the variable phenotypes observed in MLH1-deficient EC, there is evidence to suggest that immune checkpoint blockade (discussed further in 6.1.2) and potentially demethylating agents may prove valuable in this subset of patients. Ultimately the lack of available literature emphasises the gap in our scientific understanding of this subgroup of the disease and highlights that there is a large fraction of patients that may benefit from alternative treatment strategies, once understood. This knowledge has the potential to guide treatment decisions and facilitate prevention strategies for women with EC.

6.1.2 MMR and clinical response to immune checkpoint inhibitors in endometrial cancer

Given certain EC subtypes (i.e. POLE mutant/hypermutated and MSI-h) are associated with a high tumour mutational burden (TMB), the presence of tumour-infiltrating lymphocytes, and a high PD-1/PD-L1 expression they are an ideal target for immunogenic intervention [46, 391]. An increased PD-L1 expression and neoantigen production correlates with an increased mutational burden and increased CD8+ T cell immune infiltration, vs. MSS endometrial tumours, as described by Howitt *et al.* [300]. In recent years, it has been reported that tumours with a high TMB, such as MSI tumours, are immunogenic, and thus could benefit from immune checkpoint inhibition [48].

The rationale behind this has been attributed to neoantigen generation. Neoantigens are mutated proteins that arise following the acquisition of nonsynonymous somatic mutations. MHC class I molecules present peptide fragments on the surface of cancer cells following processing by the proteasome [392]. Neoantigens are specific to tumour cells, making previously hidden cancer cells identifiable as foreign by the immune system. It is thought that an increased TMB generates more neoantigens triggering an anti-tumour immune response, which can be further amplified by immune checkpoint blockade [393]. Studies have indicated that a high TMB increases the likelihood that immunogenic neoantigens expressed by tumour cells may induce a response to immunotherapy [394]. For instance, a positive correlation between TMB, neoantigen number, and overall response to immune checkpoint inhibitors (ICIs) was identified in NSCLC patients, who demonstrated improved progression-free survival, vs. those who did not respond [395]. ICIs such as anti-programmed cell death-1 (PD-1)/ -programmed death-ligand 1 (PD-L1) therapies have demonstrated high antitumor effects against MMR-deficient cancers, and although not perfect, tumour PD-L1 expression is considered a biomarker that predicts response to anti-PD-1 therapies in some cancers [396]. ICIs are immunotherapy drugs which block checkpoint proteins from binding with their partner proteins. This prevents cancer cells from evading the immune system and enables T cells to recognise and kill the cancer cells. For instance, PD-1 is a T cell checkpoint, a receptor that is expressed on the surface of

cells and plays a central role in regulating T cell exhaustion. The binding of PD-1 to its ligand, PD-L1 activates downstream signalling pathways and inhibits T cell activation [47].

Given ECs show the highest levels of PD-1/ PD-L1 expression among gynaecological cancers, with 75% and 25-100% respectively, there is a rationale for targeting this tumour-immunity interaction and as such, several clinical trials have investigated the efficacy and safety of ICIs in the disease, leading to the approval of the first an-PD-1 antibody, pembrolizumab. The KEYNOTE-028 study (NCT02054806) demonstrated the antitumour effect of pembrolizumab in PD-L1-positive EC, leading to its approval in the US and EU for the treatment of ECs with MSI-h or high TMB [397]. As the future of cancer treatment likely relies on combination therapy strategies, ongoing trials are exploring the potential of combining ICIs with chemotherapy, radiotherapy, and other targeted therapies. One of these (NCT02501096) led to the approval of pembrolizumab (anti-PD-1) in combination with the tyrosine kinase inhibitor lenvatinib for advanced MMR-proficient ECs that are not MSI-h or MMR-deficient. Results from the KEYNOTE-146 study demonstrated an increased ORR and greater median PFS of 7.5 months [398]. The KEYNOTE-868 (NCT03914612) study the addition of pembrolizumab to standard chemotherapy resulted in significantly longer PFS than with chemotherapy alone in patients with advanced or recurrent EC [55]. This highlights the relevance of targeted unique dependencies of anticancer therapies and exploring combinations with already approved agents, hence underscoring the rationale for identifying previously unknown pathways altered in the disease. This was just the start for the prospect of ICIs in EC, and more recently dostarlimab (anti-PD-1) has also been approved for the treatment of MMR-deficient advanced or recurrent MMR-deficient ECs following failed chemotherapy [399]. Recently, results from the RUBY (NCT03981796) trial demonstrated that dostarlimab plus carboplatin-paclitaxel significantly increased PFS among patients with primary advanced or recurrent EC, with a substantial benefit in the MMR-deficient MSI-h population [56].

Despite advances in immunotherapy, analysis of clinical response to immune checkpoint inhibition across several cancer types indicate that up to 85% of patients do not respond [400]. As such, there is a need not only to identify reliable predictive biomarkers to identify patients likely to respond to immune checkpoint inhibition but also the underlying mechanism to potentially identify other targetable pathways that are modified in the disease. A more robust understanding of the molecular and immunologic drivers of response and resistance will be critical to optimally design next-generation studies in EC. Moreover, the relationship between MLH1 hypermethylated endometrial tumours and response to immune checkpoint inhibition has not yet been reported on, and the consensus on the association between hypermethylated EC and PD-L1 expression is immature [301].

There is growing evidence demonstrating that mitochondrial activity, which is critical for T cell function, can be augmented by blocking PD-1 or CTLA4 signalling [401-403]. Given the central role of mitochondria in the complex interactions between cancer and the immune system, a high priority should be placed on developing combinatorial strategies in future preclinical and clinical studies. In this thesis, we identified a novel link between MLH1 loss and mitochondrial metabolism in *in vitro* EC models. To date, there has been limited research on the link between MMR loss and mitochondrial disease across any cancer types published in the literature. Previous work from our lab has demonstrated that MLH1-deficient cells have a dysfunctional mitochondrial phenotype caused by a rearrangement of mitochondrial gene expression including decreased mitochondrial biogenesis and anti-oxidant response genes [175]. Additionally, Rashid *et al*. demonstrated that MLH1-deficient cells increased the sensitivity of the cells to the Complex I inhibitor, Rotenone, and hence oxidative stress. Taken together these findings implied that impaired Complex I activity and a subsequent perturbed anti-oxidant stress response were responsible for this sensitivity and could be clinically exploited [175]. Our work provides the rationale for further investigating this correlation to determine whether targeting cancer metabolism in EC, alone or in combination with immunotherapy, is viable clinically. Evidence *in vitro* and *in vivo* supports the notion that mitochondrial metabolism provides key metabolites for macromolecule synthesis to support tumour anabolism and by generating oncometabolites necessary for tumour growth [217, 283, 404-406], thus chemotherapies targeting cancer metabolism are an attractive therapeutic option.

6.2 Endometrial cancer as a metabolic disease

There have been numerous studies investigating the link between metabolism and EC, identifying that women with metabolic disorders such as obesity and diabetes have a marked increased risk of developing EC [407-410]. Despite being well-characterised at a genetic level, the metabolism of endometrial tumours is not fully understood. Many genetic aberrations involved in EC initiation and progression are also involved in regulating cell metabolism such as the PI3K-AKT pathway. This metabolic pathway is altered in over 90% of type I endometrial tumours and results in enhanced insulin signalling and the optimal tumour microenvironment [20, 411]. Despite this knowledge, however, it is still unclear whether the flux of nutrients through metabolic pathways contributes to EC survival and tumour growth. In recent years several preclinical and clinical studies have linked the alteration of metabolic genes to the type and grade of EC, however, this field warrants further investigation to determine whether this metabolic vulnerability can be exploited therapeutically to increase progression-free survival in these patients.

In 2014, a study by Byrne *et al.* demonstrated EC cells have an increased glycolytic–lipogenic metabolism which they depend on for survival [412]. The study analysed previously reported gene expression data from women with type I EC, and identified genes involved in glycolysis and gluconeogenesis were enriched in tumour-derived endometrium. The most elevated genes were glycolytic enzymes HK2, GAPDH, pyruvate kinase 2 (PKM2), and lactate dehydrogenase isoform A (LDHA) [412]. In an independent cohort of six patients, gene expression data was validated at the protein level which corroborated the increased expression of glycolytic enzymes as well as an increased expression of enzymes involved in *de novo* lipogenesis such as ACLY, acetyl-CoA carboxylases (ACC1 and ACC2), and FASN [412]. Further *in vitro* analyses of EC cells highlighted an increased expression of GLUT6 and glycolytic-lipogenic metabolism in HEC-1-A, Ishikawa, MFE-296, MFE-319, AN3CA, RL95-2, KLE cells and two immortalized cell lines derived from noncancerous endometrial tissue, MAD-11 stromal and hUE-Ts uterine epithelial cells [412]. GLUT6 was upregulated in all seven endometrial cell lines investigated, whereas the expression of GLUT1 and other glycolytic and lipogenic enzymes varied between cell lines. Furthermore, suppression of GLUT6 expression in these cancer cells *in vitro* inhibited glycolysis and survival of endometrial cells in the study. Consistent with these findings, in our MLH1-deficient MFE-280 cells we identified an increase in genes involved in glycolysis and gluconeogenesis such as PFKP, PKM, GAPDH, PGK, GOT1/2 and HK2. Interestingly, MLH1 loss in these cells was also accompanied by a significant downregulation of phosphoenolpyruvate carboxykinase 1 (PCK1), which catalyses the formation of phosphoenolpyruvate from oxaloacetate. In a hepatocellular carcinoma cell (HCC) model, PCK1 deficiency was shown to promote proliferation through the inactivation of AMPK, suppression of p27Kip1 expression, and stimulation of the CDK/Rb/E2F pathway, consequently accelerating transition from G1 to S phase of the cell cycle in glucose-starved conditions [326]. Furthermore, Xiang *et al*. demonstrated that PCK1 knockout markedly enhanced the global *O*-GlcNAcylation levels in HCC cells under low-glucose conditions [413]. Metabolic reprogramming in PCK1-deficient hepatoma cells led to oxaloacetate accumulation and increased *de novo* uridine triphosphate synthesis contributing to uridine diphosphate-*N*-acetylglucosamine (UDP-GlcNAc) biosynthesis [413]. UDP-GlcNAc, the end product of the hexosamine-biosynthesis pathway, is proposed to be a nutrient sensor that couples metabolic and signalling pathways in cells [414, 415]. If the decreased expression of PCK1 is linked to MLH1 loss in EC cells, it is possible these cells are undergoing a similar metabolic rewiring to HCC cells in low-glucose conditions. Unfortunately, our metabolomics analysis could not detect oxaloacetate levels, a metabolite that would be interesting to measure to understand whether MLH1-deficient EC cells have a similar metabolic architecture. Further investigations are required to understand the importance of these metabolic alterations in EC cells. Our findings could provide a rationale for profiling endometrial

patient tumours to further investigate whether there is a link between MLH1 and the regulation of metabolic pathways in humans.

6.2.1 Altered amino acid metabolism in endometrial cancer

Amino acids facilitate cancer cell proliferation and survival of cancer cells under genotoxic, oxidative, and nutritional stress. In our study, we observed a significant increase in the abundance of glycine, isoleucine, leucine, arginine and citrulline in the MLH1-deficient cells. It is long recognised that cancer is a metabolic disorder with alterations to pathways such as glycolysis, tricarboxylic acid cycle, choline, and fatty acid metabolism [416], though further research is required to purpose metabolomic studies for the identification of biomarkers linked to specific histological or molecular subtypes of EC. Recently, Trousil *et al.* identified metabolic patterns that illustrate a severely altered phenotype in EC involving proliferation-associated markers such as altered amino acids metabolism and the nucleobase uracil, which are indicative of high transcriptional and proliferative activity, maintenance of intracellular redox homeostasis (glutathione), osmoregulation (inositols, taurine) and glucose [416, 417].

Targeting aberrant amino acid metabolism is an attractive anticancer therapy, though few studies to date have investigated its role specifically in EC. A study by Skorupa *et al.* investigated metabolomic characteristics associated with EC using NMR spectroscopy in 64 patients with varying grades of endometrial tumours [416]. Results demonstrated increased levels of amino acids in all ECs, regardless of the grade, including valine, isoleucine, leucine, hypotaurine, serine, lysine, ethanolamine, and choline and decreased creatine, creatinine, glutathione, ascorbate, glutamate, phosphoethanolamine and scyllo-inositol [416]. This study also revealed grade 1 and 2 endometrial tumours had increased levels of taurine relative to the control tissue, alongside elevated glycine, N-acetyl compound and lactate in grade 1 and 3 tumours [416]. In our study which adds in the additional layer of MLH1 deficiency, we observed a further increase in the levels of glutamine glutamate, a-KG, malate, asparagine, and serine in our MLH1-deficient Ishikawa cells, which could signify their importance in driving the more severe phenotype associated with MLH1 deficiency in this indication.

Furthermore, a study by Wang *et al.* uncovered the association between branched-chain amino acid aminotransferase 1 (BCAT1) expression, an aminotransferase of glutamate and branched-chain amino acids (BCAAs) in high-grade EC relative to low grade [418]. In the study, they identified the link between BCAT1 expression and proliferation, with BCAT1 knockdown significantly suppressing *in vitro* proliferative capabilities of HEC-1A and Ishikawa cells. Moreover, LC-MS/MS analysis was carried out to analyse intracellular amino acid concentrations upon BCAT1 suppression. BCAT1 knockdown

resulted in >30% decreases in the amount of intracellular isoleucine and leucine produced [418]. The increased expression of BCAT1 was also confirmed in endometrial tumours and was consistent with previous reports of BCAT1 overexpression in ovarian tumours [419]. Interestingly, in both our MLH1-deficient cell models, BCAT1 was significantly downregulated (-1.05 Log2FoldChange, p=0.007; -0.85 Log2FoldChange, p=0.006 for MLH1-deficient Ishikawa and MFE-280, respectively). The recent study by Li *et al.* analysed the expression, potential mechanisms, and clinical significance of BCAT1 in pan-cancer, and demonstrated its prognostic significance in eight cancers, including adrenocortical carcinoma, urothelial, breast, RCC, Glioma, HCC, pancreatic, and uveal melanoma [420]. Additionally, BCAT1 expression was shown to positively correlate with the levels of neutrophils, dendritic cells, CD4 T cells, and CD8 T cells in some cancers such as HNSCC [420]. This study deduced that BCAT1 expression is a likely cancer biomarker, and may signify tumour immune cell infiltration with the potential to be a marker for immunotherapy treatment [420]. Given that MLH1 deficiency in our EC cell models is associated with a reduction in BCAT1 expression, which based on the previously discussed studies should be a good prognostic indicator, there must be another mechanism underpinning the more severe disease phenotype associated with MLH1-deficient EC. However, given that a metabolite can be involved in multiple reactions, its dysregulation can be influenced by several different processes, and therefore uncovering the actual altered metabolic pathways in EC solely by metabolomic analysis is difficult, particularly *in vitro* which has several limitations [421].

6.3 Studying MLH1-deficient metabolic differences *in vitro*

6.3.1 Tools to study cancer metabolism

Cancer metabolism refers to the complex system that adapts to provide the building blocks that enable the rapid proliferation of cells, even at times of poor nutrient availability. Since the discovery of the Warburg effect which elucidated the metabolic flexibility of cancer cells, there is growing interest in how cancer cells rewire their metabolism to prevail in unfavourable environments and at times of nutrient stress [217]. Studying cancer metabolism *in vitro* has improved our knowledge of metabolic reprogramming in cancer and as such is providing new therapeutic opportunities. To investigate how cancer cells differentiate metabolically from normal cells, researchers have developed techniques to measure the levels of specific metabolic intermediates. Techniques such as liquid chromatography (LC) coupled with mass spectrometry (MS) is popular as they can measure water-soluble metabolites. Many intermediates that have been linked to promoting cancer through metabolic rewiring, have hydrophilic chemical properties [422]. Discoveries from MS-based techniques have been revolutionary in the field of cancer metabolism. An example of this is the use of LC-MS-based plasma metabolic profiling to uncover the role of BCAAs in the development of

pancreatic ductal adenocarcinoma (PDAC) [423]. Moreover, global metabolic profiling led to the discovery of oncometabolite 2-hydroxyglutarate (2-HG) in IDH mutant glioblastoma [424].

Moreover, metabolomics is being realised for its potential application in the clinic and is beginning to play a role in cancer diagnosis and treatment algorithms. For instance, metabolomics techniques are being utilised for the identification of biomarkers and predictive markers of progression, and the prediction of adverse events in response to certain therapies [425]. These techniques are also being used to investigate dietary influences on drug therapy. For instance, Warth *et al.* monitored amino acid and central carbon metabolism of breast cancer cells under palbociclib (CD4/6 inhibitor) and letrozole (anti-oestrogen) treatment, which is approved for ER+ breast cancer in the US based on the PALOMA-1 study (NCT00721409) of 165 postmenopausal women [426]. The study demonstrated that dietary xenoestrogens genistein and zearalenone had a distinct effect on cellular metabolism, oncogenic signalling, and cell proliferation during the combined treatment [426], results which provide a rationale for targeted nutritional recommendations to be made for breast cancer patients on this treatment. Metabolomics has been used for drug repurposing studies to identify novel indications for already registered drugs, with metabolomics analysis, combined with bioinformatic and pathway analysis showing great promise for advancing and potentially accelerating these programs [425, 427]. A study using isotopic tracing in combination with untargeted metabolomics to screen drug candidates targeting one-carbon metabolism identified that sertraline, a clinically used antidepressant, targeted the serine/glycine biosynthesis pathway, thus could be a candidate for cancer treatment in combination with mitochondrial inhibitors [428]. Sertraline was able to significantly reduce cell viability, proliferation, and protein synthesis in a concentration-dependent manner by inhibiting SHMT 1/2, the enzyme that converts serine to glycine and combining treatment with rotenone or antimycin A further decreased proliferation of breast cancer cells [428]. Sertraline is a clinically used drug that can safely be used in humans, whereas previously identified inhibitors of serine/glycine synthesis enzymes did not reach clinical trials. Metabolomics uncovered that sertraline may have applications as an adjuvant therapeutic strategy against serine/glycine synthesis–addicted cancers [428].

We used LC-MS to quantify the levels of specific metabolites in our MLH1-deficient EC models. In doing so we identified that MLH1-deficient EC cells have a distinct metabolic architecture, harbouring differences in the levels of metabolites involved in glycolysis, one-carbon metabolism, and the TCA cycle. We carried out the assay in two different culture mediums, DMEM and RPMI which interestingly showed different results which we will discuss in more detail below, consequently highlighting one of

the drawbacks of using *in vitro* techniques for studying cancer metabolism. As such, interpreting the biological meaning of identified metabolic differences in MLH1 deficiency is challenging, as the observed differences in metabolite levels could be an artefact of supraphysiological nutrient availability from the surrounding media. Additionally, it is important to note that these assays do not tell you why these metabolite levels are different, i.e., it could be due to changes in metabolite transport, production, or even consumption. It is useful to combine metabolite abundance data with the expression of metabolic enzymes to gauge what is happening mechanistically in cells. Additionally, it is informative to trace metabolites in dynamic systems using stable isotope tracers. Radioactive isotopic tracers have been used for many years to study metabolic alterations associated with disease, by measuring the dynamic flux of nutrients [429]. Metabolic pathway activity is inferred by tracing the incorporation of labelled substrates such as ^{13}C into metabolites. MLH1-deficient EC cells have increased incorporation of labelled carbon into metabolites associated with the TCA cycle and the serine synthesis pathway. Interestingly, we identified differences in metabolic pathway dependencies in both MLH1-proficient and deficient cell lines, according to the medium in which the cells were cultured. As such, we were interested in investigating why this may be the case, alongside deciphering the biologically significant alterations in MLH1 deficiency.

6.3.2 Traditional versus physiologically relevant cell culture media

Cell culture media was originally constituted to contain the nutrients required to sustain continuous cell proliferation *in vitro*, however recently it has been realised that their composition does not accurately reflect the tumour microenvironment *in vivo.* This leads to early research incorrectly progressing to studies in animal models and potentially human trials, guided by biologically irrelevant findings *in vitro*. Data published in 2019 by Wong *et al.* highlights that approximately only ~3% of potential oncology drugs succeed during clinical development [430]. This low success rate highlights the limitations of *in vitro* models, one of which is the media in which the cells are cultured.

For the metabolomics assay Ishikawa MLH1-proficient and deficient cells were cultured in both DMEM and RPMI media to investigate the effect each of these media has on metabolic pathway dependency. In both growth conditions, Ishikawa cells, regardless of MLH1 status, have similar levels of glucose. Interestingly in DMEM, we identified that Ishikawa cells have much lower levels of lactate, and pyruvate compared to when cultured in RPMI. This could either imply that in DMEM they have a faster rate of metabolism and therefore are metabolising these quicker, or that under these conditions (when provided with excess glucose) lactate and pyruvate are less essential, than when these cells are cultured in RPMI, and therefore they produce them at a slower rate/ require them less, possibly utilising alternative energy generating pathways. Furthermore, in DMEM, Ishikawa cells have much

higher levels of intracellular glutamine compared to when cultured in RPMI, however comparable levels of glutamate in both media. This implies that despite a higher concentration of extracellular glutamine available, the rate-limiting step of glutaminolysis determines the levels of intracellular glutamate and α-KG for entry into the TCA cycle. Consequently, we considered this information when investigating the potential therapeutic effect of specific metabolic inhibitors.

DMEM and RPMI are the most frequently used culture media in *in vitro* research but were originally only designed to provide the minimum number of nutrients required to enable the continuous proliferation of cancer cells. As such, the nutritional composition of these media differs significantly from relevant physiological values and consequently also from the nutritional tumour microenvironment. For instance, DMEM contains 25mM glucose, four times the concentration of 'normal' blood plasma levels [354, 431]. As a result, it is not surprising that studies have identified differences between *in vitro* and *in vivo* cancer cell metabolism. To combat this problem and improve *in vitro* data, Voorde *et al*. formulated a media guided by the composition of metabolites in human blood [431]. They then compared the effects of culturing TNBC in commercially available media versus 'Plasmax'. Interestingly they found that culturing these cancer cells in Plasmax, thought to contain metabolites of low nutritional value such as selenium, impacts the colony-forming capacity of these cells by inhibiting ferroptosis [354]. Moreover, Voorde *et al.* also highlighted that when cultured in Plasmax, TNBCs reprogram their metabolism and transcriptional profiles independent of cell proliferation rate. They carried out an untargeted metabolomics study to compare the profiles of cancer cells cultured in Plasmax versus DMEM-F12, demonstrating that culturing these cells in Plasmax more accurately recapitulates the metabolic environment of tumours [354]. We observed differential responses to metabolic inhibitors depending on the media in which our EC cells were cultured, most likely due to the availability and therefore dependence on certain metabolites. These differences are discussed further in the following sections.

6.3.4 Vulnerability of MLH1-deficient endometrial cancer cells to LDH inhibition

Our metabolomics results highlighted that MLH1-deficient cells were more metabolically active as we observed an increased flux of ^{13}C from glucose into metabolic intermediates involved in the TCA cycle, urea cycle and numerous essential and nonessential amino acids. Additionally, we observed differences in the abundance of certain metabolites involved in glycolysis and anaerobic metabolism, notably pyruvate and lactate. In MLH1 deficiency, we observed significantly higher levels of pyruvate and lactate alongside significantly lower levels of glucose, in comparison to the MLH1-proficient cells. Due to the high levels of lactate in MLH1-deficient cells, we hypothesised that they are upregulating

anaerobic metabolism to support their proliferation and survival, and consequently may be vulnerable to LDH inhibition.

High levels of lactate in cancer cells, the Warburg effect, results from the ability of cancer cells to uptake large amounts of glucose which produces large amounts of lactate even in the presence of oxygen. The high concentration of lactate acidifies the tumour microenvironment contributing to metastasis, angiogenesis, immunosuppression, and resistance to therapies in some cases. For some time lactate was considered only a metabolic waste product of glycolysis, however, it has now been realised that lactate can be used as a fuel source by incorporation into the TCA cycle, and in addition is an oncometabolite with signalling properties [302].

The majority of lactate in cancer cells is produced from glucose via glycolysis [432]. Where, normal mammalian cells generate most of their energy through OXPHOS in the mitochondria, cancer cells generate ATP from glycolysis in the conversion of glucose to lactate, a much less efficient process [433]. Moreover, it has also been demonstrated that glutamine can contribute to a small amount of lactate formation in cancer cells. Glutamine is the most abundant circulating amino acid [289]. In the mitochondria, glutamine is converted to glutamate catalysed by GLS1. Glutamate is further deaminated by glutamate dehydrogenase to α-KG for incorporation into the TCA cycle. Malate, a TCA cycle intermediate, can be exported to the cytosol and converted to pyruvate, the precursor to lactate, by malic enzyme [246, 302].

The conversion of pyruvate to lactate is mediated by nicotinamide adenine dinucleotide oxidoreductase LDH enzyme. This is a tetrameric enzyme composed of M and H protein subunits, encoded by the LDHA and LDHB genes [302]. These subunits can combine to form 5 homo or hetero tetramers in human tissues, but the predominant isoform found in skeletal muscle tissues is LDHA, which preferentially catalyses the reduction of pyruvate to lactate. LDHB, which is predominantly located in the human heart muscle, preferentially catalyses the conversion of lactate to pyruvate for OXPHOS or gluconeogenesis [302]. There have been several reports of increased LDHA expression and activity in a variety of tumour types, and this is associated with a reduced survival rate and increased resistance to therapy. Previous studies have demonstrated that high LDHA levels in serum could be a poor prognostic indicator in osteosarcoma, pancreatic cancer, and lung adenocarcinoma [434-437].

Consequently, there has been significant therapeutic interest in targeting lactate production in cancer cells. LDHA links glycolysis and OXPHOS. Inhibiting LDHA results in more pyruvate entering the TCA

cycle, increased oxygen consumption and increased OXPHOS activity. LDHA's role in OXPHOS is linked to fumarate hydratase activity (FH), which converts fumarate to malate. Inhibition of FH can lead to decreased OXPHOS alongside increased glycolysis. Studies demonstrate that cell lines deficient in both FH and LDHA, exhibit reduced proliferation, ATP depletion, increased apoptosis, and increased oxygen consumption and ROS, compared to cell lines deficient in only one of FH or LDHA [438, 439]. Furthermore, numerous studies have demonstrated the dependence of tumour cells on LDHA in mouse models. Fantin *et al.* highlighted the dependency of cancer cells on LDHA activity in comparison to normal cells which rely on OXPHOS [231]. Additionally, Rong *et al.* demonstrated that LDHA promotes cell proliferation in pancreatic cancer both *in vitro* and *in vivo*, and FX11, a small-molecule inhibitor of LDHA effectively inhibited tumour growth in human B-cell lymphoma and pancreatic cancer xenograft models [231, 237].

Although we do not observe a significant upregulation of LDHA at protein or mRNA level, our metabolomics data which demonstrated a significant increase in lactate levels in MLH1-deficient EC cells implies that these cells are indeed more glycolytic. This is consistent with our data which highlighted that in the absence of MLH1, these cells display a decrease in complex I activity, alongside an increase in glycolytic capacity determined by the seahorse assay. Consequently, we investigated whether MLH1-deficient EC cells were sensitive to LDH inhibition using several inhibitors including, FX11, GNE-140, and GSK2837808A. Its high anticancer efficacy makes LDHA an attractive antitumour target, however, the search for effective LDH inhibitors to use in the clinic is an ongoing process. To date, it has been relatively unsuccessful with many hopeful molecules not progressing further than early-stage *in vitro* research due to off-target effects, low renal clearance, or incompatibility with oral bioavailability [440].

Nonetheless, to investigate the mechanism driving metastasis in MLH1 deficient EC we used FX11, GNE-140 and GSK2837808A, to inhibit glycolysis in our EC cell models. FX11, an LDHA antagonist, competes with NADH, and has been shown to inhibit aerobic glycolysis and induce cell cycle arrest and apoptosis, showing preclinical efficacy in lymphoma, pancreatic, prostate cancer, and neuroblastoma [364, 365, 441]. Even though FX11 exhibits therapeutic potential, it is an unsuitable candidate drug for further clinical development as studies have implied that some of the observed effects were due to the reactive nature of the catechol groups in the molecule, as opposed to LDH inhibition [442]. Moreover, GNE-140 is a selective inhibitor of LDHA and LDHB, which Boudreau *et al*. have demonstrated the ability of the inhibitor to cause cell cycle arrest in highly glycolytic pancreatic cancer cell lines [371]. Lastly, GSK2837808A is a potent and selective LDHA inhibitor which has been

shown to inhibit lactate production and reduce proliferation, migration and invasion of breast cancer cells [443].

Interestingly, inhibiting glycolysis using FX11 and GNE-140 slowed the proliferation of our Ishikawa MLH1-deficient Ishikawa cell line, however, the opposite was observed in our MFE-280 cell lines, whereby the MLH1-proficient gCTRL cells were more sensitive to inhibition. This is likely due to the OXPHOS capability of these cell lines upon inhibition of glycolysis. We demonstrated that in the absence of MLH1, Ishikawa cells have a reduced OXPHOS capability, which we did not observe in the MLH1-deficient MFE-280 cells. Noncancerous cells depend scarcely on LDH, preferentially generating ATP via OXPHOS, thus inhibiting its activity isn't as debilitating. A study has demonstrated that in the absence of LDHA/B cells shift their metabolism to OXPHOS, alongside increasing their mitochondrial content [444]. Our MLH1-deficient MFE-280 cell lines are not deficient in OXPHOS, and in fact, our RNAseq data indicates that these cells upregulate mitochondrial energy metabolism, as well as genes involved in OXPHOS in the absence of MLH1. This could explain why we do not observe a consistent therapeutic response to LDH inhibition in both of our MLH1-deficient cell lines. The study by Boudreau *et al*. that observed their pancreatic cell lines that utilised OXPHOS over glycolysis were resistant to GNE-140 inhibition of LDH, is consistent with our findings [371]. They demonstrated that this acquired resistance to GNE-140 was driven by activation of the AMPK-mTOR-S6K signalling pathway, which led to increased OXPHOS, and inhibitors targeting this pathway could prevent resistance. Consequently, using inhibitors targeting this pathway in combination with LDH inhibitors in glycolytically independent tumours could reduce the emergence of chemoresistance [371].

To date, little to no research has been published on the prospect of targeting glycolysis in EC. Patients diagnosed with EC typically have a poor prognosis due to the lack of effective treatments, thus uncovering novel biomarkers and promising treatment strategies is essential. Tian *et al*. have paved the way in demonstrating the importance of glycolytic metabolism in EC. They investigated the role of microRNA-1271 in EC, demonstrating its ability to inhibit cell proliferation and metastasis by regulating LDHA, thus highlighting its function as a tumour suppressor [445]. Moreover, although not in EC, Zhang *et al*. have shown how LDHA is involved in cervical cancer pathogenesis and may be a promising target for therapy [446]. They demonstrated that the inhibition of LDHA activated the mitochondrial apoptosis pathway by inducing G2/M cell cycle arrest. It is possible that ECs harbouring a high expression of LDHA associated with poor patient survival could also benefit from LDH inhibition. LDH inhibition induces cell cycle arrest and apoptosis via the JNK pathway in cervical cancer cells. Future

work on our MLH1-deficient EC cell lines should investigate whether inhibiting LDH is suppressing proliferation in the same manner.

Although developing novel small molecule compounds specifically targeting LDHA has shown great promise *in vitro*, most currently available glycolytic inhibitors have low potency, or have shown limited success *in vivo*. This may be because most *in vitro* research is carried out in media containing supraphysiological concentrations of nutrients that do not resemble the *in vivo* tumour microenvironment or even 'normal' blood plasma. We saw a sensitivity of Ishikawa cells to LDH inhibitors GNE-140 and FX11 *in vitro* in DMEM, however, were intrigued to see whether this sensitivity was consistent when cultured in alternative media. Interestingly, MLH1-deficient cells were not sensitive to LDH inhibition when cultured in RPMI or Plasmax, even though all cells proliferate comparably in each media. DMEM contains the highest concentration of glucose of all three media, and interestingly no lactate. It is plausible that inhibiting LDH in cells cultured in Plasmax is less effective as the media contains a sufficient basal amount of lactate to generate ATP. Alternatively, it is possible that the inhibitor was less effective in Plasmax and RPMI compared to DMEM. It would be beneficial to monitor the levels of lactate in each cell line, cultured in each media, with the addition of each inhibitor, to compare the percentage of LDHA inhibition for each. Nonetheless, ECs with a high expression of LDHA may still benefit from a combination of LDH inhibition in conjunction with immune checkpoint blockade or radiotherapy. In non-small cell lung cancer (NSCLC), inhibition of LDH by Oxamate enhances the therapeutic effect of anti-PD-1 therapy pembrolizumab, significantly slowing tumour growth in the Hu-PBMCs-CDX mouse model [447]. The increased immunotherapeutic effect is mediated by increased infiltration of CD8+ T cells into the tumour tissue, particularly at the centre. A previous study suggested that reducing lactic acid levels in tumours downregulated PD-L1 expression, consequently blocking the PD-1/PD-L1 pathway and resulting in an increased infiltration and activity of CD8+ cytotoxic T-cells [448]. Moreover, inhibition of LDHA by Oxamate remarkably increased the radiosensitivity of NSCLC cells to ionizing radiation-induced apoptosis in preclinical studies [449]. Given the recent accelerated approval of dostarlimab for the treatment of recurrent or advanced MMR-deficient EC, these data could provide the rationale for investigating the correlation between LDHA expression and therapeutic response to immunotherapy [399].

6.3.5 Vulnerability of MLH1-deficient endometrial cancer cells to glutaminolysis inhibition

Glutamine is an important amino acid which provides building blocks, in the form of carbon and nitrogen precursors, for biosynthetic pathways. GLS catalyses the first step of glutaminolysis, the reaction that converts glutamine in the cytosol to glutamate in the mitochondria. Targeting glutamine utilisation offers promise for tumours that display an increased dependency on glutamine for energy

production, often described as “glutamine-addicted” because of their huge metabolic demands [242]. GLS1 is being explored as a therapeutic target across a range of cancer types, for instance, GLS1 inhibition in osteosarcoma preclinical models can limit metastasis [450]. Studies have demonstrated that CB-839, a first-in-class, potent and selective inhibitor of GLS1, primes the environment for immune modulation by stimulating the cytotoxic action of tumour infiltrating lymphocytes and demonstrating anti-proliferative responses in a range of preclinical cancer models including TNBC and melanoma [451, 452]. These data supported the progression of CB-839 into clinical development which, although well tolerated in patients, had limited activity as a single agent resulting in the discontinuation of several clinical trials [453].

Despite this, preclinical data by Rashmi *et al*. supported the use of CB-839 in glutamine-dependent cervical cancers resistant to radiation, demonstrating that specific mutations in the PI3K pathway predict response to CB-839 sensitivity [454]. Excitingly, this has led registration of a new Phase 2 clinical trial on clinicaltrials.gov in the US, comparing the efficacy of CB-839 in combination with standard of care (SoC) treatment, to SoC alone, in advanced cervical cancer (NCT05521997). Consequently, we were intrigued to investigate whether we saw a similar sensitivity in our MLH1-deficient endometrial cell lines by treating them with the GLS1 inhibitor, given we observed a significant increase in the levels of glutamine/glutamate alongside an increased metabolic flux in our MLH1-deficient Ishikawa cells. The intention of these experiments was to understand whether MLH1 loss in EC cells drives glutamine metabolic rewiring. Chen *et al*. described a phenotype where mtDNA mutant cells with OXPHOS impairment increased glutamine anaplerotic flux, with the severity of OXPHOS defects determining the direction of the flux [249]. Given previous studies demonstrated MLH1-deficient EC cells displayed a similar phenotype with reduced mtDNA copy number and reduced OXPHOS [175], we originally hypothesised that these cells could be comparably rewiring their metabolism. Nonetheless despite observing a slight dependency on glutamine in supplementation experiments in the MLH1-deficient Ishikawa cells, we observed no significant differences in sensitivity in our MLH1-deficient cell models to glutaminolysis inhibition by CB-839. As a result, we turned our focus to other metabolic pathways. Future work to investigate the correlation between GLS1 expression and MLH1 loss in EC patient data could provide more insight into glutamine dependency in EC and consequently whether glutaminase inhibition would be a viable treatment option.

6.4 Targeting the serine synthesis pathway in cancer cells

We observed aberrant serine synthesis *in vitro* in MLH1-deficient cell models, particularly when cultured in a physiologically relevant media such as Plasmax. In physiologically relevant media, MFE-

280 MLH1 K/O clones significantly upregulated proteins involved in the serine synthesis pathway, such as PHGDH. Interestingly these differences were not observed when MFE-280 cell lines were cultured in DMEM. Though not statistically significant, a trend towards increased PHGDH expression was also observed in the MLH1-deficient Ishikawa cell line cultured in Plasmax media. Numerous studies discuss the importance of serine/glycine biosynthesis and one-carbon metabolism in cancer cells for promoting survival and sustaining rapid proliferation, with a growing subset of cancers being identified with the ability to shunt glycolytic intermediates into the serine synthesis pathway [256, 260, 261, 455-457]. Upregulation of serine synthesis pathway metabolism in cancer cells drives tumourigenesis by generating single-carbon units for use in one-carbon (1C) metabolism, which produces proteins, nucleic acids, lipids, and other biological macromolecules to support tumour growth. The upregulation of PHGDH could explain the significantly increased levels of serine and lower levels of glycine observed in the metabolomics analysis of our MLH1-deficient Ishikawa cells. This is accompanied by significantly increased incorporation of labelled carbon into both glycine and serine in the glucose metabolic tracing study, further supporting a possible dependency on this pathway in the absence of MLH1. Whilst targeting metabolic vulnerabilities of cancers is a fast-growing field of interest, and inhibiting serine synthesis is of high clinical relevance, due to the ubiquitous nature of metabolic enzymes, more research is required before these enter the clinic due to the associated systemic toxicities [458].

Though no serine synthesis pathway inhibitors are approved for clinical use, there are preclinical studies investigating experimental inhibitors targeting PHGDH, the first enzyme in the pathway, which is considered an exciting and viable therapeutic target [267, 269]. Increased expression of PHGDH, has been linked to shorter PFS, increased metastasis, and poorer OS in patients with a range of cancers including, colorectal, gastric, breast, melanoma, and cervical [260, 261, 265, 459, 460]. Studies have shown that elevated levels of PHGDH affect redox homeostasis, cell growth and proliferation, and metastasis, along with playing a role in resistance to anti-cancer therapies [461]. By elevating PHGDH levels, cancer cells develop resistance to chemotherapies that induce apoptosis through increased ROS, as PHGDH generates the metabolic precursors for antioxidant and ROS scavenging activity [461]. Direct inhibition of PHGDH by small-molecule inhibitors decreases cellular proliferation *in vitro* and can sensitise tumour cells to various therapies [461].

Several high-throughput screening studies have identified hopeful molecules in preclinical studies, though a lack of potency *in vivo* and the potential for off-target side effects are big drawbacks. Mullarky *et al.* identified CBR-5884, a PHGDH inhibitor that disrupts the enzyme in its tetrameric

shape, favouring the dimeric conformation. This study also suggested that enzyme activity *in situ* may be regulated by fluctuations between 3D confirmations [267]. Moreover, in a comparable study, Pacold *et al*. identified a compound called NCT-503 with an improved inhibition of PHGDH [268]. Despite showing promising anti-cancer functionalities *in vitro*, these compounds have limited potency *in vivo*. Nonetheless, they do demonstrate that this approach is a viable anti-cancer therapeutic strategy and as such these compounds, and others, are undergoing optimisation for future clinical testing.

Though a growing number of studies identify the emerging link between metabolism and DNA repair, relatively few associate the MMR pathway. Our study demonstrated that MFE-280 MLH1-deficient cells were more sensitive to PHGDH inhibition, suggesting a novel link between the MMR and serine synthesis pathways. In the absence of MLH1, we propose that EC cells have an increased dependency on serine to sustain proliferation. Upon PHGDH inhibition, MLH1-deficient MFE-280 cells exhibited reduced expression of PHGDH, PSAT1, and PSPH, likely resulting in reduced *de novo* serine synthesis. The same trend in gene expression was not observed in the Ishikawa cells upon PHGDH inhibition suggesting why a similar sensitivity in MLH1 deficiency was not observed. Moreover, though the same sensitivity is not replicated upon depletion of PHGDH by siRNA, this pathway warrants further investigations to uncover the association with MLH1 deficiency in EC and decipher whether this dependency could be therapeutically targeted.

Despite drawbacks linked to PHGDH inhibition, the future holds promise, with several studies investigating ways to limit off-target side effects. For instance, Menin *et al*. hypothesized that supplementing patients with dietary exogenous serine could sustain normal, but not oncogenic, cellular function, as tumour cells favour *de novo* serine synthesis [462]. Furthermore, there is a rationale for small molecule PHGDH inhibitors with increased lipophilicity which prevents the inhibitor from crossing the blood-brain barrier, averting off-target neurodevelopmental effects observed by Yoshida *et al*. [463]. More recent scientific advances propose the use of targeted drug delivery systems such as nanoparticles, which could reduce off-target effects of anti-cancer therapies by targeting administration directly to the tumour. Currently, the leading nanomaterial for drug delivery is carboxymethyl chitosan which has been shown to suppress cell proliferation *in vitro* and cervical cancer tumour growth *in vivo* [464].

7.0 Conclusions and Future Work

This study demonstrates for the first time that MLH1-deficient EC cell lines exhibit a dependency on serine metabolism that could be exploited therapeutically. In order to understand whether this is truly EC-specific, and to gain a full understanding of the mechanism, this needs to be validated across a range of cell lines and cancer types. Moreover, the differing results between Ishikawa and MFE-280 cell lines emphasize the importance of future investigations that account for the method of MLH1 loss. It is plausible that variations in the method of MLH1 loss could could differentially influence the metabolic architecture of the cell lines. To further investigate these differences future studies should consider employing paired CRISPR methylation MLH1 knockout cell lines. Nonetheless, our findings could provide a rationale for profiling endometrial patient tumours to further investigate whether there is a link between MLH1 and the regulation of metabolic pathways in humans. In order to translate these results, an *in vivo* experiment with PHGDH inhibitors in development should be performed in mice xenografted with MLH1-deficient and proficient tumour cells, due to the drawbacks of utilising *in vitro* models for studying cancer metabolism.

8.0 References

1. Bray, F., et al., *Global cancer statistics 2018: GLOBOCAN estimates of incidence and mortality worldwide for 36 cancers in 185 countries.* CA: A Cancer Journal for Clinicians, 2018. **68**(6): p. 394-424.

2. Siegel, R.L., K.D. Miller, and A. Jemal, *Cancer statistics, 2018.* CA Cancer J Clin, 2018. **68**(1): p. 7-30.

3. Sung, H., et al., *Global Cancer Statistics 2020: GLOBOCAN Estimates of Incidence and Mortality Worldwide for 36 Cancers in 185 Countries.* CA: A Cancer Journal for Clinicians, 2021. **71**(3): p. 209-249.

4. Kitson, S.J., D.G. Evans, and E.J. Crosbie, *Identifying High-Risk Women for Endometrial Cancer Prevention Strategies: Proposal of an Endometrial Cancer Risk Prediction Model.* Cancer Prevention Research, 2017. **10**(1): p. 1.

5. Gottwald, L., et al., *Long-term survival of endometrioid endometrial cancer patients.* Archives of medical science : AMS, 2010. **6**(6): p. 937-944.

6. Lewin, S.N., et al., *Comparative Performance of the 2009 International Federation of Gynecology and Obstetrics' Staging System for Uterine Corpus Cancer.* Obstetrics & Gynecology, 2010. **116**(5).

7. Sorbe, B., C. Juresta, and C. Ahlin, *Natural history of recurrences in endometrial carcinoma.* Oncol Lett, 2014. **8**(4): p. 1800-1806.

8. Monk, B.J., et al., *Real-world outcomes in patients with advanced endometrial cancer: A retrospective cohort study of US electronic health records.* Gynecologic Oncology, 2022. **164**(2): p. 325-332.

9. Barretina-Ginesta, M.P., et al., *SEOM-GEICO clinical guidelines on endometrial cancer (2021).* Clinical & translational oncology : official publication of the Federation of Spanish Oncology Societies and of the National Cancer Institute of Mexico, 2022. **24**(4): p. 625-634.

10. Scharl, A., et al., *The Right Treatment for the Right Patient - Personalised Treatment of Breast Cancer.* Geburtshilfe Frauenheilkd, 2015. **75**(7): p. 683-691.

11. Schmandt, R.E., et al., *Understanding obesity and endometrial cancer risk: opportunities for prevention.* American journal of obstetrics and gynecology, 2011. **205**(6): p. 518-525.

12. Bogani, G., et al., *Uterine serous carcinoma.* Gynecologic Oncology, 2021. **162**(1): p. 226-234.

13. Lu, K.H. and R.R. Broaddus, *Endometrial cancer.* New England Journal of Medicine, 2020. **383**(21): p. 2053-2064.

14. Setiawan, V.W., et al., *Type I and II endometrial cancers: have they different risk factors?* Journal of clinical oncology : official journal of the American Society of Clinical Oncology, 2013. **31**(20): p. 2607-2618.

15. Varughese, J., et al., *Clear Cell Cancer of the Uterine Corpus: The Association of Clinicopathologic Parameters and Treatment on Disease Progression.* Journal of Oncology, 2011. **2011**: p. 628084.

16. Matsuzaki, S., et al., *Uterine carcinosarcoma: Contemporary clinical summary, molecular updates, and future research opportunity.* Gynecol Oncol, 2021. **160**(2): p. 586-601.

17. Soslow, R.A., et al., *Endometrial Carcinoma Diagnosis: Use of FIGO Grading and Genomic Subcategories in Clinical Practice: Recommendations of the International Society of Gynecological Pathologists.* (1538-7151 (Electronic)).

18. Levine, D.A., et al., *Integrated genomic characterization of endometrial carcinoma.* Nature, 2013. **497**(7447): p. 67-73.

19. Murali, R., R.A. Soslow, and B. Weigelt, *Classification of endometrial carcinoma: more than two types.* The Lancet Oncology, 2014. **15**(7): p. e268-e278.

20. Cancer Genome Atlas Research, N., et al., *Integrated genomic characterization of endometrial carcinoma.* Nature, 2013. **497**(7447): p. 67-73.

21. Klicka, K., et al. *The Role of miRNAs in the Regulation of Endometrial Cancer Invasiveness and Metastasis—A Systematic Review*. Cancers, 2021. **13**, DOI: 10.3390/cancers13143393.

22. Colombo, N., et al., *ESMO-ESGO-ESTRO Consensus Conference on Endometrial Cancer: diagnosis, treatment and follow-up[†].* Annals of Oncology, 2016. **27**(1): p. 16-41.

23. Oaknin, A., et al., *Endometrial cancer: ESMO Clinical Practice Guideline for diagnosis, treatment and follow-up.* Ann Oncol, 2022. **33**(9): p. 860-877.

24. Concin, N., et al., *ESGO/ESTRO/ESP guidelines for the management of patients with endometrial carcinoma.* Int J Gynecol Cancer, 2021. **31**(1): p. 12-39.

25. Oaknin, A., et al., *Endometrial cancer: ESMO Clinical Practice Guideline for diagnosis, treatment and follow-up[☆].* Annals of Oncology, 2022. **33**(9): p. 860-877.

26. Creutzberg, C.L., et al., *Surgery and postoperative radiotherapy versus surgery alone for patients with stage-1 endometrial carcinoma: multicentre randomised trial. PORTEC Study Group. Post Operative Radiation Therapy in Endometrial Carcinoma.* Lancet, 2000. **355**(9213): p. 1404-11.

27. Keys, H.M., et al., *A phase III trial of surgery with or without adjunctive external pelvic radiation therapy in intermediate risk endometrial adenocarcinoma: a Gynecologic Oncology Group study.* Gynecol Oncol, 2004. **92**(3): p. 744-51.

28. Blake, P., et al., *Adjuvant external beam radiotherapy in the treatment of endometrial cancer (MRC ASTEC and NCIC CTG EN.5 randomised trials): pooled trial results, systematic review, and meta-analysis.* Lancet, 2009. **373**(9658): p. 137-46.

29. Nout, R.A., et al., *Vaginal brachytherapy versus pelvic external beam radiotherapy for patients with endometrial cancer of high-intermediate risk (PORTEC-2): an open-label, non-inferiority, randomised trial.* Lancet, 2010. **375**(9717): p. 816-23.

30. Wortman, B.G., et al., *Ten-year results of the PORTEC-2 trial for high-intermediate risk endometrial carcinoma: improving patient selection for adjuvant therapy.* Br J Cancer, 2018. **119**(9): p. 1067-1074.

31. Maggi, R., et al., *Adjuvant chemotherapy vs radiotherapy in high-risk endometrial carcinoma: results of a randomised trial.* Br J Cancer, 2006. **95**(3): p. 266-71.

32. Susumu, N., et al., *Randomized phase III trial of pelvic radiotherapy versus cisplatin-based combined chemotherapy in patients with intermediate- and high-risk endometrial cancer: a Japanese Gynecologic Oncology Group study.* Gynecol Oncol, 2008. **108**(1): p. 226-33.

33. Hogberg, T., et al., *Sequential adjuvant chemotherapy and radiotherapy in endometrial cancer--results from two randomised studies.* European journal of cancer (Oxford, England : 1990), 2010. **46**(13): p. 2422-2431.

34. de Boer, S.M., et al., *Adjuvant chemoradiotherapy versus radiotherapy alone for women with high-risk endometrial cancer (PORTEC-3): final results of an international, open-label, multicentre, randomised, phase 3 trial.* The Lancet. Oncology, 2018. **19**(3): p. 295-309.

35. Hamilton, C.A., et al., *Endometrial cancer: A society of gynecologic oncology evidence-based review and recommendations.* Gynecol Oncol, 2021. **160**(3): p. 817-826.

36. Randall, M.E., et al., *Phase III Trial: Adjuvant Pelvic Radiation Therapy Versus Vaginal Brachytherapy Plus Paclitaxel/Carboplatin in High-Intermediate and High-Risk Early Stage Endometrial Cancer.* J Clin Oncol, 2019. **37**(21): p. 1810-1818.

37. Matei, D., et al., *Adjuvant Chemotherapy plus Radiation for Locally Advanced Endometrial Cancer.* N Engl J Med, 2019. **380**(24): p. 2317-2326.

38. León-Castillo, A., et al., *Molecular Classification of the PORTEC-3 Trial for High-Risk Endometrial Cancer: Impact on Prognosis and Benefit From Adjuvant Therapy.* Journal of clinical oncology : official journal of the American Society of Clinical Oncology, 2020. **38**(29): p. 3388-3397.

39. Creutzberg, C.L., et al., *Survival after relapse in patients with endometrial cancer: results from a randomized trial.* Gynecol Oncol, 2003. **89**(2): p. 201-9.

40. Chiantera, V., et al., *Pelvic exenteration for recurrent endometrial adenocarcinoma: a retrospective multi-institutional study about 21 patients.* Int J Gynecol Cancer, 2014. **24**(5): p. 880-4.

41. Miller, D.S., et al., *Carboplatin and Paclitaxel for Advanced Endometrial Cancer: Final Overall Survival and Adverse Event Analysis of a Phase III Trial (NRG Oncology/GOG0209).* J Clin Oncol, 2020. **38**(33): p. 3841-3850.

42. Lorusso, D., et al., *Carboplatin-paclitaxel compared to Carboplatin-Paclitaxel-Bevacizumab in advanced or recurrent endometrial cancer: MITO END-2 - A randomized phase II trial.* Gynecol Oncol, 2019. **155**(3): p. 406-412.

43. Pectasides, D., E. Pectasides, and T. Economopoulos, *Systemic therapy in metastatic or recurrent endometrial cancer.* Cancer Treat Rev, 2007. **33**(2): p. 177-90.

44. Ethier, J.L., et al., *Is hormonal therapy effective in advanced endometrial cancer? A systematic review and meta-analysis.* Gynecol Oncol, 2017. **147**(1): p. 158-166.

45. Herzog, T.J., et al., *PD-1, PD-L1 expression in 1599 gynecological cancers: implications for immunotherapy.* Gynecologic Oncology, 2015. **137**: p. 204-205.

46. Green, A.K., J. Feinberg, and V. Makker, *A Review of Immune Checkpoint Blockade Therapy in Endometrial Cancer.* American Society of Clinical Oncology Educational Book, 2020(40): p. 238-244.

47. Jiang, Y., et al., *PD-1 and PD-L1 in cancer immunotherapy: clinical implications and future considerations.* Hum Vaccin Immunother, 2019. **15**(5): p. 1111-1122.

48. Le, D.T., et al., *PD-1 Blockade in Tumors with Mismatch-Repair Deficiency.* The New England journal of medicine, 2015. **372**(26): p. 2509-2520.

49. Le, D.T., et al., *Mismatch repair deficiency predicts response of solid tumors to PD-1 blockade.* Science (New York, N.Y.), 2017. **357**(6349): p. 409-413.

50. Marabelle, A., et al., *Association of tumour mutational burden with outcomes in patients with advanced solid tumours treated with pembrolizumab: prospective biomarker analysis of the multicohort, open-label, phase 2 KEYNOTE-158 study.* Lancet Oncol, 2020. **21**(10): p. 1353-1365.

51. Oaknin, A., et al., *Clinical Activity and Safety of the Anti-Programmed Death 1 Monoclonal Antibody Dostarlimab for Patients With Recurrent or Advanced Mismatch Repair-Deficient Endometrial Cancer: A Nonrandomized Phase 1 Clinical Trial.* JAMA oncology, 2020. **6**(11): p. 1766-1772.

52. Konstantinopoulos, P.A., et al., *Phase II Study of Avelumab in Patients With Mismatch Repair Deficient and Mismatch Repair Proficient Recurrent/Persistent Endometrial Cancer.* J Clin Oncol, 2019. **37**(30): p. 2786-2794.

53. Antill, Y., et al., *LBA12 - Updated results of activity of durvalumab in advanced endometrial cancer (AEC) according to mismatch repair (MMR) status: The phase II PHAEDRA trial (ANZGOG1601).* Annals of Oncology, 2019. **30**: p. ix192.

54. Makker, V., et al., *Lenvatinib plus Pembrolizumab for Advanced Endometrial Cancer.* N Engl J Med, 2022. **386**(5): p. 437-448.

55. Eskander, R.N., et al., *Pembrolizumab plus Chemotherapy in Advanced Endometrial Cancer.* N Engl J Med, 2023. **388**(23): p. 2159-2170.

56. Mirza, M.R., et al., *Dostarlimab for Primary Advanced or Recurrent Endometrial Cancer.* N Engl J Med, 2023. **388**(23): p. 2145-2158.

57. Mirza, M.R., et al., *Palbociclib versus placebo in combination with letrozole for patients with advanced or recurrent endometrial cancer: The NSGO ENGOT-EN3/PALEO trial.* Journal of Clinical Oncology, 2017. **35**(15_suppl): p. TPS5612-TPS5612.

58. Liu, J.F., et al., *Phase II Study of the WEE1 Inhibitor Adavosertib in Recurrent Uterine Serous Carcinoma.* J Clin Oncol, 2021. **39**(14): p. 1531-1539.

59. MacKay, H.J., V.R. Freixinos, and G.F. Fleming, *Therapeutic Targets and Opportunities in Endometrial Cancer: Update on Endocrine Therapy and Nonimmunotherapy Targeted Options.* American Society of Clinical Oncology Educational Book, 2020(40): p. 245-255.

60. McAlpine, J.N., S.M. Temkin, and H.J. Mackay, *Endometrial cancer: Not your grandmother's cancer.* Cancer, 2016. **122**(18): p. 2787-2798.

61. Li, G.-M., *Mechanisms and functions of DNA mismatch repair.* Cell Research, 2008. **18**(1): p. 85-98.

62. Bell, D.W. and L.H. Ellenson, *Molecular Genetics of Endometrial Carcinoma.* Annu Rev Pathol, 2019. **14**: p. 339-367.

63. Jumaah, A.S., et al., *Mismatch repair deficiency and clinicopathological characteristics in endometrial carcinoma: a systematic review and meta-analysis.* J Pathol Transl Med, 2021. **55**(3): p. 202-211.

64. Peltomäki, P., *Lynch syndrome genes.* Fam Cancer, 2005. **4**(3): p. 227-32.

65. Wang, Y., et al., *Lynch syndrome related endometrial cancer: clinical significance beyond the endometrium.* Journal of hematology & oncology, 2013. **6**: p. 22-22.

66. Buchanan, D.D., et al., *Tumor mismatch repair immunohistochemistry and DNA MLH1 methylation testing of patients with endometrial cancer diagnosed at age younger than 60 years optimizes triage for population-level germline mismatch repair gene mutation testing.* J Clin Oncol, 2014. **32**(2): p. 90-100.

67. Lu, K.H., et al., *Gynecologic cancer as a "sentinel cancer" for women with hereditary nonpolyposis colorectal cancer syndrome.* (0029-7844 (Print)).

68. Meyer, L.A., R.R. Broaddus, and K.H. Lu, *Endometrial cancer and Lynch syndrome: clinical and pathologic considerations.* Cancer Control, 2009. **16**(1): p. 14-22.

69. Esteller, M., et al., *MLH1 promoter hypermethylation is associated with the microsatellite instability phenotype in sporadic endometrial carcinomas.* Oncogene, 1998. **17**(18): p. 2413-7.

70. Kurnit, K.C., S.N. Westin, and R.L. Coleman, *Microsatellite instability in endometrial cancer: New purpose for an old test.* Cancer, 2019. **125**(13): p. 2154-2163.

71. Umar, A., et al., *Revised Bethesda Guidelines for hereditary nonpolyposis colorectal cancer (Lynch syndrome) and microsatellite instability.* J Natl Cancer Inst, 2004. **96**(4): p. 261-8.

72. Hampel, H., et al., *Screening for Lynch syndrome (hereditary nonpolyposis colorectal cancer) among endometrial cancer patients.* Cancer Res, 2006. **66**(15): p. 7810-7.

73. Aaltonen, L., et al., *Explaining the familial colorectal cancer risk associated with mismatch repair (MMR)-deficient and MMR-stable tumors.* Clin Cancer Res, 2007. **13**(1): p. 356-61.

74. Lynch, H.T. and A. de la Chapelle, *Hereditary colorectal cancer.* N Engl J Med, 2003. **348**(10): p. 919-32.

75. Geiersbach, K.B. and W.S. Samowitz, *Microsatellite instability and colorectal cancer.* Arch Pathol Lab Med, 2011. **135**(10): p. 1269-77.

76. Lu, K.H., et al., *Gynecologic cancer as a "sentinel cancer" for women with hereditary nonpolyposis colorectal cancer syndrome.* 2005(0029-7844 (Print)).

77. Bonadona, V., et al., *Cancer risks associated with germline mutations in MLH1, MSH2, and MSH6 genes in Lynch syndrome.* Jama, 2011. **305**(22): p. 2304-10.

78. Post, C.C.B., et al., *Prevalence and Prognosis of Lynch Syndrome and Sporadic Mismatch Repair Deficiency in Endometrial Cancer.* J Natl Cancer Inst, 2021. **113**(9): p. 1212-1220.

79. Toh, J.W.T., et al., *Survival outcomes associated with Lynch syndrome colorectal cancer and metachronous rate after subtotal/total versus segmental colectomy: Meta-analysis.* Surgery, 2022. **172**(5): p. 1315-1322.

80. Steinbakk, A., et al., *Biomarkers and microsatellite instability analysis of curettings can predict the behavior of FIGO stage I endometrial endometrioid adenocarcinoma.* Mod Pathol, 2011. **24**(9): p. 1262-71.

81. Black, D., et al., *Clinicopathologic significance of defective DNA mismatch repair in endometrial carcinoma.* J Clin Oncol, 2006. **24**(11): p. 1745-53.

82. Resnick, K.E., et al., *Mismatch repair status and outcomes after adjuvant therapy in patients with surgically staged endometrial cancer.* Gynecol Oncol, 2010. **117**(2): p. 234-8.

83. Shikama, A., et al., *Clinicopathologic implications of DNA mismatch repair status in endometrial carcinomas.* Gynecologic Oncology, 2016. **140**(2): p. 226-233.

84. Mackay, H.J., et al., *Prognostic value of microsatellite instability (MSI) and PTEN expression in women with endometrial cancer: results from studies of the NCIC Clinical Trials Group (NCIC CTG).* Eur J Cancer, 2010. **46**(8): p. 1365-73.

85. Kato, M., et al., *DNA mismatch repair-related protein loss as a prognostic factor in endometrial cancers.* J Gynecol Oncol, 2015. **26**(1): p. 40-5.

86. Fountzilas, E., et al., *Prognostic implications of mismatch repair deficiency in patients with nonmetastatic colorectal and endometrial cancer.* ESMO Open, 2019. **4**(2): p. e000474.

87. Nagle, C.M., et al., *Endometrial cancer risk and survival by tumor MMR status.* J Gynecol Oncol, 2018. **29**(3): p. e39.

88. Garg, K., et al., *Endometrial carcinomas in women aged 40 years and younger: tumors associated with loss of DNA mismatch repair proteins comprise a distinct clinicopathologic subset.* Am J Surg Pathol, 2009. **33**(12): p. 1869-77.

89. Carcangiu, M.L., et al., *Lynch Syndrome—Related Endometrial Carcinomas Show a High Frequency of Nonendometrioid Types and of High FIGO Grade Endometrioid Types.* International Journal of Surgical Pathology, 2009. **18**(1): p. 21-26.

90. van den Bos, M., et al., *More differences between HNPCC-related and sporadic carcinomas from the endometrium as compared to the colon.* Am J Surg Pathol, 2004. **28**(6): p. 706-11.

91. Grzankowski, K.S., et al., *Clinical and pathologic features of young endometrial cancer patients with loss of mismatch repair expression.* Gynecol Oncol, 2012. **126**(3): p. 408-12.

92. An, H.J., et al., *Microsatellite instability in endometrioid type endometrial adenocarcinoma is associated with poor prognostic indicators.* Am J Surg Pathol, 2007. **31**(6): p. 846-53.

93. Cosgrove, C.M., et al., *Epigenetic silencing of MLH1 in endometrial cancers is associated with larger tumor volume, increased rate of lymph node positivity and reduced recurrence-free survival.* Gynecologic oncology, 2017. **146**(3): p. 588-595.

94. Loukovaara, M., A. Pasanen, and R. Bützow *Mismatch Repair Deficiency as a Predictive and Prognostic Biomarker in Molecularly Classified Endometrial Carcinoma*. Cancers, 2021. **13**, DOI: 10.3390/cancers13133124.

95. Martin, S.A., C.J. Lord, and A. Ashworth, *DNA repair deficiency as a therapeutic target in cancer.* Current Opinion in Genetics & Development, 2008. **18**(1): p. 80-86.

96. Lombard, D.B., et al., *DNA repair, genome stability, and aging.* Cell, 2005. **120**(4): p. 497-512.

97. Jeggo, P.A., L.H. Pearl, and A.M. Carr, *DNA repair, genome stability and cancer: a historical perspective.* Nat Rev Cancer, 2016. **16**(1): p. 35-42.

98. Bouwman, P. and J. Jonkers, *The effects of deregulated DNA damage signalling on cancer chemotherapy response and resistance.* Nat Rev Cancer, 2012. **12**(9): p. 587-98.

99. Ghosal, G. and J. Chen, *DNA damage tolerance: a double-edged sword guarding the genome.* Transl Cancer Res, 2013. **2**(3): p. 107-129.

100. Wolters, S. and B. Schumacher, *Genome maintenance and transcription integrity in aging and disease.* Front Genet, 2013. **4**: p. 19.

101. Hsieh, P. and Y. Zhang, *The Devil is in the details for DNA mismatch repair.* Proceedings of the National Academy of Sciences of the United States of America, 2017. **114**(14): p. 3552-3554.

102. Hsieh, P. and K. Yamane, *DNA mismatch repair: molecular mechanism, cancer, and ageing.* Mech Ageing Dev, 2008. **129**(7-8): p. 391-407.

103. Chatterjee, N. and G.C. Walker, *Mechanisms of DNA damage, repair, and mutagenesis.* Environ Mol Mutagen, 2017. **58**(5): p. 235-263.

104. Genschel, J., et al., *Isolation of MutSβ from Human Cells and Comparison of the Mismatch Repair Specificities of MutSβ and MutSα.* Journal of Biological Chemistry, 1998. **273**(31): p. 19895-19901.

105. Kolodner, R.D. and G.T. Marsischky, *Eukaryotic DNA mismatch repair.* Current Opinion in Genetics & Development, 1999. **9**(1): p. 89-96.

106. Sinicrope, F.A. and Z.J. Yang, *Prognostic and predictive impact of DNA mismatch repair in the management of colorectal cancer.* Future oncology (London, England), 2011. **7**(3): p. 467-474.

107. Kunkel, T.A. and D.A. Erie, *DNA MISMATCH REPAIR.* Annual Review of Biochemistry, 2005. **74**(1): p. 681-710.

108. Kadyrov, F.A., et al., *Endonucleolytic function of MutLalpha in human mismatch repair.* Cell, 2006. **126**(2): p. 297-308.

109. Paul Solomon Devakumar, L.J., et al., *Effective mismatch repair depends on timely control of PCNA retention on DNA by the Elg1 complex.* Nucleic Acids Res, 2019. **47**(13): p. 6826-6841.

110. Guo, S., et al., *Differential requirement for proliferating cell nuclear antigen in 5' and 3' nick-directed excision in human mismatch repair.* J Biol Chem, 2004. **279**(17): p. 16912-7.

111. Guillotin, D. and S.A. Martin, *Exploiting DNA mismatch repair deficiency as a therapeutic strategy.* Experimental Cell Research, 2014. **329**(1): p. 110-115.

112. Junop, M.S., et al., *In vitro and in vivo studies of MutS, MutL and MutH mutants: correlation of mismatch repair and DNA recombination.* DNA Repair, 2003. **2**(4): p. 387-405.

113. Prolla, T.A., et al., *Tumour susceptibility and spontaneous mutation in mice deficient in Mlh1, Pms1 and Pms2 DNA mismatch repair.* Nat Genet, 1998. **18**(3): p. 276-9.

114. Ollikainen, M., et al., *Mechanisms of inactivation of MLH1 in hereditary nonpolyposis colorectal carcinoma: a novel approach.* Oncogene, 2007. **26**(31): p. 4541-4549.

115. Wu, H., et al., *Structure of the human MLH1 N-terminus: implications for predisposition to Lynch syndrome.* Acta crystallographica. Section F, Structural biology communications, 2015. **71**(Pt 8): p. 981-985.

116. Li, Z., A.H. Pearlman, and P. Hsieh, *DNA mismatch repair and the DNA damage response.* DNA repair, 2016. **38**: p. 94-101.

117. Ellison, A.R., J. Lofing, and G.A. Bitter, *Human MutL homolog (MLH1) function in DNA mismatch repair: a prospective screen for missense mutations in the ATPase domain.* Nucleic Acids Res, 2004. **32**(18): p. 5321-38.

118. Hall, M.C., P.V. Shcherbakova, and T.A. Kunkel, *Differential ATP binding and intrinsic ATP hydrolysis by amino-terminal domains of the yeast Mlh1 and Pms1 proteins.* J Biol Chem, 2002. **277**(5): p. 3673-9.

119. Tomer, G., et al., *Contribution of human mlh1 and pms2 ATPase activities to DNA mismatch repair.* J Biol Chem, 2002. **277**(24): p. 21801-9.

120. Räschle, M., et al., *Mutations within the hMLH1 and hPMS2 subunits of the human MutLalpha mismatch repair factor affect its ATPase activity, but not its ability to interact with hMutSalpha.* J Biol Chem, 2002. **277**(24): p. 21810-20.

121. Plotz, G., et al., *Mutations in the MutSalpha interaction interface of MLH1 can abolish DNA mismatch repair.* Nucleic Acids Res, 2006. **34**(22): p. 6574-86.

122. Ban, C., M. Junop, and W. Yang, *Transformation of MutL by ATP binding and hydrolysis: a switch in DNA mismatch repair.* Cell, 1999. **97**(1): p. 85-97.

123. Kadyrova, L.Y., et al., *Human MutLγ, the MLH1-MLH3 heterodimer, is an endonuclease that promotes DNA expansion.* Proceedings of the National Academy of Sciences of the United States of America, 2020. **117**(7): p. 3535-3542.

124. Wang, T.F., N. Kleckner, and N. Hunter, *Functional specificity of MutL homologs in yeast: evidence for three Mlh1-based heterocomplexes with distinct roles during meiosis in recombination and mismatch correction.* Proc Natl Acad Sci U S A, 1999. **96**(24): p. 13914-9.

125. Lipkin, S.M., et al., *Meiotic arrest and aneuploidy in MLH3-deficient mice.* Nat Genet, 2002. **31**(4): p. 385-90.

126. Pang, Q., T.A. Prolla, and R.M. Liskay, *Functional domains of the Saccharomyces cerevisiae Mlh1p and Pms1p DNA mismatch repair proteins and their relevance to human hereditary nonpolyposis colorectal cancer-associated mutations.* Molecular and cellular biology, 1997. **17**(8): p. 4465-4473.

127. Li, G.M., *The role of mismatch repair in DNA damage-induced apoptosis.* Oncol Res, 1999. **11**(9): p. 393-400.

128. Stojic, L., R. Brun, and J. Jiricny, *Mismatch repair and DNA damage signalling.* DNA Repair, 2004. **3**(8): p. 1091-1101.

129. Chambers, S.R., et al., *The mismatch repair system reduces meiotic homeologous recombination and stimulates recombination-dependent chromosome loss.* Mol Cell Biol, 1996. **16**(11): p. 6110-20.

130. de Wind, N., et al., *Inactivation of the mouse Msh2 gene results in mismatch repair deficiency, methylation tolerance, hyperrecombination, and predisposition to cancer.* Cell, 1995. **82**(2): p. 321-30.

131. Selva, E.M., et al., *Mismatch correction acts as a barrier to homeologous recombination in Saccharomyces cerevisiae.* Genetics, 1995. **139**(3): p. 1175-88.

132. Kunz, C. and P. Schär, *Meiotic recombination: sealing the partnership at the junction.* Curr Biol, 2004. **14**(22): p. R962-4.

133. Snowden, T., et al., *hMSH4-hMSH5 adenosine nucleotide processing and interactions with homologous recombination machinery.* J Biol Chem, 2008. **283**(1): p. 145-154.

134. Allers, T. and M. Lichten, *Intermediates of yeast meiotic recombination contain heteroduplex DNA.* Mol Cell, 2001. **8**(1): p. 225-31.

135. Radman, M., *Mismatch repair and the fidelity of genetic recombination.* Genome, 1989. **31**(1): p. 68-73.

136. Kadyrova, L.Y., E.R. Blanko, and F.A. Kadyrov, *CAF-I-dependent control of degradation of the discontinuous strands during mismatch repair.* Proc Natl Acad Sci U S A, 2011. **108**(7): p. 2753-8.

137. Schöpf, B., et al., *Interplay between mismatch repair and chromatin assembly.* Proc Natl Acad Sci U S A, 2012. **109**(6): p. 1895-900.

138. Fedier, A. and D. Fink, *Mutations in DNA mismatch repair genes: implications for DNA damage signaling and drug sensitivity (review).* Int J Oncol, 2004. **24**(4): p. 1039-47.

139. Karran, P., J. Offman, and M. Bignami, *Human mismatch repair, drug-induced DNA damage, and secondary cancer.* Biochimie, 2003. **85**(11): p. 1149-60.

140. Bignami, M., I. Casorelli, and P. Karran, *Mismatch repair and response to DNA-damaging antitumour therapies.* Eur J Cancer, 2003. **39**(15): p. 2142-9.

141. Brierley, D.J. and S.A. Martin, *Oxidative stress and the DNA mismatch repair pathway.* Antioxid Redox Signal, 2013. **18**(18): p. 2420-8.

142. Russo, M.T., et al., *Different DNA repair strategies to combat the threat from 8-oxoguanine.* Mutat Res, 2007. **614**(1-2): p. 69-76.

143. Dizdaroglu, M., *Oxidatively induced DNA damage: Mechanisms, repair and disease.* Cancer Letters, 2012. **327**(1): p. 26-47.

144. Bridge, G., S. Rashid, and S.A. Martin, *DNA mismatch repair and oxidative DNA damage: implications for cancer biology and treatment.* Cancers, 2014. **6**(3): p. 1597-1614.

145. Macpherson, P., et al., *8-oxoguanine incorporation into DNA repeats in vitro and mismatch recognition by MutSalpha.* Nucleic Acids Res, 2005. **33**(16): p. 5094-105.

146. Martin, S.A., et al., *DNA Polymerases as Potential Therapeutic Targets for Cancers Deficient in the DNA Mismatch Repair Proteins MSH2 or MLH1.* Cancer Cell, 2010. **17**(3): p. 235-248.

147. Martin, S.A., et al., *Methotrexate induces oxidative DNA damage and is selectively lethal to tumour cells with defects in the DNA mismatch repair gene MSH2.* EMBO Molecular Medicine, 2009. **1**(6-7): p. 323-337.

148. Hewish, M., et al., *Cytosine-based nucleoside analogs are selectively lethal to DNA mismatch repair-deficient tumour cells by enhancing levels of intracellular oxidative stress.* British journal of cancer, 2013. **108**(4): p. 983-992.

149. Guillotin, D., et al., *Drug-Repositioning Screens Identify Triamterene as a Selective Drug for the Treatment of DNA Mismatch Repair Deficient Cells.* Clinical Cancer Research, 2017. **23**(11): p. 2880.

150. Martin, S.A., et al., *Parallel High-Throughput RNA Interference Screens Identify PINK1 as a Potential Therapeutic Target for the Treatment of DNA Mismatch Repair–Deficient Cancers.* Cancer Research, 2011. **71**(5): p. 1836.

151. Mishra, M. and R.A. Kowluru, *Retinal mitochondrial DNA mismatch repair in the development of diabetic retinopathy, and its continued progression after termination of hyperglycemia.* Invest Ophthalmol Vis Sci, 2014. **55**(10): p. 6960-7.

152. Mootha, V.K., et al., *Integrated analysis of protein composition, tissue diversity, and gene regulation in mouse mitochondria.* Cell, 2003. **115**(5): p. 629-40.

153. Colussi, C., et al., *The mammalian mismatch repair pathway removes DNA 8-oxodGMP incorporated from the oxidized dNTP pool.* Current biology, 2002. **12**(11): p. 912-918.

154. Piao, J., et al., *Mismatch repair deficient mice show susceptibility to oxidative stress-induced intestinal carcinogenesis.* International journal of biological sciences, 2013. **10**(1): p. 73-79.

155. Hardman, R.A., C.A. Afshari, and J.C. Barrett, *Involvement of mammalian MLH1 in the apoptotic response to peroxide-induced oxidative stress.* Cancer Res, 2001. **61**(4): p. 1392-7.

156. Glaab, W.E., R.B. Hill, and T.R. Skopek, *Suppression of spontaneous and hydrogen peroxide-induced mutagenesis by the antioxidant ascorbate in mismatch repair-deficient human colon cancer cells.* Carcinogenesis, 2001. **22**(10): p. 1709-13.

157. DeWeese, T.L., et al., *Mouse embryonic stem cells carrying one or two defective Msh2 alleles respond abnormally to oxidative stress inflicted by low-level radiation.* Proceedings of the National Academy of Sciences of the United States of America, 1998. **95**(20): p. 11915-11920.

158. Holt, S.M., et al., *Compromised repair of clustered DNA damage in the human acute lymphoblastic leukemia MSH2-deficient NALM-6 cells.* Mutat Res, 2009. **674**(1-2): p. 123-30.

159. Zlatanou, A., et al., *The hMsh2-hMsh6 complex acts in concert with monoubiquitinated PCNA and Pol η in response to oxidative DNA damage in human cells.* Mol Cell, 2011. **43**(4): p. 649-62.

160. Barone, F., et al., *Replication of 2-hydroxyadenine-containing DNA and recognition by human MutSalpha.* DNA Repair (Amst), 2007. **6**(3): p. 355-66.

161. Russo, M.T., et al., *Role of MUTYH and MSH2 in the control of oxidative DNA damage, genetic instability, and tumorigenesis.* Cancer Res, 2009. **69**(10): p. 4372-9.

162. Kaneko, E., et al., *MLH1 promoter hypermethylation predicts poorer prognosis in mismatch repair deficiency endometrial carcinomas.* Journal of gynecologic oncology, 2021. **32**(6): p. e79-e79.

163. Pasanen, A., M. Loukovaara, and R. Bützow, *Clinicopathological significance of deficient DNA mismatch repair and MLH1 promoter methylation in endometrioid endometrial carcinoma.* Mod Pathol, 2020. **33**(7): p. 1443-1452.

164. McMeekin, D.S., et al., *Clinicopathologic Significance of Mismatch Repair Defects in Endometrial Cancer: An NRG Oncology/Gynecologic Oncology Group Study.* Journal of clinical oncology : official journal of the American Society of Clinical Oncology, 2016. **34**(25): p. 3062-3068.

165. Guo, Z., et al., *ATM activation by oxidative stress.* Science, 2010. **330**(6003): p. 517-21.

166. Mason, P.A., et al., *Mismatch repair activity in mammalian mitochondria.* Nucleic acids research, 2003. **31**(3): p. 1052-1058.

167. Giles, R.E., et al., *Maternal inheritance of human mitochondrial DNA.* Proceedings of the National Academy of Sciences of the United States of America, 1980. **77**(11): p. 6715-6719.

168. Lightowlers, R.N., et al., *Mammalian mitochondrial genetics: heredity, heteroplasmy and disease.* Trends in Genetics, 1997. **13**(11): p. 450-455.

169. Schon, E.A., S. DiMauro, and M. Hirano, *Human mitochondrial DNA: roles of inherited and somatic mutations.* Nature reviews. Genetics, 2012. **13**(12): p. 878-890.

170. Van Houten, B., S.E. Hunter, and J.N. Meyer, *Mitochondrial DNA damage induced autophagy, cell death, and disease.* Frontiers in bioscience (Landmark edition), 2016. **21**: p. 42-54.

171. Herst, P.M., et al., *Functional Mitochondria in Health and Disease.* Frontiers in endocrinology, 2017. **8**: p. 296-296.

172. Smeitink, J., L. van den Heuvel, and S. DiMauro, *The genetics and pathology of oxidative phosphorylation.* Nat Rev Genet, 2001. **2**(5): p. 342-52.

173. Bender, D.A., *OXIDATIVE PHOSPHORYLATION*, in *Encyclopedia of Food Sciences and Nutrition (Second Edition)*, B. Caballero, Editor. 2003, Academic Press: Oxford. p. 4295-4301.

174. Sazanov, L.A., *A giant molecular proton pump: structure and mechanism of respiratory complex I.* Nature Reviews Molecular Cell Biology, 2015. **16**(6): p. 375-388.

175. Rashid, S., et al., *MLH1 deficiency leads to deregulated mitochondrial metabolism.* Cell death & disease, 2019. **10**(11): p. 795-795.

176. Sharma, L.K., J. Lu, and Y. Bai, *Mitochondrial respiratory complex I: structure, function and implication in human diseases.* Current medicinal chemistry, 2009. **16**(10): p. 1266-1277.

177. Stroud, D.A., et al., *Accessory subunits are integral for assembly and function of human mitochondrial complex I.* Nature, 2016. **538**(7623): p. 123-126.

178. Tuppen, H.A.L., et al., *The p.M292T NDUFS2 mutation causes complex I-deficient Leigh syndrome in multiple families.* Brain : a journal of neurology, 2010. **133**(10): p. 2952-2963.

179. Hofhaus, G., H. Weiss, and K. Leonard, *Electron microscopic analysis of the peripheral and membrane parts of mitochondrial NADH dehydrogenase (Complex I).* Journal of Molecular Biology, 1991. **221**(3): p. 1027-1043.

180. Hunte, C., V. Zickermann, and U. Brandt, *Functional Modules and Structural Basis of Conformational Coupling in Mitochondrial Complex I.* Science, 2010. **329**(5990): p. 448.

181. Wirth, C., et al., *Structure and function of mitochondrial complex I.* Biochimica et Biophysica Acta (BBA) - Bioenergetics, 2016. **1857**(7): p. 902-914.

182. Ju, Y.S., et al., *Origins and functional consequences of somatic mitochondrial DNA mutations in human cancer.* eLife, 2014. **3**: p. e02935.

183. Bénit, P., et al., *Large-Scale Deletion and Point Mutations of the Nuclear NDUFV1 and NDUFS1 Genes in Mitochondrial Complex I Deficiency.* The American Journal of Human Genetics, 2001. **68**(6): p. 1344-1352.

184. Piekutowska-Abramczuk, D., et al., *NDUFB8 Mutations Cause Mitochondrial Complex I Deficiency in Individuals with Leigh-like Encephalomyopathy.* The American Journal of Human Genetics, 2018. **102**(3): p. 460-467.

185. Friederich, M.W., et al., *Mutations in the accessory subunit NDUFB10 result in isolated complex I deficiency and illustrate the critical role of intermembrane space import for complex I holoenzyme assembly.* Hum Mol Genet, 2017. **26**(4): p. 702-716.

186. Perrier, S., et al., *Recessive mutations in NDUFA2 cause mitochondrial leukoencephalopathy.* Clin Genet, 2018. **93**(2): p. 396-400.

187. Hoefs, S.J., et al., *NDUFA10 mutations cause complex I deficiency in a patient with Leigh disease.* Eur J Hum Genet, 2011. **19**(3): p. 270-4.

188. Iommarini, L., et al., *Different mtDNA mutations modify tumor progression in dependence of the degree of respiratory complex I impairment.* Human molecular genetics, 2014. **23**(6): p. 1453-1466.

189. Calabrese, C., et al., *Respiratory complex I is essential to induce a Warburg profile in mitochondria-defective tumor cells.* Cancer Metab, 2013. **1**(1): p. 11.

190. Li, L.D., et al., *Down-Regulation of NDUFB9 Promotes Breast Cancer Cell Proliferation, Metastasis by Mediating Mitochondrial Metabolism.* PLoS One, 2015. **10**(12): p. e0144441.

191. Urra, F.A., et al., *The Mitochondrial Complex(I)ty of Cancer.* Frontiers in oncology, 2017. **7**: p. 118-118.

192. Philley, J.V., et al., *Complex-I alteration and enhanced mitochondrial fusion are associated with prostate cancer progression.* Journal of cellular physiology, 2016. **231**(6): p. 1364-1374.

193. Gasparre, G., et al., *Disruptive mitochondrial DNA mutations in complex I subunits are markers of oncocytic phenotype in thyroid tumors.* Proceedings of the National Academy of Sciences, 2007. **104**(21): p. 9001-9006.

194. Evangelisti, C., et al., *A mutation screening of oncogenes, tumor suppressor gene TP53 and nuclear encoded mitochondrial complex I genes in oncocytic thyroid tumors.* BMC cancer, 2015. **15**(1): p. 1-7.

195. Yu, Y., et al., *Mitochondrial ND3 G10398A mutation: a biomarker for breast cancer.* Genet Mol Res, 2015. **14**(4): p. 17426-31.

196. Su, C.-Y., et al., *The opposite prognostic effect of NDUFS1 and NDUFS8 in lung cancer reflects the oncojanus role of mitochondrial complex I.* Scientific reports, 2016. **6**(1): p. 31357.

197. Kim, H., et al., *Mutations in the mitochondrial ND1 gene are associated with postoperative prognosis of localized renal cell carcinoma.* International journal of molecular sciences, 2016. **17**(12): p. 2049.

198. Horton, T.M., et al., *Novel mitochondrial DNA deletion found in a renal cell carcinoma.* Genes, Chromosomes and Cancer, 1996. **15**(2): p. 95-101.

199. Akouchekian, M., et al., *Analysis of mitochondrial ND1 gene in human colorectal cancer.* Journal of research in medical sciences, 2011. **16**(1): p. 50.

200. Allegra, E., et al., *Mutations and polymorphisms in mitochondrial DNA in head and neck cancer cell lines.* Acta otorhinolaryngologica italica, 2006. **26**(4): p. 185.

201. Birsoy, K., et al., *An Essential Role of the Mitochondrial Electron Transport Chain in Cell Proliferation Is to Enable Aspartate Synthesis.* Cell, 2015. **162**(3): p. 540-551.

202. Sullivan, Lucas B., et al., *Supporting Aspartate Biosynthesis Is an Essential Function of Respiration in Proliferating Cells.* Cell, 2015. **162**(3): p. 552-563.

203. Wu, M., et al., *Multiparameter metabolic analysis reveals a close link between attenuated mitochondrial bioenergetic function and enhanced glycolysis dependency in human tumor cells.* Am J Physiol Cell Physiol, 2007. **292**(1): p. C125-36.

204. Mullen, A.R., et al., *Reductive carboxylation supports growth in tumour cells with defective mitochondria.* Nature, 2011. **481**(7381): p. 385-388.

205. Garcia-Heredia, J.M. and A. Carnero, *Decoding Warburg's hypothesis: tumor-related mutations in the mitochondrial respiratory chain.* Oncotarget, 2015. **6**(39): p. 41582-99.

206. Cruz-Bermúdez, A., et al., *Enhanced tumorigenicity by mitochondrial DNA mild mutations.* Oncotarget, 2015. **6**(15): p. 13628-43.

207. Ishikawa, K., et al., *ROS-generating mitochondrial DNA mutations can regulate tumor cell metastasis.* Science, 2008. **320**(5876): p. 661-4.

208. Yuan, Y., et al., *Nonsense and missense mutation of mitochondrial ND6 gene promotes cell migration and invasion in human lung adenocarcinoma.* (1471-2407 (Electronic)).

209. Gonzalez, D.M. and D. Medici, *Signaling mechanisms of the epithelial-mesenchymal transition.* Sci Signal, 2014. **7**(344): p. re8.

210. Li, L. and W. Li, *Epithelial-mesenchymal transition in human cancer: comprehensive reprogramming of metabolism, epigenetics, and differentiation.* Pharmacol Ther, 2015. **150**: p. 33-46.

211. He, X., et al., *Suppression of Mitochondrial Complex I Influences Cell Metastatic Properties.* PLOS ONE, 2013. **8**(4): p. e61677.

212. Putignani, L., et al., *Preliminary evidences on mitochondrial injury and impaired oxidative metabolism in breast cancer.* Mitochondrion, 2012. **12**(3): p. 363-9.

213. Yadav, N. and D. Chandra, *Mitochondrial DNA mutations and breast tumorigenesis.* Biochimica et biophysica acta, 2013. **1836**(2): p. 336-344.

214. Jeon, J.H., et al., *Migration and invasion of drug-resistant lung adenocarcinoma cells are dependent on mitochondrial activity.* Experimental & molecular medicine, 2016. **48**(12): p. e277-e277.

215. Thompson, C.B., et al., *How do cancer cells acquire the fuel needed to support cell growth?* Cold Spring Harb Symp Quant Biol, 2005. **70**: p. 357-62.

216. Vander Heiden, M.G., L.C. Cantley, and C.B. Thompson, *Understanding the Warburg effect: the metabolic requirements of cell proliferation.* Science (New York, N.Y.), 2009. **324**(5930): p. 1029-1033.

217. WARBURG, O., *On the origin of cancer cells.* Science, 1956. **123**(3191): p. 309-14.

218. DeBerardinis, R.J. and N.S. Chandel, *Fundamentals of cancer metabolism.* Sci Adv, 2016. **2**(5): p. e1600200.

219. Granchi, C., et al., *Inhibitors of lactate dehydrogenase isoforms and their therapeutic potentials.* Curr Med Chem, 2010. **17**(7): p. 672-97.

220. Zheng, J., *Energy metabolism of cancer: Glycolysis versus oxidative phosphorylation (Review).* Oncology letters, 2012. **4**(6): p. 1151-1157.

221. Zwerschke, W., et al., *Metabolic analysis of senescent human fibroblasts reveals a role for AMP in cellular senescence.* Biochem J, 2003. **376**(Pt 2): p. 403-11.

222. Moreno-Sánchez, R., et al., *Energy metabolism in tumor cells.* Febs j, 2007. **274**(6): p. 1393-418.

223. Locasale, J.W., *Serine, glycine and one-carbon units: cancer metabolism in full circle.* Nature Reviews Cancer, 2013. **13**(8): p. 572-583.

224. Altenberg, B. and K.O. Greulich, *Genes of glycolysis are ubiquitously overexpressed in 24 cancer classes.* Genomics, 2004. **84**(6): p. 1014-20.

225. Martins, S.F., et al., *Significance of glycolytic metabolism-related protein expression in colorectal cancer, lymph node and hepatic metastasis.* BMC cancer, 2016. **16**: p. 535-535.

226. Yamamoto, T., et al., *Over-expression of facilitative glucose transporter genes in human cancer.* Biochemical and Biophysical Research Communications, 1990. **170**(1): p. 223-230.

227. Peng, S.Y., et al., *Aberrant expression of the glycolytic enzymes aldolase B and type II hexokinase in hepatocellular carcinoma are predictive markers for advanced stage, early recurrence and poor prognosis.* Oncol Rep, 2008. **19**(4): p. 1045-53.

228. Wolf, A., et al., *Hexokinase 2 is a key mediator of aerobic glycolysis and promotes tumor growth in human glioblastoma multiforme.* J Exp Med, 2011. **208**(2): p. 313-26.

229. Kessler, R., et al., *6-Phosphofructo-2-kinase/fructose-2,6-bisphosphatase (PFKFB3) is up-regulated in high-grade astrocytomas.* J Neurooncol, 2008. **86**(3): p. 257-64.

230. Augoff, K. and K. Grabowski, *[Significance of lactate dehydrogenase measurements in diagnosis of malignancies].* Pol Merkur Lekarski, 2004. **17**(102): p. 644-7.

231. Fantin, V.R., J. St-Pierre, and P. Leder, *Attenuation of LDH-A expression uncovers a link between glycolysis, mitochondrial physiology, and tumor maintenance.* Cancer Cell, 2006. **9**(6): p. 425-434.

232. Koukourakis, M.I., et al., *Serum and tissue LDH levels in patients with breast/gynaecological cancer and benign diseases.* Gynecol Obstet Invest, 2009. **67**(3): p. 162-8.

233. von Eyben, F.E., *A systematic review of lactate dehydrogenase isoenzyme 1 and germ cell tumors.* Clin Biochem, 2001. **34**(6): p. 441-54.

234. Porporato, P.E., et al., *Anticancer targets in the glycolytic metabolism of tumors: a comprehensive review.* Frontiers in pharmacology, 2011. **2**: p. 49-49.

235. Sola-Penna, M., *Metabolic regulation by lactate.* IUBMB Life, 2008. **60**(9): p. 605-608.

236. Kolev, Y., et al., *Lactate dehydrogenase-5 (LDH-5) expression in human gastric cancer: association with hypoxia-inducible factor (HIF-1alpha) pathway, angiogenic factors production and poor prognosis.* Ann Surg Oncol, 2008. **15**(8): p. 2336-44.

237. Miao, P., et al., *Lactate dehydrogenase a in cancer: A promising target for diagnosis and therapy.* IUBMB Life, 2013. **65**(11): p. 904-910.

238. Cairns, R.A., I.S. Harris, and T.W. Mak, *Regulation of cancer cell metabolism.* Nat Rev Cancer, 2011. **11**(2): p. 85-95.

239. Luo, W., et al., *Pyruvate Kinase M2 Is a PHD3-Stimulated Coactivator for Hypoxia-Inducible Factor 1.* Cell, 2011. **145**(5): p. 732-744.

240. Luo, W. and G.L. Semenza, *Pyruvate kinase M2 regulates glucose metabolism by functioning as a coactivator for hypoxia-inducible factor 1 in cancer cells.* Oncotarget, 2011. **2**(7): p. 551-556.

241. Yang, W., et al., *ERK1/2-dependent phosphorylation and nuclear translocation of PKM2 promotes the Warburg effect.* Nature Cell Biology, 2012. **14**(12): p. 1295-1304.

242. Yang, L., S. Venneti, and D. Nagrath, *Glutaminolysis: A Hallmark of Cancer Metabolism.* Annual Review of Biomedical Engineering, 2017. **19**(1): p. 163-194.

243. Yoo, H.C., et al., *A Variant of SLC1A5 Is a Mitochondrial Glutamine Transporter for Metabolic Reprogramming in Cancer Cells.* Cell Metab, 2020. **31**(2): p. 267-283.e12.

244. Stine, Z.E. and C.V. Dang, *Glutamine Skipping the Q into Mitochondria.* Trends Mol Med, 2020. **26**(1): p. 6-7.

245. Cruzat, V., et al., *Glutamine: Metabolism and Immune Function, Supplementation and Clinical Translation.* Nutrients, 2018. **10**(11).

246. DeBerardinis Ralph, J., et al., *Beyond aerobic glycolysis: Transformed cells can engage in glutamine metabolism that exceeds the requirement for protein and nucleotide synthesis.* Proceedings of the National Academy of Sciences, 2007. **104**(49): p. 19345-19350.

247. Mullen, A.R., et al., *Reductive carboxylation supports growth in tumour cells with defective mitochondria.* Nature, 2012. **481**(7381): p. 385-388.

248. Eales, K.L., K.E.R. Hollinshead, and D.A. Tennant, *Hypoxia and metabolic adaptation of cancer cells.* Oncogenesis, 2016. **5**(1): p. e190-e190.

249. Chen, Q., et al., *Rewiring of Glutamine Metabolism Is a Bioenergetic Adaptation of Human Cells with Mitochondrial DNA Mutations.* Cell metabolism, 2018. **27**(5): p. 1007-1025.e5.

250. Lombardi, A.A., et al., *Mitochondrial calcium exchange links metabolism with the epigenome to control cellular differentiation.* Nature Communications, 2019. **10**(1): p. 4509.

251. Jain, M., et al., *Metabolite profiling identifies a key role for glycine in rapid cancer cell proliferation.* Science (New York, N.Y.), 2012. **336**(6084): p. 1040-1044.

252. Wu, Q., et al., *Serine and Metabolism Regulation: A Novel Mechanism in Antitumor Immunity and Senescence.* Aging and disease, 2020. **11**(6): p. 1640-1653.

253. Shimizu, K., et al., *ASC amino-acid transporter 2 (ASCT2) as a novel prognostic marker in non-small cell lung cancer.* Br J Cancer, 2014. **110**(8): p. 2030-9.

254. van Geldermalsen, M., et al., *ASCT2/SLC1A5 controls glutamine uptake and tumour growth in triple-negative basal-like breast cancer.* Oncogene, 2016. **35**(24): p. 3201-3208.

255. Snell, K., *Enzymes of serine metabolism in normal, developing and neoplastic rat tissues.* Adv Enzyme Regul, 1984. **22**: p. 325-400.

256. Amelio, I., et al., *Serine and glycine metabolism in cancer.* Trends in biochemical sciences, 2014. **39**(4): p. 191-198.

257. Newman, A.C. and O.D.K. Maddocks, *One-carbon metabolism in cancer.* British journal of cancer, 2017. **116**(12): p. 1499-1504.

258. Kiweler, N., et al., *Mitochondria preserve an autarkic one-carbon cycle to confer growth-independent cancer cell migration and metastasis.* Nature Communications, 2022. **13**(1): p. 2699.

259. Davis, J.L., H.J. Fallon, and H.P. Morris, *Two enzymes of serine metabolism in rat liver and hepatomas.* Cancer Res, 1970. **30**(12): p. 2917-20.

260. Locasale, J.W., et al., *Phosphoglycerate dehydrogenase diverts glycolytic flux and contributes to oncogenesis.* Nature genetics, 2011. **43**(9): p. 869-874.

261. Possemato, R., et al., *Functional genomics reveal that the serine synthesis pathway is essential in breast cancer.* Nature, 2011. **476**(7360): p. 346-350.

262. Pollari, S., et al., *Enhanced serine production by bone metastatic breast cancer cells stimulates osteoclastogenesis.* Breast Cancer Res Treat, 2011. **125**(2): p. 421-30.

263. Maddocks, O.D., et al., *Serine starvation induces stress and p53-dependent metabolic remodelling in cancer cells.* Nature, 2013. **493**(7433): p. 542-6.

264. Unterlass, J.E., et al., *Validating and enabling phosphoglycerate dehydrogenase (PHGDH) as a target for fragment-based drug discovery in PHGDH-amplified breast cancer.* Oncotarget, 2018. **9**(17): p. 13139-13153.

265. Jia, X.-Q., et al., *Increased Expression of PHGDH and Prognostic Significance in Colorectal Cancer.* Translational oncology, 2016. **9**(3): p. 191-196.

266. Muhammad, N., H.M. Lee, and J. Kim, *Oncology Therapeutics Targeting the Metabolism of Amino Acids.* Cells, 2020. **9**(8): p. 1904.

267. Mullarky, E., et al., *Identification of a small molecule inhibitor of 3-phosphoglycerate dehydrogenase to target serine biosynthesis in cancers.* Proceedings of the National Academy of Sciences of the United States of America, 2016. **113**(7): p. 1778-1783.

268. Pacold, M.E., et al., *A PHGDH inhibitor reveals coordination of serine synthesis and one-carbon unit fate.* Nature chemical biology, 2016. **12**(6): p. 452-458.

269. Wang, Q., et al., *Rational Design of Selective Allosteric Inhibitors of PHGDH and Serine Synthesis with Anti-tumor Activity.* Cell chemical biology, 2017. **24**(1): p. 55-65.

270. Davidson, S.M., et al., *Environment Impacts the Metabolic Dependencies of Ras-Driven Non-Small Cell Lung Cancer.* Cell metabolism, 2016. **23**(3): p. 517-528.

271. Guo, J., et al., *Azacoccone E inhibits cancer cell growth by targeting 3-phosphoglycerate dehydrogenase.* Bioorg Chem, 2019. **87**: p. 16-22.

272. Zheng, M., et al., *Ixocarpalactone A from dietary tomatillo inhibits pancreatic cancer growth by targeting PHGDH.* Food Funct, 2019. **10**(6): p. 3386-3395.

273. Mullarky, E., et al., *Inhibition of 3-phosphoglycerate dehydrogenase (PHGDH) by indole amides abrogates de novo serine synthesis in cancer cells.* Bioorganic & Medicinal Chemistry Letters, 2019. **29**(17): p. 2503-2510.

274. Anders, S., P.T. Pyl, and W. Huber, *HTSeq--a Python framework to work with high-throughput sequencing data.* (1367-4811 (Electronic)).

275. Hackenberg, R., et al., *Expression of placental protein 14 by the new endometrial cancer cell line MFE-280 in vitro and by endometrial carcinomas in vivo.* Anticancer Res, 1998. **18**(2a): p. 1153-8.

276. Van Nyen, T., et al., *Modeling Endometrial Cancer: Past, Present, and Future.* International journal of molecular sciences, 2018. **19**(8): p. 2348.

277. Nishida, M., *The Ishikawa cells from birth to the present.* Hum Cell, 2002. **15**(3): p. 104-17.

278. Devor, E.J., et al., *Genomic characterization of five commonly used endometrial cancer cell lines.* Int J Oncol, 2020. **57**(6): p. 1348-1357.

279. Valeri, N., et al., *Modulation of mismatch repair and genomic stability by miR-155.* Proc Natl Acad Sci U S A, 2010. **107**(15): p. 6982-7.

280. Gu, L., C.M. Ensor, and G.M. Li, *In vitro DNA mismatch repair in human cells.* Methods Mol Biol, 2012. **920**: p. 135-47.

281. Lanigan, T.M., et al., *Real time visualization of cancer cell death, survival and proliferation using fluorochrome-transfected cells in an IncuCyte(®) imaging system.* Journal of biological methods, 2020. **7**(2): p. e133-e133.

282. Liang, C.-C., A.Y. Park, and J.-L. Guan, *In vitro scratch assay: a convenient and inexpensive method for analysis of cell migration in vitro.* Nature Protocols, 2007. **2**(2): p. 329-333.

283. Warburg, O., F. Wind, and E. Negelein, *THE METABOLISM OF TUMORS IN THE BODY.* The Journal of general physiology, 1927. **8**(6): p. 519-530.

284. Lenaz, G., et al., *Mitochondrial Complex I: Structural and functional aspects.* Biochimica et Biophysica Acta (BBA) - Bioenergetics, 2006. **1757**(9): p. 1406-1420.

285. Kadenbach, B., *Complex IV – The regulatory center of mitochondrial oxidative phosphorylation.* Mitochondrion, 2021. **58**: p. 296-302.

286. Chaban, Y., E.J. Boekema, and N.V. Dudkina, *Structures of mitochondrial oxidative phosphorylation supercomplexes and mechanisms for their stabilisation.* Biochimica et Biophysica Acta (BBA) - Bioenergetics, 2014. **1837**(4): p. 418-426.

287. Greenbaum, D., et al., *Comparing protein abundance and mRNA expression levels on a genomic scale.* Genome Biology, 2003. **4**(9): p. 117.

288. Pratt, J.M., et al., *Dynamics of Protein Turnover, a Missing Dimension in Proteomics *.* Molecular & Cellular Proteomics, 2002. **1**(8): p. 579-591.

289. Wise, D.R. and C.B. Thompson, *Glutamine addiction: a new therapeutic target in cancer.* Trends in biochemical sciences, 2010. **35**(8): p. 427-433.

290. Du, K., et al., *Hedgehog-YAP Signaling Pathway Regulates Glutaminolysis to Control Activation of Hepatic Stellate Cells.* Gastroenterology, 2018. **154**(5): p. 1465-1479.e13.

291. Shiratori, R., et al., *Glycolytic suppression dramatically changes the intracellular metabolic profile of multiple cancer cell lines in a mitochondrial metabolism-dependent manner.* Scientific Reports, 2019. **9**(1): p. 18699.

292. Liberzon, A., et al., *Molecular signatures database (MSigDB) 3.0.* Bioinformatics, 2011. **27**(12): p. 1739-1740.

293. Subramanian, A., et al., *Gene set enrichment analysis: A knowledge-based approach for interpreting genome-wide expression profiles.* Proceedings of the National Academy of Sciences, 2005. **102**(43): p. 15545-15550.

294. Wei, W., et al., *A Role for Small RNAs in DNA Double-Strand Break Repair.* Cell, 2012. **149**(1): p. 101-112.

295. Wan, G., et al., *miRNA response to DNA damage.* Trends in biochemical sciences, 2011. **36**(9): p. 478-484.

296. Owusu Obeng, E., et al., *Phosphoinositide-Dependent Signaling in Cancer: A Focus on Phospholipase C Isozymes.* International journal of molecular sciences, 2020. **21**(7): p. 2581.

297. Fan, J., et al., *Phospholipase C-ε regulates bladder cancer cells via ATM/EXO1.* American journal of cancer research, 2020. **10**(8): p. 2319-2336.

298. Stålberg, P., et al., *Differentially Expressed cDNAs in PLCβ3-Induced Tumor Suppression in a Human Endocrine Pancreatic Tumor Cell Line: Activation of the Human Mismatch Repair Protein 3 Gene.* Biochemical and Biophysical Research Communications, 2001. **281**(1): p. 227-231.

299. Ghosh, S., et al., *PD-L1 recruits phospholipase C and enhances tumorigenicity of lung tumors harboring mutant forms of EGFR.* Cell Reports, 2021. **35**(8): p. 109181.

300. Howitt, B.E., et al., *Association of Polymerase e-Mutated and Microsatellite-Instable Endometrial Cancers With Neoantigen Load, Number of Tumor-Infiltrating Lymphocytes, and Expression of PD-1 and PD-L1.* JAMA Oncol, 2015. **1**(9): p. 1319-23.

301. Sloan, E.A., et al., *PD-L1 Expression in Mismatch Repair-deficient Endometrial Carcinomas, Including Lynch Syndrome-associated and MLH1 Promoter Hypermethylated Tumors.* The American Journal of Surgical Pathology, 2017. **41**(3).

302. de la Cruz-López, K.G., et al., *Lactate in the Regulation of Tumor Microenvironment and Therapeutic Approaches.* Frontiers in oncology, 2019. **9**: p. 1143-1143.

303. Nallanthighal, S., J.P. Heiserman, and D.-J. Cheon, *The Role of the Extracellular Matrix in Cancer Stemness.* Frontiers in Cell and Developmental Biology, 2019. **7**.

304. Martins, S.G., et al., *Linking Oxidative Stress and DNA Damage to Changes in the Expression of Extracellular Matrix Components.* Frontiers in genetics, 2021. **12**: p. 673002-673002.

305. Wang, F., et al., *Mitochondrial Protein Translation: Emerging Roles and Clinical Significance in Disease.* Frontiers in Cell and Developmental Biology, 2021. **9**.

306. Janiszewska, M., M.C. Primi, and T. Izard, *Cell adhesion in cancer: Beyond the migration of single cells.* The Journal of biological chemistry, 2020. **295**(8): p. 2495-2505.

307. Santo-Domingo, J. and N. Demaurex, *Calcium uptake mechanisms of mitochondria.* Biochimica et Biophysica Acta (BBA) - Bioenergetics, 2010. **1797**(6): p. 907-912.

308. Jaña, F., et al., *Complex I and II are required for normal mitochondrial Ca2+ homeostasis.* Mitochondrion, 2019. **49**: p. 73-82.

309. Chédotal, A., G. Kerjan, and C. Moreau-Fauvarque, *The brain within the tumor: new roles for axon guidance molecules in cancers.* Cell Death & Differentiation, 2005. **12**(8): p. 1044-1056.

310. Chamberlain, K.A. and Z.-H. Sheng, *Mechanisms for the maintenance and regulation of axonal energy supply.* Journal of neuroscience research, 2019. **97**(8): p. 897-913.

311. Harris, J.J., R. Jolivet, and D. Attwell, *Synaptic energy use and supply.* Neuron, 2012. **75**(5): p. 762-777.

312. Sobieski, C., M.J. Fitzpatrick, and S.J. Mennerick, *Differential presynaptic ATP supply for basal and high-demand transmission.* Journal of Neuroscience, 2017. **37**(7): p. 1888-1899.

313. Vallenius, T., *Actin stress fibre subtypes in mesenchymal-migrating cells.* Open Biology. **3**(6): p. 130001.

314. Parker, A.L., M. Kavallaris, and J.A. McCarroll, *Microtubules and their role in cellular stress in cancer.* Frontiers in oncology, 2014. **4**: p. 153-153.

315. Waters, A.M. and P.L. Beales, *Ciliopathies: an expanding disease spectrum.* Pediatric nephrology (Berlin, Germany), 2011. **26**(7): p. 1039-1056.

316. Ma, S., et al., *DNA damage promotes microtubule dynamics through a DNA-PK-AKT axis for enhanced repair.* Journal of Cell Biology, 2021. **220**(2): p. e201911025.

317. Gou, Q., et al., *Peroxisome proliferator-activated receptors (PPARs) are potential drug targets for cancer therapy.* Oncotarget, 2017. **8**(36): p. 60704-60709.

318. Tan, Y., et al., *PPAR-α Modulators as Current and Potential Cancer Treatments.* Frontiers in Oncology, 2021. **11**.

319. Hinrichsen, I., et al., *Phosphorylation-dependent signaling controls degradation of DNA mismatch repair protein PMS2.* Mol Carcinog, 2017. **56**(12): p. 2663-2668.

320. Lynch, H.T., et al., *Milestones of Lynch syndrome: 1895–2015.* Nature Reviews Cancer, 2015. **15**(3): p. 181-194.

321. Mohd, A.B., et al., *Truncation of the C-terminus of human MLH1 blocks intracellular stabilization of PMS2 and disrupts DNA mismatch repair.* DNA Repair, 2006. **5**(3): p. 347-361.

322. Perera, S. and B. Bapat, *The MLH1 variants p.Arg265Cys and p.Lys618Ala affect protein stability while p.Leu749Gln affects heterodimer formation.* Human Mutation, 2008. **29**(2): p. 332-332.

323. Briggs, S. and I. Tomlinson, *Germline and somatic polymerase ϵ and δ mutations define a new class of hypermutated colorectal and endometrial cancers.* The Journal of Pathology, 2013. **230**(2): p. 148-153.

324. Cerami, E., et al., *The cBio cancer genomics portal: an open platform for exploring multidimensional cancer genomics data.* Cancer Discov, 2012. **2**(5): p. 401-4.

325. Zhang, J., et al., *Sequential gene expression analysis of cervical malignant transformation identifies RFC4 as a novel diagnostic and prognostic biomarker.* BMC Medicine, 2022. **20**(1): p. 437.

326. Tuo, L., et al., *PCK1 negatively regulates cell cycle progression and hepatoma cell proliferation via the AMPK/p27Kip1 axis.* Journal of Experimental & Clinical Cancer Research, 2019. **38**(1): p. 50.

327. Fan, Y., et al., *Anti-Warburg effect by targeting HRD1-PFKP pathway may inhibit breast cancer progression.* Cell Communication and Signaling, 2021. **19**(1): p. 18.

328. Ooi, A.T. and B.N. Gomperts, *Molecular Pathways: Targeting Cellular Energy Metabolism in Cancer via Inhibition of SLC2A1 and LDHA.* Clinical cancer research : an official journal of the American Association for Cancer Research, 2015. **21**(11): p. 2440-2444.

329. Li, J., et al., *Wild-type IDH2 promotes the Warburg effect and tumor growth through HIF1α in lung cancer.* Theranostics, 2018. **8**(15): p. 4050-4061.

330. Xiao, Z., et al., *SDHB downregulation facilitates the proliferation and invasion of colorectal cancer through AMPK functions excluding those involved in the modulation of aerobic glycolysis.* Experimental and therapeutic medicine, 2018. **15**(1): p. 864-872.

331. Carrozzo, R., et al., *SUCLA2 mutations are associated with mild methylmalonic aciduria, Leigh-like encephalomyopathy, dystonia and deafness.* Brain, 2007. **130**(3): p. 862-874.

332. Ostergaard, E., *Disorders caused by deficiency of succinate-CoA ligase.* Journal of Inherited Metabolic Disease, 2008. **31**(2): p. 226-229.

333. Kowluru, A., M. Tannous, and H.-Q. Chen, *Localization and Characterization of the Mitochondrial Isoform of the Nucleoside Diphosphate Kinase in the Pancreatic β Cell: Evidence for Its Complexation with Mitochondrial Succinyl-CoA Synthetase.* Archives of Biochemistry and Biophysics, 2002. **398**(2): p. 160-169.

334. Lieu, E.L., et al., *Amino acids in cancer.* Experimental & Molecular Medicine, 2020. **52**(1): p. 15-30.

335. Alkan, H.F. and J.G. Bogner-Strauss, *Maintaining cytosolic aspartate levels is a major function of the TCA cycle in proliferating cells.* Mol Cell Oncol, 2019. **6**(5): p. e1536843.

336. Nguyen, T., et al., *Uncovering the Role of N-Acetyl-Aspartyl-Glutamate as a Glutamate Reservoir in Cancer.* Cell reports, 2019. **27**(2): p. 491-501.e6.

337. Lou, T.-F., et al., *Cancer-Specific Production of N-Acetylaspartate via NAT8L Overexpression in Non-Small Cell Lung Cancer and Its Potential as a Circulating Biomarker.* Cancer prevention research (Philadelphia, Pa.), 2016. **9**(1): p. 43-52.

338. Alkan, H.F., et al., *N-acetylaspartate improves cell survival when glucose is limiting.* bioRxiv, 2020: p. 2020.05.28.114629.

339. Bogner-Strauss, J.G., *N-Acetylaspartate Metabolism Outside the Brain: Lipogenesis, Histone Acetylation, and Cancer.* Frontiers in Endocrinology, 2017. **8**.

340. Zand, B., et al., *Role of Increased n-acetylaspartate Levels in Cancer.* Journal of the National Cancer Institute, 2016. **108**(6): p. djv426-djv426.

341. Chen, C.-L., et al., *Arginine Signaling and Cancer Metabolism.* Cancers, 2021. **13**(14): p. 3541.

342. Changou, C.A., et al., *Arginine starvation-associated atypical cellular death involves mitochondrial dysfunction, nuclear DNA leakage, and chromatin autophagy.* Proc Natl Acad Sci U S A, 2014. **111**(39): p. 14147-52.

343. Chen, C.-L., et al., *Arginine is an epigenetic regulator targeting TEAD4 to modulate OXPHOS in prostate cancer cells.* Nature Communications, 2021. **12**(1): p. 2398.

344. Lee, W.D., et al., *Spatial-fluxomics provides a subcellular-compartmentalized view of reductive glutamine metabolism in cancer cells.* Nature Communications, 2019. **10**(1): p. 1351.

345. Liang, C., et al., *Leucine Modulates Mitochondrial Biogenesis and SIRT1-AMPK Signaling in C2C12 Myotubes.* J Nutr Metab, 2014. **2014**: p. 239750.

346. Sun, X. and M.B. Zemel, *Leucine modulation of mitochondrial mass and oxygen consumption in skeletal muscle cells and adipocytes.* Nutrition & metabolism, 2009. **6**: p. 26-26.

347. Villena, J.A., *New insights into PGC-1 coactivators: redefining their role in the regulation of mitochondrial function and beyond.* Febs j, 2015. **282**(4): p. 647-72.

348. Ghilardi, C., et al., *PGC1α/β Expression Predicts Therapeutic Response to Oxidative Phosphorylation Inhibition in Ovarian Cancer.* Cancer Research, 2022. **82**(7): p. 1423-1434.

349. Kennedy, L., et al., *Role of Glutathione in Cancer: From Mechanisms to Therapies.* Biomolecules, 2020. **10**(10): p. 1429.

350. Bansal, A. and M.C. Simon, *Glutathione metabolism in cancer progression and treatment resistance.* The Journal of cell biology, 2018. **217**(7): p. 2291-2298.

351. Kim, J.-H., et al., *Clinicopathologic significance of DNA mismatch repair protein status in endometrial cancer.* Taiwanese Journal of Obstetrics and Gynecology, 2022. **61**(3): p. 415-421.

352. Cantor, J.R., et al., *Physiologic Medium Rewires Cellular Metabolism and Reveals Uric Acid as an Endogenous Inhibitor of UMP Synthase.* Cell, 2017. **169**(2): p. 258-272.e17.

353. Hui, S., et al., *Glucose feeds the TCA cycle via circulating lactate.* Nature, 2017. **551**(7678): p. 115-118.

354. Vande Voorde, J., et al., *Improving the metabolic fidelity of cancer models with a physiological cell culture medium.* Science advances, 2019. **5**(1): p. eaau7314-eaau7314.

355. Joly, J.H., B.T.L. Chew, and N.A. Graham, *The landscape of metabolic pathway dependencies in cancer cell lines.* PLOS Computational Biology, 2021. **17**(4): p. e1008942.

356. Nishitani, S., et al., *Branched-chain amino acids improve glucose metabolism in rats with liver cirrhosis.* American Journal of Physiology-Gastrointestinal and Liver Physiology, 2005. **288**(6): p. G1292-G1300.

357. Doi, M., et al., *Isoleucine, a potent plasma glucose-lowering amino acid, stimulates glucose uptake in C2C12 myotubes.* Biochemical and Biophysical Research Communications, 2003. **312**(4): p. 1111-1117.

358. Koukourakis, M.I., et al., *Comparison of Metabolic Pathways between Cancer Cells and Stromal Cells in Colorectal Carcinomas: a Metabolic Survival Role for Tumor-Associated Stroma.* Cancer Research, 2006. **66**(2): p. 632-637.

359. Fischer, K., et al., *Inhibitory effect of tumor cell–derived lactic acid on human T cells.* Blood, 2007. **109**(9): p. 3812-3819.

360. Riches, L.C., et al., *Pharmacology of the ATM Inhibitor AZD0156: Potentiation of Irradiation and Olaparib Responses Preclinically AID - 10.1158/1535-7163.MCT-18-1394.*

361. Oshima, N., et al., *Dynamic Imaging of LDH Inhibition in Tumors Reveals Rapid In Vivo Metabolic Rewiring and Vulnerability to Combination Therapy.* Cell reports, 2020. **30**(6): p. 1798-1810.e4.

362. Doherty, J.R. and J.L. Cleveland, *Targeting lactate metabolism for cancer therapeutics.* The Journal of Clinical Investigation, 2013. **123**(9): p. 3685-3692.

363. Sulkowski, P.L., et al., *2-Hydroxyglutarate produced by neomorphic IDH mutations suppresses homologous recombination and induces PARP inhibitor sensitivity.* Sci Transl Med, 2017. **9**(375).

364. Le, A., et al., *Inhibition of lactate dehydrogenase A induces oxidative stress and inhibits tumor progression.* Proceedings of the National Academy of Sciences of the United States of America, 2010. **107**(5): p. 2037-2042.

365. Rellinger, E.J., et al., *FX11 inhibits aerobic glycolysis and growth of neuroblastoma cells.* Surgery, 2017. **161**(3): p. 747-752.

366. Lemberg, K.M., et al., *We're Not "DON" Yet: Optimal Dosing and Prodrug Delivery of 6-Diazo-5-oxo-L-norleucine.* Molecular cancer therapeutics, 2018. **17**(9): p. 1824-1832.

367. Altman, B.J., Z.E. Stine, and C.V. Dang, *From Krebs to clinic: glutamine metabolism to cancer therapy.* Nature Reviews Cancer, 2016. **16**(10): p. 619-634.

368. Thomas, A.G., et al., *Kinetic characterization of ebselen, chelerythrine and apomorphine as glutaminase inhibitors.* Biochemical and Biophysical Research Communications, 2013. **438**(2): p. 243-248.

369. Purkey, H.E., et al., *Cell Active Hydroxylactam Inhibitors of Human Lactate Dehydrogenase with Oral Bioavailability in Mice.* ACS medicinal chemistry letters, 2016. **7**(10): p. 896-901.

370. Billiard, J., et al., *Quinoline 3-sulfonamides inhibit lactate dehydrogenase A and reverse aerobic glycolysis in cancer cells.* Cancer & metabolism, 2013. **1**(1): p. 19-19.

371. Boudreau, A., et al., *Metabolic plasticity underpins innate and acquired resistance to LDHA inhibition.* Nature Chemical Biology, 2016. **12**(10): p. 779-786.

372. Kleijn, A., et al., *A Systematic Comparison Identifies an ATP-Based Viability Assay as Most Suitable Read-Out for Drug Screening in Glioma Stem-Like Cells.* Stem cells international, 2016. **2016**: p. 5623235-5623235.

373. Giuliano, C.J., et al., *Generating Single Cell–Derived Knockout Clones in Mammalian Cells with CRISPR/Cas9.* Current Protocols in Molecular Biology, 2019. **128**(1): p. e100.

374. Gao, L., et al., *CPI-613 rewires lipid metabolism to enhance pancreatic cancer apoptosis via the AMPK-ACC signaling.* Journal of Experimental & Clinical Cancer Research, 2020. **39**(1): p. 73.

375. Rosenzweig, A., J. Blenis, and A.P. Gomes, *Beyond the Warburg Effect: How Do Cancer Cells Regulate One-Carbon Metabolism?* Frontiers in Cell and Developmental Biology, 2018. **6**.

376. Li, A.M. and J. Ye, *Reprogramming of serine, glycine and one-carbon metabolism in cancer.* Biochimica et Biophysica Acta (BBA) - Molecular Basis of Disease, 2020. **1866**(10): p. 165841.

377. Choi, B.-H., et al., *Lineage-specific silencing of PSAT1 induces serine auxotrophy and sensitivity to dietary serine starvation in luminal breast tumors.* Cell Reports, 2022. **38**(3): p. 110278.

378. Rathore, R., C.R. Schutt, and B.A. Van Tine, *PHGDH as a mechanism for resistance in metabolically-driven cancers.* Cancer drug resistance (Alhambra, Calif.), 2020. **3**(4): p. 762-774.

379. Weinstabl, H., et al., *Intracellular Trapping of the Selective Phosphoglycerate Dehydrogenase (PHGDH) Inhibitor BI-4924 Disrupts Serine Biosynthesis.* Journal of Medicinal Chemistry, 2019. **62**(17): p. 7976-7997.

380. Arlt, B., et al., *Inhibiting PHGDH with NCT-503 reroutes glucose-derived carbons into the TCA cycle, independently of its on-target effect.* Journal of Enzyme Inhibition and Medicinal Chemistry, 2021. **36**(1): p. 1282-1289.

381. Brüggmann, D., et al., *Endometrial cancer: mapping the global landscape of research.* Journal of Translational Medicine, 2020. **18**(1): p. 386.

382. Wortman, B.G., et al., *Selecting Adjuvant Treatment for Endometrial Carcinoma Using Molecular Risk Factors.* Current Oncology Reports, 2019. **21**(9): p. 83.

383. Kurpiel, B., et al., *MLH1/PMS2-deficient Endometrial Carcinomas in a Universally Screened Population: MLH1 Hypermethylation and Germline Mutation Status.* International Journal of Gynecological Pathology, 2022. **41**(1).

384. Caduff, R.F., et al., *Clinical and pathological significance of microsatellite instability in sporadic endometrial carcinoma.* Am J Pathol, 1996. **148**(5): p. 1671-8.

385. Pelletier, M.P., et al., *Microcystic, elongated, and fragmented pattern invasion is mainly associated with isolated tumor cell pattern metastases in International Federation of Gynecology and Obstetrics grade I endometrioid endometrial cancer.* Hum Pathol, 2017. **62**: p. 33-39.

386. Ribic, C.M., et al., *Tumor microsatellite-instability status as a predictor of benefit from fluorouracil-based adjuvant chemotherapy for colon cancer.* N Engl J Med, 2003. **349**(3): p. 247-57.

387. Strathdee, G., et al., *A role for methylation of the hMLH1 promoter in loss of hMLH1 expression and drug resistance in ovarian cancer.* Oncogene, 1999. **18**(14): p. 2335-2341.

388. Fink, D., et al., *The role of DNA mismatch repair in platinum drug resistance.* Cancer Res, 1996. **56**(21): p. 4881-6.

389. Drummond, J.T., et al., *Cisplatin and adriamycin resistance are associated with MutLalpha and mismatch repair deficiency in an ovarian tumor cell line.* J Biol Chem, 1996. **271**(33): p. 19645-8.

390. Zong, L., et al., *PD-L1 expression in tumor cells is associated with a favorable prognosis in patients with high-risk endometrial cancer.* Gynecologic Oncology, 2021. **162**(3): p. 631-637.

391. Eggink, F.A., et al., *Immunological profiling of molecularly classified high-risk endometrial cancers identifies POLE-mutant and microsatellite unstable carcinomas as candidates for checkpoint inhibition.* OncoImmunology, 2017. **6**(2): p. e1264565.

392. Schumacher, T.N. and R.D. Schreiber, *Neoantigens in cancer immunotherapy.* Science, 2015. **348**(6230): p. 69-74.

393. McGranahan, N., et al., *Clonal neoantigens elicit T cell immunoreactivity and sensitivity to immune checkpoint blockade.* Science, 2016. **351**(6280): p. 1463-9.

394. Anagnostou, V., et al., *Evolution of Neoantigen Landscape during Immune Checkpoint Blockade in Non-Small Cell Lung Cancer.* Cancer Discov, 2017. **7**(3): p. 264-276.

395. Rizvi, N.A., et al., *Cancer immunology. Mutational landscape determines sensitivity to PD-1 blockade in non-small cell lung cancer.* Science (New York, N.Y.), 2015. **348**(6230): p. 124-128.

396. Topalian, Suzanne L., Charles G. Drake, and Drew M. Pardoll, *Immune Checkpoint Blockade: A Common Denominator Approach to Cancer Therapy.* Cancer Cell, 2015. **27**(4): p. 450-461.

397. Ott, P.A., et al., *Safety and Antitumor Activity of Pembrolizumab in Advanced Programmed Death Ligand 1–Positive Endometrial Cancer: Results From the KEYNOTE-028 Study.* Journal of Clinical Oncology, 2017. **35**(22): p. 2535-2541.

398. Makker, V., et al., *Lenvatinib Plus Pembrolizumab in Patients With Advanced Endometrial Cancer.* Journal of clinical oncology : official journal of the American Society of Clinical Oncology, 2020. **38**(26): p. 2981-2992.

399. Redondo, A., A. Gallego, and M. Mendiola, *Dostarlimab for the treatment of advanced endometrial cancer.* Expert Review of Clinical Pharmacology, 2022. **15**(1): p. 1-9.

400. Haslam, A. and V. Prasad, *Estimation of the Percentage of US Patients With Cancer Who Are Eligible for and Respond to Checkpoint Inhibitor Immunotherapy Drugs.* JAMA Network Open, 2019. **2**(5): p. e192535-e192535.

401. Chamoto, K., et al., *Mitochondrial activation chemicals synergize with surface receptor PD-1 blockade for T cell-dependent antitumor activity.* Proceedings of the National Academy of Sciences of the United States of America, 2017. **114**(5): p. E761-E770.

402. Kouidhi, S., F. Ben Ayed, and A. Benammar Elgaaied, *Targeting Tumor Metabolism: A New Challenge to Improve Immunotherapy.* Frontiers in immunology, 2018. **9**: p. 353-353.

403. Klein, K., et al., *Role of Mitochondria in Cancer Immune Evasion and Potential Therapeutic Approaches.* Frontiers in Immunology, 2020. **11**.

404. Koppenol, W.H., P.L. Bounds, and C.V. Dang, *Otto Warburg's contributions to current concepts of cancer metabolism.* Nat Rev Cancer, 2011. **11**(5): p. 325-37.

405. Hanahan, D. and Robert A. Weinberg, *Hallmarks of Cancer: The Next Generation.* Cell, 2011. **144**(5): p. 646-674.

406. Reznik, E., et al., *Mitochondrial DNA copy number variation across human cancers.* eLife, 2016. **5**: p. e10769.

407. Calle, E.E. and R. Kaaks, *Overweight, obesity and cancer: epidemiological evidence and proposed mechanisms.* Nature Reviews Cancer, 2004. **4**(8): p. 579-591.

408. McCawley, G.M., et al., *Cancer in Obese Women: Potential Protective Impact of Bariatric Surgery.* Journal of the American College of Surgeons, 2009. **208**(6).

409. Lambe, M., et al., *Impaired glucose metabolism and diabetes and the risk of breast, endometrial, and ovarian cancer.* Cancer Causes & Control, 2011. **22**(8): p. 1163-1171.

410. Zendehdel, K., et al., *Cancer Incidence in Patients With Type 1 Diabetes Mellitus: A Population-Based Cohort Study in Sweden.* JNCI: Journal of the National Cancer Institute, 2003. **95**(23): p. 1797-1800.

411. Weigelt, B. and S. Banerjee, *Molecular targets and targeted therapeutics in endometrial cancer.* Current Opinion in Oncology, 2012. **24**(5).

412. Byrne, F.L., et al., *Metabolic Vulnerabilities in Endometrial Cancer.* Cancer Research, 2014. **74**(20): p. 5832-5845.

413. Xiang, J., et al., *Gluconeogenic enzyme PCK1 deficiency promotes CHK2 O-GlcNAcylation and hepatocellular carcinoma growth upon glucose deprivation.* The Journal of clinical investigation, 2021. **131**(8): p. e144703.

414. Zachara, N.E. and G.W. Hart, *O-GlcNAc a sensor of cellular state: the role of nucleocytoplasmic glycosylation in modulating cellular function in response to nutrition and stress.* Biochim Biophys Acta, 2004. **1673**(1-2): p. 13-28.

415. Ferrer, C.M., V.L. Sodi, and M.J. Reginato, *O-GlcNAcylation in Cancer Biology: Linking Metabolism and Signaling.* J Mol Biol, 2016. **428**(16): p. 3282-3294.

416. Skorupa, A., et al., *Grading of endometrial cancer using 1H HR-MAS NMR-based metabolomics.* Scientific Reports, 2021. **11**(1): p. 18160.

417. Trousil, S., et al., *Alterations of Choline Phospholipid Metabolism in Endometrial Cancer Are Caused by Choline Kinase Alpha Overexpression and a Hyperactivated Deacylation Pathway.* Cancer Research, 2014. **74**(23): p. 6867-6877.

418. Wang, P., et al., *BCAT1 promotes proliferation of endometrial cancer cells through reprogrammed BCAA metabolism.* International journal of clinical and experimental pathology, 2018. **11**(12): p. 5536-5546.

419. Wang, Z.-Q., et al., *BCAT1 expression associates with ovarian cancer progression: possible implications in altered disease metabolism.* Oncotarget, 2015. **6**(31): p. 31522-31543.

420. Li, G.-S., et al., *BCAT1: A risk factor in multiple cancers based on a pan-cancer analysis.* Cancer Medicine, 2022. **11**(5): p. 1396-1412.

421. Yi, R., et al., *Multi-Omic Profiling of Multi-Biosamples Reveals the Role of Amino Acid and Nucleotide Metabolism in Endometrial Cancer.* Frontiers in oncology, 2022. **12**: p. 861142-861142.

422. Kang, Y.P., N.P. Ward, and G.M. DeNicola, *Recent advances in cancer metabolism: a technological perspective.* Experimental & Molecular Medicine, 2018. **50**(4): p. 1-16.

423. Mayers, J.R., et al., *Tissue of origin dictates branched-chain amino acid metabolism in mutant Kras-driven cancers.* Science (New York, N.Y.), 2016. **353**(6304): p. 1161-1165.

424. Dang, L., et al., *Cancer-associated IDH1 mutations produce 2-hydroxyglutarate.* Nature, 2010. **465**(7300): p. 966.

425. Alarcon-Barrera, J.C., et al., *Recent advances in metabolomics analysis for early drug development.* Drug Discovery Today, 2022. **27**(6): p. 1763-1773.

426. Warth, B., et al., *Metabolomics Reveals that Dietary Xenoestrogens Alter Cellular Metabolism Induced by Palbociclib/Letrozole Combination Cancer Therapy.* Cell Chemical Biology, 2018. **25**(3): p. 291-300.e3.

427. Pushpakom, S., et al., *Drug repurposing: progress, challenges and recommendations.* Nature Reviews Drug Discovery, 2019. **18**(1): p. 41-58.

428. Geeraerts, S.L., et al., *Repurposing the Antidepressant Sertraline as SHMT Inhibitor to Suppress Serine/Glycine Synthesis–Addicted Breast Tumor Growth.* Molecular Cancer Therapeutics, 2021. **20**(1): p. 50-63.

429. Kaushik, A.K. and R.J. DeBerardinis, *Applications of metabolomics to study cancer metabolism.* Biochimica et Biophysica Acta (BBA) - Reviews on Cancer, 2018. **1870**(1): p. 2-14.

430. Wong, C.H., K.W. Siah, and A.W. Lo, *Estimation of clinical trial success rates and related parameters.* Biostatistics, 2019. **20**(2): p. 273-286.

431. Psychogios, N., et al., *The human serum metabolome.* PloS one, 2011. **6**(2): p. e16957-e16957.

432. Liberti, M.V. and J.W. Locasale, *The Warburg Effect: How Does it Benefit Cancer Cells?* Trends in biochemical sciences, 2016. **41**(3): p. 211-218.

433. van der Bliek, A.M., M.M. Sedensky, and P.G. Morgan, *Cell Biology of the Mitochondrion.* Genetics, 2017. **207**(3): p. 843-871.

434. Fu, Y., et al., *Meta-analysis of serum lactate dehydrogenase and prognosis for osteosarcoma.* Medicine, 2018. **97**(19): p. e0741-e0741.

435. Gan, J., et al., *Prognostic value of pretreatment serum lactate dehydrogenase level in pancreatic cancer patients: A meta-analysis of 18 observational studies.* Medicine, 2018. **97**(46): p. e13151-e13151.

436. Zhang, Z., et al., *Pretreatment lactate dehydrogenase may predict outcome of advanced non small-cell lung cancer patients treated with immune checkpoint inhibitors: A meta-analysis.* Cancer medicine, 2019. **8**(4): p. 1467-1473.

437. Hou, X.-M., et al., *LDH-A promotes malignant behavior via activation of epithelial-to-mesenchymal transition in lung adenocarcinoma.* Bioscience reports, 2019. **39**(1): p. BSR20181476.

438. Xie, H., et al., *LDH-A inhibition, a therapeutic strategy for treatment of hereditary leiomyomatosis and renal cell cancer.* Molecular cancer therapeutics, 2009. **8**(3): p. 626-635.

439. Ashrafian, H., et al., *Expression Profiling in Progressive Stages of Fumarate-Hydratase Deficiency: The Contribution of Metabolic Changes to Tumorigenesis.* Cancer Research, 2010. **70**(22): p. 9153-9165.

440. Cheng, C.-S., et al., *Functional inhibition of lactate dehydrogenase suppresses pancreatic adenocarcinoma progression.* Clinical and translational medicine, 2021. **11**(6): p. e467-e467.

441. Xian, Z.-Y., et al., *Inhibition of LDHA suppresses tumor progression in prostate cancer.* Tumour biology : the journal of the International Society for Oncodevelopmental Biology and Medicine, 2015. **36**(10): p. 8093-8100.

442. Feng, Y., et al., *Lactate dehydrogenase A: A key player in carcinogenesis and potential target in cancer therapy.* Cancer medicine, 2018. **7**(12): p. 6124-6136.

443. Martínez-Ordoñez, A., et al., *POU1F1 transcription factor induces metabolic reprogramming and breast cancer progression via LDHA regulation.* Oncogene, 2021. **40**(15): p. 2725-2740.

444. Ždralević, M., et al., *Double genetic disruption of lactate dehydrogenases A and B is required to ablate the "Warburg effect" restricting tumor growth to oxidative metabolism.* The Journal of biological chemistry, 2018. **293**(41): p. 15947-15961.

445. Tian, Y., A.L. Chen Yy Fau - Han, and A.L. Han, *MiR-1271 inhibits cell proliferation and metastasis by targeting LDHA in endometrial cancer.* (2284-0729 (Electronic)).

446. Zhang, W., et al., *Inhibition of LDHA suppresses cell proliferation and increases mitochondrial apoptosis via the JNK signaling pathway in cervical cancer cells.* Oncol Rep, 2022. **47**(4): p. 77.

447. Qiao, T., et al., *Inhibition of LDH-A by Oxamate Enhances the Efficacy of Anti-PD-1 Treatment in an NSCLC Humanized Mouse Model.* Frontiers in Oncology, 2021. **11**.

448. Daneshmandi, S., B. Wegiel, and P. Seth, *Blockade of Lactate Dehydrogenase-A (LDH-A) Improves Efficacy of Anti-Programmed Cell Death-1 (PD-1) Therapy in Melanoma.* Cancers, 2019. **11**(4).

449. Yang, Y., et al., *Targeting lactate dehydrogenase a improves radiotherapy efficacy in non-small cell lung cancer: from bedside to bench.* Journal of Translational Medicine, 2021. **19**(1): p. 170.

450. Ren, L., et al., *Glutaminase-1 (GLS1) inhibition limits metastatic progression in osteosarcoma.* Cancer & Metabolism, 2020. **8**(1): p. 4.

451. Gross, M.I., et al., *Antitumor Activity of the Glutaminase Inhibitor CB-839 in Triple-Negative Breast Cancer.* Molecular Cancer Therapeutics, 2014. **13**(4): p. 890-901.

452. Varghese, S., et al., *The Glutaminase Inhibitor CB-839 (Telaglenastat) Enhances the Antimelanoma Activity of T-Cell-Mediated Immunotherapies.* Molecular cancer therapeutics, 2021. **20**(3): p. 500-511.

453. Lemberg, K.M., et al., *Clinical development of metabolic inhibitors for oncology.* The Journal of Clinical Investigation, 2022. **132**(1).

454. Rashmi, R., et al., *Glutaminase Inhibitors Induce Thiol-Mediated Oxidative Stress and Radiosensitization in Treatment-Resistant Cervical Cancers.* Molecular Cancer Therapeutics, 2020. **19**(12): p. 2465-2475.

455. Kalhan, S.C. and R.W. Hanson, *Resurgence of serine: an often neglected but indispensable amino Acid.* The Journal of biological chemistry, 2012. **287**(24): p. 19786-19791.

456. Davis, S.R., et al., *Tracer-derived total and folate-dependent homocysteine remethylation and synthesis rates in humans indicate that serine is the main one-carbon donor.* Am J Physiol Endocrinol Metab, 2004. **286**(2): p. E272-9.

457. Deberardinis, R.J., et al., *Brick by brick: metabolism and tumor cell growth.* Current opinion in genetics & development, 2008. **18**(1): p. 54-61.

458. McNamee, M.J., D. Michod, and M.V. Niklison-Chirou, *Can small molecular inhibitors that stop de novo serine synthesis be used in cancer treatment?* Cell Death Discovery, 2021. **7**(1): p. 87.

459. Xian, Y., et al., *Phosphoglycerate dehydrogenase is a novel predictor for poor prognosis in gastric cancer.* OncoTargets and therapy, 2016. **9**: p. 5553-5560.

460. Jing, Z., et al., *Expression and Clinical Significance of Phosphoglycerate Dehydrogenase and Squamous Cell Carcinoma Antigen in Cervical Cancer.* International Journal of Gynecologic Cancer, 2013. **23**(8): p. 1465.

461. Rathore, R., C.R. Schutt, and B.A. Van Tine, *PHGDH as a mechanism for resistance in metabolically-driven cancers.* Cancer Drug Resistance, 2020. **3**(4): p. 762-774.

462. Svoboda, L.K., et al., *Menin regulates the serine biosynthetic pathway in Ewing sarcoma.* The Journal of Pathology, 2018. **245**(3): p. 324-336.

463. Yoshida, K., et al., *Targeted Disruption of the Mouse 3-Phosphoglycerate Dehydrogenase Gene Causes Severe Neurodevelopmental Defects and Results in Embryonic Lethality *.* Journal of Biological Chemistry, 2004. **279**(5): p. 3573-3577.

464. Jiang, L., et al., *Molecular Mechanism of Anti-Cancer Activity of the Nano-Drug C-PC/CMC-CD59sp NPs in Cervical Cancer.* Journal of Cancer, 2019. **10**(1): p. 92-104.

9.0 Supplementary Materials

TABLE 8.1. Nutritional composition of Plasmax, DMEM, and RPMI.

Nutrient	Media (μM)		
	Plasmax	DMEM	RPMI 1640
Proteinogenic Amino Acids			
Alanine	510		
Arginine	64	398	1149
Asparagine	41		379
Aspartic Acid	6		150
Cysteine	33		
Glutamate	98		136
Glutamine	650	4000	2055
Glycine	330	400	133
Histidine	120	200	97
Isoleucine	140	802	382
Leucine	170	802	382
Lysine	220	798	219
Methionine	30	201	101
Phenylalanine	68	400	91
Proline	360		174
Serine	140	400	286
Threonine	240	798	168
Tryptophan	78	78	25
Tyrosine	74	399	111
Valine	230	803	171
Non-proteinogenic Amino Acids			
Aminobutyrate	41		
Citrulline	55		
Dicysteine	65	201.3	207.7
Homocysteine	9		
Hydroxy-L-proline	13		152.7
Ornithine	80		
Pyroglutamate	20		
Amino Acid Derivatives			
Acetyl Glycine	70		
Carnosine	6		
Glutathione (reduced)	37		3.3
Putrescine			
Taurine	130		
N-Trimethylglycine (Betaine)	72		
Other components			
Acetate	42		
Acetone	55		

Acetyl carnitine	5		
Citrate	114		
Carnitine	46		
Creatine	37		
Creatinine	74		
Formate	33		
D-Glucose	5556	25000	11111
Glycerol	82		
2-Hyroxybutyrate	31		
3-Hydroxybutyrate	77		
3-Hyroxyisobutyrate	20		
Hypoxanthine	5		
Lactate	500		
Linoleic Acid			
Lipoic Acid			
Methyl acetoacetate	41		
Phenol Red	25	39.9	13.3
Pyruvate	100	1000	
Succinate	23		
Thymidine			
Uracil	2		
Urate	270		
Urea	3000		
Uridine	3		
Inorganic Salts			
Ammonium Chloride	50		
Calcium Chloride	1800	1802	
Calcium Nitrate			424
Magnesium Chloride			
Magnesium Sulphate	813	814	407
Potassium Chloride	5330	5333	5333
Potassium Nitrate			
Sodium Bicarbonate	26191	44048	23810
Sodium Chloride	118706	110345	103448
Sodium Phosphate monobasic	1010	906	
Sodium Phosphate dibasic			5634
Trace Elements			
Ammonium Metavanadate	0.0026		
Cupric Sulphate	0.0052		
Ferric Chloride			
Ferric Nitrate	0.1238	0.2475	
Ferric Sulphate	1.0428		
Manganous Chloride	0.0002		
Sodium Selenite	0.0289		
Zinc Sulphate	1.5		

Vitamins			
p-Aminobenzoate			7.3
Ascorbate	62		
D-Biotin	4.1		0.82
Choline	7.1	28.6	21.4
Myo-Inositol	2.3	9.1	2.27
Niacinamide	11.1	40	194.4
D-Calcium pantothenate	8.2	32.8	8.2
p-Aminobenzoate	2.1	8.4	0.52
Pyridoxal	4.9		
Pyridoxin		19.4	4.9
Riboflavin	0.3	1.1	0.53
Thiamine	3	11.2	3
Vitamin B12	0.005		0.0037